Aus dem Institut für Virologie
Geschäftsführender Direktor: Prof. Dr. Stephan Becker
des Fachbereichs Medizin der Philipps-Universität Marburg

# Proteolytic activation of *Zaire ebolavirus* and SARS-CoV-2 class I membrane fusion proteins by different host cell proteases

Inaugural-Dissertation zur Erlangung des Doktorgrades
der Naturwissenschaften (Dr. rer. nat.)

dem Fachbereich Medizin
der Philipps-Universität Marburg
vorgelegt von

**Dorothea Bestle**
aus Kempten (Allgäu)

Marburg, 2022

Angenommen vom Fachbereich Medizin der Philipps-Universität Marburg am:
28.11.2022

Gedruckt mit Genehmigung des Fachbereichs Medizin

Dekanin: Prof. Dr. Denise Hilfiker-Kleiner

Referentin: Prof. Dr. Eva Friebertshäuser

Korreferentin: Prof. Dr. Magdalena Huber

# Table of contents

## Abstract

The proteolytic processing of viral fusion proteins by host cell proteases is a prerequisite for the replication and infectivity of enveloped viruses. The identification of relevant proteases involved in virus activation is therefore an important step towards the development of host protease inhibitors as antiviral strategies.

In this study the proteolytic activation mechanisms of the class I fusion proteins of Zaire ebolavirus (ZEBOV) and the novel severe acute respiratory syndrome (SARS) coronavirus (CoV) 2, which both possess two cleavage sites, were investigated. The fusion protein S of SARS-CoV-2 contains two distinct cleavage sites, with a multibasic motif at the S1/S2 site and a monobasic motif at the S2' site. Co-expression in 293F cells and infection studies in Calu-3 cells in the presence and absence of protease inhibitors revealed proteolytic activation by furin and transmembrane serine protease 2 (TMPRSS2). Both proteases have been shown to be essential for efficient replication of SARS-CoV-2, as they were not able to compensate for each other. In contrast, *in vitro* experiments revealed a highly complex processing mechanism for the ZEBOV GP beyond the described classical proteolytic activation by furin and endosomal cathepsin B and L. The "non-cleavable" ZEBOV GP_AGTAA furin cleavage mutant was shown to be processed into the 20 kDa fusion competent $GP_2$ by TMPRSS2 and cathepsin L at so far unknown positions. Moreover, pseudovirus rVSVΔG ZEBOV GP growth kinetics and transcription and replication-competent virus-like particle (trVLP) entry studies in Huh-7, VeroE6 and Vero-TMPRSS2 cells in the presence and absence of protease inhibitors demonstrated, that protease-dependency of ZEBOV GP is determined by the protease repertoire of the respective cell line. Endosomal cathepsins were essential for the entry of ZEBOV GP into Huh-7 cells and combined treatment with inhibitors of furin (MI-1148), cathepsins (E64d) or TMPRSS2 (BAPA or MI-432) was able to completely abolish rVSVΔG ZEBOV GP replication. In contrast, this was not the case for VeroE6 and Vero-TMPRSS2 cells, indicating that ZEBOV GP is able to use other so far unknown protease(s) for the proteolytic processing in Vero cells. Host cell protease cleavage seems to be an essential mechanism for ZEBOV GP replication, as the generation of highly truncated GP variants resulted in either still cleavable or functionally inactive GP.

Additionally the subcellular localization of the host cell protease TMPRSS2, involved in the processing of fusion proteins of many respiratory viruses, including influenza virus HA and SARS-CoV-2 S, was analyzed in Huh-7 cells. TMPRSS2 has been found to accumulate as previously described in the TGN but was furthermore found in the ERGIC and to a certain extent in the recycling and late endosome of TMPRSS2-overexpressing Huh-7 cells.

## Zusammenfassung

Die proteolytische Prozessierung viraler Fusionsproteine durch Wirtszellproteasen ist eine Voraussetzung für die Replikation und Infektiosität umhüllter Viren. Die Identifizierung der Proteasen, die an der Aktivierung beteiligt sind, ist daher ein wichtiger Schritt zur Entwicklung von Wirtszellproteaseinhibitoren als antivirale Strategien.

In dieser Studie sollten die proteolytischen Aktivierungsmechanismen der Klasse I Fusionsproteine des Zaire-Ebolavirus (ZEBOV) und des neuartigen schweren akuten respiratorischen Syndrom (SARS) Coronavirus (CoV) 2 untersucht werden. Beide Viren werden durch die proteolytische Spaltung an zwei Stellen innerhalb des Fusionsproteins aktiviert. Das Fusionsprotein S des neuen SARS-CoV-2 besitzt zwei unterschiedliche Spaltstellen, mit einem multibasischen Motiv an der S1/S2 Stelle und einem monobasischen Motiv an der S2' Stelle. Co-Expression in 293F Zellen sowie Infektionsstudien in Calu-3 Zellen in An- und Abwesenheit von Proteaseinhibitoren zeigten die proteolytische Aktivierung durch Furin und die transmembrane Serinprotease 2 (TMPRSS2). Beide Proteasen erwiesen sich als essenziell für eine effiziente Replikation von SARS-CoV-2, da sie sich nicht gegenseitig kompensieren konnten. Im Gegensatz dazu zeigten *In-vitro*-Experimente einen hochkomplexen Prozessierungsmechanismus für das ZEBOV GP jenseits der beschriebenen klassischen proteolytischen Aktivierung durch Furin und endosomales Cathepsin B und L. Es wurde gezeigt, dass die zuvor als „nicht spaltbar“ bezeichnete ZEBOV GP_AGTAA Furin-Spaltstellenmutante durch TMPRSS2 und Cathepsin L an bisher unbekannten Positionen in das 20 kDa fusionskompetente $GP_2$ gespalten werden konnte. Darüber hinaus zeigten rVSVΔG ZEBOV GP Pseudovirus-Wachstumskinetiken und Eintrittsstudien mit transkriptions- und replikatioskompetenten Virus-ähnlichen Partikeln (trVLPs) in Huh-7-, VeroE6- und Vero-TMPRSS2-Zellen in An- und Abwesenheit von Proteaseinhibitoren, dass die Proteaseabhängigkeit von ZEBOV GP je nach Proteaserepertoire der jeweiligen Zelllinie variieren kann. Endosomale Cathepsine waren hierbei essenziell für den Eintritt von ZEBOV GP in Huh-7 Zellen und eine kombinierte Behandlung mit Inhibitoren gegen Furin (MI-1148), endosomale Cathepsine (E64d) oder TMPRSS2 (BAPA oder MI-432) war in der Lage, die rVSVΔG ZEBOV GP Replikation vollständig zu inhibieren. Dies war im Gegensatz dazu bei VeroE6- und Vero-TMPRSS2 Zellen nicht der Fall, was darauf hindeutet, dass ZEBOV GP in der Lage ist, andere bisher unbekannte Protease(n) für die proteolytische Prozessierung zu verwenden. Die Spaltung durch Wirtszellproteasen scheint ein wesentlicher Mechanismus für die ZEBOV GP Replikation zu sein, da die Erzeugung stark verkürzter GP-Varianten entweder zu noch spaltbarem oder funktionell inaktivem GP führte.

Zusätzlich wurde die subzelluläre Lokalisierung der Wirtszellprotease TMPRSS2, die an der Prozessierung der Fusionsproteine vieler respiratorischer Viren, darunter Influenzavirus HA und SARS-CoV-2 S, beteiligt ist, in Huh-7-Zellen analysiert. Es konnte gezeigt werden, dass TMPRSS2 wie zuvor beschrieben im TGN akkumuliert, darüber hinaus aber auch im ERGIC und zu einem gewissen Grad im Recycling- und spätem Endosomen von TMPRSS2-überexprimierenden Huh-7 Zellen lokalisiert ist.

# 1 Introduction

## 1.1 Membrane fusion during the replication of enveloped viruses

Fusion of the viral lipid envelope and the host cell membrane is a prerequisite for enveloped viruses in order to release the viral genome into the host cell and thus essential for replication and infectivity. The membrane fusion is mediated by viral fusion proteins, which are embedded into the virus envelope (Helenius *et al.*, 1980; White *et al.*, 1980; White & Helenius, 1980; White *et al.*, 1982). Viral fusion proteins can be divided into three different classes based on the main structural component of their fusion subunit. Class I fusion proteins such as the influenza virus hemagglutinin (HA), the coronavirus (CoV) spike (S) or the Ebola virus (EBOV) glycoprotein (GP) consist of α-helices, while class II fusion proteins from flaviviruses such as Dengue virus or alphaviruses like Chikungunya virus contain largely β-sheets. In contrast, class III viral fusion proteins like the vesicular stomatitis virus (VSV) glycoprotein (G) contain both α-helix and β-sheet structures within their fusion subunits. The class I and II fusion proteins are synthesized as trimeric inactive precursors or are retained fusion incompetent in a heterodimer with another viral chaperon-like membrane protein, respectively. In order to transfer into a fusion competent state, these proteins have to be cleaved ("primed") by host cell proteases (Lazarowitz *et al.*, 1973; Scheid & Choppin, 1974; Klenk *et al.*, 1975).

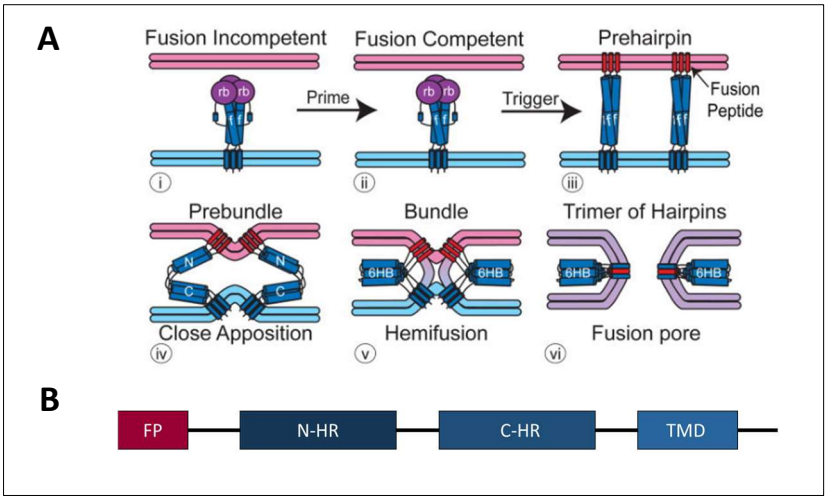


**Figure 1: Trimer-of-hairpins formation during membrane fusion.**
**A**) Fusion incompetent proteins (i) acquire their fusion competent state by proteolytic cleavage ("priming") (ii). Upon a certain trigger like low pH or co-receptor binding, the primed fusion protein inserts the fusion peptide/loop (FP) into the host cell membrane, thereby forming the prehairpin structure (iii). Profound refolding processes in which the fusion FP interacts with the transmembrane domain of the viral fusion subunit lead to the progressive formation of the fusion pore (iv-vi) (White & Whittaker, 2016). **B**) Schematic illustration of the C-terminal region of class I fusion proteins. The FP is followed by the N-terminal and C-terminal heptad repeat region (N-HR and C-HR) and the transmembrane domain (TMD). Both HR segments consist of 7 amino acids (aa) that form coiled-coiled structures that are involved in the refolding process and the formation of the trimer-of-hairpins (modified by White *et al.*, 2008; White & Whittaker, 2016).

The cleavage of the inactive precursor protein leads to the exposure of the hydrophobic fusion peptide/loop (FP) of the viral fusion protein. Induced by a triggering event, like low endosomal pH, receptor binding or both, an irreversible conformational change of the surface glycoprotein leads to the insertion of the FP into the host cell membrane (Figure 1 A, i-iii) (White *et al.*, 2008). Interestingly, the class III fusion glycoproteins of rhabdoviruses, such as Rabies virus or vesicular stomatitis virus (VSV), do not depend on proteolytic processing by host cell proteases as they are able to undergo reversible conformational changes upon a fusion trigger (Roche & Gaudin, 2002). Even though the overall structures, membrane organization and activation of the three classes of fusion proteins differ, they all share a common mechanism during virus-host membrane fusion. Crystal structures of pre- and post-fusion conformations of viral fusion proteins from class I, II and III showed that a prehairpin structure folds back into a trimer-of-hairpins form upon fusion pore formation (Figure 1 A, vi). This refolding step during membrane fusion brings the N-terminal part inserted into the host cell membrane in close proximity to the C-terminal transmembrane domain (TMD) anchored into the viral envelope thereby overcoming the barrier of hydrophobic force. Hence, the outer viral and the host membrane fuse, inducing the sequential formation of a fusion pore (Figure 1 A, iii-vi) (Kuzmin *et al.*, 2001; Lee, 2010). The key characteristics of class I fusion subunits for these folding steps are heptad repeats. They are located N-terminally (N-HR) downstream of the FP and C-terminally upstream of the TMD (C-HR) and are the basis of coiled-coil structures (Figure 1 B). During membrane fusion the N-HR folds back with a subsequent packing of the C-HR around the N-HR core, thereby bringing the two membranes close together (Weissenhorn *et al.*, 1996; Skehel & Wiley, 1998; Peisajovich & Shai, 2003). The common features of viral fusion proteins regarding fusion pathway from prehairpin to trimer-of-hairpins formation and membrane fusion dynamics are found in all three classes of fusion proteins. Nevertheless, there are still substantial differences in structure, triggering and especially, in the host cell proteases involved in the priming event even among the class I fusion proteins.

## 1.2 Viruses with class I fusion proteins

### 1.2.1 Ebola virus

The EBOV is the causative agent of the Ebola virus disease, that can lead to severe illness with hemorrhagic fever and often fatal outcome in humans and non-human primates. It belongs to the order of *Mononegavirales* and to the family of *Filoviridae* and is an enveloped virus that consists of a single-stranded RNA genome in negative orientation ((-)ssRNA). EBOV morphology

is heterogeneous, even though the mean particle diameter is 80 nm, the length of the filamentous particle can vary substantially with filaments up to 14000 nm (Feldmann & Geisbert, 2011).

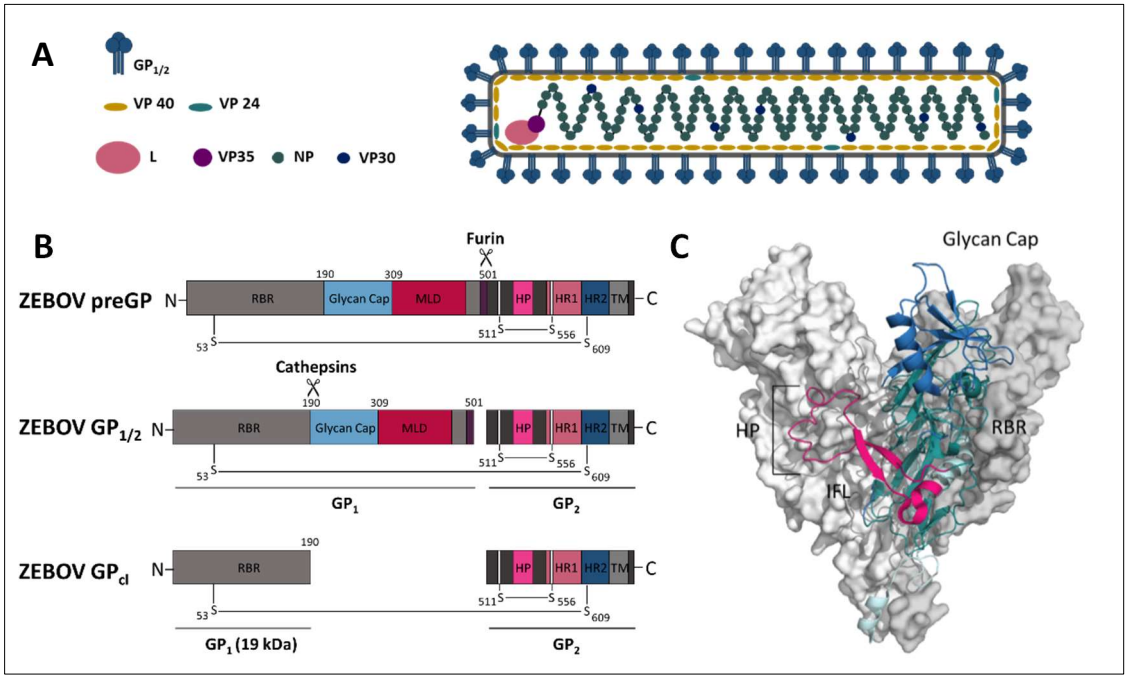


**Figure 2: Ebola virus morphology and GP priming.**
**A**) Schematic illustration of Ebolavirus particle. The trimeric surface glycoprotein (GP) is embedded into the viral membrane, while the major and minor matrix proteins (VP40 and VP24) coat the inner layer of the particle and associate with the nucleoprotein (NP), which encapsulates the viral (-)ssRNA genome. In combination with the polymerase complex consisting of the polymerase (L), VP30 and VP35 the NP-coated RNA forms the viral ribonucleoprotein (RNP) complex. **B**) Schematic protein domain structure of Zaire Ebolavirus GP. The GP is a type I transmembrane protein consisting of 676 aa. The receptor binding region (RBR) is located at the N-terminal end followed by the glycan cap and the mucin-like domain (MLD). The domains responsible for viral fusion, including the hydrophobic patch (HP) and the two heptad repeat domains (HR1 and HR2), are located at the C-terminal end of the protein. The ZEBOV GP is synthesized as an inactive precursor protein (ZEBOV preGP), that has to be proteolytically activated ("primed") in order to gain its fusion capacity. Priming of preGP is a multistep process, starting with an initial cleavage at R501 by the proprotein convertase furin, within the trans-Golgi network (TGN), into the subunits $GP_1$ and $GP_2$ (ZEBOV $GP_{1/2}$). ZEBOV $GP_{1/2}$ is then incorporated into released virus particles. After attachment and micropinocytosis at the target cell, the ZEBOV $GP_{1/2}$ is further trimmed by endosomal cysteine proteases cathepsin L and B (ZEBOV $GP_{cl}$). This leads to a loss of MLD and glycan cap domain and exposure of the RBR. **C**) Crystal structure of the trimeric GP of ZEBOV isolate Makona from 2014 (PDB: 6vkm). Monomers 1 (grey) and 2 (white) are shown in surface representation, while monomer 3 is depicted in cartoon representation. The glycan cap (blue) projects from the top of the structure covering the RBR (cyan). Underneath lies the internal fusion loop (IFL) shown in magenta, which is formed by the disulfide bond between Cys511 and Cys556. The tip of the loop contains the HP, responsible for membrane fusion (Rutten et al. 2020).

First discovered in 1976 in Central Africa, until now six species of EBOV, *Zaire ebolavirus* (ZEBOV), *Sudan ebolavirus* (SEBOV), *Taï Forest ebolavirus* (TAFV), *Reston ebolavirus* (REBOV), *Bundigugyo ebolavirus* (BDBV) and *Bombali ebolavirus* (BOMV) have been identified. The ZEBOV, SEBOV and BDBV have been associated with reoccurring outbreaks in Central and West Africa with case fatality rates ranging from 25 to 90 %, whereas for REBOV and TAFV no fatal cases have been reported so far. The largest outbreak occurring from 2014 to 2016 in West Africa (Sierra Leone, Guinea and Liberia) was caused by the ZEBOV Makona variant and led to a total of 28.652 cases with 11.325 deaths (CDC, 2019). Ebola virus disease is assumed to be a zoonotic virus infection,

which is transmitted through direct contact with virus-contaminated body fluids to open wounds or mucosal surfaces (e.g., eyes, mouth and nose). The natural reservoir and host range are not yet defined. However, recent studies showed the involvement of fruit bats in the spread of EBOV, possibly serving as the natural reservoir (Leroy *et al.*, 2005; Leendertz *et al.*, 2016).

The EBOV genome consists of 7 genes that are arranged from the 3'-leader to the 5'-trailer end in the following order: nucleoprotein (NP), phosphoprotein (VP35), major matrix protein (VP40), GP, nucleocapsid protein (VP30), minor matrix protein (VP24) and the RNA-dependent RNA polymerase (L). The encoded proteins VP30, VP35 and L together with the viral genome encapsidated by NP form the ribonucleoprotein complex. VP40 and VP24 are lined at the inner layer of the viral envelope in which the only transmembrane surface protein GP is embedded as a trimer (Figure 2 A) (Feldmann *et al.*, 1993).

### 1.2.2 Ebola virus glycoprotein (GP)

The Ebola virus GP is the sole viral surface protein that is embedded as a homotrimer into the lipid envelope of the filamentous virion. Crystal structure data revealed a chalice-like form of the GP trimer (Figure 2 C), with the $GP_2$ subunit at the base and the $GP_1$ subunit on top (Lee *et al.*, 2008). The ZEBOV GP is synthesized as a 676 amino acid (aa) inactive precursor (preGP) protein (Figure 2 B) that is proteolytically activated by furin along the secretory transport pathway within the trans-Golgi network (TGN). Furin cleaves the ZEBOV GP at the multibasic RRTRR cleavage site motif (aa 497 to 501) at position 501 (Volchkov *et al.*, 1998; Wool-Lewis & Bates, 1999). This initial processing step leads to the separation of the $GP_1$ and $GP_2$ subunits, which remain covalently linked by a disulfide bond between the C53 and C609. The cleaved $GP_{1/2}$ is transported to the host cell membrane and subsequently incorporated into newly budding filamentous particles. The $GP_2$ subunit consists of the classical class I fusion protein domain structures with the N- and C-terminal HR regions (HR1 and HR2), as well as the transmembrane domain (TM). Nevertheless, unlike most class I fusion proteins, the $GP_2$ consists of an internal fusion loop that is formed by a disulfide bridge between C511 and C556 bearing the hydrophobic patch (HP) at the tip, instead of an FP at the N-terminal end (Jeffers *et al.*, 2002; Gregory *et al.*, 2011). In its prefusion conformation, the internal fusion loop is wrapped around the GP with the hydrophobic patch packed into the nearby $GP_1$ monomer (Figure 2 C) (Lee *et al.*, 2008; Lee & Saphire, 2009). The $GP_1$ subunit harbors the receptor binding domain (RBD) that is initially masked by the heavily N- and O-glycosylated mucin-like domain (MLD) (aa 309-464) and the N-glycosylated glycan cap region (aa 228-308). Hence, ZEBOV GP is more likely to be internalized

by rather unspecific micropinocytosis than receptor-mediated endocytosis. It has been shown that ZEBOV GP attaches to the target cell by binding to C-type lectins or phosphatidyl serine (PtdSer) receptors that interact with the ZEBOV GP glycans or the PtdSer in the viral envelope, respectively (Lee & Saphire, 2009; Moller-Tank & Maury, 2015). After the internalization of EBOV GP the $GP_1$ subunit is consecutively trimmed from a 50 kDa fragment to a 19 kDa product by endosomal cathepsin B and L (CatB and CatL), with final processing at position 190 (Dube *et al.*, 2009), thereby stepwise removing the bulky MLD and glycan cap (ZEBOV $GP_{cl}$) (Chandran *et al.*, 2005; Schornberg *et al.*, 2006; Kaletsky *et al.*, 2007; Brecher *et al.*, 2012). During entry, the ZEBOV GP-containing virions are transported from the early endosome through a Rab7 GTPase-dependent manner to the late endosome and lysosome (Saeed *et al.*, 2010; Spence *et al.*, 2016). The proteolytic processing of $GP_1$ by endosomal cathepsins leads to the exposure of the RBD, which then binds to the Niemann-Pick disease, type C1 (NPC1) cholesterol transporter within the late endosome or lysosome. The endosomal receptor interaction is essential for the fusion of the filovirus and endosomal host membrane, even though receptor binding alone is not sufficient for fusion pore formation (Carette *et al.*, 2011; Côté *et al.*, 2011). Recent studies suggest the involvement of a second endosomal protein, the two-pore calcium channel 2 (TPC2). TPC2 contributes to protein trafficking within acidic compartments and has been shown to be a target for ZEBOV inhibition in cell culture infections (Grimm *et al.*, 2014; Sakurai *et al.*, 2015), with most recent live cell analysis suggesting an entry through NPC1 and TPC2 containing endolysosomes (Simmons *et al.*, 2016). Nevertheless, the exact fusion trigger and subsequent fusion mechanism have yet to be determined.

Even though the proteolytic processing of ZEBOV GP by furin and endosomal CatB and CatL was shown in several publications (Volchkov *et al.*, 1998; Wool-Lewis & Bates, 1999; Chandran *et al.*, 2005; Schornberg *et al.*, 2006; Kaletsky *et al.*, 2007; Brecher *et al.*, 2012), the necessity of host cell protease activation of ZEBOV GP has been a controversially discussed topic over the last two decades. Studies with recombinant ZEBOV possessing GP with a mutated furin cleavage site, due to substitution of the multibasic RRTRR to the non-basic AGTAA motif, showed only an initial reduction of virus replication in VeroE6 cells. Furthermore, the infectivity and virulence of these "non-cleavable" mutants were not impaired regarding the ability to infect non-human primates (Neumann *et al.*, 2002; Neumann *et al.*, 2007). Additionally, it was shown that neither *in vitro* inhibition of cathepsins nor *in vivo* knockout of CatB or CatL in mice had an adverse effect on ZEBOV replication and infectivity (Marzi *et al.*, 2012). Both groups suggested that proteolytic activation of ZEBOV GP by either furin or cathepsins is dispensable for virus replication, leaving the question whether ZEBOV GP is a unique member of the class I fusion proteins that is able to replicate independently of host cell protease activation.

### 1.2.3 Severe acute respiratory syndrome coronavirus 2 (SARS-CoV-2)

CoVs belong to the order of *Nidovirales* and to the family of *Coronaviridae*, which is divided into four genera: *Alpha-*, *Beta-*, *Gamma-* and *Deltacoronavirus* (Groot *et al.*, 2011). CoVs are able to infect a broad range of mammalian and avian hosts, including the globally circulating human CoVs (HCoVs) that mostly infect the upper respiratory tract and are associated with mild cold-like symptoms (Tyrell & Bynoe, 1965). In the last two decades, two novel CoVs were transmitted from animals to the human population causing major outbreaks. First, the severe acute respiratory syndrome (SARS)-CoV emerged in 2002 in southern China followed by the Middle Eastern respiratory syndrome (MERS)-CoV in 2012 with case fatality rates of up to 9.6 % and 36.3 %, respectively (Drosten *et al.*, 2003; CDC, 2003; Zaki *et al.*, 2012; ECDC, 2022). The 2019 newly emerged SARS-CoV-2, is the causative agent of CoV infectious disease 2019 (COVID-19), which ranges from mild respiratory symptoms to acute pneumonia. The introduction of SARS-CoV-2 into the human population has led to a worldwide pandemic with so far over 500 million cases and approximately 6 million deaths (Dong *et al.*, 2020). Sequence analysis showed that SARS-CoV-2 belongs to the genus of *Betacoronavirus* together with SARS- and MERS-CoV (Lu *et al.*, 2020; Zhou *et al.*, 2020; Zhu *et al.*, 2020).

Even though the global SARS-CoV-2 case fatality rates of approximately 1.2 % are much lower compared to other zoonotic *Betacoronavirus* members, human-to-human transmission via respiratory droplets and aerosols is more efficient in SARS-CoV-2 infections (Harrison *et al.*, 2020; van Doremalen *et al.*, 2020). The origin of the still ongoing SARS-CoV-2 pandemic could be traced to a cluster of pneumonia cases associated with a wet seafood market in the city of Wuhan in China. Although there are hints of a zoonotic spillover event from bats over an unknown intermediate host to humans, the exact initial transmission route and SARS-CoV-2 reservoir are still not clear (Zhou *et al.*, 2020).

CoVs form spherical virus particles with diameters of approximately 80 to 125 nm (Belouzard *et al.*, 2012; Haan & Rottier, 2016). The *Coronaviridae* comprise one of the largest genomes among the RNA viruses, with the SARS-CoV-2 consisting of an approximately 30 kb single-stranded genome in positive orientation ((+)ssRNA) (Khailany *et al.*, 2020). It contains 14 open reading frames, encoding for up to 16 non-structural, nine accessory and only four structural proteins. The structural proteins are the RNA-complexing nucleocapsid protein (N), the envelope-associated matrix protein (M), the envelope protein (E) as well as the entry-mediating spike (S) (Figure 3 A) (Belouzard *et al.*, 2012; Harrison *et al.*, 2020). During virus replication S, M and E are synthesized at the rough endoplasmic reticulum (ER) and further transported to the

ER-Golgi intermediate compartment (ERGIC), where virion assembly with the nucleocapsid and subsequent budding takes place (Krijnse-Locker *et al.*, 1994; Stertz *et al.*, 2007; Collins *et al.*, 2021). Thus, CoV particles are transported along the secretory pathway and released by exocytosis (Haan & Rottier, 2016).

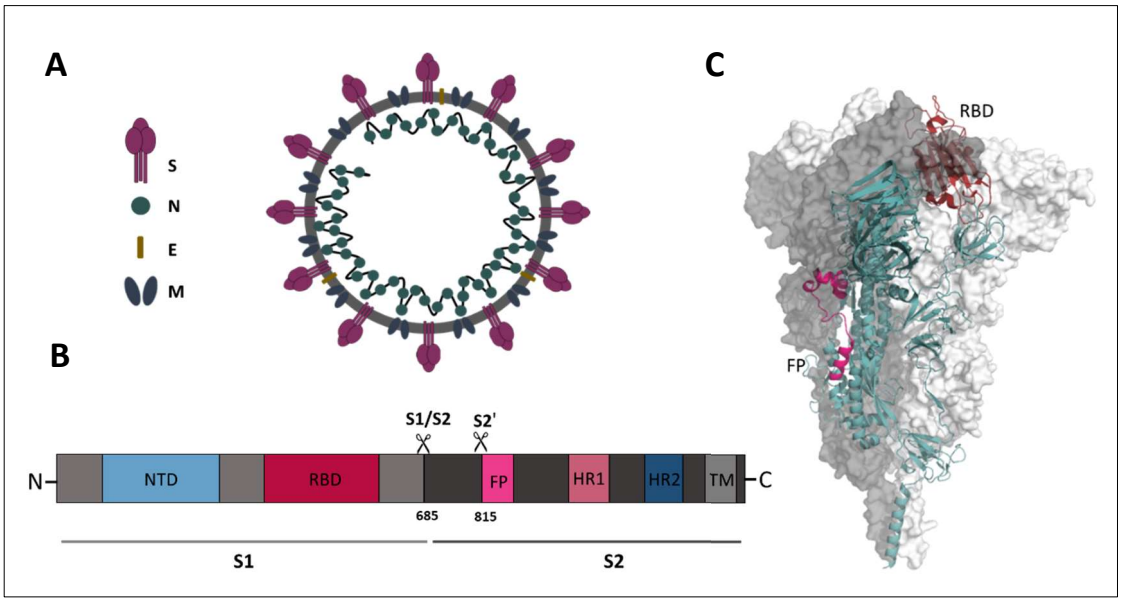


**Figure 3: SARS-CoV-2 virus morphology and spike protein.**
**A**) Schematic illustration of SARS-CoV-2 virus particle. The three major structural proteins matrix (M), envelope (E) and Spike (S) are embedded into the viral membrane, while the nucleoprotein (NP) coats the viral RNA genome. **B**) Schematic illustration of the S membrane glycoprotein. The S protein consists of 1273 aa with an N-terminal domain (NTD) followed by the receptor binding domain (RBD). In the C-terminal direction, the fusion peptide (FP) and the heptad repeat 1 and 2 (HR1 and HR2) are located in front of the transmembrane domain (TM). The S protein is synthesized as an inactive precursor protein that possesses two potential cleavage sites. The S1/S2 at aa position 685 separates the S1 (light grey) from the S2 (dark grey) subunit, whereas processing at the S2' cleavage site at aa position 815 exposes the FP within the S2 subunit. **C**) Cryogenic electron microscopy structure of S trimer (PDB_6XR8). Monomers 1 (grey) and 2 (white) are shown in surface representation, while monomer 3 is depicted in cartoon representation (cyan). The FP and the RBD within the protein structure are shown in magenta and red, respectively (Cai *et al.*, 2020).

### 1.2.4 SARS-CoV-2 spike (S)

The SARS-CoV-2 glycoprotein S is embedded as a homotrimer into the virus membrane. It protrudes in a corona-like structure from the virion that was detected in electron microscopy and gave the family of *Coronaviridae* its name (Berry & Almeida, 1968). The sole surface protein S consists of 1273 aa and is, like the EBOV GP, responsible for receptor-mediated entry and membrane fusion (Tortorici & Veesler, 2016). CoVs share an overall domain structure of their S protein with an N-terminal domain (NTD) followed by the receptor binding domain (RBD), a C-terminal FP with the subsequent two heptad repeat domains (HR1 and HR2) and a TMD (Figure 3 B). The CoV S protein belongs to the class I fusion proteins, which are synthesized as an inactive precursor. In order to gain a fusion competent state, the CoV S has to be processed by host cell

proteases (Bosch *et al.*, 2003). Proteolytic activation of CoV S protein is a multistep process requiring the cleavage of S at two distinct sites. The proteolytic cleavage at the S1/S2 site leads to the separation of the S1 and S2 subunits, which remain non-covalently bound while processing at the S2' site leads to the exposure of the FP (Figure 3 B) (Bosch *et al.*, 2008; Belouzard *et al.*, 2009; Millet & Whittaker, 2015). Cryogenic electron microscopy data show the S1 harboring RBD at the tip of the club-like S homotrimer, while the FP within the S2 subunit is located at the stem (Figure 3 C) (Kirchdoerfer *et al.*, 2016; Cai *et al.*, 2020).

Receptor binding has been shown to be a critical step for CoV entry and fusion, as the interaction with the host cell receptor initiates a conformational change that is pivotal for S to transfer into post-fusion conformation (Song *et al.*, 2018). For SARS-CoV, the cellular membrane enzyme angiotensin-converting enzyme 2 (ACE2) has been identified as host cell receptor (Li *et al.*, 2003; Li *et al.*, 2005). As phylogenetic analysis displayed clustering of SARS-CoV and SARS-CoV-2 S (Zhu *et al.*, 2021), it was suggested that the newly emerged SARS-CoV-2 might also use ACE2 as a cellular receptor, which could rapidly be verified (Hoffmann *et al.*, 2020; Lan *et al.*, 2020; Letko *et al.*, 2020; Zhou *et al.*, 2020).

Several host cell proteases have been described to proteolytically activate CoV S, including the pH-dependent endosomal CatL, proprotein convertases (PCs) like furin, as well as the trypsin-like transmembrane serine protease 2 (TMPRSS2) and human airway trypsin-like protease (HAT) (Millet & Whittaker, 2015; Hoffmann *et al.*, 2018). Nevertheless, protease specificity and spatial localization upon activation seem to differ among the CoVs (Matsuyama *et al.*, 2005; Park *et al.*, 2016). CoV members belonging to the genus *Alphacoronavirus* as well as the *Betacoronavirus* SARS-CoV, have been described to bud from the cell without S1/S2 cleavage, which implicates a subsequent activation upon cellular entry at or near the plasma membrane (Bisht *et al.*, 2004; Haan & Rottier, 2016). Following studies with SARS-CoV S revealed that pH-dependent replication by CatL cleavage in cell culture could be shifted to a pH-independent entry route by treatment of adsorbed virions with exogenous trypsin (Matsuyama *et al.*, 2005). Moreover, the respiratory epithelium serving as primary entry site for respiratory CoVs has been shown to express only insufficient levels of CatL for an efficient MERS-CoV activation (Park *et al.*, 2016). Clinical human isolates of CoV like HCoV-229E, HCoV-OC43 and HKU1 preferred activation by TMPRSS2, but are able to switch to CatL activation as an adaptation to passaging in TMPRSS2-deficient cell cultures. However, with the change to endosomal cathepsin activation human CoV lose the ability to infect human primary bronchial tracheal epithelial cells (Kawase *et al.*, 2009; Shirato *et al.*, 2017; Shirato *et al.*, 2018). This implicates an important role of TMPRSS2 in the physiological human CoV activation. Based on the data collected for the

*Betacoronaviruses* SARS- and MERS-CoV, as well as the clinical HCoVs, the so far unknown proteolytic activation of SARS-CoV-2 S by different host cell proteases should be characterized in this study.

## 1.3 Virus-activating host cell proteases

Proteolytic activation of virus fusion proteins requires processing by host cell proteases. These proteases are enzymes that are able to hydrolyze peptide bonds within a peptide or protein substrate (Barrett *et al.*, 2012). Proteolytic cleavage is an irreversible posttranslational protein interaction that was previously mainly linked to degradation processes. However, processing by enzymes plays a crucial role in the regulation of the biological function of proteins (Klein *et al.*, 2018). So far 588 human peptidases have been identified, which can be assigned to five catalytic enzyme classes with various members: 21 aspartyl, 192 metallo, 27 threonine, 164 cysteine and 184 serine proteases (Pérez-Silva *et al.*, 2016). Hence, approximately 3.1 % of the human encoded proteins are peptidases that are involved in a broad range of biological processes, including cell cycle progression, protein trafficking, cell death, immune response and cell proliferation (Deu *et al.*, 2012). Furthermore, studies over the last five decades have shown that not only cellular processes of the host organism rely on protease processing, but also enveloped viruses are able to hijack host cell proteases for the proteolytic activation of their membrane fusion proteins (1.1 and 1.2). Intact peptide bonds found in ancient human remains revealed that these bonds can be highly stable at neutral pH and moderate temperature, with a half time of over 100 years. Hence, proteolytic enzymes are needed to catalyze peptide hydrolysis (Radzicka & Wolfenden, 1996; Janko *et al.*, 2010). Overall, protease processing is able to profoundly alter the biological properties, localization and stability of proteins (Klein *et al.*, 2018). Proteolytic enzymes can further be classified based on their cleavage mode into (i) endopeptidases (EC 3.4.21-25) that target peptide bonds within a protein, (ii) amino- (EC.3.4.11-14) and (iii) carboxypeptidases (EC 3.4.15-18), which cleave up to three aa from the N- or C-terminal end, respectively, and are therefore referred to as exopeptidases.

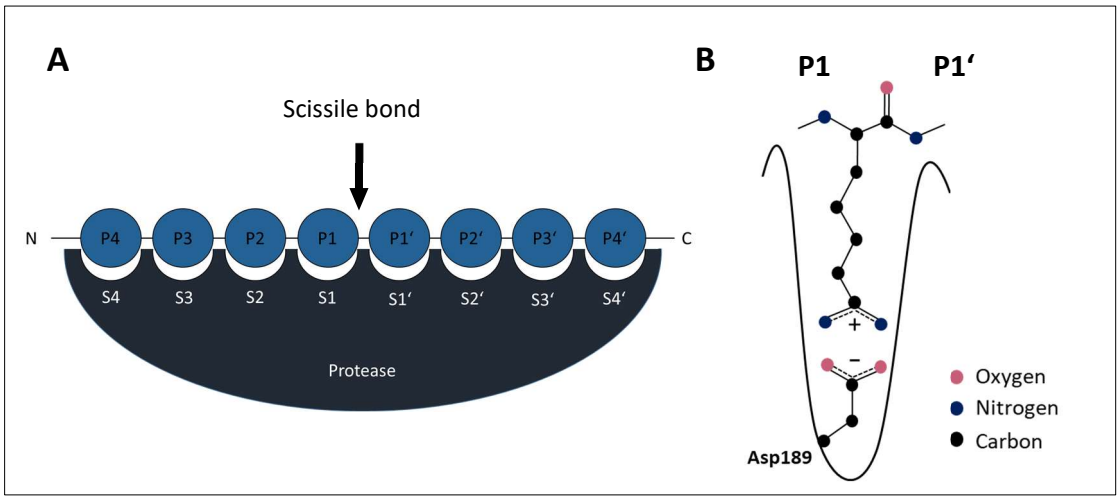


**Figure 4: Protease cleavage specificity.**
**A**) Schematic illustration of Schechter and Berger nomenclature. The letter S indicates protease binding pockets, whereas the substrate peptide residues are marked with the letter P. Peptides are cleaved at the P1-P1’ site (scissile bond). **B**) Protease substrate specificity on the example of the serine protease trypsin. The negatively charged residue of aspartate (Asp189) projects from the bottom of the trypsin S1 binding pocket, therefore non-covalently binds to basic aa like arginine (R) and lysine (K) through a salt bridge. This mechanism explains the substrate specificity of trypsin and trypsin-like serine proteases towards basic aa.

Proteases bind their substrate primarily through hydrophobic and electrostatic interaction with the substrate aa side chain residues and the enzyme binding pocket or through hydrogen bonds between the enzyme and the peptide backbone (Deu *et al.*, 2012). Subsequently, the peptide is cleaved at the catalytic site of the protease between P1 and P1' at the so-called scissile bond (Figure 4 A) (Schechter & Berger, 1967). The serine protease trypsin is a prominent example of specific substrate recognition at the catalytic site of proteases. Trypsin cleaves its peptide substrates at a single basic residue at P1, like arginine (R) or lysine (K). This specificity for positively charged aa results from a negatively charged aspartate (Asp189) side chain residue in its S1 binding pocket that non-covalently binds the substrate by forming a salt bridge (Figure 4 B). Cysteine, serine and asparagine proteases are named after the central aa side chain within their catalytic dyade or triade, which is used in the general mechanism to catalyze the peptide bond cleavage. The respective aa side chain initiates a nucleophilic attack, thereby forming a covalent acyl-enzyme intermediate stabilized by the other catalytic side chains and the oxyanion hole forming aa residues. Subsequent hydrolysis by water leads to the release of the cleaved peptide and reconstitution of the catalytic site (Deu *et al.*, 2012; Klein *et al.*, 2018).

### 1.3.1 Transmembrane serine protease 2 (TMPRSS2)

TMPRSS2 belongs to the family of the type II transmembrane serine proteases (TTSPs), whose members are transmembrane anchored proteins with a serine protease activity. TMPRSS2 was first described and cloned from the human chromosome 21 in 1997 (Paoloni-Giacobino *et al.*, 1997). The protein comprises 492 aa with an N-terminal TMD followed by a stem region with a low-density lipoprotein receptor class A domain (LDLRA) and a scavenger receptor cysteine-rich domain (SRCR) (Figure 5A). Located at the C-terminal end is the trypsin-like serine protease catalytic domain, containing the catalytic triad consisting of histidine (H), aspartic acid (D) and serine (S). Like the serine protease trypsin, TMPRSS2 recognizes substrates with monobasic aa residues in P1 position, like R or K (**R/K↓**) (Böttcher *et al.*, 2006; Lucas *et al.*, 2014). Like most proteolytic enzymes, TMPRSS2 is synthesized as an inactive precursor (zymogen) to prevent premature activity, which is autocatalytically activated at a highly conserved arginine at position R255 (Figure 5 A) (Afar *et al.*, 2001).

Human TMPRSS2 is expressed in the prostatic tissue with an androgen-dependent upregulation in patients with prostatic cancer, but could also be detected in the colon, pancreas, urogenital tract (Afar *et al.*, 2001; Vaarala *et al.*, 2001; Lucas *et al.*, 2008; Bugge *et al.*, 2009). Furthermore, TMRPSS2 expression was found in nose and epiglottis tissue of the upper respiratory tract as well as in all parts of the lower respiratory tract including the trachea, bronchi and lung (Böttcher *et al.*, 2006; Bertram *et al.*, 2012; Limburg *et al.*, 2019). The *TMPRSS2* gene has been predicted in all vertebrate genomes with several homologous variants already found in the respiratory tract of several species including mouse (Tarnow et al., 2014), swine (Peitsch et al., 2014), duck (Bestle *et al.*, 2021) and chicken (Bertram et al., 2012). The physiological role of TMPRSS2 is still not clear. Even though functional expression studies in *Xenopus laevis* oocytes showed that TMPRSS2 might contribute to the regulation of the airway surface liquid volume by decreasing the level of epithelium sodium channels (ENaC) within the human airway epithelium, recently contradicting observations have been made indicating a role of TMPRSS2 as an ENaC activator (Donaldson *et al.*, 2002; Sure *et al.*, 2022). Studies in TMPRSS2 knockout (*tmprss2*$^{-/-}$) mice displayed a reduced inflammatory response to toll-like receptor 3 stimulation, suggesting a possible involvement in the host cell's innate immune response (Iwata-Yoshikawa *et al.*, 2019). However, protease deficient mice do not show any phenotypical alterations in comparison to their wildtype littermates. Thus, indicating a functional redundancy of this serine protease or involvement in a specialized process that is not essential for the vitality of the mice (Kim et al., 2006).

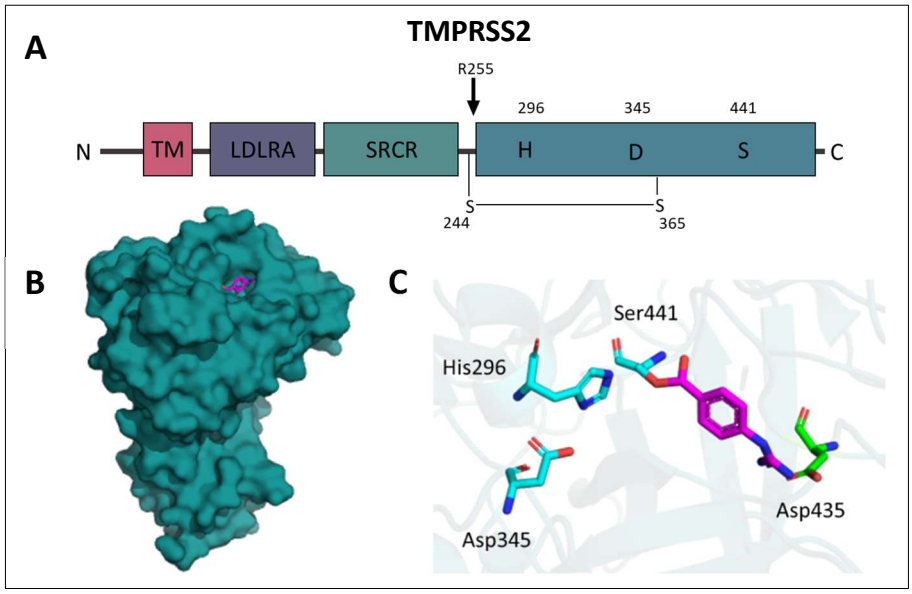


**Figure 5: Trypsin-like transmembrane serine protease 2 (TMPRSS2).**
**A**) Schematic illustration of the protein domain structure of the 492 aa human TMPRSS2, with an N-terminal transmembrane region that is followed by low-density lipoprotein receptor class A domain (LDLRA) and a scavenger receptor cysteine-rich domain (SRCR). The serine protease domain containing the catalytic triad histidine (H296), aspartic acid (D345) and serine (S441) is located at the C-terminal end. The inactive zymogen is autocatalytically activated at a single arginine at aa position R255 after which the catalytic domain is still linked to the N-terminal subunit by a disulfide bond (C244 and C365). **B**) Structure of TMPRSS2 in complex with the small molecule inhibitor nafamostat (magenta) based on the crystal structure (PDB_7MEQ). **C**) Cartoon representation of TMPRSS2 with nafamostat (carbons in magenta, oxygen in red and nitrogen in blue). The catalytic triade His296, Asp345 and Ser441 are depicted in cyan sticks, whereas the Asp435 within the S1 binding pocket is shown in green. The binding of nafamostat leads to acetylation of Ser441 (Fraser *et al.*, 2022).

The recently solved crystal structure of TMPRSS2 in complex with the serine protease inhibitor nafamostat revealed a club-like structure with a prominent confined S1 binding pocket (Figure 5 B). As TMPRSS2 is a serine protease it hydrolysis proteins by the nucleophilic attack of the substrates scissile bond by its catalytic site (Ser441), which leads to the formation of an acyl-enzyme intermediate. The Asp345 stabilizes the His296, which functions as a proton donor in the catalytic reaction. Subsequently, the substrate-enzyme intermediate is hydrolyzed by water, leading to the release of the cleaved peptide and the reconstitution of the active site residues (Klein *et al.*, 2018). A closer view of the serine peptidase domain showed the initial interaction of the inhibitor is mediated by its guanidine group with the Asp435 in the S1 binding pocket of TMPRSS2, which is typical for trypsin-like proteases (Figure 4 B). Furthermore, the structure revealed the interaction of nafamostat with the aa residues of the catalytic triade His296, Asp345 and Ser441, and here especially the acylation of Ser441 that renders the protease inactive (Figure 5 C) (Fraser *et al.*, 2022).

TMPRSS2 has been shown to play a crucial role in the processing and activation of almost all influenza A virus (IAV) subtypes in human and murine airway epithelium cells (Limburg *et al.*, 2019; Bestle *et al.*, 2021) as well as *in vivo* in mice (Hatesuer *et al.*, 2013; Sakai *et al.*, 2014; Lambertz *et al.*, 2019; Lambertz *et al.*, 2020). Furthermore, the involvement of TMPRSS2 in the

proteolytic activation of zoonotic SARS- and MERS-CoV has been described by several groups (Glowacka *et al.*, 2011; Shulla *et al.*, 2011; Park *et al.*, 2016; Iwata-Yoshikawa *et al.*, 2019).

### 1.3.2 Furin

The PC furin, also known as PACE/PCSK3, is a type I membrane protein belonging to the kex2/subtilisin-like serine protease family. It is encoded by the *fur* gene, which is located upstream of the *c-fes/fps* proto-oncogene (Roebroek *et al.*, 1986). Due to its high similarity with the Kex2p catalytic domain found in *Saccharomyces cerevisiae*, human furin was proposed to be a subtilisin-like prohormone processing endoprotease (Fuller *et al.*, 1989). Since then it has been shown that furin is a $Ca^{2+}$-dependent protease involved in the proteolytic maturation of various precursor proteins, including mammalian growth hormones, neuropeptides and receptors. Moreover, the processing of bacterial exotoxins by furin, including anthrax, diphtheria and Shiga toxin, has been described as a prerequisite for the uptake into host cells (Garten, 2018). Furthermore, animal studies revealed that furin is a vital factor in physiological fetal development as knockout of furin is lethal at day 11 of embryogenesis, with multiple defects (Scamuffa *et al.*, 2006). Nevertheless, animals with a tissue-specific conditional furin knockout have been shown to be viable with no obvious pathological alterations in the affected organ (Roebroek *et al.*, 2004).

Furin is ubiquitously expressed in eukaryotic cells and tissue, where it is synthesized as an inactive proenzyme (Figure 6A). During the transport along the secretory pathway, the prodomain is initially cleaved at position R107 (**R**A**KR**↓) within the ER in an autocatalytic reaction. The propeptide then stays associated with the protease domain, containing the catalytic triad D153, H194 and S368, until a second cleavage at position R75 (**R**GVT**KR**↓) occurs. This cleavage is a prerequisite for the transport of furin to the TGN, where the propeptide diffuses from the active protease form that is stabilized by the P domain (Leduc *et al.*, 1992; Vey *et al.*, 1994; Zhou *et al.*, 1998). Furin has been shown to accumulate within the TGN, but also cycles from there to the plasma membrane and can even be secreted in an active form after cleavage within the ectodomain at the R683 (**R**↓) (Molloy *et al.*, 1999; Plaimauer *et al.*, 2001)

PCs share a basic recognition motif R/K-$[X]_{0,2,4,6}$-R/K with any aa in the position of X (Vey *et al.*, 1992; Seidah *et al.*, 2008). Substrates of furin possess multibasic R-X-K/R-R and to a lesser extent dibasic R-X-X-R motifs, with the basic aa arginine in the P1 and P4 position (Molloy *et al.*, 1992; Vey *et al.*, 1992). These are essential for the proteolytic cleavage of the substrates, whereas a basic K or R in P2 is dispensable (Krysan *et al.*, 1999). The crystal structure of furin, together with

the substrate analog inhibitor MI-1148, shows that furin displays a club-like shape with a broad binding site with deep substrate binding pockets that fit the multibasic substrate residues (Figure 6 B). A closer view of the aa side chain residues Asp153, His194, Ser368 of the catalytic triade and the oxyanion stabilizing Asn295 reveals that MI-1148 binds non-covalently to furin and occupies its S1 binding pocket with its guanidine group in P1 position (Figure 6 C).

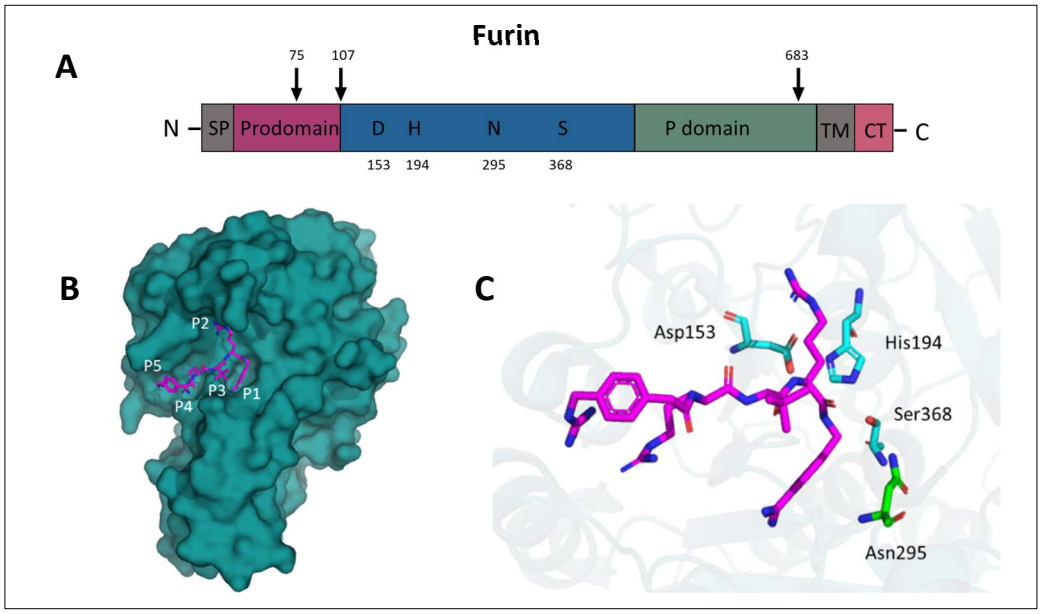


**Figure 6: Substilisin/kexin-like proproteine convertase furin.**
**A**) Protein domain structure of proprotein convertase furin (PACE/PCSK3). The type I transmembrane protein consists of an N-terminal signal peptide (SP) for the ER luminal transport as well as a prodomain which renders the protease inactive during the transport. Initial autocatalytic cleavage at aa position 107 (RAKR) within the ER is a prerequisite for the exit of ER into the Golgi. Acidic and $Ca^{2+}$ conditions in the TGN lead to a second cleavage at the aa position 70-75 (RGVTKR) within the propeptide. The catalytic domain containing the catalytic triad and oxyanion hole determining aa D (Asp153), H (His194), S (Ser368) and N (Asn295) **B**) Structure of furin in complex with substrate analog furin inhibitor MI-1148 (magenta) based on the crystal structure (PDB_4RYD). Peptide mimetic active binding site residues P1 to P4 are marked in white (Hardes et al. 2015). **C**) Cartoon representation of furin with MI-1148 (carbons in magenta, oxygen in red and nitrogen in blue). The catalytic triade aa Asp153, His194, Ser368 is shown in cyan stick representation, while the oxyanion stabilizing Asn295 is depicted in green sticks (Creemers et al. 1993).

Besides the previously mentioned eukaryotic and bacterial proproteins, that are proteolytically activated by furin there is a vast variety of viral surface glycoproteins that use furin for their priming to a fusion competent state. The first viral proteins identified to be activated by furin were the HAs of the subtypes H7 and H5 of the highly pathogenic avian influenza viruses (HPAIV) (Stieneke-Gröber *et al.*, 1992; Vey *et al.*, 1992; Garten *et al.*, 1994). Over time it has been shown that furin plays a critical role not only in the activation of surface glycoproteins of RNA viruses like influenza, measles or CoVs but also proteolytically cleaves the fusion proteins of the retrovirus HIV-1 and DNA viruses from the *Herpesviridae* family. Furthermore, is furin involved in the cleavage of viral chaperon proteins like the prM protein of *Flaviviridae* such as Yellow fever and Zika virus, therefore indirectly activating these viral fusion proteins (Garten, 2018).

### 1.3.3 Cathepsins B and L

CatB and CatL belong to the CA clan of cysteine proteases and to the papain-like family C1. Cysteine cathepsins are a large group of 11 members (cathepsin B, C, F, H, K, L, O, S, V, W, X/Z) of which the majority is ubiquitously expressed in human tissues and cell types (Rossi *et al.*, 2004; Rawlings *et al.*, 2010; Brix, 2018). They were initially described to be active under slightly reduced pH conditions in the endolysosomal compartments, where they were mainly connected with the degradation of proteins delivered through endocytosis or autophagy (Turk *et al.*, 2012). However, during the last two decades, they have been shown to play a key role in several other intra- and extracellular processes, in which they exhibit a very specific and directed proteolytic activity. Thus, contributing to various physiological processes, including MHC class-II antigen presentation, neuropeptide and hormone processing, apoptosis, cell cycle control as well as shaping of extracellular matrix proteins (Buck *et al.*, 1992; Honey & Rudensky, 2003; Funkelstein *et al.*, 2008; Brix, 2018). The endosomal CatB and CatL are expressed in a broad variety of tissues and cells. Their physiological function has been characterized in animal knockout studies. There, mice homozygote for CatL knockout (*ctsL*$^{-/-}$) show a slightly increased mortality of 16 % compared to 6 % of their wildtype littermates during the weaning period, while there is no similar phenotype in CatB knockout (*ctsB*$^{-/-}$) animals. Nevertheless, the single knockout *in vivo* models revealed an involvement of CatL in highly physiological processes like epidermal homeostasis, hair morphogenesis and MHC class II antigen presentation in the thymus. On the other hand side, CatB has been described to play a role in pathophysiological processes like TNFα-induced hepatocyte apoptosis, pancreatitis and tumor progression (Reinheckel *et al.*, 2001; Mijanović *et al.*, 2019). Animal studies with different knockout combinations revealed that CatB and CatL are able to compensate for each other, but a complete CatB and CatL depletion (*ctsB*$^{-/-}$/*L*$^{-/-}$) resulted in a lethal infant phenotype with mice succumbing to severe neuronal atrophy after two to four weeks (Felbor *et al.*, 2002).

Endosomal cathepsins are synthesized as inactive preproenzymes to avoid premature proteolytic activation (Figure 7 A). The signal peptide at the N-terminal end leads to the insertion of the newly synthesized cathepsin into the ER lumen. Here, signal peptidases remove the signal peptide resulting in the zymogen proenzyme. The still attached prodomain has two functions, as it acts as a chaperon for proper protein folding and as an inhibitor by binding to the active site during the transport from the rough ER to the TGN. Binding to cation-dependent mannose 6-phosphate receptors (CD-MPRs) in the TGN leads to sorting and transport to the endosomal compartments. The pH reduction during endosome maturation leads to the dissociation of the procathepsin from the CD-MPRs in the late endosome. Here, proteolytic processing by

asparaginyl endopeptidases or autocatalysis results in an active soluble cysteine protease (Duve & Wattiaux, 1966; Erickson *et al.*, 2013; Brix, 2018).

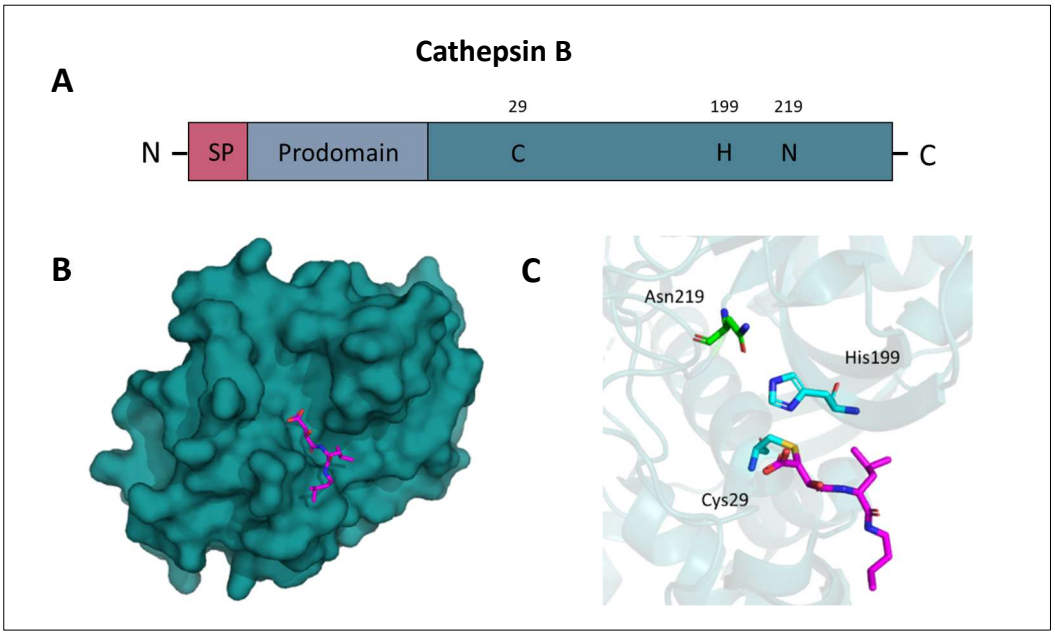


**Figure 7: Papain-like cysteine protease cathepsin B (CatB).**
**A**) Schematic illustration of the protein domain structure of cysteine proteases on the example of CatB. The preproenzyme consists of an N-terminal signal peptide (SP) that is co-transcriptionally removed by signal peptidases within the ER lumen. The inhibitory N-terminal prodomain holds the CatB in an inactive zymogen form during the transport through the TGN and endosomal compartments. Proteolytic removal of the prodomain in the late endosome leads to the releases of the C-terminal catalytic domain containing the catalytic dyade (C29 and H199) and the histidine-stabilizing aa (N219). **B**) Surface representation of bovine CatB in complex with cysteine protease inhibitor E64d based on the crystal structure (PDB_1ITO) (Yamamoto et al. 2002). **C**) Cartoon representation of bovine CatB in complex with E64d (carbons in magenta, oxygen in red and nitrogen in blue). The catalytic dyade consisting of aa Cys29 and His199 and the histidine-stabilizing Asn219 of the active enzyme domain are depicted in cyan and green sticks, respectively (Musil et al. 1991).

Active CatB and CatL display an endopeptidase activity, whereas CatB is also able to act as an exopeptidase (Brix *et al.*, 2008). Similar to serine proteases, the cysteine of the catalytic dyade initiates a nucleophilic attack at the scissile bond, leading to a covalently bound thioacyl-enzyme intermediate with the oxyanion hole stabilizing the intermediate. Subsequent, hydrolysis by water results in the release of the cleaved peptide and reconstitution of the catalytic cysteine side chain residue. As the active site thiol of cysteine is very susceptible to oxidation, these proteases are most active at a low pH and/or slightly reducing conditions (Klein *et al.*, 2018). Early studies with the cysteine protease papain revealed the recognition of seven peptide residues from S4 to S3', with further crystal structure data displaying that substrates are bound in an extended conformation (Schechter & Berger, 1967; Turk *et al.*, 1998). The crystal structure of papain family member CatB, in complex with the inhibitor E64d, displays a rather flat, long binding cleft of the protease (Figure 7 B). A closer view of the catalytic domain revealed the covalent interaction of E64d with the catalytic Cys29 near the proton donor His199 (Figure 7 C).

Endosomal CatB and CatL have a broad substrate spectrum with no clearly defined cleavage recognition sequence like it is known for furin and TMPRSS2. However, these proteases show a preference for basic (R) and bulky hydrophobic (e.g. phenylalanine, F) aa residues in the P1 position, with CatB also accepting substrates with an additional basic residue in P2 (Turk *et al.*, 2012; Rawlings & Salvesen, 2013).

For Hendra and Nipah virus it was demonstrated that CatL is responsible for the proteolytic activation of the F protein within the early and recycling endosomal compartments of Vero cells (Diederich *et al.*, 2005; Pager & Dutch, 2005). Studies with the Nipah virus in MDCK cells revealed an alternate cleavage of F by CatB (Diederich *et al.*, 2012). Moreover, endosomal CatB and CatL have also been described to be involved in the more complex sequential proteolytic activation of enveloped viruses entering the host cell through the endosomal pathway, like SARS-CoV and ZEBOV. Here, CatB and CatL act in combination with other host cell proteases, such as furin or TMPRSS2, in rather early stages of virus entry through the early or late endosomal compartments (Simmons *et al.*, 2005; Schornberg *et al.*, 2006).

## 1.4 Host cell proteases as antiviral targets

The identification and characterization of host cell proteases that activate viral surface fusion proteins not only sheds light on the activation mechanism of enveloped viruses but is a crucial step for the development of potent antiviral drugs. Antiviral therapeutics directed against viral proteins have been efficient in the treatment of HIV and hepatitis C virus over the last years. Nevertheless, the prolonged potency of antiviral therapeutics is often limited by the emergence of viral escape mutations. Especially RNA viruses, such as IAVs, display a high mutation rate due to a lack of proofreading of the viral polymerase (Sanjuán *et al.*, 2010; Richman & Nathanson, 2016). Inhibitors directed against two key proteins within the IAV life cycle, the M2 ion channel and the neuraminidase, have been clinically used as antivirals. However, the high frequency of occurring resistance mutations is a pressing issue in anti-influenza therapy (Bright *et al.*, 2005; Hussain *et al.*, 2017). Therefore, the targeting of host cell proteases is a promising approach to inhibit viral replication without applying high selective pressure on virus proteins.

Host cell proteases are well-known drug targets, with a number of inhibitors approved or in clinical trials (Steinmetzer & Hardes, 2018). Broad-spectrum serine protease inhibitors, such as the peptide mimetic BAPA and the natural peptide inhibitor aprotinin, have been shown to inhibit fusion protein activation and suppress IAV replication in cell culture (Böttcher-Friebertshäuser *et al.*, 2010; Zhirnov *et al.*, 2011; Böttcher-Friebertshäuser *et al.*, 2012).

Furthermore, a therapeutic effect in human influenza and parainfluenza virus infections could be demonstrated in aprotinin-aerosol-treated patients (Ovcharenko & Zhirnov, 1994; Zhirnov *et al.*, 1996; Zhirnov *et al.*, 2011). Even though non-selective inhibitors are able to suppress virus replication, they still possess the risk of side effects due to their indiscriminating inhibition of other host cell proteases. Hence, more selective inhibitory molecules are designed based on the growing availability of cryogenic electron microscopy and crystallographic structures of cellular proteases. The substrate analog inhibitor MI-1148 has been shown to potently inhibit the PC furin ($K_i$ 5.5 pM) resulting in a strong antiviral effect against a variety of enveloped viruses including HPAIV subtypes H5N1 and H7N1, Semliki Forest, chikungunya, West Nile, Dengue-2, mumps as well as the respiratory syncytial virus in cell culture models. Unfortunately, even though MI-1148 was not toxic in cell culture assays, it displayed substantial toxicity in rodents due to its highly basic character (van Lam van *et al.*, 2021). Therefore the less basic canavanine-based derivate MI-1851 was designed, which is a slightly less potent furin inhibitor but well tolerated in animal models (Hardes *et al.*, 2015; van Lam van *et al.*, 2021). Hence, the development of selective and non-toxic inhibitory molecules that target host cell proteases is a promising step toward new antiviral therapeutics.

## 1.5 Objectives

The fusion of virus and host cell membranes is a crucial step during the replication of enveloped viruses that allows the release of the viral genome into the host cell. Viral fusion proteins play a key role in this step, as they mediate membrane interaction and the subsequent fusion. The class I viral fusion proteins are synthesized as fusion-incompetent precursors and need to be proteolytically activated by host cell proteases to gain their fusion competent state. Activation of viral fusion proteins such as the influenza virus HA has been shown to be essential for viral infectivity and replication. Therefore, the identification and characterization of the host cell proteases involved in the proteolytic activation of enveloped viruses is an important step toward the development of specific protease inhibitors as a new antiviral strategy.

In this thesis, the proteolytic activation of two viral type I fusion proteins was investigated on protein level, as well as in the context of cell culture infection. The processing of the ZEBOV GP has been a controversial subject over the past two decades. Several publications described a sequential activation of the ZEBOV GP during the replication cycle by furin within the secretory pathway and by the endosomal cysteine proteases CatB and CatL upon cell entry. Nevertheless, unaltered replication of recombinant ZEBOV with a "non-cleavable" AGTAA mutant instead of

the multibasic RRTRR furin recognition motif in cell culture and in non-human primates as well as infection studies in CatB or CatL knockout mice raised the question whether proteolytic activation of ZEBOV GP is crucial for membrane fusion activity and virus entry. In order to address this question under BSL-2 conditions, the replication of furin-primed and -unprimed recombinant rVSVΔG ZEBOV GP should be analyzed in the presence and absence of host cell protease inhibitors in different cell lines. Moreover, the proteolytic processing of ZEBOV GP_AGTAA furin cleavage mutant should be investigated on protein level in co-expression experiments with trypsin-like serine proteases, like human TMPRSS2. The functionality of further generated ZEBOV GP cleavage mutants should be analyzed with transcription and replication-competent virus-like particles (trVLPs).

Furthermore, the viral fusion protein of the 2019 newly emerged SARS-CoV-2 should be investigated in this thesis. CoVs have been shown to be proteolytically activated at two distinct sites, the S1/S2 and the S2'site, within the surface protein S. Sequence analysis of SARS-CoV-2 revealed that this new variant possesses an unusual multibasic insertion at the S1/S2 cleavage site, suggesting a possible activation by PCs, including furin. The presence of a monobasic aa motif at the S2' site implicated the processing by a trypsin-like serine protease, like TMPRSS2 which has been shown to proteolytically process SARS-CoV and MERS-CoV. Here, the proteolytic activation of the new SARS-CoV-2 S protein should be characterized in co-expression experiments with the human TMPRSS2 in the presence and absence of furin and serine protease inhibitors. Furthermore, infection experiments under BSL-3 conditions should be performed with an early SARS-CoV-2 isolate (Munich 929) in human bronchial epithelial Calu-3 cells treated with different host cell protease inhibitors.

As IAV and CoV glycoproteins are proteolytically activated by TMPRSS2 at different cellular compartments and time points during their replication cycle, the subcellular localization of overexpressed human TMPRSS2 was of special interest. Therefore, TMPRSS2 should be transiently expressed in Huh-7 cells. The co-localization with the cellular compartment marker proteins EEA1, Rab7, ERGIC53 and TGN38 should then be analyzed in IF-staining image data using Fiji.

# 2 Material

## 2.1 Chemicals and consumptions

**Table 1: Chemicals and consumptions**

| Name | Manufacturer |
|---|---|
| 1 kb ladder | New England Biolabs, Ipswich (USA) |
| 2-Mercaptoethanol | Sigma-Aldrich, Steinheim (Germany) |
| 4',6-diamidino-2-phenylindole (DAPI) | Thermo Fisher Scientific, Waltham (USA) |
| **A**cetic acid | Merck, Darmstadt (Germany) |
| Acteone | Sigma-Aldrich, Steinheim (Germany) |
| Ammonium Persulfate (APS) | Bio-Rad Laboratories, Inc., Hercules (USA) |
| Ampicillin | Serva, Heidelberg (Germany) |
| **B**acto agar | BD Biosciences, Laagstraat (Netherlands) |
| Blasticidin | Invitrogen, Waltham (Germany) |
| Blotting paper, 0.35 mm | Hahnemühle GmbH, Dassel (Germany) |
| Bovine serum albumin (BSA) lyophilized | SERVA, Heidelberg (Germany) |
| Bromophenol blue | Sigma-Aldrich, Steinheim (Germany) |
| **C**alcium chloride ($CaCl_2$) | Merck, Darmstadt (Germany) |
| Cannula G 21 | B.Braun, Melsungen (Germany) |
| Cell culture dish (35 mm) | Greiner, Frickenhausen (Germany) |
| Cell culture flask (25 $cm^2$, 75 $cm^2$) | Greiner, Frickenhausen (Germany) |
| Cell culture plate (6, 12, 24, 96 Well) | Greiner, Frickenhausen (Germany) |
| CelLyticM | Sigma-Aldrich, Steinheim (Germany) |
| Centrifugation falcon (15 ml, 50 ml) | Greiner, Frickenhausen (Germany) |
| Collagen type I (rat tail) | Corning, Bedford (USA) |
| Cryo tubes | Sarstedt, Nümbrecht (Germany) |
| **D**imethyl sulfoxide (DMSO) | Merck, Darmstadt (Germany |
| Disodium hydrogen phosphate ($Na_2HPO_4$) | Merck, Darmstadt (Germany) |
| DL-Dithiothreitol (DTT) | Sigma-Aldrich, Steinheim (Germany) |
| DMEM/F-12 (1:1) + GlutaMAX-I | Gibco, Karlsruhe (Germany) |
| *Dulbeccos Modified Eagle`s Medium* (DMEM) 1x | Gibco, Karlsruhe (Germany) |
| **E**thanol | Sigma-Aldrich, Steinheim (Germany) |
| Ethylenediaminetetraacetic acid (EDTA) | Carl Roth, Karlsruhe (Germany) |
| **F**etal calf serum (FCS) | Life Technologies, Darmstadt (Germany) |
| Filter tips 10, 100, 1000 µl | Starlab, Hamburg (Germany) |
| **G**el Loading Dye (6x) | New England Biolabs, Ipswich (USA) |
| GelGreen Nucleic Acid Stain | Merck, Darmstadt (Germany) |
| GeneRuler 1kb Plus DNA ladder | Thermo Fisher Scientific, Waltham (USA) |
| **I**mmersion oil, liquid type F | Leica Microsystems, Wetzlar (Germany) |
| **L**-Glutamine | Life Technologies, Darmstadt (Germany) |
| Lipofectamine 2000 | Invitrogen, Waltham (Germany) |
| **M**ethanol | Honeywell, Seelze (Germany) |
| Micro plate 96-well, black | Thermo Fisher Scientific, Waltham (USA) |
| Micro plate 96-well, lumitrac white | Bio-Rad Laboratories, Inc., Hercules (USA) |
| Milk powder | Saliter, Obergünzburg (Germany) |
| **O**ptiMem | Gibco, Karlsruhe (Germany) |
| **P**age ruler | Thermo Fisher Scientific, Waltham (USA) |
| Paraformaldehyde (PFA) | Carl Roth, Karlsruhe (Germany) |
| Penicillin/Streptomycin | Life Technologies, Darmstadt (Germany) |
| Peptone | Merck, Darmstadt (Germany) |
| Petri dish, 92x16 mm | Sarstedt, Nümbrecht (Germany) |
| Polyvinylidene difluorid (PVDF) membrane | GE Healthcare, Chicago (USA) |
| Potassium chloride (KCl) | Sigma-Aldrich, Steinheim (Germany) |
| Potassium dihydrogen phosphate ($KH_2PO_4$) | Merck, Darmstadt (Germany) |
| **R**eaction tube (1,5 ml, 2 ml) | Eppendorf, Hamburg (Germany) |
| Rotiphorese Gel 30 (37,5:1) | Carl Roth, Karlsruhe (Germany) |

| | |
|---|---|
| **S**odium chloride (NaCl) | Sigma-Aldrich, Steinheim (Germany) |
| Sodium dodecyl sulfate (SDS) | Carl Roth, Karlsruhe (Germany) |
| SuperSignal West Dura Extended Duration Substrate | Thermo Fisher Scientific, Waltham (USA) |
| SuperSignal West Femto Maximum Sensitivity Substrate | Thermo Fisher Scientific, Waltham (USA) |
| Syringe 1 ml | B.Braun, Melsungen (Germany) |
| **T**etramethylethylenediamine (TEMED) | Bio-Rad Laboratories, Inc., Hercules (USA) |
| Tips 10, 100, 1000 µl | Starlab, Hamburg (Germany) |
| Tris acetate (Tris) | Carl Roth, Karlsruhe (Germany) |
| Triton-X-100 | Serva, Heidelberg (Germany) |
| Tween (20) | Sigma-Aldrich, Steinheim (Germany) |
| Tween (80) | Sigma-Aldrich, Steinheim (Germany) |
| **Y**east extract | Carl Roth, Karlsruhe (Germany) |

## 2.2 Mammalian cell culture

**Table 2: Mammalian cell lines**

| Name | Organism | Specification | Reference |
|---|---|---|---|
| 293F | *Homo sapiens* | Embryonal kidney epithelial cells | RRID: CVCL_6642 |
| Calu-3 | *Homo sapiens* | Airway epithelial cells (Adenocarcinoma) | RRID: CVCL_0609 |
| HeLa | *Homo sapiens* | Cervical epithelial cells (Adenocarcinoma) | RRID: CVCL_0030 |
| Huh-7 | *Homo sapiens* | Hepatic epithelial cells (Hepatoma) | RRID: CVCL_0336 |
| VeroE6 | *Chlorocebus sabaeus* | Kidney epithelial cells | RRID: CVCL_0574 |
| Vero-TMPRSS2 | *Chlorocebus sabaeus* | Stable expression of TMPRSS2 in VeroE6 cells | (Hoffmann *et al.*, 2020) |

**Table 3: Cell culture media**

| Name | Ingredients |
|---|---|
| Co-transfection medium (pH 7.5 or pH 4.5) | DMEM<br>1 % [v/v] Glutamine<br>1 % [v/v] Penicillin/Streptomycin<br>0.1 % [v/v] BSA |
| Culture medium (3 % DMEM +++) | DMEM<br>1 % [v/v] Glutamine<br>1 % [v/v] Penicillin/Streptomycin<br>3 % [v/v] FCS |
| Growth medium (10 % DMEM +++) | DMEM<br>1 % [v/v] Glutamine<br>1 % [v/v] Penicillin/Streptomycin<br>10 % [v/v] FCS |
| Growth medium for Calu-3 cells | DMEM/F-12 (1:1) + GlutaMAX™-I<br>1 % [v/v] Glutamine<br>1 % [v/v] Penicillin/Streptomycin<br>10 % [v/v] FCS |

| | |
|---|---|
| Infection medium (DMEM ++) | DMEM<br>1 % [v/v] Glutamine<br>1 % [v/v] Penicillin/Streptomycin<br>0 % [v/v] FCS |
| Transfection medium | OptiMem |

## 2.3 Prokaryotic cell culture

**Table 4: Bacteria strains**

| Name | Manufacturer |
|---|---|
| *Escherichia Coli*, Strain XL1-blue | Agilent Technologies, Santa Clara (USA) |
| *Escherichia Coli*, Strain DH5alpha | New England Biolabs, Ipswich (USA) |

**Table 5: Bacterial culture media**

| Name | Ingredients |
|---|---|
| Lysogeny broth (LB)-medium<br>+ Ampicillin (100 µg/ml) | 2.5 g Yeast extract<br>5.0 g Peptone<br>2.5 g Sodium chloride (NaCl)<br>ad 500 ml $dH_20$ |
| LB-agar<br>+ Ampicillin (100 µg/ml) | 2.5 g Yeast extract<br>5.0 g Peptone<br>5.0 g Sodium chloride (NaCl)<br>7.5 g Bacto agar<br>ad 500 ml $dH_20$ |

## 2.4 Viruses

**Table 6: Virus isolate**

| Name | Reference |
|---|---|
| SARS-CoV-2 isolate Munich 929 | Christian Drosten, Institute of Virology, Charité Berlin (Germany) |

**Table 7: Recombinant viruses**

| Name | Reference |
|---|---|
| rVSVΔG ZEBOV GP (Makona C7 isolate) | Institute of Virology, Marburg (Germany) |

## 2.5 Buffer and solutions

**Table 8: Buffer and solutions**

| Name | Ingredients |
|---|---|
| Cell lysis buffer | 1 % [v/v] Protease inhibitor cocktail<br>in CelLyticM |
| Immunofluorescence (IF) blocking buffer | 2 % [v/v] BSA<br>5 % [v/v] Glycerin<br>0.2 % [v/v] Tween (20)<br>in PBS |

| | |
|---|---|
| Laemmli buffer (6x) | 12 % [w/v] SDS<br>0.6 % [w/v] Bromophenol blue<br>47 % [v/v] Glycerin<br>60 mM Tris (pH6.8)<br>0.6 M DTT<br>in $dH_2O$ |
| Methanol/Acetone [1:1] | 50 % [v/v] Methanol<br>50 % [v/v] Acetone |
| Paraformaldehyde | 4 % [w/v] Paraformaldehyde<br>in PBS |
| PBS (pH 7.5) | 137 mM NaCl<br>2.7 mM KCl<br>10 mM $Na_2HPO_4$<br>1.8 mM $KH_2PO_4$<br>in $dH_2O$ |
| SDS buffer (10x) | 1 % [w/v] SDS<br>250 mM Tris<br>2 M Glycine<br>in $dH_2O$ |
| TAE buffer (50x) | 2 M Tris<br>1 M Acetic acid<br>50 mM EDTA (pH 8.0)<br>in $dH_2O$ |
| TNE buffer (autoclaved) | 1 mM EDTA (pH 8)<br>150 mM NaCl<br>10 mM Tris-HCl (pH 7.4)<br>in $dH_2O$ |
| Triton-X-100 | 0.1 % [v/v] Triton-X-100<br>in PBS |
| Western blot blocking buffer | 7 % [v/v] milk powder<br>0.1 % [v-/v] Tween (80)<br>in PBS |
| Western blot transfer buffer | 20 % Ethanol<br>48 mM Tris<br>39 mM Glycine<br>in $dH_2O$ |
| Western blot wash buffer | 0.1 % [v/v] Tween (80)<br>in PBS |

## 2.6 Antibodies

### 2.6.1 Primary Antibodies

**Table 9: Immunocytochemistry (ICC)**

| Name | Host | Dilution | Manufacturer |
|---|---|---|---|
| α-CD71 (polyclonal) | rabbit | 1:50 | Cell Signaling Technology, Danvers (USA) |
| α-EEA1 (monoclonal) | rabbit | 1:150 | Thermo Fisher Scientific, Waltham (USA) |
| α-FLAG-tag (monoclonal) | mouse | 1:50 | Sigma-Aldrich, Steinheim (Germany) |
| α-LMAN1 (monoclonal) | mouse | 1:50 | Thermo Fisher Scientific, Waltham (USA) |
| α-Rab7 (monoclonal) | rabbit | 1:50 | Abcam, Cambridge (UK) |
| α-TGN38 (serum) | rabbit | 1:200 | Institute of Virology, Marburg (Germany) |

**Table 10: Western blot analysis (WB)**

| Name | Host | Dilution | Manufacturer |
|---|---|---|---|
| α-EBOV#36 (serum) | goat | 1:20000 | Institute of Virology, Marburg (Germany) |
| α-Myc-tag (monoclonal) | mouse | 1:1000 | Cell Signaling Technology, Danvers (USA) |
| α-V5 epitope-tag (monoclonal) | rabbit | 1:1500 | Novus Biologicals, Littleton (USA) |
| α-beta actin (monoclonal) | mouse | 1:5000 | Abcam, Cambridge (UK) |

### 2.6.2 Secondary antibodies

**Table 11: HRP-conjugated antibodies (WB)**

| Name | Host | Dilution | Manufacturer |
|---|---|---|---|
| α-goat HRP-conjugated | rabbit | 1:8000 | Invitrogen, Waltham (Germany) |
| α-mouse HRP-conjugated | rabbit | 1:6000 | DAKO, Glostrup (Denmark) |
| α-rabbit HRP-conjugated | goat | 1:6000 | DAKO, Glostrup (Denmark) |

**Table 12: Fluorochrome-conjugated antibodies (IF)**

| Name | Host | Dilution | Manufacturer |
|---|---|---|---|
| α-mouse Alexa 488-conjugated | goat | 1:100/250 | Invitrogen, Waltham (Germany) |
| α-mouse Alexa 568-conjugated | goat | 1:100/250 | Institute of Virology, Marburg (Germany) |
| α-rabbit Alexa 488-conjugated | chicken | 1:100/250 | Life Technologies, Carlsbad (USA) |
| α-rabbit Alexa 568-conjugated | goat | 1:100/250 | Life Technologies, Carlsbad (USA) |

## 2.7 Oligonucleotides

All oligonucleotides were synthesized by biomers.net GmbH, Ulm (Germany).

### 2.7.1 TMPRSS2 mRNA detection primer

**Table 13: TMPRSS2 mRNA detection primer**

| Name | Sequence (5´-3´) | Reference |
|---|---|---|
| hTMPRSS2-108-fwd | CTACGAGGTGCATCC | Böttcher-Friebertshäuser et al., 2011 |
| hTMPRSS2-1336-rev | CCAGAGGCCCTCCAGCGTCACCC TGGCAA | Böttcher-Friebertshäuser et al., 2011 |

### 2.7.2 Sequencing primer

**Table 14: Sequencing primer**

| Name | Sequence (5´-3´) | Reference |
|---|---|---|
| pHW50-fwd | CTCACTATAGGGAGACCC | Institute of Virology, Marburg (Germany) |
| pHW50-rev | GAGGTATATCTTTCGCTCC | Institute of Virology, Marburg (Germany) |
| pCAGGS_std_fwd | CCTCTGCTAACCATGTTCATGC | Institute of Virology, Marburg (Germany) |
| pCAGGS_std_rev | CATATGTCCTTCCGAGTGAGAG | Institute of Virology, Marburg (Germany) |

### 2.7.3 Site-directed mutagenesis primer

The responsible nucleotides for the alanine scanning substitution are underlined.

**Table 15: Site-directed mutagenesis primer**

| Name | Sequence (5´-3´) |
|---|---|
| ZEBOV GP_AGTAA_K478A_fwd | CCAGCAGCGGGGCACTAGGCTTAATTACC |
| ZEBOV GP_AGTAA_K478A_rev | GGTAATTAAGCCTAGTGCCCCGCTGCTG |
| ZEBOV GP_AGTAA_E502A_fwd | GGGACTGCTGCCGCCGTAATTGTCAATGC |
| ZEBOV GP_AGTAA_E502A_rev | GCATTGACAATTACGGCGGCAGCAGTCCC |
| ZEBOV GP_AGTAA_V503A_fwd | GACTGCTGCCGAAGCTATTGTCAATGCTCAACC |
| ZEBOV GP_AGTAA_V503A_rev | GGTTGAGCATTGACAATAGCTTCGGCAGCAGTC |
| ZEBOV GP_AGTAA_I504A_fwd | GCTGCCGAAGTAGCTGTCAATGCTCAACCC |
| ZEBOV GP_AGTAA_I504A_rev | GGGTTGAGCATTGACAGCTACTTCGGCAGC |
| ZEBOV GP_AGTAA_V505A_fwd | GAGAAGTAATTGCAAATGCTCAACCCA |
| ZEBOV GP_AGTAA_V505A_rev | TGGGTTGAGCATTTGCAATTACTTCTC |
| ZEBOV GP_AGTAA_N506A_fwd | GAAGTAATTGTCGCTGCTCAACCCAAA |
| ZEBOV GP_AGTAA_N506A_rev | TTTGGGTTGAGCAGCGACAATTACTTC |
| ZEBOV GP_AGTAA_Q508A_fwd | GTCAATGCTGCACCCAAATGCAACC |
| ZEBOV GP_AGTAA_Q508A_rev | GGTTGCATTTGGGTGCAGCATTGAC |
| ZEBOV GP_AGTAA_P509A_fwd | GTCAATGCTCAAGCAAAATGCAACC |
| ZEBOV GP_AGTAA_P509A_rev | GGGGTTGCATTTTGCTTGAGCATTGAC |
| ZEBOV GP_AGTAA_K510A_fwd | AATTGTCAATGCTCAACCCGCATGCAACCCCAA |
| ZEBOV GP_AGTAA_K510A_rev | TTGGGGTTGCATGCGGGTTGAGCATTGACAATT |
| ZEBOV GP_AGTAA_502-505_fwd | GCAGCTAATGCTCAACCCAAATGCAACCCC |
| ZEBOV GP_AGTAA_502-505_rev | GGCAGCGGCAGCAGTCCCTGCCCC |
| ZEBOV GP_AGTAA_506-510_fwd | AGCCGCATGCAACCCCAATTTACATTAC |
| ZEBOV GP_AGTAA_506-510_rev | GCAGCTGCGACAATTACTTCGGCAGC |
| ZEBOV GP_AGTAA_H516A_fwd | CCCCAATTTAGCTTACTGGACTACTCAGG |
| ZEBOV GP_AGTAA_H516A_rev | CCTGAGTAGTCCAGTAAGCTAAATTGGGG |
| ZEBOV GP_RRTRR_V5_Δ502-510_Δ190-496_4A_fwd | GCTGCATGCAACCCCAATTTACATTAC |
| ZEBOV GP_RRTRR_V5_Δ502-510_Δ190-496_4A_rev | GGCTGCTCTTCGAGTCCTTCTAGC |
| ZEBOV GP_RRTRR_V5_Δ502-510_Δ190-496_5A_fwd | TGCAGCCTGCAACCCCAATTTACATTAC |
| ZEBOV GP_RRTRR_V5_Δ502-510_Δ190-496_5A_rev | GCGGCTGCTCTTCGAGTCCTTCTAGC |
| ZEBOV GP_RRTRR_V5_Δ502-510_Δ190-496_9A_fwd | CGCAGCCGCTGCATGCAACCCCAATTTACATTAC |
| ZEBOV GP_RRTRR_V5_Δ502-510_Δ190-496_9A_rev | GCTGCAGCGGCTGCTCTTCGAGTCCTTCTAGC |

**Table 16: Deletion primer**

| Name | Sequence (5´-3´) |
|---|---|
| ZEBOV GP_AGTAA_V5_Δ465-496 fwd | GCAGGGACTGCTGCCGAA |
| ZEBOV GP_AGTAA_V5_Δ465-496 rev | AGTGTTGTTGTTGCCAGCAGTC |
| ZEBOV GP_AGTAA_V5_Δ502-510 fwd | TGCAACCCCAATTTACATTACTGGACTACTC |
| ZEBOV GP_AGTAA_V5_Δ502-510 rev | GGCAGCAGTCCCTGCCCC |
| ZEBOV GP_AGTAA_V5_Δ465-496/502-510 fwd | AGAAGGACTCGAAGATGC |
| ZEBOV GP_AGTAA_V5_Δ465-496/502-510 rev | AGTGTTGTTGTTGCCAGC |
| ZEBOV GP_RRTRR_V5_Δ502-510 fwd | TGCAACCCCAATTTACATTAC |
| ZEBOV GP_RRTRR_V5_Δ502-510 rev | TCTTCGAGTCCTTCTCCC |
| ZEBOV GP_RRTRR_V5_Δ502-510 _Δ190-496_fwd | AGAAGGACTCGAAGATGC |
| ZEBOV GP_RRTRR_V5_Δ502-510 _Δ190-496_rev | AGCTTGGGGCAGTATCAG |
| ZEBOV GP_RRTRR_V5_Δ190-496_fwd | TGCTCAACCCAAATGCAACCCCAATTTACATTAC |
| ZEBOV GP_RRTRR_V5_Δ190-496_rev | TTGACAATTACTTCTCTTCGAGTCCTTCTAGC |
| ZEBOV GP_RRTRR_V5_Δ190-486_fwd | CTGATCACAGGCGGGAGAAGGACTCGAAGAGAAG |
| ZEBOV GP_RRTRR_V5_Δ190-486_rev | TCCTGCTACTCCAGCAGCTTGGGGCAGTATCAG |

## 2.8 Protease inhibitors

**Table 17: Protease inhibitors**

| Name | Manufacturer |
|---|---|
| MI-0001 (BAPA)<br>MI-432<br>MI-1148<br>MI-1851<br>MI-1900 | Prof. Dr. Torsten Steinmetzer, Pharmaceutical Chemistry Marburg (Germany) |
| Aprotinin | AppliChem GmbH, Darmstadt (Germany) |
| Protease inhibitor cocktail | Sigma-Aldrich, Steinheim (Germany) |
| E64d | Sigma-Aldrich, Steinheim (Germany) |

## 2.9 Plasmids

**Table 18: Plasmids**

| Name | Resistance | Origin |
|---|---|---|
| pCAGGS NP | Ampicillin | Institute of Virology, Marburg (Germany) |
| pCAGGS VP35 | Ampicillin | Institute of Virology, Marburg (Germany) |
| pCAGGS VP30 | Ampicillin | Institute of Virology, Marburg (Germany) |
| pCAGGS VP40 | Ampicillin | Institute of Virology, Marburg (Germany) |
| pCAGGS VP24 | Ampicillin | Institute of Virology, Marburg (Germany) |
| pCAGGS T7 | Ampicillin | Institute of Virology, Marburg (Germany) |
| 3E5E Renilla | Ampicillin | Institute of Virology, Marburg (Germany) |
| pGL4-Firefly | Ampicillin | Institute of Virology, Marburg (Germany) |
| pCAGGS human TMPRSS2-FLAG | Ampicillin | Institute of Virology, Marburg (Germany) |
| pCAGGS empty vector | Ampicillin | Institute of Virology, Marburg (Germany) |
| pHW2000 empty vector | Ampicillin | Institute of Virology, Marburg (Germany) |
| pCAGGS SARS-Cov-2 S-Myc-6xHis (Wuhan Hu-1) | Ampicillin | Institute of Virology, Marburg (Germany |
| pCAGGS ZEBOV GP_AGTAA-V5 | Ampicillin | Generated in master thesis (Bittel, 2019) |
| pCAGGS ZEBOV GP_AGTAA_E502A-V5 | Ampicillin | Generated in this thesis |
| pCAGGS ZEBOV GP_AGTAA_V503A-V5 | Ampicillin | Generated in this thesis |
| pCAGGS ZEBOV GP_AGTAA_I504A-V5 | Ampicillin | Generated in this thesis |

| | | |
|---|---|---|
| pCAGGS ZEBOV GP_AGTAA_V505A-V5 | Ampicillin | Generated in this thesis |
| pCAGGS ZEBOV GP_AGTAA_N506A-V5 | Ampicillin | Generated in this thesis |
| pCAGGS ZEBOV GP_AGTAA_Q508A-V5 | Ampicillin | Generated in this thesis |
| pCAGGS ZEBOV GP_AGTAA_P509A-V5 | Ampicillin | Generated in this thesis |
| pCAGGS ZEBOV GP_AGTAA_K510A-V5 | Ampicillin | Generated in master thesis (Bittel, 2019) |
| pCAGGS ZEBOV GP_AGTAA_H516A-V5 | Ampicillin | Generated in this thesis |
| pCAGGS ZEBOV GP_AGTAA_K478A-V5 | Ampicillin | Generated in this thesis |
| pCAGGS ZEBOV GP_AGTAA_502-505A-V5 | Ampicillin | Generated in this thesis |
| pCAGGS ZEBOV GP_AGTAA_506-510A-V5 | Ampicillin | Generated in this thesis |
| pCAGGS ZEBOV GP_AGTAA_Δ465-496-V5 (Δ1) | Ampicillin | Generated in this thesis |
| pCAGGS ZEBOV GP_AGTAA_Δ502-510-V5 (Δ2) | Ampicillin | Generated in this thesis |
| pCAGGS ZEBOV GP_AGTAA_Δ465-496Δ502-510-V5 (Δ1&2) | Ampicillin | Generated in this thesis |
| pCAGGS ZEBOV GP_RRTRR-V5 | Ampicillin | Generated in master thesis (Bittel, 2019) |
| pCAGGS ZEBOV GP_RRTRR_Δ190-464 Δ465-496-V5 (Δ1_Δgly/muc) | Ampicillin | Generated in this thesis |
| pCAGGS ZEBOV GP_RRTRR_Δ190-464Δ465-496Δ502-510-V5 (Δ1&2Δgly/muc) | Ampicillin | Generated in this thesis |
| pCAGGS ZEBOV GP_RRTRR_Δ190-464Δ465-496Δ502-510_4A-V5 (Δ1&2Δgly/muc_4A) | Ampicillin | Generated in this thesis |
| pCAGGS ZEBOV GP_RRTRR_Δ190-464Δ465-496Δ502-510_5A-V5 (Δ1&2Δgly/muc_5A) | Ampicillin | Generated in this thesis |
| pCAGGS ZEBOV GP_RRTRR_Δ190-464Δ465-496Δ502-510_9A-V5 (Δ1&2Δgly/muc_9A) | Ampicillin | Generated in this thesis |
| pCAGGS ZEBOV GP_RRTRR_Δ190-486-V5 | Ampicillin | Generated in this thesis |

## 2.10 Enzymes

**Table 19: Enzymes**

| Name | Manufacturer |
|---|---|
| BglII | New England Biolabs, Ipswich (USA) |
| DpnI | Thermo Fisher Scientific, Waltham (USA) |
| EndoH | New England Biolabs, Ipswich (USA) |
| NotI | New England Biolabs, Ipswich (USA) |
| PNGaseF | New England Biolabs, Ipswich (USA) |
| Recombinant human Cathepsin B | R&D Systems, Minneapolis (USA) |
| Recombinant human Cathepsin L | R&D Systems, Minneapolis (USA) |
| T4 Ligase | New England Biolabs, Ipswich (USA) |
| Thermolysin | Promega, Madison (USA) |
| Trypsin/EDTA | Gibco, Karlsruhe (Germany) |
| Trypsin/TPCK | Sigma-Aldrich, Taufkirchen (Germany) |

## 2.11 Commercially available reaction kits

**Table 20: Reaction Kits**

| Name | Manufacturer |
|---|---|
| Beetle-Juice Luciferase assay Firefly | PJK, Kleinblittersdorf (Germany) |
| Cathepsin B Activity Assay Kit | PromoCell, Heidelberg (Germany) |
| Cathepsin L Activity Assay Kit | PromoCell, Heidelberg (Germany) |
| CellTiter-Glo Luminescent Cell Viability Assay | Promega, Madison, USA |
| E.N.Z.A. Gel Extraction Kit | Omega Bio Tek, Norcross (USA) |
| E.N.Z.A. Plasmid Mini Kit | Omega Bio Tek, Norcross (USA) |
| E.Z.N.A. Transfilter Plasmid Maxi Kit | Omega Bio Tek, Norcross (USA) |
| E.Z.N.A. Cycle Pure Kit | Omega Bio Tek, Norcross (USA) |
| OneStep RT-PCR Kit | Qiagen, Hilden (Germany) |
| Pierce BCA Protein Assay Kit | Thermo Fisher Scientific, Waltham (USA) |
| Q5 Site-Directed Mutagenesis Kit | New England Biolabs, Ipswich (USA) |
| Renilla-Juice Luciferase Assay | PJK, Kleinblittersdorf (Germany) |
| RNase-Free DNase Set | Qiagen, Hilden (Germany) |
| Rneasy Mini Kit | Qiagen, Hilden (Germany) |
| QuikChange II Site-Directed Mutagenesis Kit | Agilent Technologies, Santa Clara (USA) |

## 2.12 Software and programs

**Table 21: Software and programs**

| Name | Provider |
|---|---|
| Citavi 6 | Swiss Academic Software, Wädenwil (Switzerland) |
| Fiji | Open-Source Software (ImageJ2) |
| Gen5 3.11 | Agilent (BioTek), Santa Clara (USA) |
| GraphPad PRISM 8 | GraphPad Software, San Diego (USA). |
| ImageLab 5.2 | Bio-Rad, Hercules (USA) |
| PyMOL Molecular Graphics System 2.0 | DeLano Scientific LLC, Schrödinger, New York (USA) |
| Serial Cloner 2.6.1 | Serial Basics |
| SnapGene Viewer 5.0.7 | GSL Biotech LLC, San Diego (USA) |

# 3 Methods

## 3.1 Cell culture methods

### 3.1.1 Cultivation of mammalian cell lines

Cultivation of immortalized cell lines including Huh-7, HeLa, VeroE6, Vero-TMPRSS2, Calu-3 or 293F involves regular passage in order to avoid overgrowth and cell death. The cells were cultivated in growth medium (Table 3) within 25 or 75 $cm^2$ cell culture flasks at 5 % $CO_2$ and 37 °C. The confluent cells were passaged, depending on their individual growth rate, once or twice a week with a ratio of 1:2.5 to 1:20. Therefore, the cell culture medium was discarded and the cell layer was washed once with 1.8 ml trypsin/EDTA to remove medium residues containing FCS. Subsequently, the confluent cell layer was incubated with another 1.8 ml of trypsin/EDTA, which leads to a loss of $Ca^{2+}$-dependent cell-cell contacts and a following detachment of the cell layer. After the cell layer was dissolved from the cell culture flask the reaction was stopped by the addition of 8.2 ml growth medium and a single cell suspension was generated by thorough resuspension. Finally, the cells were seeded into a new flask or cell culture plates for further cultivation in a Labotec C200 incubator at 5 % $CO_2$ and 37 °C (Labotec, Göttingen (Germany)). The Vero cells stably expressing TMPRSS2 (Vero-TMPRSS2, (Hoffmann *et al.*, 2020)) were cultivated under selective conditions in 10 % +++ DMEM containing 12 µg/ml blasticidin.

### 3.1.2 Transient expression of plasmid DNA in mammalian cell culture

'Naked'-plasmid DNA is not able to pass the cell membrane due to its negatively charged phosphate backbone. In order to introduce DNA into eukaryotic cells including HeLa, Huh-7, VeroE6, Vero-TMPRSS2 and 293F cells transfection reagents have to be used. These agents form cationic liposomes that are able to engage with the negatively charged DNA and therefore form positively charged complexes. These liposome complexes, containing plasmid DNA, can fuse with the negatively charged eukaryotic cell membrane releasing the DNA into the eukaryotic cell. The transfection leads to a transient expression of the plasmid-encoded mRNA, which is subsequently translated into the protein of interest.

The transfection experiments of viral glycoproteins were performed with Lipofectamine 2000 in 12 to 24-well cell culture plates with 0.8 µg to 1.6 µg of plasmid DNA (Table 18), respectively. For co-transfection studies with plasmid-encoded host cell proteases 15 ng or 30 ng were added

to the glycoprotein plasmid mix (1:53 ratio). Plasmid DNA and Lipofectamine 2000 (1:2.5 ratio) were separately mixed with serum free OptiMem (Table 3) and incubated for 5 min at room temperature (RT). In the next step, the plasmid DNA and Lipofectamine 2000 were mixed well and incubated at RT for an additional 20 min to form liposome complexes. The growth medium of 80 % confluent cells was discarded and fresh BSA containing co-transfection medium (Table 3) was added to the cells. The transfection mixture was then carefully added by dropping and incubated at 37 °C and 5 % $CO_2$ for 24 to 48 h.

### 3.1.3 Cell viability assay

Cell viability under protease inhibitor treatment was assessed by measuring the cellular ATP content, which indicates metabolically active cells, using the "*CellTiter-Glo luminescent cell viability assay*" (Table 20). Therefore, Calu-3 cells were grown in 96-well plates and incubated with 50 µM of protease inhibitor (aprotinin, MI-1851, MI432, MI-1900 and E64d) or 0.5 % DMSO for 72 h, untreated cells were used as control. Subsequently, the cells were incubated with 100 µl of the CellTiter-Glo reagent for 2 min on an orbital shaker in order to induce lysis of the cells. The plate was then incubated for 10 min at RT to equilibrate the luminescence signal. Afterward, 100 µl of the cellular lysates were transferred to a white 96-well lumitrac plate and luminescence was measured using a Centro LB 960 luminometer (Berthold Technologies, Bad Wildbad (Germany)). The relative luminescence of the untreated control was set to 100 % cell viability and compared to the inhibitor or DMSO treated cells.

## 3.2 Molecular biological methods

### 3.2.1 Total RNA isolation from mammalian cells

To investigate the mRNA expression of a cellular protein of interest, total RNA present in the cell was isolated. The RNA was extracted with the "*RNeasy Mini Kit*" (Table 20) according to the manufacturer's protocol, which is used to purify the RNA on a silica membrane within a spin column.

Cells of interest were cultivated in a 24-well plate until confluency. The cell layer was harvested in 1 ml phosphate buffered saline (PBS), transferred to a 1.5 ml sample tube and centrifuged for 5 min at 8000xg. The supernatant was discarded and the cellular pellet was resuspended in

600 µl RLT lysis buffer containing 6 µl $\beta$-mercaptoethanol. Subsequently, the sample was homogenized with a 1 ml syringe and a G21 cannula, using shear forces to break up the cells. The cell homogenate was centrifuged at 13000xg for 3 min to remove cellular debris. Afterward, the supernatant containing the intracellular soluble compounds was collected. The addition of 70 % ethanol facilitates the binding of the soluble RNA to the spin column membrane. To remove possible DNA contaminations the column-bound RNA was incubated for 15 min with DNase I, after several washing steps the RNA was eluted with RNase-free water and stored at -80 °C.

### 3.2.2 DNA and RNA quantification

The isolated DNA and RNA probes were quantified using the UV/Vis photometric-based NanoPhotometer NP80 (Implen, Munich (Germany)). This device allows the measurement of concentrations up to 15 000 µg/µl, without prior sample dilution. For DNA and RNA measurements, 1 µl sample volume was applied between two optical pedestals that form a liquid column. The sample concentration was calculated by photometric measurement of the absorption in the UV spectrum (260 nm wavelength).

### 3.2.3 Reverse transcription and polymerase chain reaction (PCR)

The mRNA of a certain gene of interest can be detected in total cellular RNA isolates by polymerase chain reaction (PCR), even if it is only present in low amounts. The mRNA is first transcribed by a reverse transcriptase, an RNA-dependent DNA-polymerase, into cDNA. Subsequently, the cDNA fragments can be amplified using small oligonucleotides complementary to the desired template sequence of interest. These so-called primers bind to the 3'-end of a DNA strand and serve as the transcriptional start for DNA-dependent DNA-polymerases. The most commonly used are heat-resistant polymerases, which were isolated from thermostable aquatic bacteria (e.g., *Taq* polymerase). The first step of a PCR reaction is the denaturation of the double-stranded DNA fragment under high temperatures by breaking up the hydrogen bonds of the DNA base pairs. By lowering the reaction temperature, the complementary primer oligonucleotides are able to anneal to the single-stranded DNA molecules. After the primers have bound to the cDNA template, the polymerase elongates the oligonucleotides, resulting in copied double-stranded DNA fragments. A PCR reaction contains

several cycles of these temperature changes, thereby exponentially amplifying the desired DNA fragment (Mullis *et al.*, 1986; Saiki *et al.*, 1988).

### 3.2.4 Detection of *TMPRSS2* mRNA with one-step RT-PCR

Detection of *TMPRSS2* mRNA after total RNA isolation (3.2.1) was performed in a one-step reverse transcription PCR (RT-PCR) reaction with a ProFlex PCR system cycler (Applied Biosystems, Waltham (USA)). Here, mRNA transcription by an reverse transcriptase into cDNA and amplification of the cDNA with a specific primer set for the detection of *TMPRSS2* mRNA (Table 13) are combined in a single RT-PCR reaction (Table 22).

**Table 22: One-step RT-PCR**

| Reaction mix | Quantity | Cycler program | | Cycles |
|---|---|---|---|---|
| RNA | 500 ng | 50 °C | 30 min | 1 |
| 10x buffer | 5 µl | 95 °C | 15 min | 1 |
| dNTPs | 1 µl | 94 °C | 30 sec | 35 |
| Primer rev | 1.25 µl | 60 °C | 30 sec | |
| Primer fwd | 1.25 µl | 72 °C | 1 min | |
| Enzyme mix | 1 µl | 72 °C | 10 min | 1 |
| $dH_2O$ | ad 50 µl | 4 °C | ∞ | 1 |

### 3.2.5 Site-directed mutagenesis PCR (Pfu and Q5)

For the substitution or insertion of aa into the ZEBOV GP plasmid DNA site-directed mutagenesis PCR kits were used (Table 20). Therefore, specific forward and reverse primers carrying the desired nucleotide exchanges were designed to mutate and amplify the ZEBOV GP plasmid in the pHW2000 vector (Table 15 and Table 16). For single amino acid substitution (e.g., alanine scan) the Agilent "*QuikChange II Site-Directed Mutagenesis Kit*" protocol was used (Table 23).

**Table 23: QuikChange II mutagenesis**

| Reaction mix | Quantity | Cycler program | | Cycles |
|---|---|---|---|---|
| Plasmid DNA | 50 ng | 95 °C | 30 sec | 1 |
| 5x buffer | 5 µl | 95 °C | 30 sec | 18 |
| dNTPs | 1 µl | 55 °C | 1 min | |
| Primer rev | 1.25 µl | 68 °C | 6 min | |
| Primer fwd | 1.25 µl | 4 °C | ∞ | 1 |
| *Pfu Ultra* HF DNA polymerase | 1 µl | | | |
| $dH_2O$ | ad 50 µl | | | |

In order to remove the non-mutated parental strand of the dsDNA plasmid, the complete reaction mix was digested with 1 µl DpnI for 1 h at 37 °C.

For insertions or deletions in the pHW2000 vector the NEB "*Q5 Site-Directed Mutagenesis Kit*"' was used, according to the manufacturer's protocol (Table 24). In this process, the plasmid DNA is opened for the PCR reaction, which facilitates the insertion or deletion of broad amino acid stretches with relatively short specific oligonucleotides. After the mutagenesis PCR, the linear PCR products are DpnI digested, phosphorylated and ligated in a single reaction (Table 25).

**Table 24: Q5 site-directed mutagenesis**

| Reaction mix | Quantity | Cycler program | | Cycles |
|---|---|---|---|---|
| Plasmid DNA | 25 ng | 98 °C | 30 sec | 1 |
| 2x Q5 Hot Start HF Mix | 12.5 µl | 98 °C | 10 sec | 25 |
| Primer rev | 1.25 µl | 50-72 °C | 1 min | |
| Primer fwd | 1.25 µl | 72 °C | 3 min | |
| $dH_2O$ | ad 25 µl | 72 °C | 2 min | 1 |
| | | 4 °C | ∞ | 1 |

**Table 25: Kinase, ligase and DpnI treatment (KLD)**

| Reaction mix | Quantity | Incubation |
|---|---|---|
| PCR product | 10 µl | |
| 2x KLD reaction buffer | 5 µl | 5 min at RT |
| 10x KLD enzyme mix | 1 µl | |
| $dH_2O$ | 3 µl | |

### 3.2.6 Agarose gel electrophoresis (DNA)

DNA fragments can be separated based on their length and the density of the used three-dimensional polysaccharide polymer gel matrix. The negatively charged sugar-phosphate backbone of the DNA enables the migration of DNA towards the anode within an electric field. The different DNA fragments can be visualized within the agarose gel by GelGreen (Table 1), which intercalates into the DNA and emits light after being exposed to 470 nm blue light on a transilluminator.

For the agarose gel electrophoresis, 5 µl of a DNA sample were mixed with 1 µl gel loading dye (Table 1) prior to the gel loading. A DNA marker (1 kb DNA ladder, NEB) was used for size determination of the sample fragments. The DNA separation was performed with 0.8 % agarose solved in 1x TAE-Buffer (Table 8), under the following conditions: 120 V and 200 mA for 60 min. Afterward, the DNA gel was incubated for 30 min in a GelGreen solution and documented with the ChemicDoc XRS+ Imaging Systems (Bio-Rad, Hercules (USA)). DNA fragments of interest were excised from the gel, purified with the OMEGA *"E.N.Z.A. Gel Extraction Kit"* and analyzed by sequencing (3.2.7).

### 3.2.7 DNA Sequencing

The DNA samples were sequenced by Seqlab in Göttingen with the use of the chain termination sequencing method (Sanger & Coulson, 1975). Therefore, 1.2 µg of DNA was premixed with 3 pmol primers, then $dH_2O$ was added to achieve a final volume of 15 µl.

### 3.2.8 Restriction digestion of plasmid DNA

DNA fragments can be cloned into a plasmid vector using specific restriction enzymes, which were first identified in bacteria and archaea. These enzymes are endonucleases with specific recognition motifs within nucleotide sequences, that excise viral insertions from their genomes as an antiviral mechanism. This defense mechanism can be utilized for the insertion of eukaryotic and viral DNA fragments into a bacterial vector (Morrow *et al.*, 1974).

Site-directed mutagenesis, as well as insertion and deletion PCR, were performed in the pHW2000 vector, for further experiments the DNA fragments were subcloned into the pCAGGS plasmid vector. All ZEBOV GP DNA fragments contain the recognition sequence for BglII at the 3'-end and the NotI sequence at the 5'-end. As these recognition sequences are also present in the pCAGGS expression vector, both ZEBOV GP in pHW2000 and pCAGGS were digested with NotI and BglII for 1.5 h at 37 °C (Table 26). The digestion mix was subsequently incubated for 20 min at 65 °C in order to inactivate NotI, preventing star activity. The digested insert and the remaining pHW2000 plasmid DNA were separated on a 0.8 % agarose gel and purified by gel extraction (3.2.6).

**Table 26: Restriction digestion**

| Digestion mix | Quantity |
|---|---|
| Plasmid DNA | 2 µg |
| NotI (10 U/µl) | 2 µl |
| BglII (10 U/µl) | 2 µl |
| 3.1 buffer | 5 µl |
| $dH_2O$ | ad 50 µl |

### 3.2.9 Dephosphorylation of plasmid DNA

The relegation of restriction enzyme-digested linear plasmid DNA is prevented by the removal of the phosphate groups of the free 5'-ends by the shrimp alkaline phosphatase (SAP) (Table 27).

**Table 27: SAP dephosphorylation**

| SAP reaction mix | Quantity |
|---|---|
| Digested plasmid DNA | 1 pmol DNA ends (1 µg of 3 kb plasmid) |
| 10x SAP reaction buffer | 2 µl |
| SAP (1 U/µl) | 1 µl |
| $dH_2O$ | ad 20 µl |

The SAP dephosphorylation reaction was incubated for 1 h at 37 °C with a subsequent inactivation step at 65 °C for 15 min. The dephosphorylated plasmid DNA was purified with the OMEGA "*E.Z.N.A. Cycle Pure Kit*" (Table 20), according to the manufacturer's protocol, on a silica matrix and stored at -20 °C until further use.

### 3.2.10 Ligation of insert and plasmid DNA

DNA ligases are enzymes, that are able to connect the complementary ends (sticky ends) of the digested insert and the vector fragments by catalyzing the formation of phosphodiester bonds. For the subcloning of mutated ZEBOV GP in pHW2000 into the pCAGGS expression vector, the T4 ligase was used (Table 19). To ensure efficient ligation of the insert into the plasmid vector, the insert is added in excess with a ratio of 3:1. The amount of insert used in the reaction can be calculated with the following formula:

$$Insert\ [ng] = \frac{Vektor[ng] \times Insert[bp]}{Vektor[bp]} \times Ratio\ \left[\frac{Insert}{Vektor}\right]$$

The digested and purified plasmid and insert DNA were incubated either overnight at 16 °C or for 10 min at RT (Table 28). Subsequently, *E. coli* of the DH5α-strain were transformed with 10 µl of the ligation reaction mix (3.3.1).

**Table 28: T4 ligase reaction (3:1)**

| T4 ligation mix | Quantity |
|---|---|
| T4 DNA Ligase Buffer (10x) | 2 µl |
| Vector DNA (4.7 kb) | 50 ng |
| Insert DNA (2.1 kb) | 67 ng |
| T4 Ligase | 1 µl |
| $dH_2O$ | ad 20 µl |

### 3.2.11 Immunocytochemistry (ICC) staining of cellular compartment markers and TMPRSS2

The cellular localization of proteins of interest can be investigated by immunocytochemistry staining. Human Huh-7 cells are a suitable cell line as their cell morphology is advantageous for microscopic analysis. The cells grow in an even monolayer and the prominent cytoplasmic area around the nucleus allows the detection of various cellular compartments. Proteins within the Huh-7 cells can be visualized with specific primary antibodies that bind to antigenic properties of the protein of interest. Subsequent incubation with a secondary fluorogenic-conjugated antibody enables the detection with fluorescence microscopy.

For the ICC staining, $4x10^4$ Huh-7 cells were seeded onto collagen-coated 12mm coverslips in a 24-well cell culture plate. After 24 h the cells were transfected with 600 ng of FLAG-tagged human TMPRSS2 in pCAGGS (3.1.2) in 10 % DMEM +++ and incubated at 37 °C and 5 % $CO_2$ for an additional 24 h. Subsequently, the cells were fixed either with 4 % PFA or with methanol/acetone [1:1], depending on the primary antibody, for 15 min at RT or on ice, respectively. As the methanol/acetone fixation dissolves all lipids from the cellular membrane structures, the cells were already permeabilized and therefore directly blocked in immunofluorescence (IF) blocking buffer (Table 8) for 1 to 2 h. The PFA-fixated cells were incubated with 0.1 M glycine for 10 min and in the following steps permeabilized with 0.1 % Triton-X-100 in PBS for 20 min and blocked for 1 to 2 h in IF blocking buffer. Primary antibodies for cellular compartment marker proteins EEA1 for early endosomes, Rab7 for late endosomes, the transferrin receptor CD71 for recycling endosomes, TGN38 for the TGN, ERGIC53 for the ERGIC and the FLAG-tag epitope of transiently expressed TMPRSS2 (Table 9) were incubated in IF blocking buffer for 1.5 h at RT and afterward washed five times with PBS to remove non-bound antibodies. In the following step, the Alexa-488- or Alexa-568-conjugated secondary antibodies (Table 12) were incubated for 45 min together with DAPI for a counter staining of cellular nuclei. After five washing steps in PBS, the coverslips were mounted with fluroshield onto glass slides and stored at 4 °C until IF microscopy. The Coverslips were analyzed by confocal laser scanning microscopy (CLSM Leica TCS SP5 II, Leica Microsystems, Wetzlar (Germany)) which enables the excitation of fluorophore-labeled proteins on a precise level within the Huh-7 cells. Co-localization was determined by image analysis using FIJI software and the Coloc2 program (Table 21).

### 3.2.12 SDS-PAGE and Western blot analysis

Denaturing sodium dodecyl sulfate-polyacrylamide gel electrophoresis (SDS-PAGE) can be used to separate viral and cellular proteins solemnly by their size within an electric field. Therefore, the protein quaternary structure is disrupted by the use of the reducing compound DTT, followed by a vigorous heating step dissolving the tertiary protein structure. The linearized proteins still possess their various charged side chain residues, which would affect the migration pattern within an electrical field. To give all fragments within the protein mixture an equal negative charge they are incubated with the anionic detergent SDS, which is able to attach uniformly to the protein fragments (Laemmli, 1970; Nelson, 1971). In the discontinuous gel electrophoresis, the negatively charged sample proteins are initially collected in a stacking gel layer (pH 6.8). After the transit into the separation gel (pH 8.8), the fragments are subsequently separated upon their size. In the following step, the proteins can be transferred from the polyacrylamide gel matrix onto a polyvinylidene difluoride (PVDF) membrane. As these membranes are highly hydrophobic, an initial activation step with methanol is necessary to improve the protein transfer in aqueous solutions, like the western bolt transfer buffer (Table 8). The PVDF membrane-bound proteins can then be detected and visualized with specific primary antibodies and an HRP-conjugated secondary antibody using chemiluminescent substrates (Towbin *et al.*, 1979; Burnette, 1981).

For SDS-PAGE and Western blot analysis transfected cells were harvested with PBS and centrifuged at 8000xg for 5 min at 4 °C. The supernatant was discarded and the cellular pellet was resuspended in 50 µl of lysis buffer (Table 8) and incubated for 30 min on ice. After the lysis cellular debris was removed by centrifugation at 8000xg for 5 min at 4 °C. The cellular lysate was then transferred into a fresh 1.5 ml tube and 10 µl of reducing Laemmli buffer (6x) (Table 8) were added. The samples were denaturized at 95 °C for 10 min and further subjected to an 8 % to 12 % SDS PAGE (Table 29) together with a protein standard (Table 1).

**Table 29: Polyacrylamide gels**

| **Ingredients** | **Stacking gel** | **Separation gels** | | |
|---|---|---|---|---|
| | **4.4 %** | **8 %** | **10 %** | **12 %** |
| Acrylamide:Bis-acrylamide (37.5:1) | 750 µl | 2.7 ml | 3.3 ml | 4 ml |
| Tris-HCl | 1.3 ml (pH 6.8) | 2.5 ml (pH 8.8) | 2.5 ml (pH 8.8) | 2.5 ml (pH 8.8) |
| SDS | 100 µl | 100 µl | 100 µl | 100 µl |
| TEMED | 10 µl | 10 µl | 10 µl | 10 µl |
| APS | 60 µl | 100 µl | 100 µl | 100 µl |
| $dH_2O$ | 2.9 ml | 4.6 ml | 4 ml | 3.3 ml |

Afterward, the polyacrylamide gel was placed on a PVDF membrane that was activated for 2 min in 100 % methanol and then soaked in Western blot transfer buffer (Table 8) between wet filter paper in the following order:

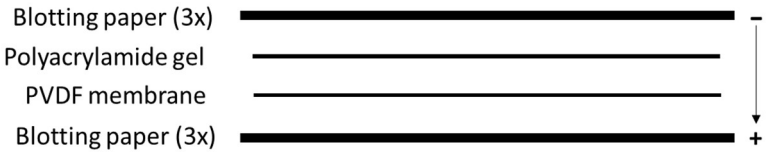


For the protein transfer the electric current was set to 2.5 mA/cm$^2$ blotting membrane for 1 h in a blotting chamber (Keutz, Reiskirchen (Germany)). The PDVF membrane was then incubated in Western blot blocking buffer (Table 8) in order to saturate the membrane and avoid unspecific antibody binding. The primary antibody (Table 10), diluted in Western blot blocking buffer, was incubated overnight at 4 °C. Afterward, the membrane was washed with 0.1 % PBS/Tween four times on a shaker. Subsequently, the HRP-conjugated secondary antibody (Table 11) directed against the host species of the primary antibody was incubated for 1 h at RT. After thorough washing steps to remove unbound antibody, the membrane was incubated with dura or femto substrate (Table 1) and documented on the ChemicDoc XRS+ Imaging Systems (Bio-Rad, Hercules (USA)).

### 3.2.13 Cleavage of transiently expressed ZEBOV GP by exogenous proteases

For the characterization of ZEBOV GP cleavage by exogenous proteases, ZEBOV GP was transiently expressed in 293F cells as described above (3.1.2) for 24 h. Subsequently, the cellular monolayer was harvested in PBS and centrifuged at 8000xg for 5 min at 4 °C. The supernatants were discarded and the remaining cell pellet was resuspended in co-transfection medium with either pH 7.2 for thermolysin or pH 4.5 for recombinant CatB or CatL (rCatB or rCatL) cleavage. The cell suspension was incubated with the 25 µg/µl of the exogenous proteases for 20 min at 37 °C. Afterward, the cells were pelleted at 8000xg for 5 min at 4 °C, then resuspended in 50 µl cell lysis buffer and incubated for 30 min on ice. The cell lysate supernatants were then prepared as described above for further SDS-PAGE and Western blot analysis (3.2.12).

### 3.2.14 EndoH and PNGaseF digestion

The location of glycosylated proteins during the secretory transport along the ER and TGN can be determined by their specific glycosylation state. Newly synthesized proteins within the ER are rich in high mannose oligosaccharides, these sugars are exchanged for more complex oligosaccharides along the transport within the TGN. For the characterization of the oligosaccharide state, and therefore indirectly the location of a protein of interest, the EndoH and PNGaseF glycosidases (Table 19) can be used. PNGaseF is able to remove almost all N-linked oligosaccharides including high mannose and complex sugars, whereas EndoH is only able to cleave high mannose oligosaccharides.

For the deglycosylation, cellular lysates, prepared for SDS-PAGE, were incubated with either PNGaseF or EndoH for 1 h at 37 °C (Table 30) and subsequently subjected to SDS-PAGE (3.2.12).

**Table 30: Deglycosylation reactions**

| EndoH | Quantity | PNGaseF | Quantity |
|---|---|---|---|
| SDS-sample | 10 µl | SDS-sample | 10 µl |
| Glycobuffer 3 | 2 µl | Glycobuffer 2 | 2 µl |
| EndoH | 2 µl | 10x NP 40 | 2 µl |
| | | PNGaseF | 1 µl |

### 3.2.15 Cathepsin L and B activity assays

Protease activity can be measured by fluorescence-based assays. Here, the substrate specificity of certain proteases is utilized by coupling the preferred amino acid cleavage site sequence with the fluorogenic 7-amino-4-trifluoromethyl-coumarin (AFC). The free fluorophore AFC is able to emit light at 505 nm wavelength when exited at 400 nm. However, AFC coupled to amide bond aa does not respond to the light excitation. Hence, only unconjugated AFC can be detected at these wavelengths after the proteolytic cleavage of the peptide amide bond.

For detection of CatL and CatB activity commercially available assay kits were used (Table 20). Therefore, T75 cell culture flasks with VeroE6, Huh-7 and Vero-TMPRSS2 cells were harvested at 100 % confluency in PBS and pelleted at 4000xg for 10 min at 4 °C. The cellular pellets were then resuspended in either CL-buffer for CatL activity or in CB-buffer for CatB activity detection, and incubated for 30 or 10 min on ice, respectively. Cellular debris was removed by centrifugation at 8000xg for 5 min at 4 °C and 25 µl cell lysate were used to determine protein concentration by BCA assay (Table 20) analysis. The total protein concentration was then adjusted to 100 µg/ml in either CL-buffer or CB-buffer. For the detection of unwanted cross-inhibition with the used inhibitory molecules, 50 µl of cell lysates were pre-incubated with protease inhibitors in

standard assay concentrations from 20 to 50 µM for 1 h on ice in a black 96-well microplate. Afterward, 50 µl of either CL-buffer containing 1 µl DTT and 1 µl of AC-FR-AFC substrate or 50 µl of CB-reaction buffer with 1 µl Ac-RR-AFC substrate were added to each well. Protease activity was then measured with the Synergy H1 fluorimeter (Agilent (BioTek), Santa Clara (USA)) in an enzyme kinetic over 2.5 h at 37 °C with measurements taken every minute after a 5 sec shaking step. CatB and CatL activity was then presented as the maximum slope (RFU/sec) within the linear range of the measurement.

## 3.3 Microbiological methods

### 3.3.1 Transformation of $CaCl_2$-competent *Escherichia coli*

The introduction of foreign DNA into bacteria is called transformation. Certain bacteria are naturally able to uptake free DNA from their environment, but the most commonly used laboratory representative *Escherichia coli* (*E. coli*) does not belong to these. Thus, the bacteria have to be pretreated, either with electroporation or chemical agents, to achieve competent organisms. In this thesis, chemically generated $CaCl_2$-competent *E. coli* were used (Cohen *et al.*, 1972; Chassy *et al.*, 1988).

For the transformation of $CaCl_2$-competent *E. coli* were thawed on ice and 500 to 1000 ng of plasmid DNA were added, followed by a heat shock at 42 °C for 1 min. Then, the bacteria were again placed on ice for 5 min, and 500 µl of ampicillin-free lysogeny broth (LB)-medium (Table 5) were transferred to the tube. The solution was incubated at 37 °C for 1 h at 400 rpm. Depending on the next step the bacteria solution was either directly transferred to 200 ml LB-medium containing 100 µg/ml ampicillin for plasmid preparation (3.3.2) or the *E. coli* were pelleted at 8000xg for 5 min and subsequently resuspended in 80 µl of LB-medium. The bacteria were then transferred to an LB-agar plate with 100 µg/ml ampicillin for colony formation. The transformed bacteria in liquid solution were incubated overnight at 37 °C on a laboratory shaker, whereas the solid agar cultures were incubated without shaking.

### 3.3.2 Preparation of plasmid DNA from *E. coli*

Plasmid DNA was isolated from *E. coli* bacteria with the OMEGA "*E.Z.N.A. Transfilter Plasmid Maxi Kit*" or "*E.N.Z.A. Plasmid Mini Kit*" (Table 20) according to the manufacturer's protocol, which are based on a modified alkaline lysis reaction (Bimboim & Doly, 1979).

The transformed bacteria overnight culture was stored on ice and centrifuged at 4000xg for 10 min at 4 °C. The bacterial pellet was resuspended in the first lysing solution containing EDTA and RNase A, which inhibits DNases and degrades the RNA, respectively. After this step, the second solution with SDS and sodium hydroxide was applied to destroy the cell membrane and denature the DNA. Subsequently, the addition of potassium acetate leads to a neutralization of the solution and precipitation of bacterial proteins. Under these conditions, the small plasmid DNA is able to renature, while the chromosomal DNA remains in the precipitate. The free plasmid DNA within the solution was then isolated by binding to a silica gel membrane under high salt conditions and eluted with 1.5 ml $dH_2O$. The plasmid DNA was stored at -20 °C until further use.

## 3.4 Virological methods

### 3.4.1 Virus titration using tissue culture infection dose 50 ($TCID_{50}$)

Virus solutions can be titrated on cell culture for the determination of the total amount of infectious viral particles. The 50 % tissue culture infectious dose ($TCID_{50}$) is an endpoint dilution assay to determine the quantity and infectivity of a virus-containing sample. The $TCID_{50}$ is defined by the virus dilution in which 50 % of the infected cell culture wells show a typical virus cytopathic effect (CPE). The corresponding virus titer can be determined by Spearman and Kärber calculations (Hierholzer & Killington, 1996).

Prior to the virus dilution assay VeroE6 cells were seeded into 96-well cell culture plates with a density of 1:5 within 100 µl of culture medium with 3 % FCS (Table 3) until 70 % confluency. Serial dilutions from $10^{-1}$ to $10^{-6}$ were generated in FCS-free infection medium in quadruplicates within a 96-well plate. From each dilution, 100 µl were transferred to the 96-well cell culture plate and incubated for 72 h at 37 °C and 5 % $CO_2$. Three days after the inoculation the last dilution value, in which 50 % of the VeroE6 cells show CPE is assessed and the viral titers are calculated.

### 3.4.2 Virus stock generation of rVSVΔG ZEBOV $GP_{1/2}$ and rVSVΔG ZEBOV $GP_0$ in Huh-7

The ZEBOV GP-dependent virus replication can be studied under BSL-2 conditions using recombinant VSV-based pseudoviruses. Here, the surface glycoprotein G of VSV is deleted from the viral genome and substituted with the GP of ZEBOV (Makona C7). The generated VSV particles bearing ZEBOV GP (rVSVΔG ZEBOV GP) on their surface can be used for infection studies.

For the propagation of rVSVΔG ZEBOV GP, Huh-7 cells were grown to 70 % confluency in 10 % +++ DMEM. The cellular monolayer was washed with ++ DMEM and inoculated with rVSVΔG ZEBOV GP (Table 7) at a low multiplicity of infection (MOI) of 0.001 for 1 h at 37 °C and 5 % $CO_2$. After the infection, the inoculum was discarded and the monolayer was washed four times with PBS to remove non-attached and defective viral particles. Subsequently, fresh 10 ml of 10 % +++ DMEM were added to the culture flask and the cells were further incubated for 24 h (>50 % CPE) at 37 °C and 5 % $CO_2$. For the generation of rVSVΔG ZEBOV $GP_0$ expressing uncleaved GP surface protein, Huh-7 cells were infected at a MOI of 0.5 as described above and further incubated in 10 % DMEM containing 30 µM MI-1148 for 24 h before the virus stock was harvested. Virus containing medium was transferred to a 15 ml falcon and centrifuged at 2500 rpm for 10 min to remove cellular debris from the virus solution. Afterward, the virus stock preparation was divided into 300 µl aliquots and stored at -80 °C.

### 3.4.3 Multicycle replication of SARS-CoV-2 in Calu-3 cells

Calu-3 cells were cultivated to 90 % confluency in a 12-well cell culture plate in Calu-3 growth medium (Table 3). Prior to the SARS-CoV-2 infection experiments in the BSL-3 facility, the cell layer was washed with PBS and 500 µl serum-free ++ DMEM were added for the transport. Inside the BSL-3 facility, the medium was carefully discarded and the cellular monolayer was infected at a low MOI of 0.001 with SARS-CoV-2 Munich isolate 929 (Table 6) in ++ DMEM for 1.5 h at 37°C and 5 % $CO_2$. After the inoculation, the cells were washed twice with PBS to remove non-attached and defective viral particles. Subsequently, 1.8 ml of fresh 3 % +++ DMEM with or without protease inhibitor were added and incubated for 72 h at 37 °C and 5 % $CO_2$. At 16, 24, 48 and 72 h postinfection (p.i.), 180 µl of cellular supernatants were collected and frozen at -70 °C. The viral titers were determined by $TCID_{50}$ titration (3.4.1).

### 3.4.4 Multicycle replication of rVSVΔG ZEBOV GP in Huh-7, VeroE6 and Vero-TMPRSS2 cells

Multicycle replication experiments with rVSVΔG ZEBOV GP were performed in Huh-7, VeroE6 and Vero-TMPRSS2 cells, which were cultivated to 70 % confluency in a 12-well cell culture plate in 10 % +++ DMEM. Prior to the rVSVΔG ZEBOV GP infection, the growth medium was removed and the cells were pre-incubated with or without protease inhibitor in 3 % +++ DMEM for 1 h at 37 °C and 5 % CO2. Afterward, the inhibitor solution was removed and the cells were washed twice with PBS to clear them from inhibitor residues. In the following step, the cellular monolayer was inoculated with rVSVΔG ZEBOV $GP_{1/2}$ or rVSVΔG ZEBOV $GP_0$ at a low MOI of 0.005 for Huh-7 and VeroE6 cells or 0.0005 for Vero-TMPRSS2 cells and incubated for 1 h at 37 °C and 5 % CO2. Next, the inoculum was discarded and the cells were washed four times with PBS to remove non-attached and defective viral particles. Subsequently, 1 ml of the 3 % +++ DMEM with or without protease inhibitor was again added and incubated for 72 h at 37 °C and 5 % CO2. At 16, 24, 48 and 72 h after the infection, 100 µl of cellular supernatants were collected and frozen at -80 °C. The viral titers were determined by $TCID_{50}$ titration (3.4.1).

### 3.4.5 Reverse genetics system for transcription and replication-competent virus-like particles (trVLP)

Replication and transcription studies of BSL-4 classified viruses as the ZEBOV under BSL-2 conditions can be performed with a reverse genetic system for transcription and replication-competent virus-like particles (trVLPs). Here, the ZEBOV genome is exchanged with a luciferase reporter-containing minigenome (Mühlberger *et al.*, 1998; Hoenen *et al.*, 2006; Hoenen & Feldmann, 2014). The monocistronic minigenome reporter plasmid consists of the luciferase genome and the non-coding regions of the 3'-end of the NP gene and the 5'-region of the L gene. These leader and trailer regions contain all necessary signals for the polymerase complex to start replication and transcription. In p0 producer cells the initial minigenome plasmid is transcribed by the T7 polymerase. Afterward, the transiently expressed proteins belonging to the RNP complex (NP, VP35, L & VP30) use this template for luciferase-reporter mRNA transcription and replication. The additional expression of VP24, VP40 and GP proteins leads to the formation and budding of trVLPs, which contain the minigenome-RNP complex. The protein of interest GP is embedded into the particle membrane. Subsequent infection of NP,

VP35, VP30 and L pre-transfected p1 cells leads to minigenome replication as well as primary and secondary luciferase-reporter gene transcription (Figure 8).

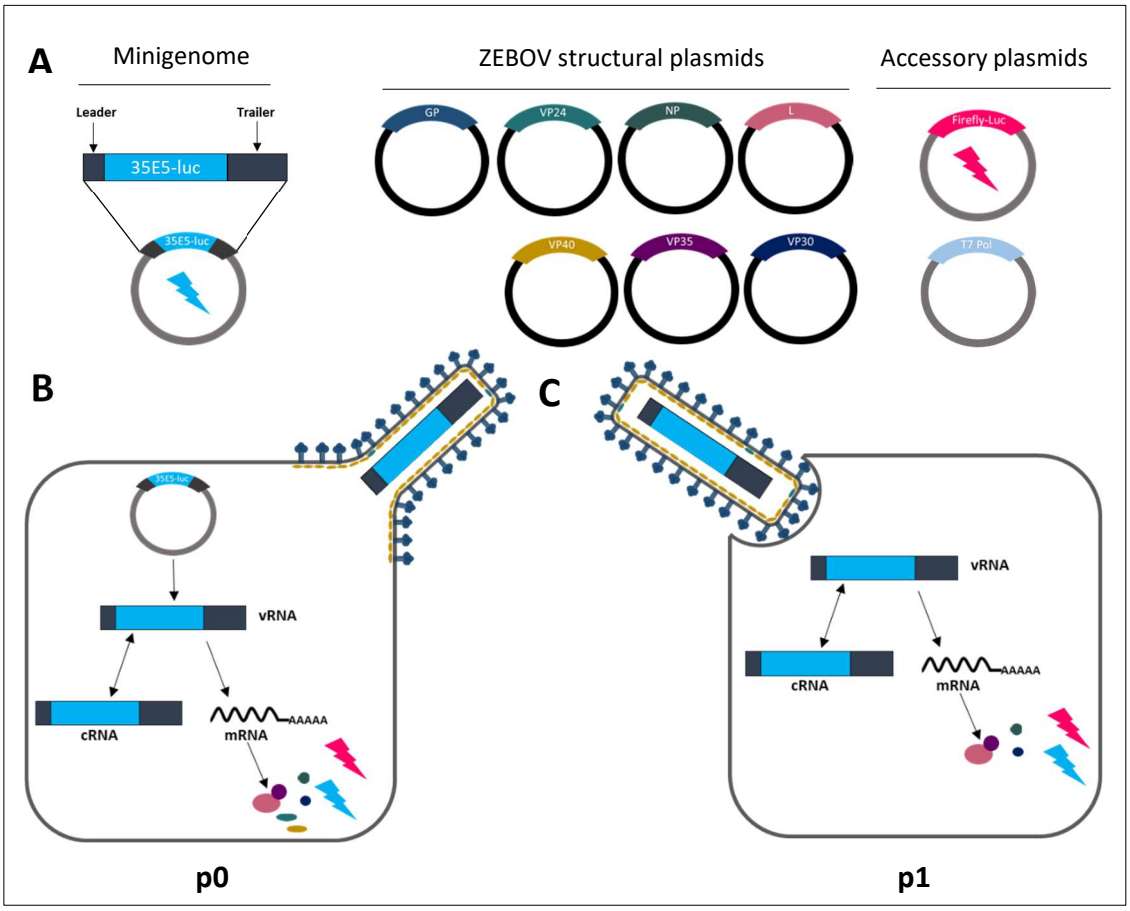


**Figure 8: Schematic illustration of trVLP assay.**
**A**) Plasmid system for the production of trVLPs. The monocistronic minigenome E3E5 consists of the renilla luciferase with the non-coding leader and trailer regions responsible for replication and transcription. Structural ZEBOV plasmids encoding for VP23, VP30, V35, VP40, NP, L and GP as well as the accessory plasmids coding for the T7 polymerase and the firefly luciferase are used. **B**) Production of trVLP in p0 (239F) cells. Transfection of p0 cells with the T7 polymerase and the E3E5 reporter minigenome leads to transcription of negative-stranded vRNA, which is used by the RNP complex proteins (VP30, VP35, NP and L) as a template for transcription of mRNA and genome replication. Additional expression of VP24, VP 40 and GP leads to the formation of trVLPs at the plasma membrane. Transcription of minigenome vRNA can be detected by luciferase assay, here co-expression of firefly luciferase is used for normalization. **C**) Pre-transfected p1 cells, expressing the RNP complex proteins VP30, VP35, NP and L are infected with trVLPs. Here, minigenome reporter activity represents on the one hand site primary transcription that reflects genome replication in p0 cells and on the other hand site secondary transcription of the luciferase reporter gene in the p1 cells. Co-expression of firefly luciferase is used for normalization.

For the trVLP generation, 293F cells were grown to a confluency of 60 % in a 6-well cell culture plate. The cells were then transfected (3.1.2) with different amounts of plasmid DNA (Table 31) to ensure efficient trVLP production. The total plasmid DNA was transfected with Lipofectamine 2000 (ratio of 1:3) in 1.8 ml 3 % +++ DMEM and incubated for 72 h at 37 °C and 5 % $CO_2$ to facilitate sufficient trVLP generation and release to the cell culture medium (Figure 8 A & B).

**Table 31: trVLP transfection plasmids**

| Plasmid | Quantity [ng] |
|---|---|
| pCAGGS NP | 125 |
| pCAGGS VP35 | 125 |
| pCAGGS VP30 | 100 |
| pCAGGS L or empty vector | 1000 |
| pCAGGS VP40 | 250 |
| pCAGGS VP24 | 30 |
| pCAGGS T7 | 250 |
| 3E5E Renilla | 250 |
| pGL4-Firefly | 100 |
| pCAGGS GP | 250 |

The trVLP containing supernatants were harvested and centrifuged at 2500 rpm for 10 min at 4 °C to remove cellular debris. For further concentration of trVLPs the cleared supernatant was carefully loaded onto a 1ml or 2 ml sucrose cushion (20 % sucrose in TNE buffer) in an SW41 or SW60 ultracentrifugation tube, respectively. The trVLPs were then centrifuged for 2 h at 40.000 rpm and 4°C in an Optima L-80XT ultracentrifuge (Beckman Coulter, Krefeld (Germany)) to form a solid particle pellet. Subsequently, the supernatant was discarded and the trVLP pellet was resuspended in 100 µl PBS and stored on ice until the infection of Huh-7, VeroE6 or Vero-TMPRSS2 cells. For expression control 20 µl trVLP suspension were subjected to SDS-PAGE and Western blot analysis.

### 3.4.6 Infection of Huh-7, VeroE6 and Vero-TMPRSS2 cells with trVLP

Pre-transfection of the p1 cells with the ZEBOV plasmids forming the RNP complex for 24 h prior to the trVLP infection increases the detected luciferase reporter gene activity. The RNP complex induces an additional secondary minigenome transcription, therefore leading to a higher luciferase reporter expression (Figure 8 C).

The p1 Huh-7, VeroE6 and Vero-TMPRSS2 cells were pre-transfected with VP30, VP35, NP and L plasmids as described above (3.4.5) upon seeding in a 6-well cell culture plate. The cells were grown to a confluency of 80 % and the cellular supernatant was removed. The p1 cells were then inoculated with 80 µl of the concentrated trVLP in PBS (3.4.5) mixed with 520 µl of ++DMEM for 2 h at 37 °C and 5 % $CO_2$ while the plate was carefully rotated every 30 min to ensure proper distribution on the cellular monolayer. Afterward, 3.5 ml of 3 % +++ DMEM were added and further incubated for 72 h at 37 °C and 5 % $CO_2$. Renilla and firefly reporter gene expression was measured with commercially available luciferase kits (3.4.7).

### 3.4.7 Reporter gene activity detection with luciferase assay

Reporter gene activity in trVLP producing p0 and trVLP infected p1 cells was detected by luciferase assays. Therefore, the cell medium was removed and the cellular monolayer was washed once with PBS. Afterward, the cells were harvested in 1 ml PBS and centrifuged at 8000 rpm for 5 min at 4 °C. The supernatant was discarded and the cell pellet was resuspended in 100 µl lysis buffer and incubated for 30 min on ice. Subsequently, the cell lysate was centrifuged at a high speed of 13 000 rpm for 5 min and 4 °C to remove cellular debris. For the luciferase assay, 30 µl of the cell lysate were transferred into a white 96-well lumitrac plate. Renilla and firefly reporter gene expression was measured with commercially available luciferase kits (Table 20) and detected with the Centro LB 960 luminometer (Berthold, Bad Wildbad (Germany)). In order to control the inter-sample variation of the detected renilla luminescence signal during trVLP generation and trVLP infection of pre-transfected p1 cells, due to varying transfection efficiency, a firefly luciferase in the pGL4 vector was co-transfected as an internal control. The assay renilla signal was subsequently normalized against the renilla control signal by calculating the (renilla:firefly) ratio.

# 4 Results

Proteolytic activation of viral fusion proteins by host cell proteases is a prerequisite for the replication of most enveloped viruses, as it enables the fusion of the virus and host cell membranes and subsequently results in genome release. Several studies have shown that virus-activating host cell proteases are promising antiviral drug targets (Helenius *et al.*, 1980; White *et al.*, 1982; Steinmetzer & Hardes, 2018). Therefore, the identification and characterization of proteolytic processing of fusion proteins from existing and newly emerging viruses are fundamental for the development of antiviral drugs and pandemic preparedness. In this study, the proteolytic activation mechanisms of the ZEBOV GP and the novel SARS-CoV-2 S should be addressed.

## 4.1 Characterization of ZEBOV GP by host cell proteases

### 4.1.1 Inhibition of furin by MI-1148 prevents cleavage of ZEBOV preGP

The ZEBOV surface fusion protein GP possesses the multibasic RRTRR sequence at position 497 to 501, with basic aa in P1, P2 and P4 being a classical recognition motif for the PC furin (Molloy *et al.*, 1992; Vey *et al.*, 1992). Previous studies showed a proteolytic cleavage of ZEBOV GP at aa position R501 by furin (Volchkov *et al.*, 1998; Wool-Lewis & Bates, 1999). The inhibitor MI-1148 has been described as a potent substrate analog furin inhibitor with a $K_i$ value of 5.5 pM. Proteolytic activation of HPAIV possessing multibasic cleavage sites by furin was efficiently inhibited by MI-1148 treatment (Hardes *et al.*, 2015). Therefore, the effect of MI-1148 on the processing of transiently expressed ZEBOV GP should be investigated. In order to characterize the cleavage of ZEBOV GP by endogenous furin, 293F cells were transfected with a pCAGGS plasmid encoding for the GP of the 2014 emerged Makona C7 ZEBOV isolate in the presence and absence of the furin inhibitor MI-1148 for 24 h (3.1.2). Subsequently, the cells were harvested and the samples subjected to SDS-PAGE and further analyzed by Western blotting using an EBOV-specific serum (EBOV#36). For further determination of the GP glycosylation state, samples were digested with either EndoH or PNGaseF for 1 h at 37 °C (3.2.14).

Western blot analysis of the GP-transfected 293F cells revealed two distinct bands at 140 kDa and 120 kDa (Figure 9 A, first lane). Both bands were sensitive to PNGaseF digestion resulting in a 110 kDa and a 90 kDa deglycosylated product, respectively (Figure 9 A, second lane). In contrast to that, only the smaller 120 kDa band was sensitive to EndoH treatment, reducing the band size to a 90 kDa product (Figure 9 A, third lane). Therefore, the 140 kDa band was designated $GP_{1/2}$ as it represents the complex N-glycosylated and furin-cleaved ZEBOV GP within the TGN. Whereas, the 120 kDa product was denoted $preGP_{ER}$ as only the synthesized precursor of GP within the ER consists of high mannose oligosaccharides that can be removed by EndoH.

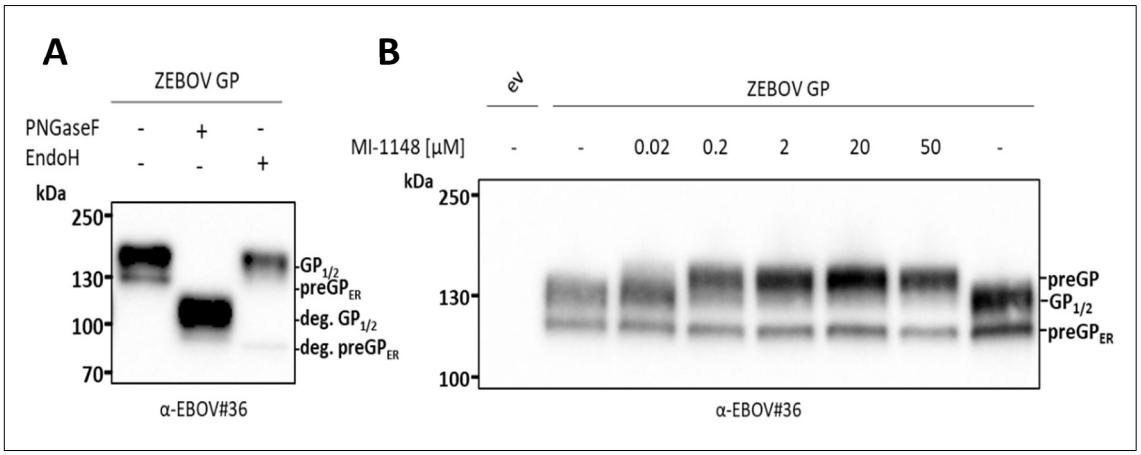


**Figure 9: Transient expression of ZEBOV GP in 293F cells under MI-1148 treatment.**
ZEBOV GP was transiently expressed in 293F cells in the presence or absence of furin inhibitor MI-1148 for 24 h. **A**) Cellular pellets were lysed and further digested with EnodH or PNGaseF glycosidases for 1 h at 37 °C. Samples were subjected to SDS-PAGE and analyzed by Western blot analysis with anti-EBOV#36 serum. **B**) Transfected cells were simultaneously treated with furin inhibitor MI-1148 in concentrations ranging from 0.02 to 50 µM. Transfection of pCAGGS empty vector (ev) served as a negative control. The cells were harvested, lysed and subjected to an 8 % SDS-PAGE. ZEBOV GP was detected by immunoblotting with an EBOV-specific serum (α-EBOV#36).

Transiently expressed ZEBOV GP was very efficiently processed in 293F cells, as no precursor protein (preGP) was detected in the Western blot analysis. Treatment of ZEBOV GP-transfected cells with 50 µM of the furin inhibitor MI-1148 for 24 h was able to completely inhibit preGP cleavage. Thus, only the uncleaved 160 kDa preGP was expressed. MI-1148 very potently inhibited the furin activity during ZEBOV GP transfection, as even low amounts of 0.2 µM MI-1148 were sufficient to abrogate preGP processing, while only at inhibitor concentrations of 0.02 µM a shift towards the cleaved $GP_{1/2}$ 140 kDa product was visible (Figure 9 B). Moreover, as expected the treatment with MI-1148 had no effect on the newly synthesized 120 kDa $preGP_{ER}$ form of ZEBOV GP residing within the ER.

### 4.1.2 Generation of a surrogate virus with uncleaved GP surface fusion protein (rVSVΔG ZEBOV $GP_0$)

The role of protease cleavage of ZEBOV GP during virus infection and replication was studied under biosafety level 2 (BSL-2) conditions with a recombinant VSV pseudovirus. This surrogate virus contains all VSV structural proteins except for the surface glycoprotein G, which was deleted and substituted with ZEBOV GP. The rVSVΔG virions, expressing ZEBOV GP (rVSVΔG ZEBOV GP), were used for infection and replication studies (4.1.3, 4.1.4, 4.1.5 and 4.1.9). As treatment of 293F cells upon transient expression of ZEBOV GP with the furin inhibitor MI-1148 led to efficient inhibition of furin cleavage, this protease inhibitor was used to further investigate the proteolytic activation mechanism during infection. Therefore, VeroE6 cells were infected with rVSVΔG ZEBOV GP at a low MOI of 0.005 for 1 h and subsequently incubated for 72 h (3.4.4) in the presence or absence of 20 µM of MI-1148. The cellular monolayer was then harvested, lysed and subjected to SDS-PAGE and Western blot analysis (3.2.12). For the detection of ZEBOV GP, expressed upon virus infection, the EBOV #36 serum was used.

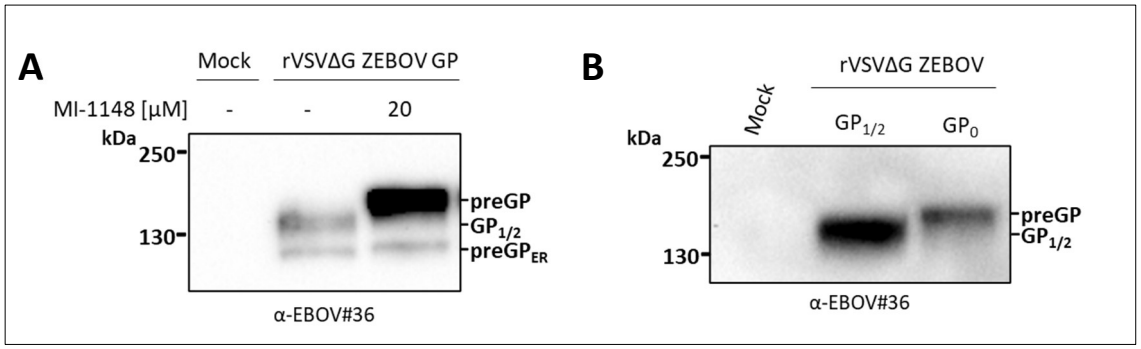


**Figure 10: Generation of uncleaved rVSVΔG ZEBOV GP pseudo-type virus.**
**A)** GP expression in rVSVΔG ZEBOV GP infected VeroE6 cell in the presence and absence of MI-1148 furin inhibitor. VeroE6 cells were inoculated with rVSVΔG ZEBOV GP at a MOI of 0.005 and incubated with or without peptidomimetic furin inhibitor MI-1148 at a concentration of 20 µM for 72 h. Infected cells were then harvested, lysed and subsequently, ZEBOV GP expression was analyzed using a 8 % SDS-PAGE and Western blot analysis. For the detection of GP, the polyclonal anti-EBOV#36 serum was used. **B**) GP expression on virus particles of furin-cleaved VSVΔG ZEBOV $GP_{1/2}$ and uncleaved $GP_0$. Both rVSVΔG ZEBOV $GP_{1/2}$ and $GP_0$ virus stocks were propagated in Huh-7 cells. For the generation of VSV pseudovirus bearing uncleaved $GP_0$ on the surface, cells were incubated with 30 µM of MI-1148 for 24 h. Virus supernatants were then subjected to an 8 % SDS-PAGE and analyzed with the anti-EBOV#36 serum by Western blot analysis.

Infection of VeroE6 cells with rVSVΔG ZEBOV GP for 72 h resulted in the translation of ZEBOV GP which was subsequently cleaved by furin along the secretory transport pathway into $GP_{1/2}$ (140 kDa). In contrast, treatment with 20 µM MI-1148 for 72 h upon rVSVΔG ZEBOV GP infection led to the expression of uncleaved GP ($GP_0$) with a size of 160 kDa (Figure 10 A). In addition, the 120 kDa precursor protein ZEBOV $preGP_{ER}$ was again not affected by the treatment with MI-1148 upon infection in VeroE6 cells, similar to the transiently expressed ZEBOV GP in 293F cells.

Based on these results a rVSVΔG ZEBOV $GP_0$ virus stock was generated in Huh-7 cells, which are highly susceptible to rVSVΔG ZEBOV infections, for maximum virus yield. Therefore, the cell monolayer was inoculated with rVSVΔG ZEBOV $GP_{1/2}$ virus stock at a high MOI of 0.5 for 1 h. Subsequently, the cells were treated with 30 µM of MI-1148 for 24 h (3.4.2). After the incubation period, the viral supernatants were harvested and GP expression on rVSVΔG ZEBOV virions was analyzed by SDS-PAGE and immunoblotting using the EBOV#36 serum.

Samples of rVSVΔG ZEBOV $GP_{1/2}$ virus stock showed a distinct 140 kDa band indicating complete cleavage of preGP by furin during pseudovirus replication in Huh-7. Treatment with MI-1148 upon infection with rVSVΔG ZEBOV GP resulted in uncleaved rVSVΔG ZEBOV $GP_0$, as only a single 160 kDa band was detected (Figure 10 B). In the following, the generated furin-cleaved rVSVΔG ZEBOV $GP_{1/2}$ and the unprocessed rVSVΔG ZEBOV $GP_0$ were used to investigate the importance of furin processing prior to the infection of new target cells. Therefore, VeroE6 cells were infected with the two virus stocks in the presence and absence of classical ZEBOV GP-activating host cell proteases furin and endosomal CatB and CatL.

### 4.1.3 Multicycle replication of rVSVΔG ZEBOV $GP_{1/2}$ and $GP_0$ under combined cathepsin and furin inhibitor treatment in VeroE6 cells

The proteolytic activation of ZEBOV GP has been controversially discussed within the last decades. Work from Neumann and colleagues focused on the proteolytic activation of ZEBOV GP by furin and showed that mutation of the multibasic furin cleavage site RRTRR to the non-basic AGTAA motif led to only initial reduction of recombinant ZEBOV titers in VeroE6 cells. Furthermore, loss of furin cleavage did not impair the infectivity and virulence of this mutant virus in non-human primates (Neumann *et al.*, 2002; Neumann *et al.*, 2007). In addition to these findings, the group of Marzi and colleagues examined the effect of the endosomal cysteine proteases CatB and CatL on ZEBOV GP activation. They observed that neither *in vitro* inhibition of cathepsins nor *in vivo* knockout of CatB or CatL in mice had an adverse effect on ZEBOV GP replication and infectivity (Marzi *et al.*, 2012). However, these studies examined the two cleavage events isolated from each other. In this study, a combined inhibitory approach was used to address the question whether proteolytic cleavage of ZEBOV GP is needed for replication after all. Thus, VeroE6 cells were inoculated with the previously described rVSVΔG ZEBOV GP surrogate viruses expressing cleaved and uncleaved GP (4.1.2) under a combined inhibition of furin and endosomal cathepsins.

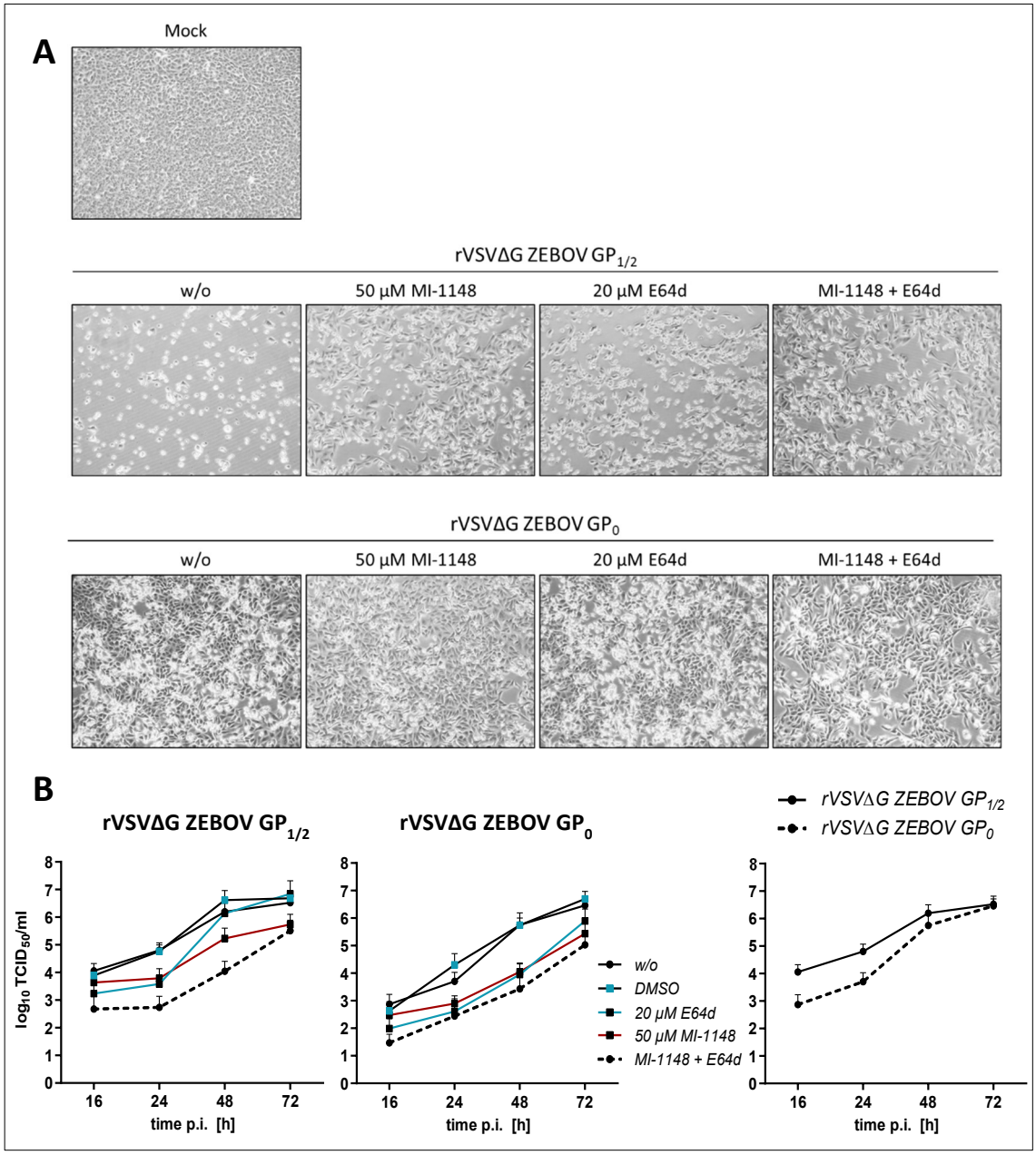


**Figure 11: Multicycle replication of rVSVΔG ZEBOV expressing cleaved ($GP_{1/2}$) and uncleaved ($GP_0$) glycoprotein.** Multicycle replication of rVSVΔG ZEBOV $GP_{1/2}$ or $GP_0$ in the presence or absence of furin and endosomal cathepsin inhibitors. VeroE6 cells were treated with furin inhibitor MI-1148 (50 µM) and/or CatB and CatL inhibitor E64d (20µM), or 0.5 % DMSO for 1 h. Afterward, the cells were infected with rVSVΔG ZEBOV $GP_{1/2}$ or $GP_0$ at a low MOI of 0.005 for 1 h. Protease inhibitor treatment was continued during 72 h incubation period. **A**) Comparison of viral cytopathic effect (CPE) between rVSVΔG ZEBOV $GP_{1/2}$ or $GP_0$ infected VeroE6 cells. After 72 h of rVSVΔG ZEBOV $GP_{1/2}$ or $GP_0$ infection, the virus-induced CPE was determined by microscopy using phase contrast and a 4x magnification. Uninfected cells (Mock) served as a negative control. **B**) Viral growth kinetics in VeroE6 cells in the presence or absence of protease inhibitors. Virus supernatants of the infected VeroE6 were collected at 16, 24, 48 and 72 h postinfection (p.i). Viral titers were determined by $TCID_{50}$ endpoint dilution assay. Data shown are means (±SD) of five independent experiments (n=5).

For the infection experiments, VeroE6 cells were inoculated with rVSVΔG ZEBOV $GP_{1/2}$ or rVSVΔG ZEBOV $GP_0$ at a MOI of 0.005 for 1 h and then further incubated in the presence or absence of protease inhibitors MI-1148 and E64d for 72 h (3.4.4). The cytopathic effect (CPE) caused by rVSVΔG ZEBOV $GP_{1/2}$ and $GP_0$ in infected VeroE6 cells after the incubation time was observed under a light microscope. While uninfected (Mock) control cells showed a confluent

monolayer after 72 h, the cell layer of rVSVΔG ZEBOV $GP_{1/2}$ inoculated VeroE6 cells was almost completely dissolved with the few remaining cells displaying a round detached phenotype. Cells treated with 20 µM E64d were also mostly detached with only a few physiologically shaped cells left. The single inhibition of furin with 50 µM MI-1148 led to an increase of attached VeroE6 cells, but a clear CPE was still visible. However, the combination of E64d and MI-1148 showed further improvement of the cell phenotype even though a profound viral CPE was still visible after 72 h. In contrast, the cell morphology of rVSVΔG ZEBOV $GP_0$ infected VeroE6 cells was different compared to the rVSVΔG ZEBOV $GP_{1/2}$ inoculated cells. The cellular monolayer was mostly intact even though virus CPE was clearly visible in untreated (w/o) and E64d treated cells, while viral CPE was further reduced in cells treated with a combination of MI-1148 and E64d (Figure 11 A).

For more precise information, viral growth kinetics from the respective rVSVΔG ZEBOV $GP_{1/2}$ and $GP_0$ infection studies were compiled by virus titration. Therefore, virus supernatants were collected at 16, 24, 48 and 72 h p.i. and viral titers were determined by $TCID_{50}$ endpoint dilution assay (3.4.1). Comparison of the viral titer from the infections with cleaved and uncleaved rVSVΔG ZEBOV GP stocks showed, that even though rVSVΔG ZEBOV $GP_0$ was not initially cleaved by endogenous furin within the TGN of the producing Huh-7 cells, the virus was still able to replicate efficiently in VeroE6 cells. The rVSVΔG ZEBOV $GP_0$-infected cells reached similar viral titers of $2.9x10^6$ $TCID_{50}$/ml compared to the rVSVΔG ZEBOV $GP_{1/2}$ with $3.3x10^6$ $TCID_{50}$/ml after 72 h. The treatment of DMSO served as a control for the DMSO-solved E64d and no negative effect on the viral replication was observed. Single inhibitor treatment with 20 µM E64d and 50 µM MI-1148 led to an up to 16-fold reduction of viral titers at early time points of infection with rVSVΔG ZEBOV $GP_{1/2}$. Nevertheless, after 48 h the inhibitory effect of E64d was completely diminished, whereas viral titers in MI-1148 treated samples displayed a steady 6- to 9-fold reduction over 48 h and 72 h, respectively. In contrast, rVSVΔG ZEBOV $GP_0$ replication was steadily suppressed by both MI-1148 and E64d single inhibitor treatment over the 72 h incubation period, with a prominent 50-fold reduction at 48 h p.i. The combined inhibition of endosomal cathepsins and furin had a synergistic effect on rVSVΔG ZEBOV $GP_{1/2}$ replication with a constant 1- to 2-log reduction over 72 h. An additive effect of furin and cathepsin inhibitors was also observed for the uncleaved rVSVΔG ZEBOV $GP_0$ infected cells, but viral titer reduction was slightly less efficient with a 2-log reduction only after 48 h (Figure 11 A and Figure 11 B). The direct comparison of multicycle replication of furin-cleaved and the uncleaved rVSVΔG ZEBOV GP virus stocks in untreated VeroE6 cells revealed an initial growth defect of rVSVΔG ZEBOV pseudovirus bearing $GP_0$, with a 1-log reduction at 16 and 24 h after infection. However, after 48 h rVSVΔG ZEBOV $GP_0$ was able to compensate for the replication

disadvantage, even reaching similar viral titers to rVSVΔG ZEBOV $GP_{1/2}$ after 72 h incubation (Figure 11 B). Thus, the uncleaved $GP_0$ was initially less sufficient but seemed to be subsequently proteolytically activated over time.

### 4.1.4 Multicycle replication of rVSVΔG ZEBOV $GP_{1/2}$ and $GP_0$ with additional trypsin-like protease inhibitor treatment in VeroE6 cells

As rVSVΔG ZEBOV $GP_0$ was able to overcome the initial growth delay and due to the incomplete abrogation of virus replication in the combined furin and cathepsin inhibitor treated VeroE6 cells, there might be a trypsin-like protease present substituting for the lack of classical ZEBOV GP-activating proteases. Thus, the triple inhibition of furin, cathepsins and trypsin-like proteases in VeroE6 cells infected with rVSVΔG ZEBOV $GP_{1/2}$ and $GP_0$ was further investigated. Here, the broad-spectrum trypsin-like protease inhibitors aprotinin and MI-0001 (BAPA), as well as the more specific structure-based TMPRSS2/matriptase inhibitor MI-432 were used.

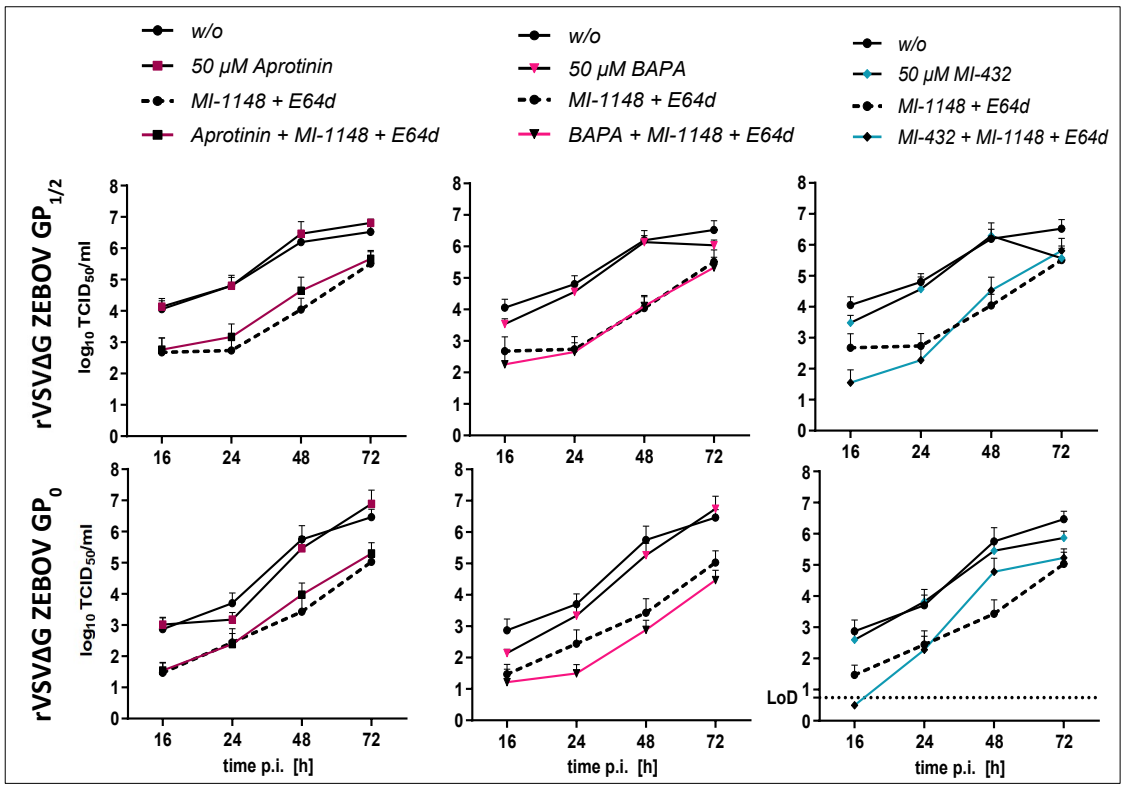


**Figure 12: Multicycle replication of rVSVΔG ZEBOV expressing cleaved ($GP_{1/2}$) and uncleaved ($GP_0$) glycoprotein under triple protease inhibitor treatment in VeroE6 cells.**
Comparative growth kinetics of rVSVΔG ZEBOV $GP_{1/2}$ or $GP_0$ in VeroE6 cells. Multicycle replication of rVSVΔG ZEBOV $GP_{1/2}$ or $GP_0$ during the combined treatment with E64d, MI-1148 and trypsin-like protease inhibitors aprotinin, BAPA and MI-432. For all studies, VeroE6 cells were incubated with 50 µM MI-1148, 20 µM E64d and 50 µM of the respective trypsin-like protease inhibitors for 1 h prior to infection. Afterward, the cells were infected with rVSVΔG ZEBOV $GP_{1/2}$ or $GP_0$ at a low MOI of 0.005 for 1 h. Protease inhibitor treatment was continued during the following 72 h incubation period. Virus supernatants were collected at the indicated time points. Viral titers were determined by $TCID_{50}$ endpoint dilution assay with the assay limit of detection (LoD) indicated as a dashed line. Data shown are means (±SD) of three to five independent experiments (n=3-5).

Single trypsin-like protease inhibitor treatment, in the presence of furin and cathepsin activity, with aprotinin, BAPA and MI-432 did not inhibit viral replication of both rVSVΔG ZEBOV $GP_{1/2}$ and $GP_0$. In rVSVΔG ZEBOV $GP_{1/2}$ infected VeroE6 cells treated with MI-1148 and E64d no additional effect of aprotinin and only a small initial virus titer reduction for BAPA was observed after 16 h. Treatment with MI-432 further suppressed rVSVΔG ZEBOV $GP_{1/2}$ replication at early time points of infection with a 1-log reduction 16 h p.i. However, after 48 h the additional inhibitory effect of triple treatment with MI-432 vanished. Similar effects were observed for rVSVΔG ZEBOV $GP_0$ inoculated VeroE6 cells, with no virus titer reduction by additional aprotinin treatment and only an initial 1-log reduction for MI-432 incubation after 16 h. However, triple inhibition with BAPA further suppressed the viral replication for the entire 72 h with an additional 3- to 8-fold reduction compared to the combined MI-1148 and E64d treatment (Figure 12).

### 4.1.5 Multicycle replication of rVSVΔG ZEBOV $GP_{1/2}$ and $GP_0$ in Vero-TMPRSS2 cells under combined inhibitor treatment

The previous viral growth kinetics in VeroE6 cells indicated the possible involvement of a trypsin-like protease in the proteolytic activation of ZEBOV GP expressing surrogate viruses. Thus, a corresponding experiment was performed in Vero cells, stably expressing TMPRSS2 (Vero-TMPRSS2) (Hoffmann *et al.*, 2020). TMPRSS2 has been shown to play an important role in the proteolytic activation of influenza viruses, as it has been shown to be the major activating host cell protease for almost all human and avian IAVs in human respiratory epithelial cells, with only few exceptions (Limburg *et al.*, 2019; Bestle *et al.*, 2021). Furthermore, TMPRSS2 has been described to be involved in the activation of MERS- and SARS-CoV, which also possess two cleavage sites like the ZEBOV GP (Glowacka *et al.*, 2011; Park *et al.*, 2016). Hence, TMPRSS2 was an interesting host cell protease candidate for the subsequent activation of ZEBOV GP in the absence of its usual activating-proteases furin and cathepsins.

The initial MOI of 0.005 used in VeroE6 cell infection experiments appeared to be too high for the replication of rVSVΔG ZEBOV $GP_{1/2}$ and $GP_0$ in Vero-TMPRSS2 cells, with virus titers peaking already at 16 or 24 h, respectively (data not shown). Therefore, infection studies were performed at a 10-fold lower MOI of 0.0005, which led to steady viral growth kinetics (Figure 13 A). Both rVSVΔG ZEBOV $GP_{1/2}$ and $GP_0$ replicated similarly in Vero-TMPRSS2 cells over 72 h, with titers peaking at $3.9 \times 10^6$ $TCID_{50}$/ml after 48 h (Figure 13 A). Again, DMSO treatment had no

effect on the replication of both pseudoviruses (Figure 13 B). Hence, any inhibitory effect of E64d was not due to the DMSO solvent.

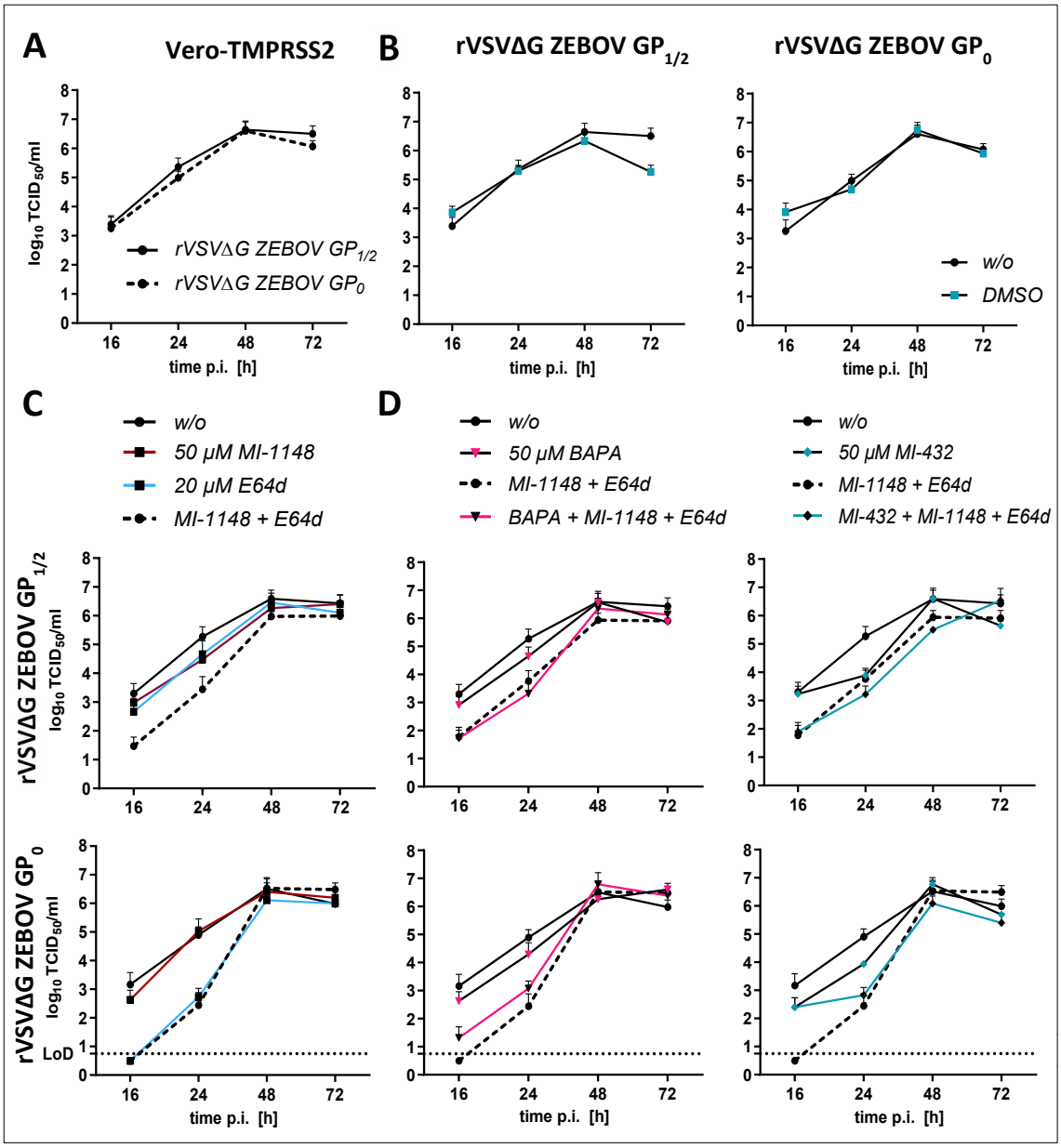


**Figure 13: Multicycle replication of rVSVΔG ZEBOV expressing cleaved ($GP_{1/2}$) and uncleaved ($GP_0$) glycoprotein in the presence of additional trypsin-like protease inhibitors in Vero-TMPRSS2 cells.**
Comparative growth kinetics of rVSVΔG ZEBOV $GP_{1/2}$ or $GP_0$ in Vero-TMPRSS2 cells infected at a MOI of 0.0005. **A**) Viral titers of rVSVΔG ZEBOV $GP_{1/2}$ or $GP_0$ in untreated Vero-TMPRSS2 cells. **B**) Growth kinetics in the presence of the solvent DMSO, with a concentration of 0.5 %, served as a control. **C**) Multicycle replication of rVSVΔG ZEBOV $GP_{1/2}$ or $GP_0$ during single and combined E64d and MI-1148 treatment. **D**) Growth kinetics under triple inhibitor treatment with E64d, MI-1148 and the broad trypsin-like protease inhibitor BAPA or the structure-based TMPRSS2 inhibitor MI-432. Vero-TMPRSS2 cells were treated with 50 µM MI-1148, 20 µM E64d and 50 µM of trypsin-like protease inhibitors (BAPA or MI-432) for 1 h prior to infection. Afterward, the cells were infected with rVSVΔG ZEBOV $GP_{1/2}$ or $GP_0$ at a low MOI of 0.0005 for 1 h. Protease inhibitor treatment was continued during the 72 h incubation period. For all studies, virus supernatants were collected at 16, 24, 48 and 72 h p.i. Viral titers were determined by TCID50 endpoint dilution assay, with the assay limit of detection (LoD) indicated as a dashed line. Data shown are means (±SD) of three to five independent experiments (n=3-5).

The incubation with single inhibitors for furin or CatB and CatL resulted in only a minor 1- to 6-fold titer reduction of rVSVΔG ZEBOV $GP_{1/2}$ in Vero-TMPRSS2 cells at the early time points of infection, whereas the combined treatment resulted in an additive 67-fold decrease of viral titers. Interestingly, for rVSVΔG ZEBOV $GP_0$, lacking the initial furin cleavage, the single E64d treatment completely suppressed virus replication after 16 h, followed by a 2-log reduction 24 h p.i. However, at later time points this effect was diminished with virus titers comparable to the untreated control. The incubation with MI-1148 did not hinder virus replication, which was also seen in the virus titers of the combined inhibitor-treated cells, as there no synergistically increased inhibition was observed (Figure 13 C). Like in the previous VeroE6 studies, single treatment with BAPA and MI-432 had no effect on the viral titers of both the cleaved and uncleaved rVSVΔG ZEBOV GP pseudoviruses. Interestingly, the triple inhibition of furin, endosomal cathepsins and trypsin-like proteases, by either adding BAPA or MI-432, were in contrast to the observations made in Vero E6 cells, not able to suppress viral replication beyond the combined E64d and MI-1148 treatment in both rVSVΔG ZEBOV $GP_{1/2}$ or rVSVΔG ZEBOV $GP_0$ infected Vero-TMPRSS2 cells (Figure 13 D). Nevertheless, the loss of the initial growth defect of rVSVΔG ZEBOV $GP_0$ in the TMPRSS2 expressing Vero cells indicated the involvement of TMPRSS2 in the activation of the uncleaved $GP_0$ during the early steps of virus replication (Figure 13A).

### 4.1.6 Functional analysis of trVLP bearing ZEBOV GP_RRTRR and ZEBOV GP_AGTAA in Huh-7 cells

The infection studies with rVSVΔG ZEBOV $GP_0$ under the combined inhibitor treatment with MI-1148, E64d and BAPA in VeroE6 and the loss of its initial replication disadvantage in Vero-TMPRPSS2 cells hinted that a trypsin-like protease could be involved in the subsequent activation of ZEBOV GP (4.1.4 and 4.1.5). In order to particularly address the viral entry and its dependence on host cell proteases, a reporter minigenome assay with transcription and replication-competent virus-like particles (trVLPs) was used (3.4.5). The trVLPs are able to infect cells and the subsequent measured reporter genome activity represents genome release and transcription (Hoenen *et al.*, 2006; Hoenen & Feldmann, 2014). For the generation of trVLPs 293F (p0) cells were transfected (3.1.2) with plasmids encoding for the structural and replication complex proteins, as well as with either ZEBOV GP containing the wildtype RRTRR motif or the furin cleavage mutant with the AGTAA sequence. Additional reporter gene plasmid transfection with the renilla luciferase-encoding minigenome and a firefly luciferase-encoding plasmid, enabled the detection and normalization of minigenome replication and transcription during

trVLP production, respectively (3.4.7). After 72 h the cellular supernatants were harvested and the trVLPs concentrated on a sucrose cushion by ultracentrifugation (3.4.5). The trVLP pellet was resuspended in 100 µl PBS and 20 µl were subjected to SDS-PAGE and immunoblotting. The Huh-7 (p1) cells were pre-transfected with the replication complex proteins VP30, VP35, NP and L for 24 h upon cell cultivation. Prior to the trVLP infection, the p1 cells were either treated with 20 µM E64d, 50 µM MI-1148, 50 µM BAPA or double or triple combinations of the protease inhibitors for 1 h or remained untreated. Subsequently, the p1 cells were inoculated with equal amounts of ZEBOV GP_RRTRR- or GP_AGTAA-bearing trVLPs for 2 h and further incubated in the presence or absence of the respective inhibitor for 72 h (3.4.6). Afterward, the cells were harvested and luciferase reporter gene expression was analyzed in the cellular lysates (3.4.7).

Western blot analysis of the concentrated trVLPs containing ZEBOV GP_RRTRR or furin cleavage site mutant ZEBOV GP_AGTAA with the EBOV#36 serum demonstrated similar expression of the matrix protein VP40 and GP in both trVLP preparations. In the samples of ZEBOV GP_RRTRR generated trVLPs the furin-cleaved $GP_{1/2}$ was detected with a molecular weight of 140 kDa, whereas predominantly unprocessed 160 kDa preGP was incorporated into the GP_AGTAA-bearing trVLPs. Subsequent staining with the V5 epitope-tag antibody enabled the detection of C-terminal furin cleavage product ($GP_2$). Here, a prominent 20 kDa $GP_2$ band was detected in the trVLPs samples containing the wildtype ZEBOV GP_RRTRR, which was cleaved by furin during trVLP production in p0 cells. Interestingly, a light $GP_2$ band could also be observed in the trVLP preparations with the ZEBOV GP_AGTAA (Figure 14 A). The renilla luciferase reporter gene activity was measured in lysates of p0 cells and normalized to co-transfected firefly plasmid expression, then the normalized renilla to firefly ratio of ZEBOV GP_RRTRR was set to 1. The relative luciferase activity during trVLP production did not differ for ZEBOV GP_RRTRR and ZEBOV GP_AGTAA plasmid transfection after 72 h (Figure 14 B).

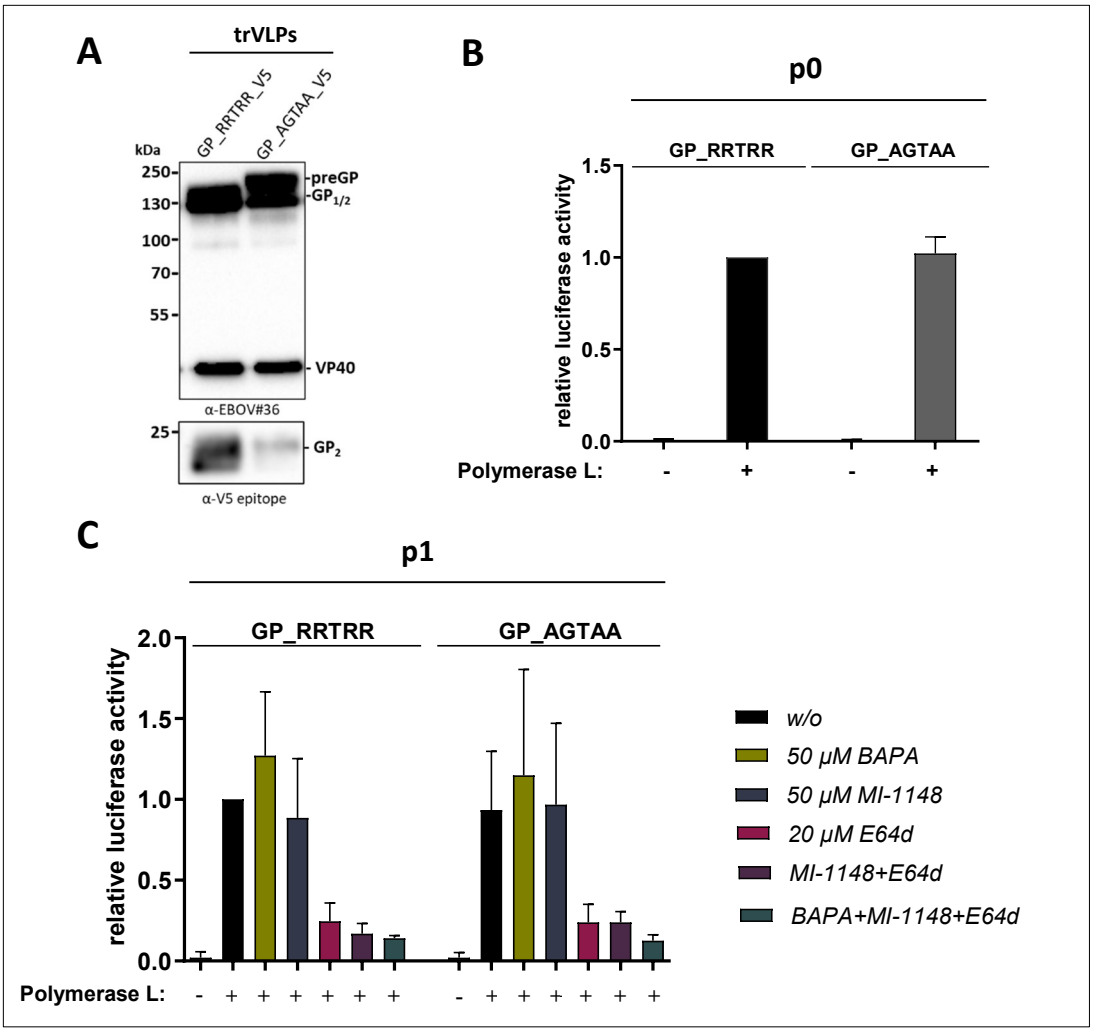


**Figure 14: Functional analysis of furin cleavage site mutant ZEBOV GP_AGTAA in Huh-7 cells.**
**A**) Generation of transcription and replication-competent virus-like particles (trVLPs) expressing either ZEBOV GP_RRTRR or the furin cleavage site mutant ZEBOV GP_AGTAA in human 293F cells. 293F cells (p0) were simultaneously transfected with pCAGGS NP, VP24, VP30, VP35, VP40, L and pCAGGS plasmids encoding either for ZEBOV GP_RRTRR or ZEBOV GP_AGTAA, as well as the plasmids for the monocistronic reporter genome E5E3 (renilla luciferase), T7 polymerase and pGL4 (firefly luciferase). After 72 h cellular supernatants were harvested and trVLPs were concentrated on a sucrose cushion by ultracentrifugation at 40.000 rpm for 2 h. The trVLP pellets were resuspended in PBS, samples were then subjected to a 10 % SDS-PAGE and analyzed by Western blot. For detection of ZEBOV proteins, the EBOV#36 serum was used, while the specific $GP_2$ cleavage site product was detected with an antibody directed against the V5 epitope at the C-terminal end of ZEBOV GP. **B**) Luciferase reporter activity in producing p0 cells. After 72 h of plasmid transfection for trVLP generation with and without polymerase L plasmid, the cells were harvested and lysed for 30 min on ice. The corresponding luminescence signal to renilla and firefly activity within the cell lysates was measured after substrate incubation. The renilla reporter gene signal was normalized to firefly expression. Relative luciferase activity over ZEBOV GP_RRTRR signal is shown. Data are mean values (±SD) of three independent experiments (n=3). **C**) Luciferase reporter activity in trVLP infected Huh-7 cells. Huh-7 (p1) cells were pre-transfected with NP, V30, VP35 and L 24 h prior to trVLP inoculation for primary and secondary transcription of reporter minigenome upon infection. The following day pre-transfected p1 cells were incubated for 1 h either with 50 µM BAPA, 20 µM E64d, 50µM MI-1148 or a triple combination, untreated cells served as control (w/o). Afterward, p1 cells were inoculated with either ZEBOV GP_RRTRR- or GP_AGTAA-bearing trVLP and incubated in the presence or absence of protease inhibitor for 72 h. Subsequently, renilla reporter gene activity was measured as described above. Data are mean values (±SD) of three independent experiments (n=3).

The expression of the ZEBOV GP_AGTAA mutant did not impair trVLP production, as a comparable reporter gene activity was detected in both p0 cells. Furthermore, the Western blot analysis of the trVLP preparations showed similar protein expression levels. Hence, pre-transfected p1 cells were inoculated with the same amount of concentrated trVLPs in the presence or absence of protease inhibitors for 72 h. Normalized luciferase activity of untreated p1 cells inoculated with wildtype GP-expressing trVLPs was again set to 1. The relative reporter gene activity showed no difference between infections with GP_RRTRR- and GP_AGTAA-expressing trVLPs in untreated p1 cells (Figure 14 C, black bars). Furthermore, treatment of p1 cells with BAPA and MI-1148 did not inhibit minigenome release and transcription for both trVLPs. For so far unknown reasons there was a slight increase of reporter activity observed for both GP variants during trVLP infection under BAPA treatment. However, inhibition of endosomal CatB and CatL with E64d resulted in an over 75 % reduction of reporter gene activity in ZEBOV GP_RRTRR- and GP_AGTAA-bearing trVLP infections. The combination of MI-1148 and E64d had only a minor additional effect on luciferase activity in GP_RRTRR trVLP inoculated p1 cells and no further reduction was observed for the GP_AGTAA trVLP variant. Interestingly, in both trVLP infections, the reporter gene activity was not suppressed to the level of the negative control trVLPs, lacking the ZEBOV polymerase L, similar to the growth kinetics in VeroE6 and Vero-TMPRSS2 cells with rVSVΔG ZEBOV $GP_{1/2}$ and $GP_0$. Nevertheless, triple inhibitor treatment with BAPA, MI-1148 and E64d was able to further suppress the luciferase minigenome signal, especially in p1 cells infected with trVLPs expressing ZEBOV GP_AGTAA. Thus, a less efficient trypsin-like protease might not only process ZEBOV GP post-translationally during trVLP production but could also be involved in the proteolytic activation upon cell entry, when classical virus-activating proteases, like furin and CatB and CatL are impaired (Figure 14 C, colored bars).

### 4.1.7 Characterization of the proteolytic cleavage site of TMPRSS2 within ZEBOV GP

The trVLP studies showed, that the previously proposed "non-cleavable" ZEBOV GP_AGTAA variant was partially cleaved and incorporated during trVLP production in 293F cells (4.1.8). Moreover, the unprocessed rVSVΔG ZEBOV $GP_0$ has been shown to overcome its initial replication disadvantage, compared to the furin-cleaved rVSVΔG ZEBOV $GP_{1/2}$ observed in VeroE6 cells when inoculated in TMPRSS2-expressing Vero cells (4.1.3 and 4.1.5). Hence, the data indicate that a trypsin-like protease, as TMPRSS2 might be able to proteolytically activate

the ZEBOV GP with the AGTAA cleavage site mutation during the posttranslational secretory transport, thereby substituting for furin cleavage.

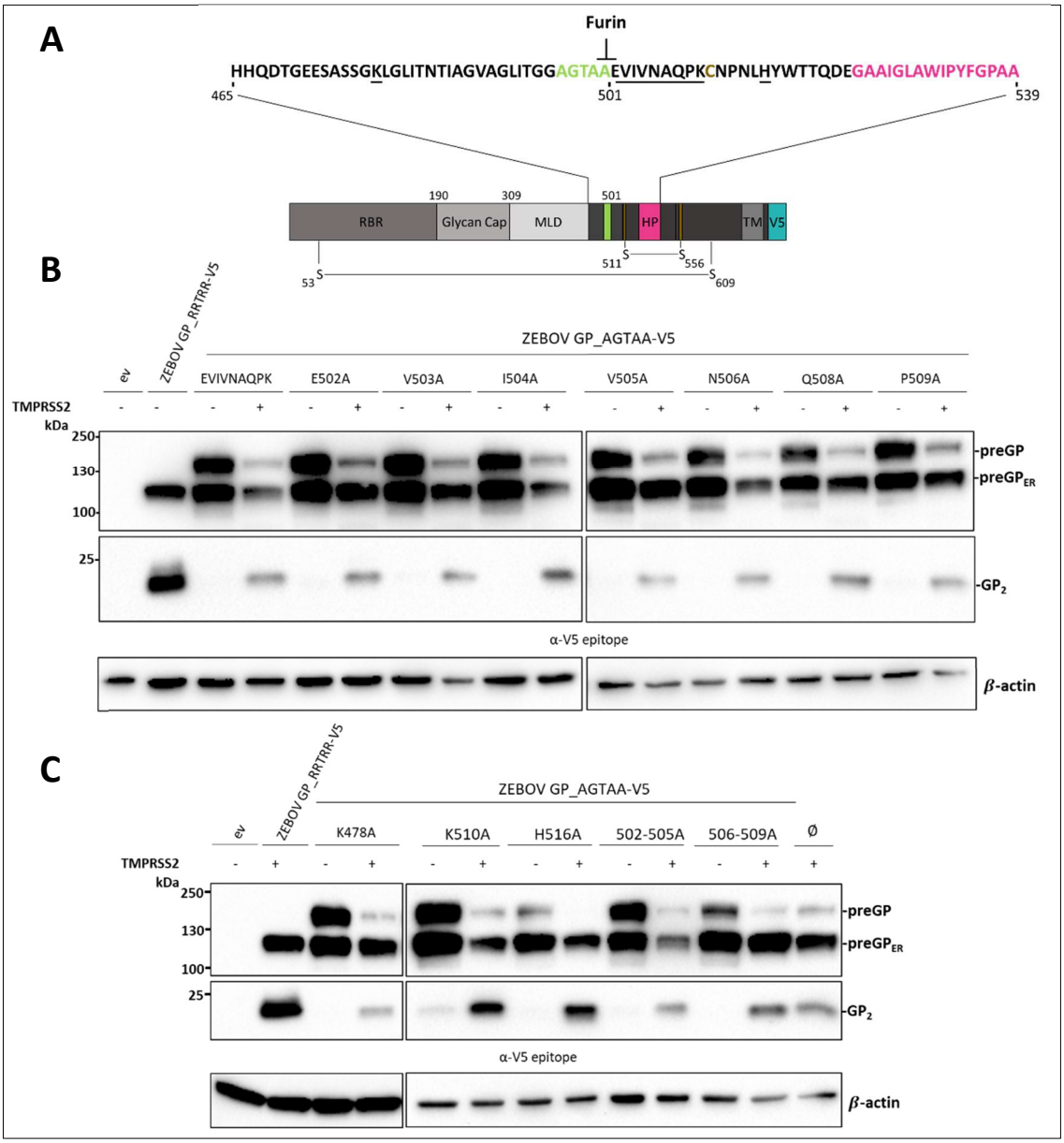


**Figure 15: Alanine scanning mutations to identify the TMPRSS2 cleavage site in ZEBOV GP.**
**A**) Schematic illustration of C-terminal V5-tagged ZEBOV GP. The region of interest from aa 465 to 539 is enlarged, with the mutated furin cleavage site AGTAA motif (green), the aa forming the hydrophobic patch (magenta) and the C511 (yellow) involved in the disulfide bridge forming the internal fusion loop. Underlined aa were exchanged to alanine either in a single or multiple mutations. **B**) HeLa cells were co-transfected with ZEBOV GP_RRTRR, ZEBOV GP_AGTAA without aa exchange or alanine scanning mutants from aa position 502 to 509 and human TMPRSS2 plasmid for 24 h. **C**) HeLa cells were co-transfected ZEBOV GP_RRTRR, ZEBOV GP_AGTAA without aa exchange (Ø) or alanine exchange mutants for basic aa in positions K478, K510 and H516 as well as multiple alanine mutants from aa position 502-505, 506-509 and human TMPRSS2 plasmid for 24 h. Afterward, the cells were lysed and the samples were analyzed using a 10 % SDS-PAGE and immunoblotting. ZEBOV GP cleavage forms were detected with an antibody directed against the C-terminal V5 epitope of ZEBOV GP. ß-Actin staining was used as a loading control. Western blots shown are representative immunoblots from three independent experiments (n=3).

Therefore, the proteolytic cleavage of ZEBOV GP_AGTAA was examined in co-transfection experiments with the human serine protease TMPRSS2. Here, the plasmid encoding for ZEBOV GP_AGTAA containing a C-terminal V5-tag for cleavage product detection was

co-expressed with the human TMPRSS2 plasmid in 80 % confluent HeLa cells for 24 h (3.1.2). Afterward, the cells were harvested and cellular lysates were subjected to SDS-PAGE and analyzed by Western blot with an antibody directed against the V5 epitope-tag.

Western blot analysis revealed that ZEBOV GP_AGTAA was cleaved by TMPRSS2 upon transient co-expression in HeLa cells to an approximately 20 kDa $GP_2$ product. The cleavage product had a similar molecular weight as observed for the ZEBOV GP_RRTRR processed by endogenous furin (Figure 15 B, lane 2-4). To examine the TMPRSS2 cleavage site of ZEBOV GP_AGTAA, a systematic alanine scan near the mutated furin cleavage site from aa 502 to 509 (EVIVNAQP) was performed (Figure 15 A). Here, the alanine exchange was used to determine possible aa responsible for TMPRSS2 substrate recognition. As alanine possesses only a small non-bulky and non-reactive methyl group it is often used to identify the contribution of aa side chains to the stability or function of a protein of interest. Single aa substitutions to alanine (A) at position E502, V503, I504, V505, N506, Q508 or P509 did neither alter the protein expression nor change the cleavability of ZEBOV GP_AGTAA by TMPRSS2 (Figure 15 B, lane 5-18). Serine proteases, like TMPRSS2, prefer basic aa in the P1 position of their substrates. Therefore, in a next alanine scanning approach the three most adjacent basic aa K478, K510 and H516 were mutated. However, K478A, K510A and H516A were still cleaved by TMPRSS2, indicating that none of these basic aa was involved in the cleavage of ZEBOV GP_AGTAA upon TMPRSS2 co-expression (Figure 15 C, lane 3-8). As the single aa substitutions were not able to inhibit TMPRSS2 cleavage, an unconventional stretch of aa could be used as a substrate for TMPRSS2. Thus, further mutants with an alanine exchange from position 502 to 505 (502-505A) and 506 to 509 (506-509A) were generated. Nevertheless, co-expression of the multiple alanine exchange mutants and TMPRSS2 did not result in the abrogation of ZEBOV GP_AGTAA cleavage by TMPRSS2 (Figure 15 C, lane 9-12).

Identification of the exact cleavage site within the ZEBOV GP_AGTAA was not successful with specific single or multiple alanine exchanges in close proximity to the altered AGTAA cleavage site motif. Therefore, a more radical approach was used in the next experiments. Broad aa deletions were made upstream from the start of the AGTAA motif to the end of the mucin-like domain (MLD) (aa 465 to 496), designated Δ1, and downstream from the end of the AGTAA motif to aa 510 (Δ2). As C511 together with C556 forms the fusion loop within the ZEBOV $GP_2$ subunit, this aa should remain in the deletion construct. An additional mutant, lacking both upstream and downstream stretches (Δ1&2), was also generated (Figure 16 A).

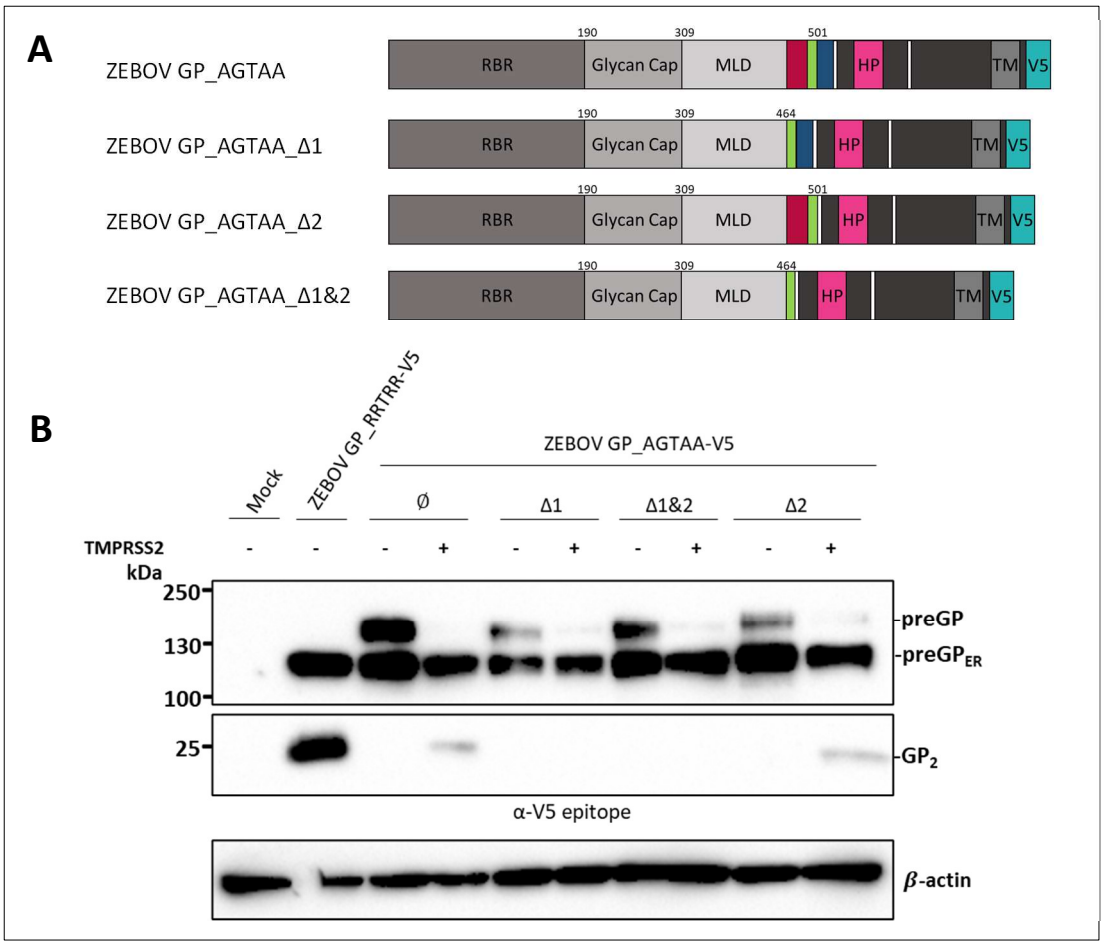


**Figure 16: Proteolytic cleavage of ZEBOV GP_AGTAA deletion mutants by human TMPRSS2.**
**A**) Schematic illustration of different ZEBOV GP_AGTAA deletion mutants. Single deletion of aa 465 to 496 (Δ1, red) and 502 to 510 (Δ2, blue) as well as simultaneous deletion of both regions (Δ1&2). **B**) Proteolytic cleavage of ZEBOV GP_AGTAA deletion mutants by human TMPRSS2. Hela cells were co-transfected with plasmids encoding for ZEBOV GP_AGTAA, ZEBOV GP_AGTAAΔ1, ZEBOV GP_AGTAAΔ2 and ZEBOV GP_AGTAAΔ1&2 and human TMPRSS2 for 24 h. The cells were then harvested, lysed and the samples subjected to a 10 % SDS-PAGE and immunoblotting. ZEBOV GP cleavage forms were detected with an antibody directed against the C-terminal V5 epitope of ZEBOV GP. ß-Actin staining was used as a loading control. Western blots shown are representative immunoblots of three independent experiments (n=3).

Despite the deletion of 9, 32 or 41 aa, all preGP forms of the three ZEBOV GP_AGTAA deletion mutants were similarly expressed upon transfection in HeLa cells, with a slight decrease in the detection of uncleaved preGP compared to the non-mutated ZEBOV GP_AGTAA (Figure 16 B, lane 3, 5, 7 and 9). Co-transfection experiments with the ZEBOV GP_ Δ2 deletion mutant showed, that the 9 aa after the AGTAA motif were not involved in the cleavage of the furin cleavage site mutant by TMPRSS2, as the $GP_2$ cleavage product could still be detected (Figure 16 B, lane 2, 4 and 10). In contrast, the deletion of 32 aa upstream of the AGTAA motif resulted in the inhibition of TMPRSS2 cleavage in both ZEBOV GP_AGTAAΔ1 and ZEBOV GP_AGTAAΔ1&2 mutants (Figure 16 B, lane 6 and 8). These data suggest, that either a stretch of unusual aa is recognized by TMPRSS2 within the area from position 465 to 496, or the deletion of these 32 aa leads to a conformational change in the ZEBOV GP protein that sterically hinders TMPRSS2 cleavage. Nevertheless, it was of interest, whether these ZEBOV GP_AGTAAΔ1 and AGTAAΔ1&2

deletion mutants, which no longer were proteolytically processed by furin and TMPRSS2, were still able to mediate membrane fusion upon cell entry.

### 4.1.8 Functional analysis of trVLP bearing ZEBOV GP_AGTAA and ZEBOV GP_AGTAAΔ1&2 in Huh7, VeroE6 and Vero-TMPRSS2 cells

The previous co-transfection experiments showed, that the deletion of the aa from position 465 to 496 within the ZEBOV GP_AGTAA resulted in a protein that was no longer cleaved by furin and TMPRSS2 upon expression in HeLa cells. As the even smaller ZEBOV GP_AGTAAΔ1&2 construct was less likely to be proteolytically activated by further unknown proteases upon trVLP production in 293F cells, further studies should be performed with this variant. Hence, the functionality of the uncleaved ZEBOV GP_AGTAAΔ1&2 deletion mutant was investigated in trVLP entry studies in order to examine the necessity of proteolytic GP activation for ZEBOV replication.

The trVLPs bearing ZEBOV GP_RRTRR, GP_AGTAA and GP_AGTAAΔ1&2 were generated in 293F (p0) cells and harvested as described above (3.4.5 and 4.1.6). Western blot analysis of the concentrated trVLPs with the EBOV#36 serum showed equal expression levels of the matrix protein VP40 in all three trVLP preparations with comparable levels of incorporated ZEBOV $GP_{1/2}$ for the ZEBOV GP_RRTRR and preGP for ZEBOV GP_AGTAA and GP_AGTAAΔ1&2. Detection of C-terminal cleavage products with the α-V5 epitope-tag again displayed a faint $GP_2$ band for ZEBOV GP_AGTAA with a similar molecular weight of 20 kDa as the furin-cleaved ZEBOV GP_RRTRR. In contrast, no $GP_2$ cleavage product could be observed in trVLPs bearing the ZEBOV GP_AGTAAΔ1&2 deletion mutant (Figure 17 A). The reporter gene activity measured in the p0 cell lysates showed no difference during trVLP production with ZEBOV GP_AGTAA and AGTAAΔ1&2 compared to the ZEBOV GP_RRTRR wildtype (Figure 17 B), indicating no interference of the GP mutation with minigenome transcription and translation.

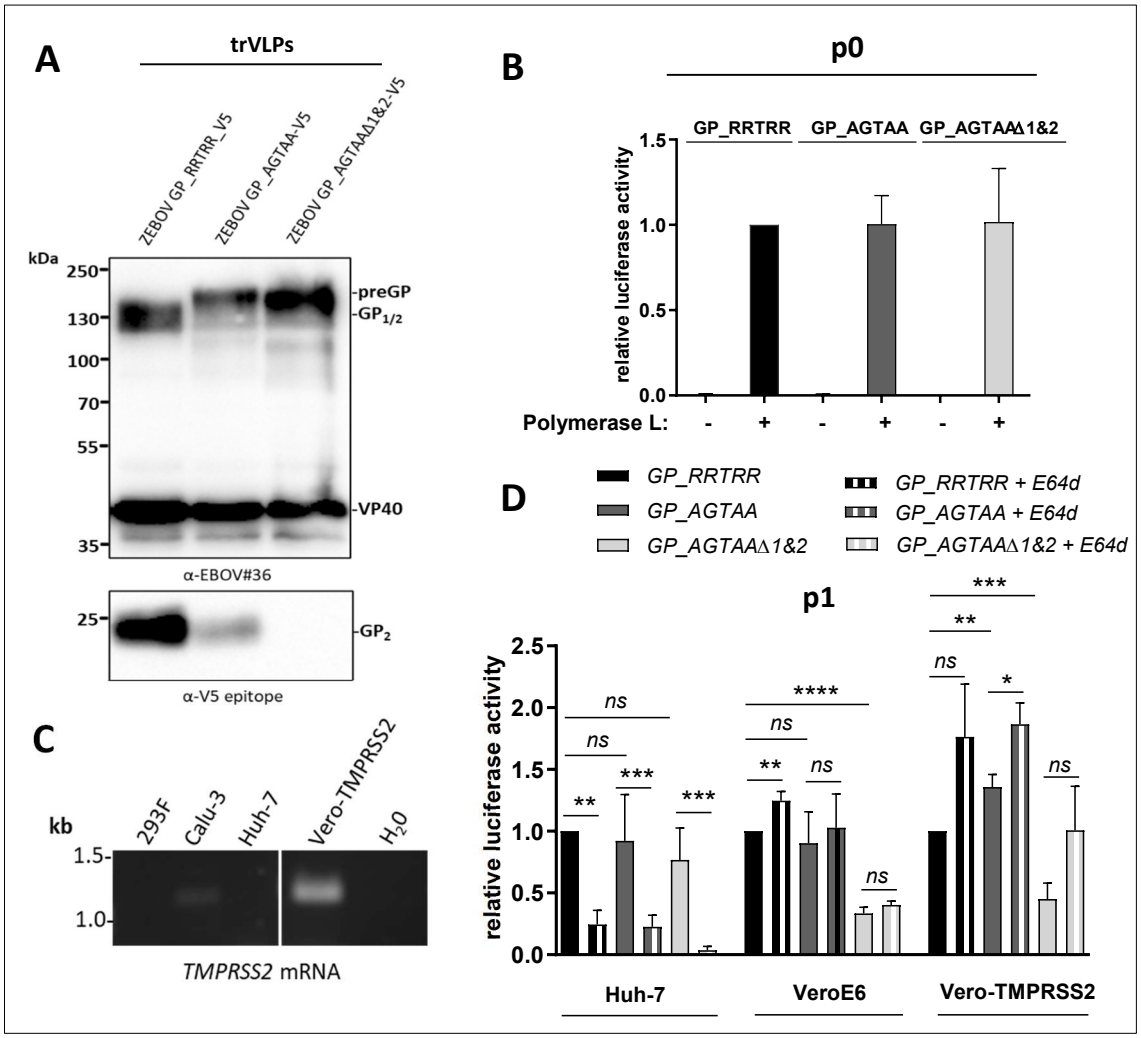


**Figure 17: Functional analysis of ZEBOV GP_AGTAA and GP_AGTAAΔ1&2 in trVLP assay.**
**A**) Generation of transcription and replication-competent virus-like particles (trVLPs) in human 293F cells. 293F (p0) cells were simultaneously transfected with pCAGGS NP, VP24, VP30, VP35, VP40, L and pCAGGS plasmids encoding either for ZEBOV GP_RRTRR, ZEBOV GP_AGTAA furin cleavage site or ZEBOV GP_AGTAAΔ1&2 deletion mutant, as well as the plasmids for the monocistronic reporter genome E5E3 (renilla luciferase), T7 polymerase and pGL4 (firefly luciferase). After 72 h cellular supernatants were harvested and trVLPs were concentrated on a sucrose cushion by ultracentrifugation at 40.000 rpm for 2 h. The trVLP pellets were resuspended in PBS, samples were subjected to a 10 % SDS-PAGE and analyzed by Western blot. For detection of ZEBOV proteins, the EBOV#36 serum was used while for specific detection of $GP_2$ cleavage site product the V5 epitope antibody was used. **B**) Reporter gene activity in p0 producer cells. Relative luciferase activity was measured in lysates of p0 cells, in which ZEBOV GP_RRTRR, GP_AGTAA and GP_AGTAAAΔ1&2 trVLPs were generated. Renilla luciferase reporter gene signal was normalized to firefly luciferase activity and GP_RRTRR activity was set to 1. Data shown are mean values (±SD) of five to nine (n=5-9) independent experiments. **C**) RT-PCR detection of *TMPRSS2* mRNA in different cell lines. Total cellular RNA was isolated from 293F, Calu-3, Huh-7 and Vero-TMPRSS2 cells and *TMPRSS2* mRNA (1228 bp) was amplified using TMPRSS2-specific oligonucleotides. $H_2O$ was used as a negative control. **D**) Entry and reporter genome replication of ZEBOV GP trVLPs. Huh-7, VeroE6 and Vero-TMPRSS2 cells were incubated with or without E64d (20 µM) for 1 h and subsequently inoculated with trVLPs bearing ZEBOV GP_RRTRR, GP_AGTAA or GP_AGTAAΔ1&2 for 72 h. Afterward, the cells were harvested and lysed for 30 min on ice. Renilla luciferase reporter gene signal was normalized to firefly luciferase activity and GP_RRTRR activity was set to 1. Data shown are mean values (±SD) of three to five (n=3-5) independent experiments. For statistical group analysis of differences between untreated ZEBOV GP variants, a one-way ANOVA with subsequent Dunnett´s multiple comparison test was performed. Further comparison of treated and untreated samples was statistically analyzed by two-sample t-test with Welch's correction. Statistically significant p values are represented as followed: ≤ 0.05 (*), ≤ 0.01 (**), ≤ 0.001 (***) and ≤ 0.0001 (****), whereas p values of >0.05 were considered not significant (ns).

Entry studies with the three trVLP variants were performed as previously described in pre-transfected Huh-7 cells, as well as in VeroE6 and Vero-TMPRSS2 cells, that were also used in rVSVΔG ZEBOV GP pseudovirus growth kinetics (4.1.3, 4.1.4 and 4.1.5). TMPRSS2-specific mRNA detection in a broad panel of immortalized cell lines with one-step RT-PCR (3.2.4) showed no *TMPRSS2* mRNA expression in 293F and Huh-7 cells, whereas low levels of endogenous *TMPRSS2* mRNA could be detected in human bronchial epithelial Calu-3 cells, that were used as a positive control. In comparison to the relatively small amounts of *TMPRSS2* mRNA present in Calu-3 cells, the Vero cells stably expressing TMPRSS2 displayed high levels of *TMPRSS2* mRNA (Figure 17 C). Huh-7, VeroE6 and Vero-TMPRSS2 cells were pre-transfected with the replication complex proteins VP30, VP35, NP and L upon seeding into 6-well cell culture plates and cultivated for 24 h. Prior to the trVLP infection, the three cell lines were either treated with 20 µM E64d for 1 h to block endosomal CatB and CatL or remained untreated. Subsequently, the Huh-7, VeroE6 and Vero-TMPRSS2 cells were inoculated with equal amounts of concentrated trVLPs bearing ZEBOV GP_RRTRR, GP_AGTAA or GP_AGTAAΔ1&2 for 2 h and further incubated in the presence or absence of E64d for 72 h.

The measurement of luciferase reporter signal in Huh-7 cell lysates showed no difference of the relative luciferase activity of ZEBOV GP_RRTRR, GP_AGTAA and GP_AGTAAΔ1&2. Whereas, the treatment with E64d had a significant adverse effect on ZEBOV GP_RRTRR, GP_AGTAA and GP_AGTAAΔ1&2 reporter gene activity. In VeroE6 cells, there was also no decrease in relative luciferase activity of ZEBOV GP_AGTAA-bearing trVLPs compared to the GP_RRTRR wildtype. Interestingly, the infection of Vero-TMPRSS2 cells with ZEBOV GP_AGTAA-containing trVLPs showed a significant increase in reporter gene activity compared to the wildtype GP-bearing trVLPs. In contrast to that, a significant reduction in reporter gene activity was detected for ZEBOV GP_AGTAAΔ1&2-bearing trVLPs in both Vero-TMPRSS2 and VeroE6 cells of 55 % and 67 %, respectively. Treatment with E64d did not reduce the reporter gene activity in VeroE6 cells and Vero-TMPRSS2 cells, with a tendency to increase the luciferase reporter signal. Moreover, for ZEVOV GP_RRTRR and GP_AGTAA inoculated VeroE6 and Vero-TMPRSS2, respectively, an even significant increase in reporter activity was observed under E64d treatment (Figure 17 D). Due to the strikingly different outcome in the trVLP entry studies in Huh-7 cells compared to the VeroE6 and Vero-TMPRSS2 cells multicycle replication of rVSVΔG ZEBOV GP with furin-cleaved and uncleaved GP should be further investigated in Huh-7 cells.

### 4.1.9 Multicycle replication of rVSVΔG ZEBOV $GP_{1/2}$ and $GP_0$ in Huh-7 cells

The previous studies with trVLPs bearing different variants of ZEBOV GP revealed a discrepancy between the entry of reporter luciferase genomes in Huh-7 cells compared to VeroE6 and Vero-TMPRSS2 cells. Hence, growth kinetics with rVSVΔG ZEBOV $GP_{1/2}$ and $GP_0$ virus stocks were performed in Huh-7 cells as already described for VeroE6 and Vero-TMPRSS2 infections (3.4.4).

Huh-7 cells are, like VeroE6 cells, highly susceptible to rVSVΔG ZEBOV GP pseudovirus infection. Hence, similar growth kinetics for rVSVΔG ZEBOV $GP_{1/2}$ and rVSVΔG ZEBOV $GP_0$ were observed in Huh-7 cells (Figure 18). The rVSVΔG ZEBOV $GP_{1/2}$, possessing furin-cleaved GP reached titers of 1.3 x $10^7$ $TCID_{50}$/ml after 48 to 72 h. The rVSVΔG ZEBOV bearing $GP_0$ was also able to efficiently infect the Huh-7 cells and reached viral titers of 1.4 x $10^7$ $TCID_{50}$/ml after 72 h. However, virus growth was delayed in the first 24 h p.i., similar to VeroE6 cell infections (Figure 18 A). As these results again suggested, that there might be a subsequent activation of rVSVΔG ZEBOV $GP_0$ upon infection, further growth kinetics in the presence or absence of MI-1148 and E64d were generated. The treatment of Huh-7 cells with DMSO had no effect on virus replication and served as a control for the DMSO-solved E64d (Figure 18 B). Interestingly, replication of rVSVΔG ZEBOV $GP_{1/2}$ under MI-1148 treatment was only slightly reduced, whereas incubation with E64d had a strong inhibitory effect, especially at early time points of infection, with a 3-log reduction of viral titers after 24 h. Combination of MI-1148 and E64d led to complete inhibition of virus replication in the first 24 h p.i. and resulted in a 5-log reduction of virus titers after 72 h. Similar results were observed for rVSVΔG ZEBOV $GP_0$ infected Huh-7 cells. Here, treatment with MI-1148 had no effect on viral titers, whereas even the single E64d incubation led to a complete initial inhibition of virus replication with a slight increase after 48 h p.i. Moreover, incubation of combined MI-1148 and E64d was not able to further reduce the viral titers (Figure 18 C). Even though E64d had strongly inhibited rVSVΔG ZEBOV GP replication in Huh-7 cells, the effect of additional trypsin-like protease inhibitors BAPA and MI-432 was further investigated. Single treatment with the broad serine protease inhibitor BAPA had no effect on both rVSVΔG ZEBOV $GP_{1/2}$ and $GP_0$ replication. Nevertheless, combined treatment of MI-1148, E64d and BAPA led to complete abrogation of virus replication in Huh-7 cells independent of the processing state of the ZEBOV GP at the point of infection (Figure 18 D, left panel). Interestingly, under the treatment with the structure-based TMPRSS2 inhibitor MI-432 a strong suppressive effect of the single treatment was observed with a 2- to 4-log reduction for both rVSVΔG ZEBOV $GP_{1/2}$ and $GP_0$. Again, the combination of MI-1148, E64d and MI-432 was able to completely inhibit viral replication in Huh-7 cells regardless whether ZEBOV GP was previously primed by furin or not (Figure 18 D, right panel). Due to the high sensitivity of ZEBOV GP to E64d

in pseudovirus and trVLP infections and especially the lack of difference between the response of the individual ZEBOV GP cleavage mutants in the trVLPs studies in Huh-7 cells, the involvement of endosomal CatB and CatL in the processing of ZEBOV $GP_2$ was further investigated.

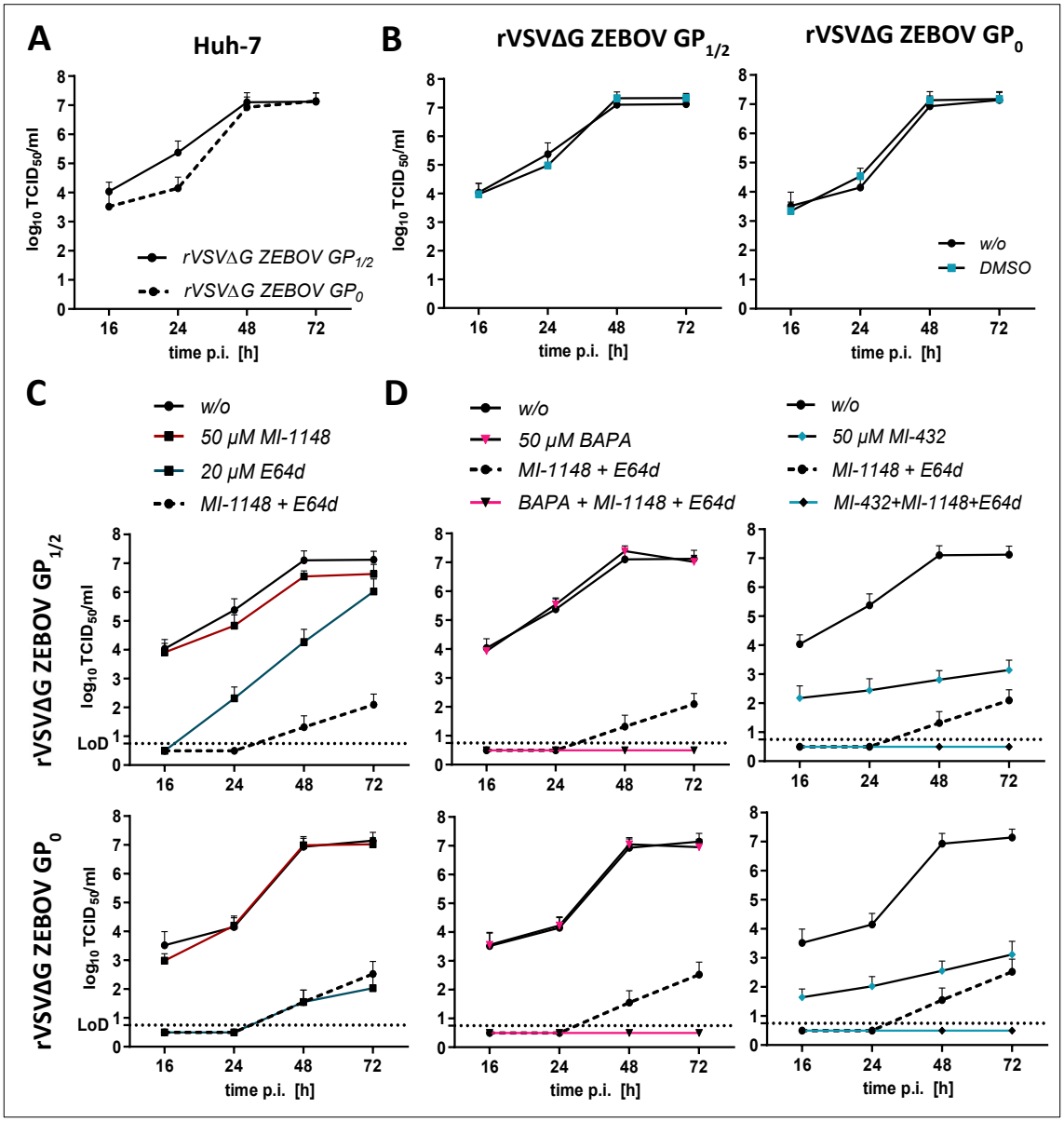


**Figure 18: Multicycle replication of rVSVΔG ZEBOV expressing cleaved ($GP_{1/2}$) or uncleaved ($GP_0$) glycoprotein in the presence or absence of protease inhibitors in Huh-7 cells.**
Comparative growth kinetics of rVSVΔG ZEBOV $GP_{1/2}$ or $GP_0$ in Huh-7 cells infected with a MOI of 0.005. **A**) Viral titers of rVSVΔG ZEBOV $GP_{1/2}$ or $GP_0$ without inhibitor treatment. **B**) Growth kinetics in the presence of the solvent DMSO as a control. Applied concentration corresponds to the amount used in DMSO-solved inhibitor E64d. **C**) Multicycle replication of rVSVΔG ZEBOV $GP_{1/2}$ or $GP_0$ during single and combined E64d and MI-1148 treatment. **D**) Growth kinetics under triple inhibitor treatment with E64d, MI-1148 and broad trypsin-like protease inhibitor BAPA or the structure-based TMPRSS2 inhibitor MI-432. For all studies, Huh-7 cells were treated with 50 µM MI-1148, 20 µM E64d and 50 µM of trypsin-like protease inhibitors (BAPA and MI-432) for 1 h prior to rVSVΔG ZEBOV GP infection. Afterward, the cells were infected with rVSVΔG ZEBOV $GP_{1/2}$ or $GP_0$ at a MOI of 0.005 for 1 h. Protease inhibitor treatment was continued during 72 h incubation period. Virus supernatants were collected at 16, 24, 48 and 72 h p.i. Viral titers were determined by $TCID_{50}$ endpoint dilution assay. Data shown are means (±SD) of three to five independent experiments (n=3-5).

### 4.1.10 Proteolytic cleavage of ZEBOV GP_AGTAA and ZEBOV GP_AGTAAΔ1&2 by recombinant CatB and CatL

The high sensitivity of rVSVΔG ZEBOV GP in Huh-7 cells to E64d and especially the prominent entry inhibition of trVLP bearing ZEBOV GP cleavage variants in these cells led to the conclusion, that endosomal cathepsins might play an additional role in the processing of the ZEBOV $GP_2$ subunit. Hence, ZEBOV GP_AGTAA and ZEBOV GP_AGTAAΔ1&2 were transiently expressed in HeLa cells for 24 h as described above (3.1.2) and subsequently processed by recombinant CatB (rCatB), recombinant CatL (rCatL) or thermolysin (3.2.13). Thermolysin has been described to functionally mimic the proteolytic cleavage of the ZEBOV $GP_1$ subunit by CatB and CatL very efficiently (Schornberg *et al.*, 2006; Kaletsky *et al.*, 2007; Dube *et al.*, 2009; Schornberg *et al.*, 2009), and was therefore used as a positive control. After the treatment of the cellular pellets with the exogenous proteases, the pellets were lysed and subjected to SDS-PAGE and immunoblotting (3.2.12).

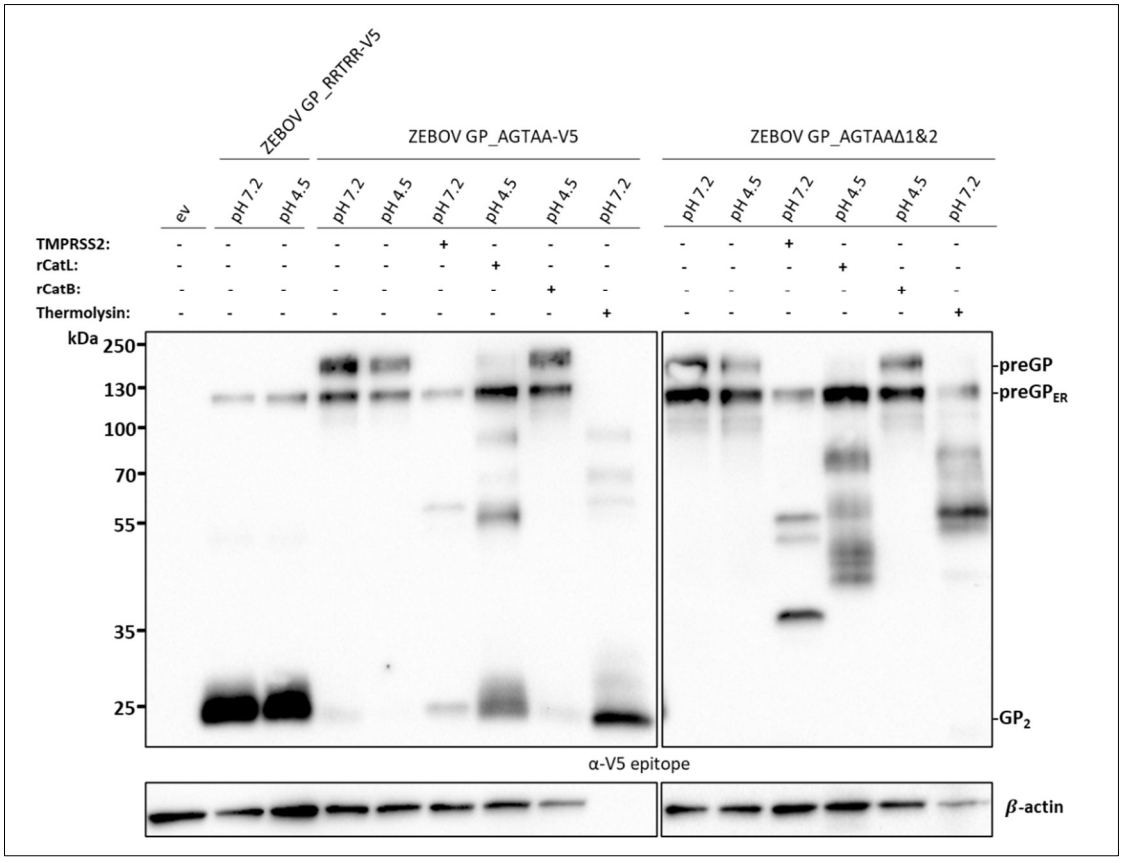


**Figure 19: Proteolytic cleavage of ZEBOV GP_AGTAA and GP_AGTAAΔ1&2 by recombinant CatB and CatL.** Hela cells were co-transfected with plasmids encoding for ZEBOV GP_AGTAA or ZEBOV GP_AGTAAΔ1&2 and human TMPRSS2 or pCAGGS (ev) for 24 h. Subsequently, the cells were harvested and cellular pellets were incubated with 25 µg/ml of recombinant CatB or CatL (rCatB or rCatL) in co-transfection medium at pH 4.5 or with 25 µg/ml thermolysin at pH 7.5 for 1 h at 37 °C. Then, the pellets were lysed and the samples subjected to a 10 % SDS-PAGE and immunoblotting. ZEBOV GP cleavage products were detected using an antibody specific for V5 epitope at the C-terminal end of ZEBOV GP. Detection of cellular ß-actin was used as a loading control. Western blots shown are representative immunoblots of four independent experiments (n=4).

The GP cleavage products were analyzed by immunoblotting using a V5-epitope antibody. Incubation of ZEBOV GP_RRTRR-, GP_AGTAA- and GP_AGTAAΔ1&2-expressing HeLa cell pellets in co-transfection medium with pH 4.5 did not alter furin cleavage of GP_RRTRR or induce endogenous cleavage of the GP_AGTAA and GP_AGTAAΔ1&2 protein and served as a control for the cathepsin low pH medium conditions (Figure 19, lane 2-5 and 10-11). Interestingly, the Western blot analysis revealed a very efficient cleavage of ZEBOV GP_AGTAA by thermolysin and rCatL into a 20 kDa $GP_2$ product that was also generated by co-expression with TMPRSS2. In contrast, incubation with rCatB was not able to process preGP as no detectable reduction of the 160 kDa precursor was observed. The detected faint $GP_2$ band was found with the same intensity in one of the untreated controls and was therefore considered as background (Figure 19, lane 4 and 8). Treatment of the generated furin and TMPRSS2 cleavage mutant ZEBOV GP_AGTAAΔ1&2 with exogenous thermolysin and rCatL did not process the GP protein into the 20 kDa $GP_2$ product. However, several cleavage fragments with higher molecular weights appeared between 80 and 45 kDa. Again, incubation with rCatB had no effect on the cleavage of the preGP of ZEBOV GP_AGTAAAΔ1&2. Interestingly, co-expression of TMPRSS2 with this furin and TMPRSS2 cleavage mutant of ZEBOV GP also displayed a pattern of cleaved GP with two cleavage fragments appearing at a high molecular weight and a very prominent 40 kDa protein band (Figure 19, lane 12-15). These data suggested, that proteolytic processing of ZEBOV GP_AGTAA into the fusion-competent 20 kDa $GP_2$ could not only be provided by furin and TMPRSS2, but also unexpectedly by rCatL. In addition, the detected cleavage products with higher molecular weights appearing for ZEBOV GP_AGTAAΔ1&2 might still be able to fold into the GP fusion loop and therefore explain the fusion competent phenotype in trVLP studies. To investigate the possible effect of endosomal cathepsins on the different outcome of the previous rVSVΔG ZEBOV GP pseudovirus and trVLP infection studies, CatB and CatL activity in Huh-7, VeroE6 and Vero-TMPRSS2 cells were analyzed.

### 4.1.11 CatB and CatL activity in Huh-7, VeroE6 and Vero-TMPRSS2 cells

Growth kinetics with rVSVΔG ZEBOV GP pseudovirus and entry studies with ZEBOV GP-bearing trVLPs in Huh-7 cells demonstrated a high sensitivity towards the CatB and CatL inhibitor E64d (4.1.8 and 4.1.9). In contrast, in VeroE6 and Vero-TMPRSS2 cells this prominent effect of endosomal cathepsin inhibition on virus entry and replication was not observed (4.1.8, 4.1.5 and 4.1.3). The previous data showed an unexpected efficient processing of ZEBOV GP_AGTAA at or near the mutated furin cleavage site by rCatL. Taken together with the already described trimming of the $GP_1$ subunit by CatB and CatL for RBD exposure (Chandran *et al.*, 2005; Schornberg *et al.*, 2006; Kaletsky *et al.*, 2007; Brecher *et al.*, 2012), it should be further investigated, whether endosomal CatB and CatL levels could be responsible for the different cell line observations. Thus, the activity of CatB and CatL in Huh-7, VeroE6 and Vero-TMPRSS2 cell lysates was determined, using commercially available cathepsin activity assay kits.

CatB and CatL activity was measured in whole cell lysates of confluent Huh-7, VeroE6 and Vero-TMPRSS2 cells grown in T75 cell culture flasks. The cellular monolayer was harvested on ice and centrifuged at 8000xg for 5 min at 4 °C. Subsequently, the cell pellets were resuspended in CatB or CatL lysis buffer and kept on ice for 10 or 30 min, respectively. Then 5 µg of the cellular lysates were transferred to a black 96-well plate and incubated either with protease inhibitors BAPA, MI-1148 or E64d or remained untreated for 1 h on ice. Afterward, the Ac-RR-AFC substrate for CatB or the Ac-FR-AFC substrate for CatL activity detection was added. The fluorescence signal of free AFC after cathepsin cleavage was measured over 2.5 h to generate enzyme kinetics of CatB and CatL in the cellular lysates.

As commercially available kits were used, the specificity of the provided AFC substrates was initially determined with rCatB and rCatL. Incubation of Ac-RR-AFC substrate provided in the CatB activity kit with rCatL showed no luminescence signal over time, indicating that there is no cleavage of the substrate. In contrast to that, rCatB was able to cleave the Ac-FR-AFC substrate provided in the CatL activity kit. The enzyme kinetics displayed a fast turnover of AFC substrate by rCatB, which was inhibited by the treatment with E64d (Figure 20 A). The CatB assay kit was therefore specific for the activity of CatB, while in the following studies CatL activity had to be considered as a mixed substrate cleavage by CatL and CatB.

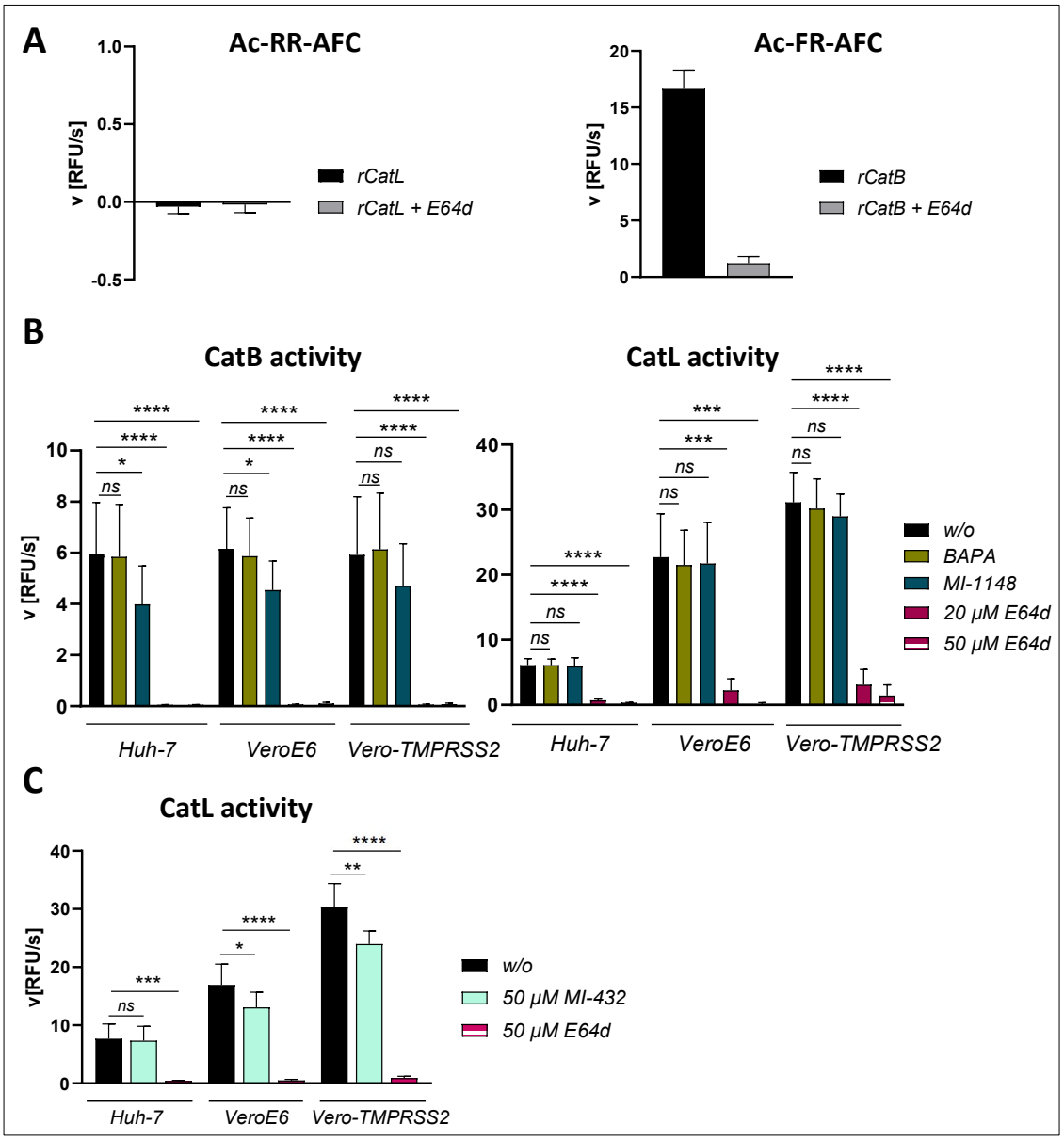


**Figure 20: CatB and CatL activity in Huh-7, VeroE6 and Vero-TMPRSS2 cell lysates.**
**A**) Specificity assessment of commercial CatB and CatL activity assay kits. Recombinant CatL (rCatL) was incubated with Ac-RR-AFC substrate from CatB assay kit while rCatB was incubated with the Ac-FR-AFC substrate from CatL assay kit. Protease activity of 10 ng recombinant protein was measured as substrate turnover within 2.5 h (PFU/s). Treatment with cysteine protease inhibitor E64d (20 µM) was used as a control for specific cathepsin activity in the sample. The shown data are means of six to ten replicates (± SD) from three independent experiments (n=3). **B**) Lysates of Huh-7, VeroE6 and Vero-TMPRSS2 cells were incubated with or without the protease inhibitors BAPA, MI-1148, or E64d in the indicated concentrations for 1 h on ice. Subsequently, either Ac-RR-AFC (CatB) or Ac-FR-AFC substrate (CatL) (PromoCell) were added to the samples and substrate turnover was detected as fluorescent signal over 2.5 h (RFU/s). The shown data are means of four to nine replicates (± SD) from three independent experiments (n=3). **C**) Lysates of Huh-7, VeroE6 and Vero-TMPRSS2 cells were incubated with or without protease inhibitors M-432 and E64d in the indicated concentrations for 1 h on ice. Subsequently, CatL substrate Ac-FR-AFC (Novus Biologicals) was added to the samples and substrate turnover was detected as fluorescent signal over 2.5 h (RFU/s). The shown data are means of seven replicates (± SD) from three independent experiments (n=3). For statistical analysis of untreated cathepsin activity in comparison to inhibitor-treated samples, a two-sample t-test with Welch's correction was performed. Statistically significant p values are represented as followed: ≤ 0.05 (*), ≤ 0.01 (**), ≤ 0.001 (***) and ≤ 0.0001 (****), whereas p values of >0.05 were considered not significant (ns).

The measurement of CatB activity in Huh-7, VeroE6 and Vero-TMPRSS2 cell lysates showed no difference between the three cell lines with a maximum turnover rate, measured as increase of fluorescence over time, of about 6 RFU/s. The incubation with BAPA had no effect on CatB activity, while MI-1148 decreased the substrate turnover rate to 4.4 RFU/s. This could be due to a low background processing of the dibasic RR motif of the CatB substrate by endogenous furin within the cellular lysates. Incubation with 20 and 50 µM E64d led to a strong significant inhibition of enzyme activity with reduced turnover rates of about 0.07 and 0.1 RFU/s, respectively (Figure 20 B, left panel). Different observations were made for CatL activity in the three cell lines. CatL substrate cleavage in Huh-7 cell lysates had a comparable velocity of 6 RFU/s to the measured CatB activity. Nevertheless, the detected activity was not inhibited by BAPA or MI-1148 but could be completely abrogated by E64d treatment. In contrast to that, CatL activity clearly differed in VeroE6 and Vero-TMPRSS2 cells. The velocity of Ac-FR-AFC substrate turnover measured in VeroE6 cells was 3 times higher with values of 22.7 RFU/s and even 5 times higher in Vero-TMPRSS2 cells with 31.1 RFU/s compare to the Huh-7 cell lysate activity. In both Vero cell lines, inhibitor treatment with BAPA and MI-1148 did not reduce CatL activity. Whereas, the incubation of Vero-TMPRSS2 cells with 20 or 50 µM E64d resulted in a highly significant 10- to 20-fold decrease of measured protease activity, respectively. Moreover, treatment of VeroE6 cells with 50 µM E64d led to a 200-fold reduced cathepsin substrate turnover. Interestingly, low levels of cathepsin activity were still measured in the cell lysates of VeroE6 and Vero-TMPRSS2 cells with the assay standard concentration of 20 µM E64d as used in the trVLP and rVSVΔG ZEBOV GP studies (Figure 20 B, right panel). Due to a change in CatL activity assay kit provider the effect of MI-432 was measured separately in Huh7, VeroE6 and Vero-TMPRSS2 cell lysates. The untreated control cell lysates of each cell line resulted in similar substrate turnover rates with 7.3 RFU/s for Huh7, 16.7 RFU/s for VeroE6 and 29.6 RFU/s in Vero-TMPRSS2 lysates (Figure 20 C). Again treatment with 50 µM E64d led to the complete inhibition of CatL activity with a maximum of 1 RFU/s. Interestingly, the treatment with the serine protease inhibitor MI-432 had no effect in Huh-7 cell lysates but CatL activity was reduced to 13 RFU/s in VeroE6 and to 23.7 RFU/s in Vero-TMPRSS2 cell lysates. Taken together, CatB and CatL activities found in whole cellular lysates of each cell line were strongly inhibited by E64d, even though complete activity abrogation was only achieved with higher concentrations of 50 µM, while incubation with MI-432 and MI-1148 only slightly reduced enzyme activity of CatL and CatB, respectively.

### 4.1.12 Recognition of highly truncated ZEBOV GP variants by furin

The data so far showed that the ZEBOV GP_AGTAA cleavage mutant could be proteolytically processed, at or adjacent to the mutated furin motif, not only by the serine protease TMPRSS2 but also by the endosomal cysteine protease CatL. Furthermore, this cleavage could not be abrogated by the ZEBOV GP_AGTAAΔ1&2 mutants with broad deletions of 32 aa upstream and 9 aa downstream of the AGTAA motif. Even though cleavage products of ZEBOV GP_AGTAAΔ1&2 appeared to have a higher molecular weight than the fusion competent 20 kDa $GP_2$, trVLP assays revealed functionality of those higher molecular weight $GP_2$ forms. Therefore, the main goal was to generate an in fact uncleavable GP variant in order to prove the importance of proteolytic activation for ZEBOV. Thus, highly truncated ZEBOV GP mutants were generated, to further decrease the possibility of proteolytic cleavage at an unknown position by proteases expressed in the host cell. As the broad deletion of aa sequences could result in extensive conformational changes, the initial approach was to generate the truncated ZEBOV GP in the wildtype sequence. The retained RRTRR furin cleavage site motif would enable the recognition of non-functional alterations of the ZEBOV GP.

Based on the already slightly truncated ZEBOV GP_RRTRRΔ1&2_V5 pCAGGS construct, first the glycan cap, as well as the MLD, were deleted (ZEBOV GP_RRTRRΔgly/mucΔ1&2) by site-directed mutagenesis using specific oligonucleotide pairs (3.2.5) (Table 15 and Table 16). This was followed by stepwise insertions of 4, 5 and 9 alanine at position 502 (ZEBOV GP_RRTRRΔgly/mucΔ1&2_4A, 5A, 9A) and the restored EVIVNAQPK motif (ZEBOV GP_RRTRRΔgly/mucΔ1). The ZEBOV GP_RRTRRΔgly/mucΔ1 was further enlarged with a 10 aa wildtype AGVAGLITGG sequence upstream of the furin cleavage site motif (ZEBOV GP_RRTRRΔ190-486). The generated constructs (Figure 21 A) were transiently expressed in HeLa cells for 24 h (3.1.2) to allow for endogenous furin cleavage. Subsequently, the harvested cell pellets were incubated in cell lysis buffer and further analyzed by SDS-PAGE and Western blot analysis using the V5 epitope tag antibody (3.2.12).

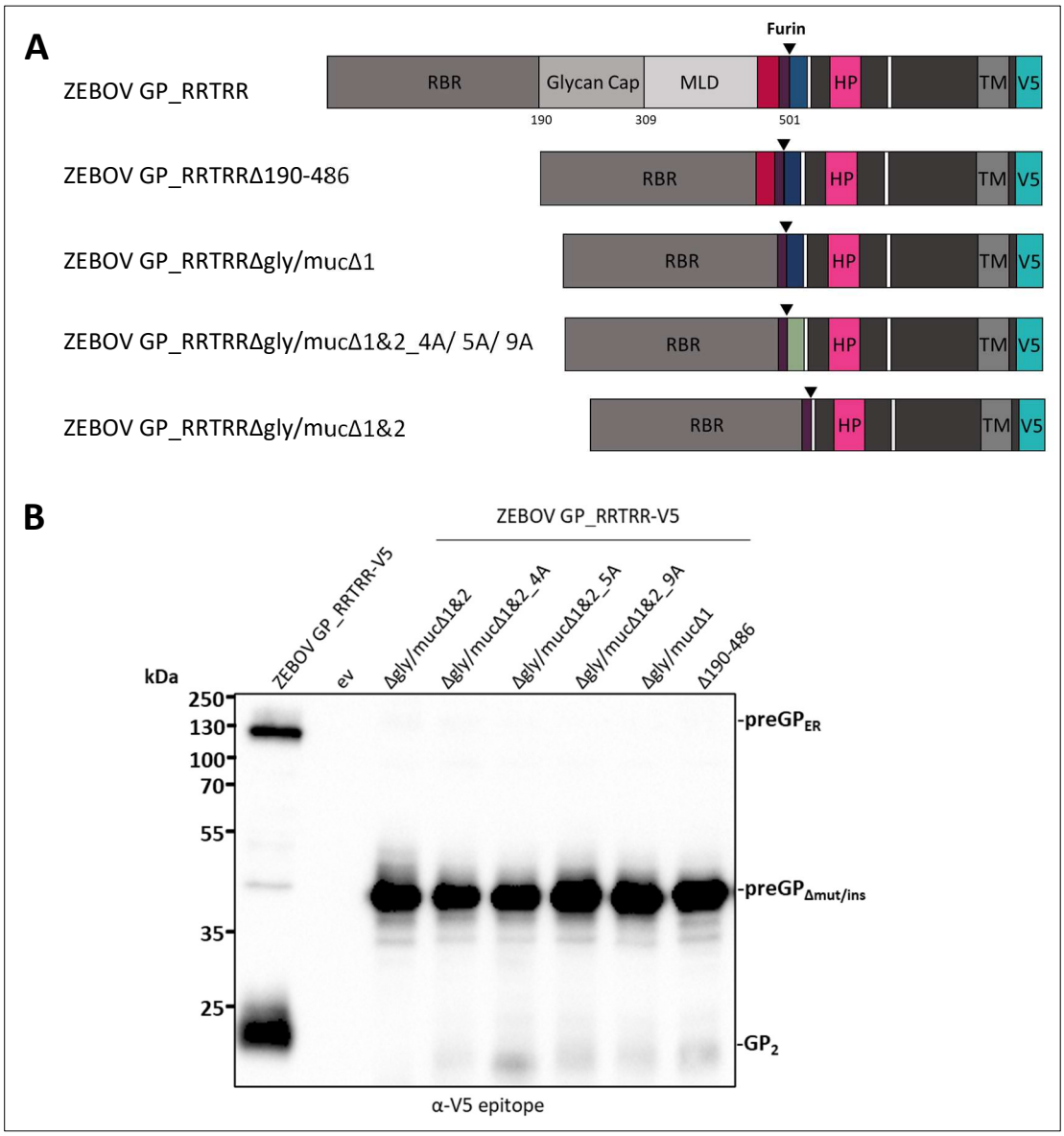


**Figure 21: Recognition of highly truncated ZEBOV GP_RRTRR variants by furin.**
**A**) Schematic illustration of different ZEBOV GP_RRTRR deletion and insertion mutants. Deletion of the glycan cap and MLD (Δgly/muc) in combination with aa deletions from position 465 to 496 and 502 to 510 (Δ1&2). Furthermore, ZEBOV GP_RRTRRΔgly/mucΔ1&2 variants with alanine (A) insertions at position 502 with stretches of 4, 5 or 9A and upstream wildtype sequence 465 to 496 (Δ1) restoration, as well as downstream wildtype sequence insertions from 465 to 486 (Δ190-486). The furin cleavage site within the truncated GP variants is indicated by an arrowhead. **B**) Proteolytic cleavage of ZEBOV GP_RRTRR mutants by endogenous furin. HeLa cells were transfected with ZEBOV GP_RRTRR variants in pCAGGS or ev for 24 h. The cells were then harvested, lysed and the samples subjected to a 12 % SDS-PAGE and analyzed by immunoblotting. ZEBOV GP cleavage products were detected with a V5 epitope-specific antibody. Non-mutated full-length ZEBOV GP_RRTRR was used as a positive control for furin cleavage. Western blots shown are representative immunoblots of two independent experiments (n=2).

Transient expression of the ZEBOV GP_RRTRR wildtype protein resulted in the prominent 20 kDa furin cleavage product that would also be expected for the truncated ZEBOV GP_RRTRR variants, as long as the deletions did not lead to drastic conformational changes (Figure 21 B, lane 1). The Western blot analysis displayed that all truncated variants were efficiently expressed with strong detectable preGP bands at approximately 45 kDa (Figure 21 B, lane 3-8). Nevertheless, cleavage of the transiently expressed highly truncated ZEBOV GP_RRTRRΔgly/mucΔ1&2 by endogenous

furin was abrogated (Figure 21 B, lane 3). The insertion of 4, 5 and 9 alanine stretches at position 502, as well as up- and downstream wildtype sequence insertions were able to restore the processing of ZEBOV GP_RRTRRΔgly/mucΔ1&2 by furin, with the five alanine construct showing the most prominent cleavage product (Figure 21 B, lane 4-8). However, furin processing was much less efficient in all shortened GP variants compared to the ZEBOV GP_RRTRR wildtype, with only faint detectable bands at 20 kDa, leaving the question whether the restored $GP_2$ cleavage products would still be functional.

The studies in rVSVΔG ZEBOV GP pseudovirus infected cells under combined MI-1148, E64d and BAPA treatment revealed a possible involvement of at least one trypsin-like protease in the activation of ZEBOV GP. TMPRSS2 expression did increase rVSVΔG ZEBOV GP pseudovirus replication and was furthermore able to process the furin cleavage mutant ZEBOV GP_AGTAA at an unknown position between aa 465-496 into the fusion competent $GP_2$ product. Moreover, a so far not described cleavage of ZEBOV GP_AGTAA by rCatL at or around the mutated furin cleavage site was shown. Interestingly, the protease dependency of ZEBOV GP clearly differed in Huh-7, VeroE6 and Vero-TMPRSS2 cells. Endosomal cathepsins were crucial for the entry of ZEBOV GP trVLPs in Huh-7 cells, while this was not the case for the used Vero cell lines. Hence, other host cell protease(s) seemed to be involved in VeroE6 and Vero-TMPRSS2 cells at this step. Taken together, the proteolytic activation of ZEBOV GP has been shown to be more complex than the previously described activation by furin and endosomal CatB and CatL, with ZEBOV GP highly accessible to various host cell proteases.

## 4.2 Characterization of SARS-CoV-2 S processing by host cell proteases

### 4.2.1 Proteolytic cleavage of SARS-CoV-2 S by furin and TMPRSS2

The 2019 newly emerged SARS-CoV-2 has led to a worldwide pandemic, which two years after its onset is still ongoing. CoVs belong to a large family of enveloped, (+)ssRNA viruses. The viral 30 kDa genome encodes for several viral proteins, including the surface fusion S protein (Harrison *et al.*, 2020; Khailany *et al.*, 2020). Similar to the ZEBOV GP, it has been observed that S of the *Sarbecovirus* lineage member SARS-CoV is activated in a multistep cleavage process. The S protein has been shown to be cleaved at two distinct sites, the S1/2 and the S2' site within the protein. Cleavage at the S1/2 site resulted in the separation of the subunits S1 and S2 which subsequently remain non-covalently bound. The second S2' cleavage site is located upstream of the fusion peptide. Hence, processing of the S2' site leads to a fusion competent S2' subunit (Belouzard *et al.*, 2009; Millet & Whittaker, 2015). Several host cell proteases have been shown

to proteolytically activate CoV in vitro including furin, TMPRSS2 and CatL (Hoffmann *et al.*, 2018), but whether the novel SARS-CoV-2 S shares the proteolytic activation mechanism and the involved host cell proteases should be investigated in the following.

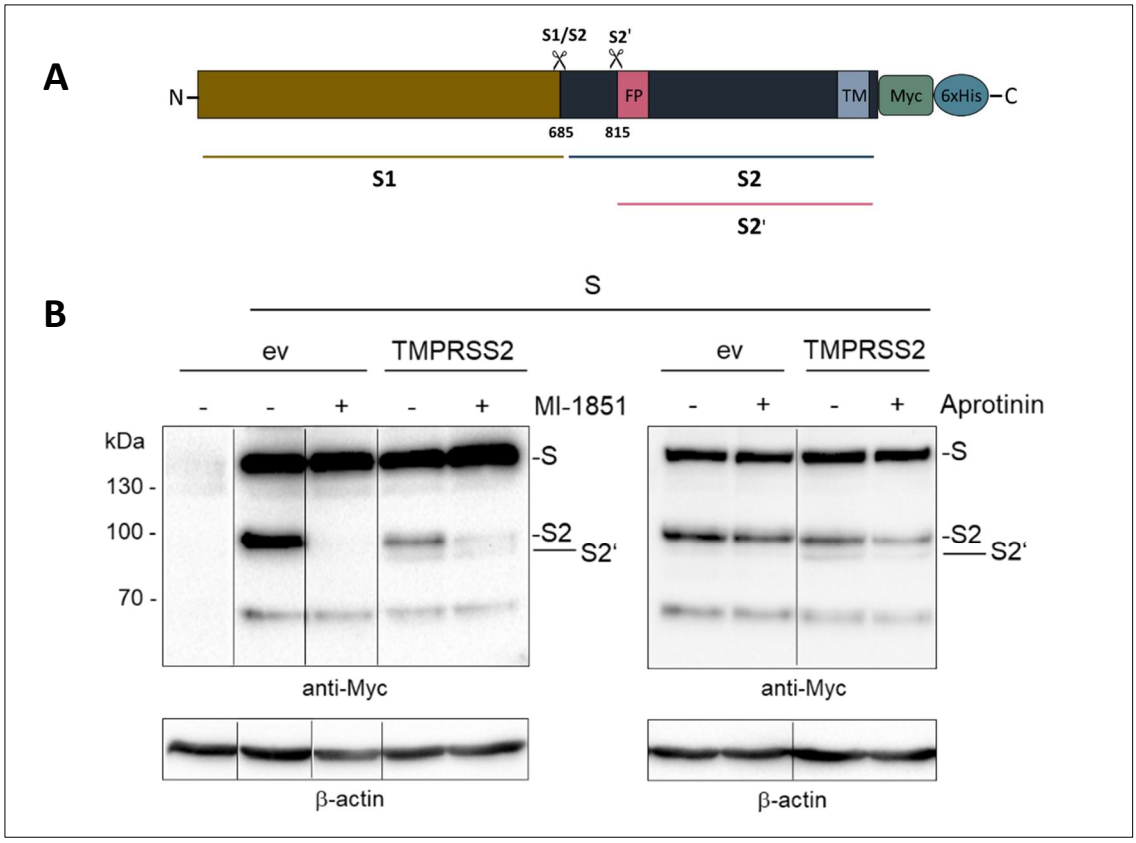


**Figure 22: Proteolytic cleavage of SARS-CoV-2 spike (S) by furin and TMPRSS2.**
**A**) Schematic illustration of the SARS-CoV-2 precursor protein with the two proposed cleavage sites at position 685 (S1/2) and at position 815 (S2'). Cleavage at S1/2 separates S into the S1 (yellow) and S2 (dark blue) subunits, while further cleavage at S2' results in the smaller S2' (pink) segment. The FP and TM domain located in the S2 subunit, as well as the C-terminal Myc-6xHis-tag for immunochemical detection are indicated. **B**) 293F cells were co-transfected with codon-optimized SARS-CoV-2 S-Myc-6xHis (Isolate Wuhan-Hu-1) and human TMPRSS2 in pCAGGS or ev control in the presence or absence of 50 µM furin inhibitor MI-1851 or trypsin-like protease inhibitor aprotinin for 48 h. The cells were harvested and cell lysates were subjected to SDS-PAGE and further analyzed by Western blotting using an antibody directed against the C-terminal Myc-tag. Subsequent β-actin staining served as a loading control. For the shown Western blots spliced lanes from one representative immunoblot of three independent experiments (n=3) were merged together.

Sequence analysis of SARS-CoV-2 S suggested a possible activation of S1/2 cleavage site with the multibasic **RR**A**R**↓ motif by furin, even though the sequence lacks a basic aa at P2, which is preferred. Furthermore, the monobasic PKS**R** motif of the S2' site could be processed by a trypsin-like host cell protease (Appendix Table 33). To investigate the proteolytic activation of the novel SARS-CoV-2 S, the codon-optimized cDNA of the isolate Wuhan-Hu-1 (Table 18) with a C-terminal Myc-6xHis-tag in the expression vector pCAGGS was co-transfected with either empty vector or human TMPRSS2 in 293F cells. The cells were incubated in the presence or absence of furin inhibitor MI-1851 or the broad serine protease inhibitor aprotinin for 48 h. Subsequently, the cellular monolayer was harvested, lysed on ice and subjected to SDS-PAGE

and immunoblotting. The different cleavage products of SARS-CoV-2 S, S2 and S2' were detected with an antibody directed against the C-terminal Myc-tag (Figure 22 A).

Western blot analysis of transiently expressed SARS-CoV-2 S in 293F cells showed that the 160 kDa precursor of S was cleaved by an endogenous protease at the S1/2 cleavage site resulting in a 100 kDa S2 cleavage product (Figure 22 B, left panel, lane 2). Treatment of the cells upon SARS-CoV-2 S transfection with furin inhibitor MI-1851 hindered the cleavage of S precursor (Figure 22 B, left panel, lane 3). Moreover, co-transfection of SARS-CoV-2 S with the plasmid encoding for human TMPRSS2 resulted in an additional smaller 90 kDa cleavage product, designated S2' (Figure 22 B, left panel, lane 4). Simultaneous treatment with MI-1851 resulted in a strong reduction of both cleavage products but did not completely inhibit the processing of S into S2 and S2' (Figure 22 B, left panel, lane 5).

To further investigate the proteolytic cleavage of SARS-CoV-2 S by trypsin-like host cell proteases the transfected 293F cells were incubated with the broad serine protease inhibitor aprotinin, which had no effect on the processing of the S1/2 site by endogenous furin (Figure 22 B, right panel, lane 1-2). In contrast to that, co-expression of SARS-CoV-2 S and TMPRSS2 in the presence of aprotinin resulted in a decrease of the 90 kDa S2' cleavage product (Figure 22 B, right panel, lane 3-4). The data strongly suggested an involvement of both furin and TMPRSS2 in the proteolytic activation of the novel SARS-CoV-2 S protein. Hence, infection studies in human bronchial epithelial Calu-3 cells were performed with authentic SARS-CoV-2 isolate (Table 6) under BSL-3 conditions, in order to investigate protease processing during virus replication in respiratory cells.

### 4.2.2 Replication of SARS-CoV-2 in human Calu-3 airway epithelial cells with furin and TMPRSS2 inhibitors

The previous *in vitro* data showed, that SARS-CoV-2 S was processed by furin at the S1/2 and by TMPRSS2 at the S2' cleavage site (4.2.1). Nevertheless, the proteolytic processing of authentic SARS-CoV-2 S could differ in the context of virus infection in the human target cells. Hence, for the following experiments human Calu-3 airway epithelial cells that express endogenous levels of TMPRSS2 and the SARS-CoV-2 entry receptor ACE2 (Tseng *et al.*, 2005; Böttcher-Friebertshäuser *et al.*, 2011), were infected with the early SARS-CoV-2 isolate Munich 929 under BSL-3 conditions.

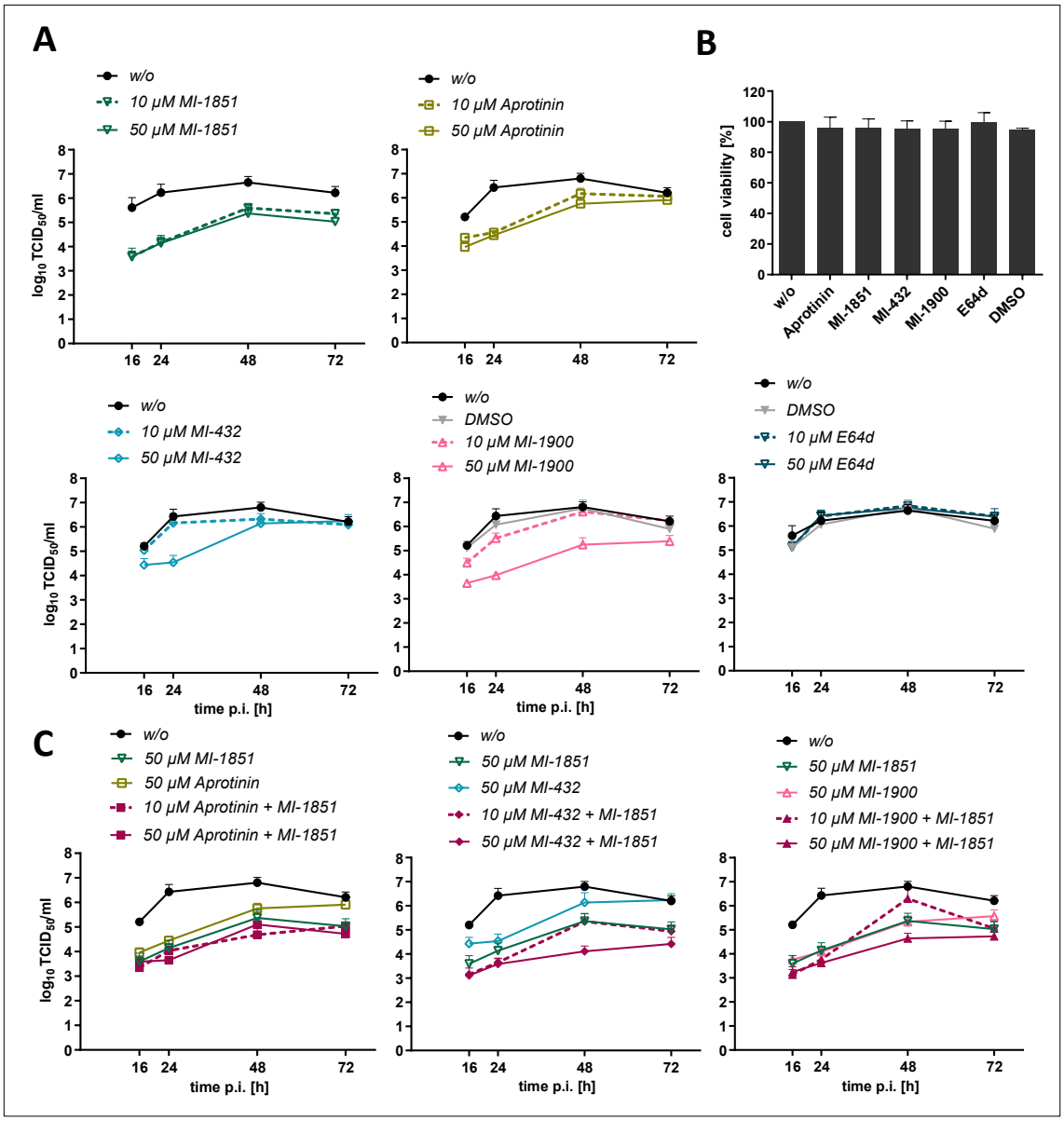


**Figure 23: Multicycle replication of SARS-CoV-2 under furin and trypsin-like protease inhibitor treatment in human Calu-3 cells.**
**A**) Growth kinetics of SARS-CoV-2 (Isolate Munich 929) in human Calu-3 epithelial airway cells. Cells were inoculated with SARS-CoV-2 at a low MOI of 0.001 and incubated in the absence (w/o) or in the presence of trypsin-like protease inhibitors (aprotinin, MI-432 and MI-1900), the furin inhibitor MI-1851 or the cysteine protease inhibitor E64d in the indicated concentrations for 72 h. The incubation with DMSO (0.5 %) served as a control for DMSO-solved inhibitors MI-1900 and E64d. Virus supernatants were collected at 16, 24, 48 and 72 h p.i. Viral titers were determined by $TCID_{50}$ endpoint dilution assay. Data shown are means (±SD) of three to five independent experiments (n=3-5). **B**) Cell viability of Calu-3 cells under protease inhibitor treatment. Calu-3 cells were incubated with 50 µM of the indicated protease inhibitor for 72 h. Untreated cells (w/o) and DMSO-treated cells were used as controls. Cell viability of untreated cells was set as 100 %. Results are mean values (± SD) of three independent experiments (n=3). **C**) Inhibitory effect of combined furin and trypsin-like protease inhibitor treatment in human airway epithelial cells. Calu-3 cells were inoculated with SARS-CoV-2 at a low MOI of 0.001 as described above. The cells were then incubated in the presence of single protease inhibitors or combined inhibitor treatment at the indicated concentrations. Virus supernatants were collected at 16, 24, 48 and 72 h p.i. and viral titers were determined by $TCID_{50}$. Data shown are means (±SD) of three independent experiments (n=3).

Calu-3 cells were inoculated with SARS-CoV-2 at a low MOI of 0.001 for 1.5 h. Subsequently, the cells were cultivated in the presence and absence of protease inhibitors for 72 h (3.4.3). Virus supernatants were collected at 16, 24, 48 and 72 h p.i. and viral titers were determined by $TCID_{50}$

endpoint dilution assay (3.4.1). Growth kinetics in SARS-CoV-2 infected Calu-3 cells showed, that the novel CoV variant sufficiently replicated in human airway epithelial cells reaching maximum titers of 6.4 x $10^6$ $TCID_{50}$/ml after 48 h. Treatment of Calu-3 cells with E64d, an inhibitor for endosomal cathepsins, had no effect on the replication of SARS-CoV-2 (Figure 23 A). In contrast, incubation with the furin inhibitor MI-1851 at a low concentration of 10 µM led to a 2-log reduction of viral titers within the first 24 h p.i., with no further inhibition in the 50 µM higher dose treated cells. Similar inhibitory effects on SARS-CoV-2 replication were observed in Calu-3 cells treated with the broad serine protease inhibitor aprotinin. The replication of SARS-CoV-2 was also strongly inhibited in cells incubated with 10 µM aprotinin, with a 36-fold reduction of viral titers 24 h p.i. Here the higher dose treatment with 50 µM aprotinin had a minor additional effect (Figure 23 A, upper panels). Treatment with the structure-based serine protease inhibitor MI-432 caused a 34-fold reduction of SARS-CoV-2 replication in the early time points at a concentration of 50 µM, while the treatment with a lower concentration (10 µM) had no inhibitory effect. Similar to that, the treatment with another structure-based peptide-mimetic inhibitor MI-1900 also displayed no prominent reduction of viral titers with 10 µM concentrations. Nevertheless, the incubation with 50 µM MI-1900 led to a prolonged 1.5- to 2.5-log inhibition of virus growth over 72 h that was superior to aprotinin treatment in the same concentration (Figure 23 A, lower panels).

In order to exclude a direct adverse effect of the used inhibitors on cell metabolism and viability, the Calu-3 cells were incubated for 72 h with the inhibitors in the highest assay concentration of 50 µM. Subsequently, the cell viability was determined using the "*CellTiter-Glo luminescent cell viability assay*" (Table 20). None of the used protease inhibitors showed a reduction in cell viability compared to the untreated control (Figure 23 B), therefore the antiviral effect was solely carried out by inhibition of the respective host cell proteases.

As the single inhibition of furin and TMPRSS2 led to a strong reduction of viral titers in Calu-3 cells, both seemed to be crucial for the replication of SARS-CoV-2. Thus, it was further assessed whether the combination of furin and TMPRSS2 inhibitors display a possible additive or even synergistic antiviral effect. Simultaneous treatment with 10 µM of MI-1851 and aprotinin was able to suppress SARS-CoV-2 replication with a 4- to 11-fold reduction beyond the respective 50 µM single inhibitor treatment at 48 h p.i. and up to 249-fold lower titers compared to the untreated SARS-CoV-2 growth kinetics (Figure 23 C, left panel). The incubation with higher doses (50 µM) of each MI-1851 and aprotinin had no additional effect. In contrast, the combined treatment of 50 µM MI-1851 and MI-432 led to a continuous reduction of SARS-CoV-2 titers compared to the single 50 µM treated Calu-3 cells, with an additional 17- to 98-fold decrease of

viral titers over the respective single inhibitor treatment at 48 h p.i. (Figure 23 C, middle panel). Compared to the untreated control the simultaneous treatment with 50 µM MI-1851 and MI-432 led to an even up to 598-fold decrease. Similar titer reductions were observed for the 10 µM combination at 16 and 24 h p.i., however, this effect was not sustained. Interestingly, despite the single inhibitor treatment with 50 µM MI-1900 displayed a striking viral titer reduction similar to 50 µM MI-1851, the synergistic antiviral effect of the combined inhibitor treatment did not exceed the inhibition of 50 µM MI-1851 and MI-432 combination (Figure 23 C, right panel). Nevertheless, SARS-CoV-2 replication was strongly inhibited over the 72 h incubation time despite a 4- to 7-fold virus titer reduction over the single inhibitor treatment, the combined incubation of 50 µM MI-1900 and MI-1851 led to a maximum of 640-fold decrease over the untreated control at 24 h p.i.

The co-expression data clearly showed that, as the sequence analysis predicted, the novel SARS-CoV-2 S was processed by endogenous furin at the S1/S and by TMPRSS2 and the S2' site. Furthermore, infection studies under inhibitor treatment with wildtype SARS-CoV-2 in human airway epithelial Calu-3 cells displayed that the cleavage of both furin and TMPRSS2 are crucial for the replication of SARS-CoV-2, as the proteases were not able to compensate for each other.

## 4.3 Subcellular localization of transiently expressed TMPRSS2 in Huh-7 cells

Over the last decades, the involvement of TMPRSS2 in the proteolytic activation of various enveloped viruses has been described (Böttcher-Friebertshäuser *et al.*, 2018). Since its detection in primary human bronchial epithelial cells (HBEC) (Böttcher *et al.*, 2006), it has been shown that cleavage of most IAV HAs strongly depends on TMPRSS2 expression in human and murine airway epithelial cells (Tarnow *et al.*, 2014; Limburg *et al.*, 2019; Bestle *et al.*, 2021). Here, the newly synthesized HA is processed by TMPRSS2 during the transport along the secretory pathway within the TGN (Böttcher-Friebertshäuser *et al.*, 2013), whereas a subsequent activation at the plasma membrane could not be observed (Böttcher-Friebertshäuser *et al.*, 2010). However, proteolytic activation seems to be more complex for other enveloped viruses. Certain CoVs from the *Alpha*- and *Betacoronaviruses*, including HCoV-229E and SARS-CoV, have been described to bud from the host cell with uncleaved S incorporated into the virions, resulting in a subsequent activation by TMPRSS2 at or near the plasma membrane of primary HBECs upon entry (Bisht *et al.*, 2004; Haan & Rottier, 2016; Shirato *et al.*, 2017). The altered cleavage mechanism might be due to the unusual budding site within the ERGIC compartment (Krijnse-Locker *et al.*, 1994;

Stertz *et al.*, 2007), thereby circumventing TMPRSS2 as activating host cell protease during S synthesis and transport. However, as TMPRSS2 was not able to activate IAV at the plasma membrane (Böttcher-Friebertshäuser *et al.*, 2010), it still remains unclear whether CoV S in contrast can be processed at the cell surface or TMPRSS2 is active in the endosomal compartments. Furthermore, our previously shown data suggest a so far not described possible role of TMPRSS2 in the processing of ZEBOV GP, in the absence of the classical activation proteases furin and endosomal cathepsins *in vitro* (4.1.4, 4.1.5 and 4.1.7), leaving the question at which point TMPRSS2 activation of ZEBOV GP could take place. Even though TMPRSS2 has been identified as an important activating host cell protease for the processing of several enveloped viruses, the precise subcellular distribution and localization have yet to be defined. Human Calu-3 and HBECs only display low levels of endogenous TMPRSS2 (Limburg *et al.*, 2019), therefore co-localization studies were performed in transiently TMPRSS2-expressing Huh-7 cells.

Co-localization experiments with cellular compartment proteins were performed in Huh-7 cells, that were seeded onto 12 mm coverslips and subsequently transfected with the pCAGGS TMPRSS2-FLAG plasmid for 24 h (3.1.2). The cells were then fixed either with 4 % PFA or methanol/acetone [1:1], permeabilized and stained with antibodies directed against the FLAG-tag of TMPRSS2 and against the specific compartment proteins EEA1 for the early endosome, Rab7 for the late endosome, the transferrin receptor CD71 for the recycling endosome, TGN38 for the TGN or ERGIC53 for the ERGIC for 1.5 h. Subsequently, the primary antibodies were detected with Alexa-488 or Alexa-568 fluorophore-coupled secondary antibodies that were incubated for 45 min. The IF analysis was performed with the confocal laser scanning microscope, while co-localization was determined on the obtained images with the coloc2 plugin (Fiji).

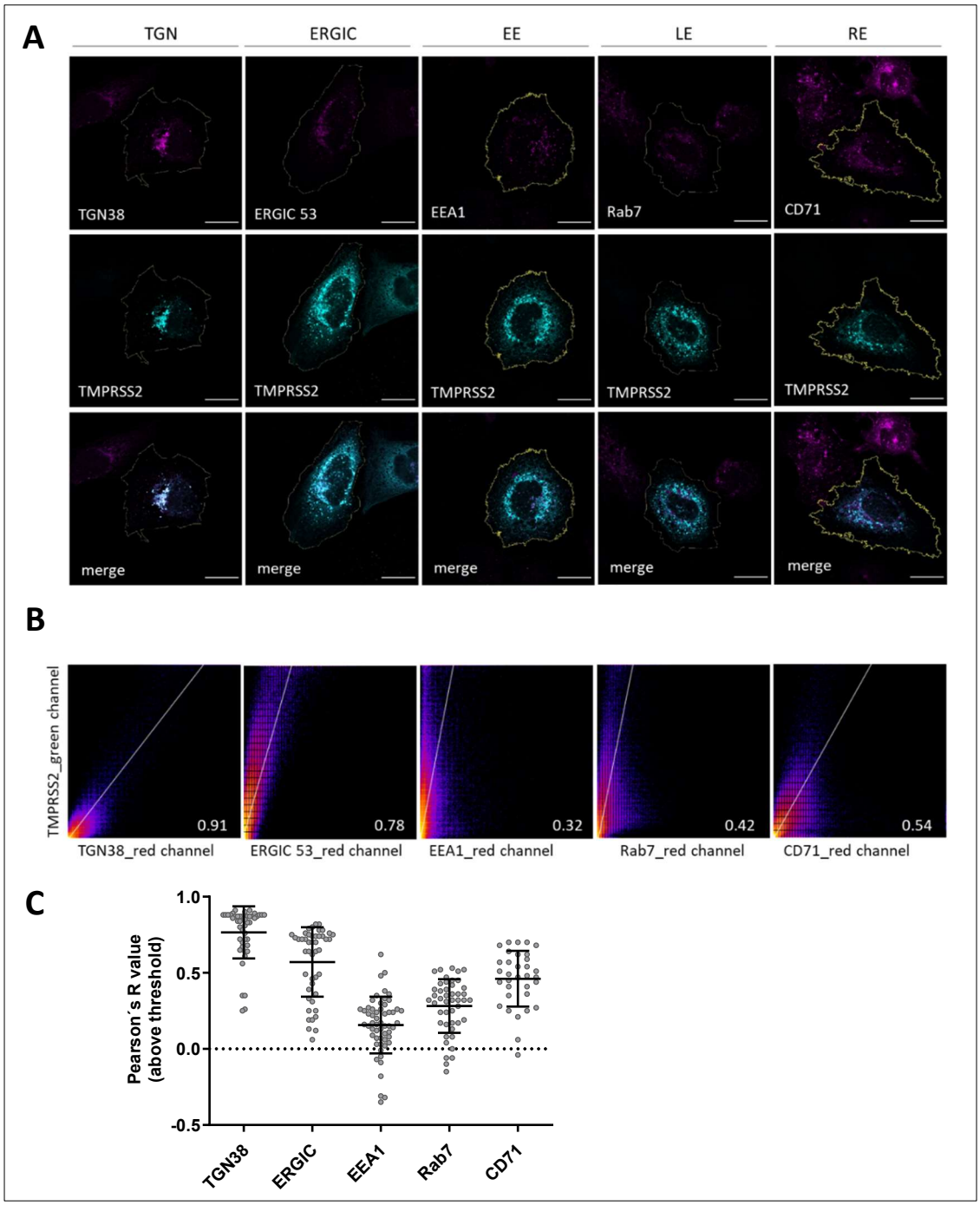


**Figure 24: Subcellular localization of transiently expressed TMPRSS2 in Huh-7 cells.**
**A**) Co-localization of transiently expressed human TMPRSS2 with cellular compartment markers. Huh-7 cells were transfected with pCAGGS encoding for human TMPRSS2 with a C-terminal FLAG-tag for 48 h. Subsequently, the cells were fixed with 4 % PFA or methanol/acetone. Immunocytochemistry (ICC) staining of human TMPRSS2 was performed with a specific FLAG-tag antibody and an Alexa-488-coupled secondary antibody. The subcellular compartments were co-stained with specific antibodies against EEA1 (early endosome, EE), Rab 7 (late endosome, LE), TGN 38 (TGN), ERGIC 53 (ERGIC) and CD71 (recycling endosome, RE) and an Alexa-568-conjugated secondary antibody. The images shown are representative IF images displayed in the red and green channel, as well as a merge. The cellular membrane border (yellow) was defined as the region of interest (ROI), which was used for co-localization analysis (Coloc2, Fiji). **B**) Two-dimensional (2D) intensity histograms with regression line and the Pearson's coefficient above threshold of the representative images shown in A. **C**) Quantification of co-localization with Pearson´s correlation coefficient of human TMPRSS2 with intracellular compartment marker proteins. Data shown are mean values (±SD) of 33 to 56 analyzed cells from three to five independent experiments (n=3-5).

A prominent accumulation of TMPRSS2 in close proximity to the cell nucleus, but also smaller vesicular structures could be observed for the transiently expressed protease in Huh-7 cells (Figure 24 A, middle panels, green channel). Antibody staining against the TGN marker protein TGN38 confirmed previous findings in MDCK II cells (Böttcher-Friebertshäuser *et al.*, 2013), displaying a strong co-localization with TMPRSS2. This was further validated by co-localization analysis, as the two-dimensional (2D) intensity histograms with regression line and the Pearson's coefficient above threshold of this image proved a strong correlation of pixel intensities in red and green channels with an R value of 0.91 (Figure 24 B). ERGIC53 detection in TMPRSS2 transfected Huh-7 cells also showed a high overlap with the FLAG-tag signal of TMPRSS2, with an R value of 0.78. In contrast, early and late endosomal compartment markers EEA1 and Rab7 displayed a relatively low co-localization with the expressed TMPRSS2 with R values of 0.32 and 0.42, respectively. Whereas, the detection of the recycling endosome protein CD71 seemed to partially co-localize with TMPRSS2 to a greater extent, with an R value of 0.54 (Figure 24 A and B). In order to quantify the determined co-localization of TMPRSS2 with the subcellular compartment marker proteins 33 to 56 individual cells were analyzed and Pearson´s R values above threshold were depicted in a dot plot representation (Figure 24 C). The quantification of TGN marker co-localization confirmed the picture of the single image analysis with the highest mean correlation indicated by the Pearson's R value above threshold at 0.76, whereas a population shift to R values of 0.8 to 0.9 was visible. A similar observation was made in ERGIC53 stained cells, with a mean R value of 0.57. However, here also a distinct population with higher R values of 0.7 to 0.8 appeared. In contrast, the measured R values in endosomal compartment protein stained Huh-7 cells were distributed around the mean R values, with almost no co-localization with TMPRSS2 for the EEA1 with a mean R value of 0.15, as an R value of 0 represents random distribution of measured pixels of both channels. For Rab7 the R value with 0.27 was slightly increased hinting toward only low co-localization in the late endosome. The co-staining of TMPRSS2 and CD71 transferrin receptor indicated a partial co-localization within the recycling endosome with an R value of 0.46.

Taken together, the data suggested that transiently expressed TMPRSS2 was not only located as described bevor in the TGN but also in the ERGIC, furthermore partial co-localization also hinted at the abundance of TMPRSS2 in recycling endosome and to a lesser extent in the late endosome compartments.

## 4.4 Summary of the results

In this study, the proteolytic activation of two class I viral fusion proteins by host cell proteases was investigated using *in vitro* infections, as well as co-expression experiments. It was shown that processing of ZEBOV GP is a highly complex process, beyond the furin- and cathepsin-mediated activation. Combined inhibition of these classical activating proteases did not lead to a complete abrogation of rVSVΔG ZEBOV GP replication. Moreover, additional treatment with trypsin-like serine protease inhibitor BAPA revealed the involvement of at least one serine protease during ZEBOV GP activation. Subsequently, the host cell protease TMPRSS2 was shown to enhance rVSVΔG ZEBOV GP replication and proteolytically processed the "non-cleavable" ZEBOV GP_AGTAA mutant at a so far unknown position between aa 465 and 496, leading to a fusion competent $GP_2$ product. Interestingly, human rCatL also cleaved ZEBOV GP_AGTAA at a similar position revealing an up to this date new role of endosomal CatL in ZEBOV GP cleavage besides the trimming of $GP_1$ for NPC1 receptor binding. Subsequently, it was shown that ZEBOV GP protease dependency differed in the used cell lines. In Huh-7 cells active endosomal cathepsins were essential for the entry of ZEBOV GP trVLPs while they were dispensable in VeroE6 and Vero-TMPRSS2 cells indicating the involvement of a so far unknown protease(s) at this step. The ZEBOV GP has been shown to be highly accessible to different host cell proteases, as efforts to generate in fact non-cleavable ZEBOV GP resulted in either residual cleavage or non-functional surface protein.

Our co-transfection studies with the novel SARS-CoV-2 S confirmed the sequence data suggestion that S is processed at the S1/S2 site by furin and at the S2' by TMPRSS2. Moreover, BSL-3 infection experiments in human bronchial Calu-3 cells revealed an essential role for both host cell proteases in the replication of SARS-CoV-2 isolate Munich 929. Replication of SARS-CoV-2 was strongly suppressed by the combination of furin inhibitor MI-1851 and trypsin-like protease inhibitors aprotinin, MI-432 and MI-1900, indicating a high potential of these protease inhibitors as antiviral drugs against COVID-19.

TMPRSS2 was identified as an activating host cell protease for both ZEBOV GP and SARS-CoV-2 S, which have been shown to use different cellular compartments during their replication. Co-localization studies in Huh-7 cells overexpressing human TMPRSS2 revealed a strong accumulation of TMPRSS2 signal within the TGN and ERGIC, with a further partial overlap in the recycling endosomal and to a lesser extent in the late endosomal compartment.

Taken together our studies highlight the importance and necessity of viral fusion protein characterization as it sheds light on the therapeutic potential and range of host cell protease inhibitors for the respective virus. Furthermore, a deeper understanding of the subcellular localization of host cell proteases, like TMPRSS2, helps to assess the spatial-temporal mode of action of protease inhibition.

# 5 Discussion

## 5.1 Cleavage of ZEBOV GP is an important process for virus entry and replication

Conflicting observations have been made over the last decades concerning the proteolytic activation of the ZEBOV GP. *In vitro* studies revealed a sequential activation of ZEBOV GP during virus replication. Endogenous furin initially cleaves the newly synthesized precursor GP at a multibasic RRTRR motif at aa position 501 along the secretory pathway within the TGN (Volchkov *et al.*, 1998; Wool-Lewis & Bates, 1999). The processed ZEBOV $GP_{1/2}$ is then incorporated into newly budding virus particles. After cellular attachment and entry via micropinocytosis, the $GP_1$ subunit is further trimmed by endosomal CatB and CatL in order to expose the RBD (Chandran *et al.*, 2005; Kaletsky *et al.*, 2007; Schornberg *et al.*, 2009; Brecher *et al.*, 2012). This is considered as an essential step for ZEBOV replication, as binding to the endosomal NPC1 receptor has been described as a crucial fusion trigger (Carette *et al.*, 2011; Côté *et al.*, 2011). Nevertheless, subsequent *in vitro* and *in vivo* studies observed no decrease in infectivity and pathogenicity of ZEBOV in CatB or CatL deficient systems (Marzi *et al.*, 2012). Similar results were found for the abrogation of furin cleavage by the exchange of the multibasic RRTRR motif to a non-basic AGTAA motif. Replication and infectivity of these "non-cleavable" GP variants in cell culture and non-human primates were not severely altered (Wool-Lewis & Bates, 1999; Neumann *et al.*, 2002; Neumann *et al.*, 2007), with Wool-Lewis and Bates stating that processing of ZEBOV GP is not required for virus replication.

In this study, the proteolytic activation of ZEBOV GP and especially the previously described ZEBOV GP_AGTAA furin cleavage mutant was further investigated. Replication and initiation of host cell and viral membrane fusion without prior proteolytic activation by host cell proteases is a unique process that has been so far only described for the class III fusion proteins, like the VSV G (Roche & Gaudin, 2002). Protease-independent fusion has not been observed for class I viral surface proteins and would be a highly unusual mechanism for ZEBOV GP. Transient expression of pCAGGS-encoded ZEBOV GP of the 2014 Makona C7 isolate in 293F cells in the presence of the highly potent furin inhibitor MI-1148 very efficiently abrogated the processing of preGP into the $GP_{1/2}$ product even in low concentrations of 0.2 µM (Figure 9 B). Thus, cultivation of recombinant VSVΔG pseudoviruses expressing ZEBOV GP together with 30 µM MI-1148 resulted in the release of virions with incorporated uncleaved preGP (Figure 10 B). Comparative growth kinetics with cleaved rVSVΔG ZEBOV $GP_{1/2}$ and uncleaved rVSVΔG ZEBOV $GP_0$ revealed an initial replication disadvantage for the unprimed $GP_0$, which was overcome after 48 h (Figure 11 B). This difference in the respective replication curves was similar

to the effect observed in VeroE6 infection studies with recombinant ZEBOV viruses with mutated furin cleavage site from the multibasic RRTRR to the non-basic AGTAA motif (Neumann *et al.*, 2002). Thus, suggesting that there might be a furin-independent processing of ZEBOVGP_AGTAA during viral replication. The separate treatment of VeroE6 cells with inhibitors against furin or endosomal cathepsins led to reduced viral titers in rVSVΔG ZEBOV $GP_{1/2}$ and $GP_0$ infected cells, but neither was able to abrogate viral replication. Nevertheless, a combined treatment of infected VeroE6 cells with MI-1148 and E64d had a synergistic effect on the replication of both rVSVΔG ZEBOV $GP_{1/2}$ and $GP_0$ (Figure 11 B). However, even though viral titers could be strongly suppressed by the combined treatment with furin and cathepsin inhibitors no complete suppression of viral multiplicity was observed. The viral titers seemed to increase in all treated samples over time indicating a possible loss of inhibitor potency either by exhaustion due to newly synthesized cellular proteases or inhibitor degradation. Repeated treatment with MI-1148 and E64d over the 72 h infection period might further decrease rVSVΔG ZEBOV GP titers with a prolonged inhibitory effect. Hence, it was hypothesized that processing ZEBOV GP was important for the replication of rVSVΔG ZEBOV, and was mainly performed by furin and endosomal cathepsins. However, other host cell protease(s) could substitute for the cleavage in the absence of classical ZEBOV GP-activating enzymes.

### 5.1.1 Trypsin-like serine protease TMPRSS2 is involved in the activation of rVSVΔG ZEBOV $GP_0$ and was able to process ZEBOV GP_AGTAA *in vitro*

Trypsin-like serine proteases, like TMPRSS2, have been described to proteolytically activate various fusion proteins of enveloped viruses, such as the IAV HA and the S protein of CoVs (Galloway *et al.*, 2018; Hoffmann *et al.*, 2018). Thus, trypsin-like serine proteases could be potential candidates substituting for the processing of ZEBOV GP in the absence of the classical activating proteases furin and endosomal cathepsins. The broad serine protease inhibitor BAPA, exhibiting activity against common TTSPs including HAT, matriptase and TMPRSS2 (Hellstern *et al.*, 2007; Sielaff *et al.*, 2011; Maiwald *et al.*, 2016), further suppressed virus replication in rVSVΔG ZEBOV $GP_0$ infected VeroE6 cells treated with MI-1148 and E64d. In contrast, only a minor additional effect was observed in rVSVΔG ZEBOV $GP_{1/2}$ inoculated cells at 16 h p.i. (Figure 12). Similar to that, the incubation with the structure-based TMPRSS2 and matriptase inhibitor MI-432 (Hammami *et al.*, 2012; Meyer *et al.*, 2013), together with MI-1148 and E64d could suppress replication in early time points of rVSVΔG ZEBOV $GP_{1/2}$ and $GP_0$ infection. However, the combination did not reach the prolonged effect of BAPA seen in rVSVΔG ZEBOV $GP_0$ infections,

probably due to the narrower inhibition spectrum of MI-432. In contrast, no additional antiviral activity was observed for the Kunitz-type proteinaceous inhibitor aprotinin, inhibiting various trypsin-like proteases (Ascenzi *et al.*, 2003). Aprotinin is a polypeptide consisting of 58 aa, with a molecular weight of approximately 6 kDa. Due to the size of this natural inhibitor, the protease inhibition was most likely limited to the extracellular space and plasma membrane. Even though studies observed a low-density lipoprotein receptor-related protein 2 (LRP2)/gp330 receptor-mediated entry and subsequent accumulation of aprotinin in absorptive epithelial cells of the renal proximal tube, uptake into VeroE6 cells seemed to be insufficient (Moestrup *et al.*, 1995; Steinmetzer & Hardes, 2018). Thus, indicating that processing of uncleaved ZEBOV GP rather took place intracellularly than at the plasma membrane. Nevertheless, the findings suggested a role of trypsin-like proteases in the activation of rVSVΔG ZEBOV GP in the absence of furin and endosomal cathepsins. To further investigate the possibility of an alternative activation of ZEBOV GP by TTSPs, such as TMPRSS2, Vero cells stably expressing TMPRSS2 were infected with the furin primed or unprimed rVSVΔG ZEBOV GP viruses (Hoffmann *et al.*, 2020). Interestingly, in this cell line virus replication was highly efficient, as a 10-fold lower initial infectious dose had to be used for similar growth kinetics compared to VeroE6 cells. Moreover, the initial replication disadvantage of rVSVΔG ZEBOV $GP_0$ observed in VeroE6 cell infections completely disappeared in the TMPRSS2-overexpressing Vero cells (Figure 13 A).

However, triple combination using BAPA or MI-432 in addition to MI-1148 and E64d had no further effect on the replication of both rVSVΔG ZEBOV $GP_{1/2}$ and $GP_0$ in Vero-TMPRSS2 cells (Figure 13 D). These cells express high levels of *TMPRSS2* mRNA compared to the endogenous levels detected in Calu-3 cells (Figure 17 C). As these elevated mRNA levels most likely correlate with an increased TMPRSS2 protein expression and activity, the standard assay concentration of 50 µM for the trypsin-like serine protease inhibitors could be insufficient to suppress TMPRSS2 activity in these cells. Therefore, the infection experiments should be repeated with higher doses of BAPA and MI-432 to further prove the involvement of TMPRSS2 in the replication of rVSVΔG ZEBOV in Vero-TMPRSS2 cells. Nevertheless, the data from the comparative growth kinetics of rVSVΔG ZEBOV $GP_{1/2}$ and $GP_0$ strongly implied a role of TMPRSS2 in the proteolytic processing of the uncleaved ZEBOV $GP_0$ variant, suggesting proteolytic cleavage at or around the furin cleavage site upon entry into the host cell.

Hence, the furin-independent proteolytic cleavage of ZEBOV GP was investigated using the previously described AGTAA furin cleavage mutant of ZEBOV GP (Wool-Lewis & Bates, 1999; Neumann *et al.*, 2002; Neumann *et al.*, 2007). Infection studies in Huh-7 cells with trVLPs bearing either ZEBOV GP_RRTRR or GP_AGTAA on their surface, displayed no difference in reporter

activity, representing the entry of reporter genome after membrane fusion, for both GP variants (Figure 14 C). Even though cleavage of ZEBOV GP_AGTAA by furin has been shown to be prevented, the Western blot analysis of trVLP particles revealed alternative processing of GP_AGTAA in the 293F producer cells (Figure 14 A). However, cleavage of ZEBOV GP_AGTAA was not as efficient as for the wildtype GP_RRTRR. Similar observations had been made for a non-basic SGTGG exchange mutant, where about 5 % of the surface GP was still cleaved (Volchkov *et al.*, 2016). Interestingly, small amounts of processed GP seemed to be sufficient for trVLP fusion and entry in Huh-7 cells. Examination of the Western blots generated by Neumann *et al*. with recombinant ZEBOV GP_AGTAA furin cleavage mutants displayed small amounts of 140 kDa $GP_1$, suggesting residual processing at or around the exchanged furin cleavage site during virus production (Neumann *et al.*, 2002). The pretreatment of the Huh-7 cells with protease inhibitor for 1 h prior to trVLP infection showed a 75 % reduction of relative luciferase reporter activity only in E64d treated cells for both GP variants. Single treatment with BAPA or MI-1148 had no negative effect on reporter gene entry, on the contrary enhancing the reporter gene signal to a certain extent. Combined inhibition of furin and endosomal cathepsins displayed a slight additional reduction of reporter signal for ZEBOV GP_RRTRR-bearing trVLPs, but not for the GP_AGTAA exchange mutant. The marginal effect of the E64d and MI-1148 combination for ZEBOV GP_RRTRR-bearing trVLP entry could be due to the cycling of furin between the secretory pathway and the plasma membrane (Molloy *et al.*, 1999). Furthermore, reporter gene expression was slightly reduced in both trVLP variants by the additional treatment with BAPA (Figure 14 C). Together with the data from the rVSVΔG ZEBOV GP infection studies in VeroE6 cells, the entry experiments further displayed the important role of furin and in particular endosomal cathepsins. However, in the absence of both activating proteases trypsin-like protease(s) seemed to be involved in the cleavage of ZEBOV GP during replication and/or possibly upon viral entry. The data indicate that ZEBOV activation is not strictly limited to furin and cathepsin activity, with the ability to use different cellular proteases for the processing of GP.

### 5.1.2 Processing of ZEBOV GP_AGTAA by TMPRSS2 at an unknown position

The subsequent infection studies in Vero-TMPRSS2 cells strongly suggested that the host cell protease TMPRSS2 could play a role in the proteolytic processing of ZEBOV GP during viral replication. A previous study by Wool-Lewis and Bates implicated a high accessibility of the furin cleavage site within the ZEBOV GP structure, resulting in recognition and cleavage by a possible

broad variety of host cell proteases. The exchange of the RRTRR motif to the AGTYF chymotrypsin recognition sequence was still exposed and allowed in vitro cleavage of ZEBOV GP. Moreover, ZEBOV GP was shown to be quite insensitive to mutations at the furin cleavage site, as the dibasic RATAR and more interestingly the monobasic RATAA variants were still processed upon transient expression in 293T cells, whereas only the non-basic AGTAA mutant was not cleaved anymore (Wool-Lewis & Bates, 1999).

In this work, co-expression experiments with TMPRSS2 and a C-terminally tagged ZEBOV GP_AGTAA construct in HeLa cells, revealed processing of ZEBOV GP_AGTAA by TMPRSS2 into a $GP_2$ product with similar molecular weight as the wildtype ZEBOV GP_RRTRR cleaved by endogenous furin (Master thesis, Linda Bittel 2019 and Figure 15 B). TMPRSS2 belongs to the family of TTSPs and preferentially cleaves substrates with a single basic aa, including R or K at the P1 position (Böttcher *et al.*, 2006; Lucas *et al.*, 2014). Interestingly, the ZEBOV GP possesses no basic aa in close proximity to the AGTAA motif. The only three basic aa found were the two lysines K478 and K510, as well as the histidine H516 (Figure 15 A). Mutation of the basic aa to alanine did not alter the recognition and processing by co-expressed TMPRSS2, implicating a more unusual substrate sequence recognized by TMPRSS2 within the ZEBOV GP_AGTAA (Figure 15 C). As the molecular weight of the furin cleavage site mutant processed $GP_2$ by TMPRSS2 did not significantly differ from the furin-cleaved ZEBOV GP_RRTRR wildtype, the proteolytic cleavage had to occur at or near the exchanged AGTAA motif. Nevertheless, a systematic alanine scan of the EVIVNAQP sequence from position 502 to 509, including multiple aa stretches from 502 to 505 (AAAANAQP) and from 506 to 509 (EVIVAAAA), did not abrogate proteolytic processing by TMPRSS2 (Figure 15 B and C). TMPRSS2 seemed to use a rather unconventional aa sequence within the ZEBOV GP_AGTAA protein as a substrate that could not be identified with single or multiple aa exchanges. Hence, as a next step broad sequence stretches of 32 aa upstream (Δ1) and 9 aa downstream (Δ2) of the AGTAA motif were deleted. Transient transfection of HeLa cells with the ZEBOV GP_AGTAA deletion constructs (Figure 16 A) together with TMPRSS2 revealed that proteolytic processing by TMPRSS2 most likely takes place in the upstream region of ZEBOV GP, as only with the Δ1-bearing constructs no 20 kDa $GP_2$ could be detected (Figure 16 B).

High-throughput screening of fluorogenic peptide libraries and mass spectrometry profiling identified the most preferential recognition sequences for TMPRSS2 with a nearly exclusive occurrence of the basic R/K in P1, but also low occupancy of S and H. Nevertheless, a high aa variability in the P2 to P4 positions was observed, with T/F/W/A/Y in P2, E/M/Q/G/Y/V in P3 and G/I/M/P/H in P4. In contrast, other TTSP family members, like hepsin or matriptase, seemed to

be more strict in their aa preferences (Lucas *et al.*, 2014; Mahoney *et al.*, 2021). Studies in our group with IAV demonstrated that TMPRSS2 expression is critical for the activation of almost all IAV HA subtypes. Even though some HAs of these TMPRSS2-dependent subtypes as the A/duck/Ukraine/1/1963 (H3N8) possess these described highly favorable aa in their monobasic cleavage site motif (K**QTR**), other strictly dependent subtypes including the A/Anhui/1/13 (H7N9) with its PKG**R** motif clearly differ, suggesting that TMPRSS2 recognition motifs can be highly variable in the P2 to P4 position (Limburg *et al.*, 2019; Bestle *et al.*, 2021). Sequence analysis of the ZEBOV GP region identified for TMPRSS2-mediated processing from aa 465 to 496 revealed only one monobasic $_{475}$SSG**K**$_{478}$ motif possibly responsible for TMPRSS2 substrate recognition. The aa sequence did not resemble a highly preferred TMPRSS2 substrate motif but could explain the lower levels of cleavage product compared to the RRTRR wildtype $GP_2$ levels detected in the Western blot analysis (Figure 15 and Figure 19). Nevertheless, cleavage of the single alanine exchange mutant ZEBOV GP_AGTAA_K478A by TMPRSSS2 was not inhibited (Figure 15 C), suggesting that the processing in this region is highly unusual. Computational binding analysis of bovine pancreatic trypsin inhibitor (BPTI or aprotinin) P1 variants with trypsin showed, that even though binding of R or K in P1 had the highest affinity, other aa residues like S, H or T showed also low levels of free binding energy, indicating a certain interaction with the S1 pocket of trypsin (Brandsdal *et al.*, 2001). Hence, there could be further tolerated possible substrate aa residues in the P1 position for TMPRSS2 beyond the highly preferred basic R and K. Nevertheless, so far no substrate with a non-basic aa in P1 has been described for TMPRSS2. Studies with the trypsin-like serine proteases matriptase and prostasin revealed a proteolytic cascade within the epidermis, with active matriptase necessary for prostasin activation (Netzel-Arnett *et al.*, 2006). Thus, TMPRSS2 could possibly function as an activation factor for other so far unknown ZEBOV GP_AGTAA activating proteases with a potential broader aa recognition panel in P1. Interestingly, further Western blot analysis displayed an intermediate phenotype of the ZEBOV GP_AGTAA_K478A mutant with a great portion of the ZEBOV GP still cleaved into the 20 kDa $GP_2$. However, a smaller fraction was processed into the higher molecular weight product also detected in the ZEBOV GP_AGTAAΔ1 and GP_AGTAAΔ1&2 variants (Appendix Figure 26). Hence, TMPRSS2 or a downstream protease seemed to be able to process ZEBOV GP_AGTAA_K478A sufficiently, but the loss of the basic K478 initiated the beginning of a switch toward the higher molecular weight products observed for the deletion mutants of ZEBOV GP_AGTAA. The alanine mutation at K478 and the deletion of aa 465-496 might impair the accessibility of the untypical cleavage site, leading to the dislocation of TMPRSS2 or another TMPRSS2-activated protease to a possible new substrate recognition site further upstream, which was either not accessible before and/or less preferential.

The MLD within the $GP_1$ subunit contains several K residues as possible alternative recognition sites for TMPRSS2, including $_{313}$NGP**K**$_{316}$ or $_{297}$LTR**K**$_{300}$ with predicted $GP_2$ cleavage products with molecular weights of 40.51 and 42.22 kDa, respectively (Serial Cloner2.6.1). Thus, processing of the overexpressed ZEBOV GP_AGTAAΔ1&2 within the MLD could lead to the observed higher molecular weight cleavage products during TMPRSS2 co-expression. Whether this possible cleavage mechanism by TMPRSS2 could occur during viral replication is not clear as the MLD is removed by endosomal cathepsins during ZEBOV entry. As a basic aa in the P1 position usually is a prerequisite for trypsin-like protease substrate recognition, it is still not clear where and especially whether TMPRSS2 is directly processing the ZEBOV GP_AGTAA to the approximately 20 kDa product. For a final elucidation of the exact cleavage site, the $GP_2$ subunit of ZEBOV GP_AGTAA resulting from TMPRSS2 co-expression should be analyzed by N-terminal protein sequencing (Laursen, 1971). However, $GP_2$ detection in Coomassie or silver gel staining has been challenging (data not shown) and needs to be further optimized.

Proteolytic cleavage of ZEBOV GP_AGTAA by the trypsin-like serine protease TMPRSS2 was shown to take place at a so far unknown cleavage motif within the region between aa 465 and 496 and resulted in an approximately 20 kDa cleavage product similar to the furin processed ZEBOV GP_RRTRR. Moreover, replication of unprocessed rVSVΔG ZEBOV $GP_0$ in Vero-TMPRSS2 cells had no initial growth delay in contrast to infected VeroE6 cells lacking TMPRSS2, clearly showing a possible additional direct or indirect activation by TMPRSS2.

### 5.1.3 Proteolytic activation of ZEBOV GP is a complex mechanism that could be performed by different host cell proteases

Even though the classical activating proteases furin and CatB and CatL seem to be the host cell proteases predominantly responsible for the processing of ZEBOV GP during virus replication, the previously described data have shown that especially furin cleavage can be substituted by other host cell proteases, including TMPRSS2 at a so far unknown position (Figure 15). Nevertheless, the entry experiments with trVLP bearing ZEBOV GP_AGTAA and GP_AGTAAΔ1&2 variants in Huh-7 compared to VeroE6 cells indicated a strong role of endosomal cathepsins depending on the infected cell type. This could be the reason for highly contradicting findings on cathepsin dependency for the EBOV subtypes over the last years. Inhibition of CatB and CatL in 293T cells led to decreased viral entry for REBOV, BEBOV, SEBOV and TAFV suggesting a conserved role of cathepsin activation in the EBOV family, while this overall effect was not

observed in cysteine protease inhibitor-treated VeroE6 cells (Gnirss *et al.*, 2012; Marzi *et al.*, 2012).

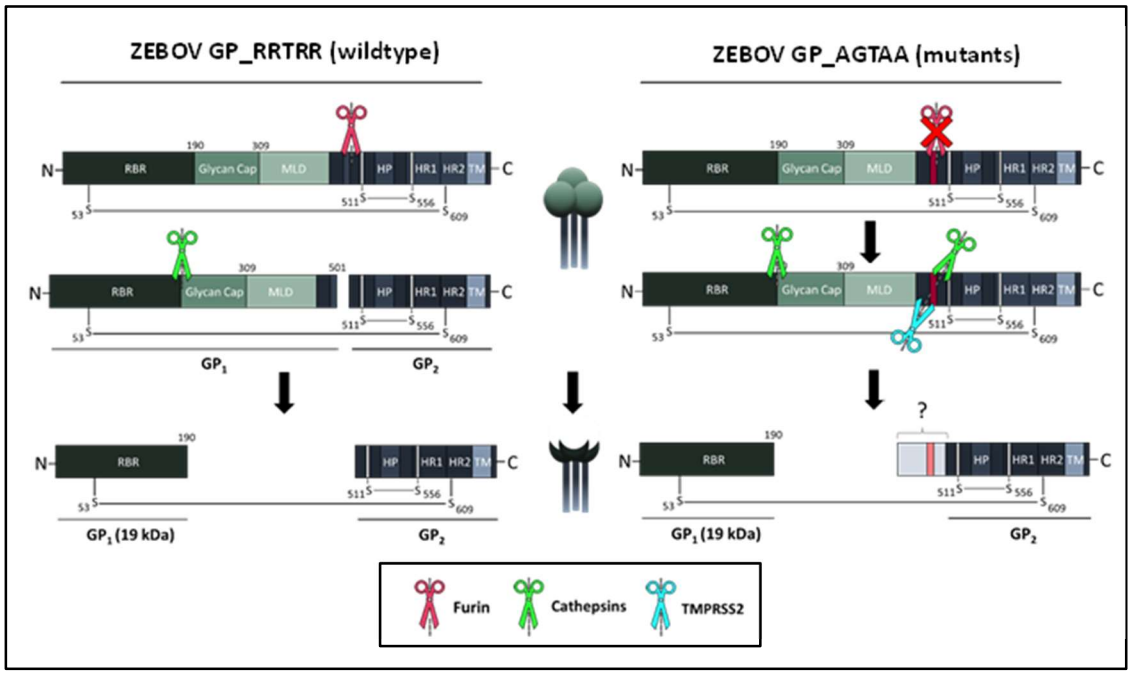


**Figure 25: Alternative proteolytic activation of ZEBOV GP_AGTAA and GP_AGTAAΔ1&2.**
Schematic illustration of proteolytic activation of wildtype ZEBOV GP_RRTRR by furin and endosomal cathepsins, leading to a fusion competent GP with exposed receptor binding region (RBR). Abrogated furin cleavage observed for ZEBOV GP AGTAA and ZEBOV GP_AGTAAΔ1&2 was substituted by other host cell proteases including TMPRSS2 and CatL. Processing of the mutated GP occurred at so far unknown positions leading to cleavage products with different molecular weight, which remained fusion competent.

More strikingly, in this study the Western blot analysis revealed that CatL has the ability to process the ZEBOV GP_AGTAA mutant to the 20 kDa $GP_2$ fragment (Figure 19), revealing a possible hitherto unknown highly dynamic mechanism of $GP_{1/2}$ processing by CatL during viral entry. Thus, ZEBOV GP seems to be broadly accessible to several host cell proteases, particularly around the furin cleavage site region. Moreover, the unique structure of the internal fusion loop of $GP_2$ might contribute to the vast resistance of ZEBOV GP to cleavage site mutations (Figure 25). In contrast to many other class I fusion proteins, including influenza HA with the FP situated at the free N-terminus after proteolytic processing, the hydrophobic patch of $GP_2$ is located at the tip of the internal fusion loop formed by a disulfide bridge between C511 and C556. The interaction of both cysteine residues has been shown to be pivotal for the transduction efficiency of GP-bearing reporter viruses (Jeffers *et al.*, 2002; Gregory *et al.*, 2011). Hence, the formation of the hairpin structure could be allowed even with longer overlaps than the 9 aa resulting from furin cleavage at position 501, as long as the C511 remains intact. This could explain the conserved functionality of the ZEBOV GP_AGTAAΔ1&2 variants in trVLP entry assays. Even though no 20 kDa product was detected in the trVLP purifications, *in vitro* processing of ZEBOV GP_AGTAAΔ1&2 by TMPRSS2 and CatL revealed higher molecular weight products

presumably still fusion competent (Figure 17 and Figure 19). Taken together, the ZEBOV seems to have evolved a quite complex proteolytic activation mechanism of GP facilitating the entry into various host cells, as it displays a vast cell tropism from the main early target of macrophages and dendritic cells to the liver, spleen and endothelial cells as well as reports of neuronal cell infections (Ito *et al.*, 2001; Bray & Geisbert, 2005; Martines *et al.*, 2015; McWilliams *et al.*, 2019).

Lassa virus, another hemorrhagic fever virus, has been shown to be dependent on the post-translational processing of its surface fusion protein by the PC SKI-1 at an RRLL motif. Furthermore, cleavage of Lassa virus GP is a prerequisite for the incorporation into the budding virus particles (Lenz *et al.*, 2001). In contrast, both cleaved and uncleaved ZEBOV GP were integrated into trVLPs (Figure 14 A and Figure 17 A), pseudoviruses and recombinantly generated ZEBOV (Wool-Lewis & Bates, 1999; Neumann *et al.*, 2002). Hence, proteolytic processing by furin was not a prerequisite for the integration of GP into virus particles, as well as for viral infectivity. However, in this study protease processing has been shown to be important for viral entry and replication (4.1). The mode of activation appeared to be relatively flexible depending on the expression profile of host cell proteases in the respective infected cell line. The initial growth kinetics of rVSVΔG ZEBOV $GP_{1/2}$ and $GP_0$ only slightly differed in Huh-7 compared to VeroE6 cells with a more efficient replication in Huh-7 cell (Figure 11 B and Figure 18 A). The subsequent inhibitor studies clearly showed that activation in Huh-7 cells was vastly dependent on endosomal cathepsin activity as the single treatment with E64d abrogated replication of rVSVΔG ZEBOV $GP_0$ in the first 24 h p.i. (Figure 18 C). Thus, processing of the uncleaved GP seemed to be executed predominantly by endosomal cysteine proteases upon entry. These observations were further supported by the trVLP studies performed in Huh-7 cells. The measured reporter activity indicated sufficient proteolytic processing of all three ZEBOV GP variants, as there was no reduced mini genome entry into Huh-7 cells. In contrast, treatment with E64d resulted in a significantly lower reporter gene expression for ZEBOV GP_RRTRR, GP_AGTAA and GP_AGTAAΔ1&2 (Figure 17 D), suggesting a cathepsin-dependent entry mechanism in this liver cell line. Moreover, only in Huh-7 cells replication of rVSVΔG ZEBOV GP could be completely inhibited by a combined treatment of MI-1148, E64d and BAPA (Figure 18 D). The same impact was observed for the triple inhibition using MI-432, but here already the single treatment strongly inhibited rVSVΔG ZEBOV GP replication. This effect was not due to direct inhibition of cathepsins, as tested CatL activity in cell lysates of Huh-7 cells was not affected by MI-432 incubation (Figure 20 C). Hence, the inhibition under MI-432 treatment could be an indirect off-target effect. One possible side effect could be the inhibition of the asparaginyl endopeptidase, also called legumain, which is responsible for the processing of the

autocatalytically cleaved single-chain form of CatB and CatL into a two-chain form. Both generated forms are active, however, inhibition of the two-chain product could result in lower overall active cathepsin levels (Shirahama-Noda *et al.*, 2003). In summary, infected Huh-7 cells display a very distinct phenotype under the treatment with protease inhibitors MI-1148, E64d, BAPA and MI-432, indicating a rather limited protease profile involved in the proteolytic activation of ZEBOV GP upon viral entry and replication (Table 32).

In contrast, proteolytic activation of ZEBOV GP in VeroE6 and Vero-TMPRSS2 cells appeared to be more complex. Infections with trVLPs bearing the deletion mutant ZEBOV GP_AGTAAΔ1&2 showed a significant decrease in reporter activity compared to the ZEBOV GP_RRTRR wildtype indicating that endosomal cathepsins are, unlike in Huh-7 cells, not fully capable of activating the ZEBOV GP_AGTAAΔ1&2 cleavage mutant in these cells (Figure 17 D). The data did not correlate with the whole cell lysate cathepsin activity levels, displaying enhanced CatL enzymatic substrate processing in VeroE6 and Vero-TMPRSS2 cells (Figure 20 B), suggesting a higher CatL activity upon entry into these cells compared to the Huh-7 cells. Hence, the trVLP entry studies revealed that levels of enzymatic active cathepsins most likely differ in the respective endosomal compartments, which could not be reflected by the whole cell lysate approach. Instead, activity-based probes should be used in further experiments for the correct identification of cathepsin activity in certain subcellular locations (Brix & Jordans, 2005). Moreover, treatment of VeroE6 cells with E64d had no adverse effect on reporter gene activity for neither used ZEBOV GP variant, with even a tendency to increase reporter activity (Figure 17 D). These observations indicated, a so far unknown additional GP-activating protease(s) within the endosomal compartments with similarly low cleavage efficiency. In VeroE6 cells, this protease(s) were able to compensate for the absence of CatB and CatL in ZEBOV GP_AGTAAΔ1&2 expressing trVLP infections, but could not restore the ZEBOV GP_RRTRR wildtype reporter activity.

Interestingly, in Vero-TMPRSS2 cells the reporter expression was enhanced to a greater extent for all three ZEBOV GPs, with a significant increase of reporter gene activity for the ZEBOV GP_AGTAA-bearing trVLPs (Figure 17 D), suggesting that here another protease(s) could benefit from the inhibition with E64d. Endocytic trafficking is a very dynamic process with several compartments participating and interacting (Huotari & Helenius, 2011), therefore the increased entry under inhibition of endosomal CatB and CatL could be an effect of prolonged temporal residence of ZEBOV GP in certain compartments. In general, the endocytic transport is a very fast process with the localization of endocytosed proteins within the early endosome after roughly 2 min, the late endosome within further 10 min and in the lysosomal compartments after 30 to 60 min (Mukherjee & Maxfield, 2004; Lakadamyali *et al.*, 2006). The

inhibition of active CatB and CatL in the lysosomes could slow down the degradation of endocytosed ZEBOV GP_AGTAA and GP_AGTAAΔ1&2 mutants that are more likely to be processed slower than the wildtype GP, due to poorer accessibility of alternative cleavage sites and less efficient protease(s) involved in the processing. This could allow other substituting endosomal proteases to process sufficient amounts of ZEBOV GP for an efficient entry.

Alternate proteolytic processing within the endosomal compartment upon entry of ZEBOV GP into the host cell could be performed by different host cell proteases. While rVSVΔG ZEBOV $GP_0$ replication was further reduced by the additional treatment with a broad trypsin-like protease inhibitor (Figure 12), combined incubation with E64d and BAPA did not further reduce reporter activity in ZEBOV GP_AGTAAΔ1&2 trVLP infected VeroE6 cells (data not shown). Suggesting, that trypsin-like proteases are more likely involved in the post-translational activation of ZEBOV GP in VeroE6 cells. Proteolytic enzymes of other families are most likely able to substitute especially for the trimming of the $GP_1$ subunit for receptor binding upon viral entry. Metalloproteases like the a disintegrin and metalloprotease 17 (ADAM17/TACE), is a so-called 'sheddase' involved in the release of TNF-α from the cell surface. Moreover, TACE has been shown to shed the ectodomain of ZEBOV GP (shedGP) from the cell surface after cleavage at position D637 close to the transmembrane domain (Dolnik *et al.*, 2004). Thus, in general interaction and processing of ZEBOV GP by metalloproteases is possible. Unlike TACE, secreted matrix metalloproteinases (MMPs) have been more associated with the reshaping of the extracellular matrix. However, recent additional findings have been made, suggesting intracellular targets of MMPs within the mitochondria and cytosol (Cauwe & Opdenakker, 2010; Bock *et al.*, 2015; Jobin *et al.*, 2017). Moreover, cellular uptake of soluble MMPs from the extracellular space by clathrin- or caveolin-mediated endocytosis with co-localization of MMPs with markers of the early endosome has been described (Jiang *et al.*, 2001; Remacle *et al.*, 2003). Studies with neurotropic mouse hepatitis virus (MHV), belonging to the CoV, revealed the involvement of metalloproteases in the neuronal cell tropism of this strain (Phillips *et al.*, 2017). Thus, ZEBOV GP could also be processed by metalloproteases in different cells and tissues, therefore contributing to the broad tropism of ZEBOV. Another family of possible ZEBOV GP-activating endopeptidases are the lysosomal aspartidyl proteases, including cathepsin E and D. Similar to the cysteine proteases CatB and CatL, cathepsin D is ubiquitously expressed in various tissues and cell types and could be responsible for subsequent processing of ZEBOV GP upon cellular uptake (Brix, 2005). Cathepsin D displays a preference for bulky hydrophobic aa in P1 and P1' like phenylalanine (F), with a described cleavage of fluorogenic substrates with the FF motif (Yasuda *et al.*, 1999). The ZEBOV GP consists of only three FF motifs within its $GP_1$ subunit and one in particular at position F193 and F194 very close to the trimming site of endosomal CatB and CatL.

Therefore, cathepsin D could substitute for the cleavage around the RBD of $GP_1$ but is most likely not able to process at or around the furin cleavage site. The more recently identified threonine proteases have been so far described to be active within the cytoplasm and are rarely identified in lysosomal compartments (Brix, 2005; Bier *et al.*, 2011). Nevertheless, as the dogma of strict intracellular and extracellular distribution of cathepsins and MMPs, respectively, has more and more changed over the last years there might be other revelations concerning the cellular localization and substrate specificity of the so far not well-characterized threonine proteases.

**Table 32: Host cell proteases involved in rVSVΔG ZEBOV GP growth kinetics**

| Activating protease\cell line | Huh-7 | VeroE6 | Vero-TMPRSS2 |
|---|---|---|---|
| Furin | + | ++ | + |
| CatB & CatL | +++ | ++ | ++ |
| TMPRSS2 | N.E.[1)] | N.E.[2)] | + |
| Unknown trypsin-like serine proteases | + | + | (+) |
| Unknown other proteases | - | + | (+) |

+: importance for rVSVΔG ZEBOV GP replication; -: no involvement; (): possible additional involvement;
N.E.: not expressed (Figure 17 C)[1], (Kleine-Weber *et al.*, 2018)[2]

Taken together, proteolytic activation of ZEBOV GP clearly differed in the used Huh-7, VeroE6 and Vero-TMPRSS2 cells. While the protease profile of ZEBOV GP-activating host cell proteases seemed to be rather narrow in Huh-7 cells, processing in VeroE6 and Vero-TMPRSS2 cells appeared to be more complex with so far unknown proteases able to compensate for furin cleavage and CatB and CatL trimming (Table 32).

### 5.1.4 Highly truncated ZEBOV GP variants are expressed but not incorporated into trVLPs

This study indicated an essential role of protease activation in the replication of ZEBOV and showed a highly dynamic and complex mode of proteolytic processing of ZEBOV GP upon entry and subsequent replication. Since all alanine scanning efforts resulted in still cleaved ZEBOV GP, the GP was stepwise truncated to generate a variant that could no longer be processed by host cell proteases. In order to identify defective deletion variants, the initial mutants were generated in pCAGGS ZEBOV GP constructs containing the wildtype furin recognition sequence RRTRR.

From previous ZEBOV GP vaccination platform studies in HIV and VSV pseudovirus systems, it was known that deletion of the MLD had no negative effect on virus generation with even reported enhanced infectivity of these mutants (Manicassamy *et al.*, 2005; Bhatia *et al.*, 2021).

Furthermore, recombinant VSV viruses bearing ZEBOV GP with an additional deletion of the glycan cap region together with the MLD from aa 228 to 489 were able to replicate efficiently in VeroE6 cells (Bhatia *et al.*, 2021). Cathepsin processing of ZEBOV GP has been proposed to take place at a loop from aa 190 to 213 with further biochemical analysis of the 19 kDa cleavage product ZEBOV $GP_{Cl}$ after thermolysin treatment indicating the final cathepsin cleavage most likely occurs at position 190 (Dube *et al.*, 2009; Lee & Saphire, 2009). For the generation of a GP variant with no cathepsin processing site the glycan cap and MLD from the ZEBOV GP_RRTRRΔ1&2 construct together with all aa from 190 to 227 were removed, resulting in the ZEBOV GP_RRTRRΔgly/mucΔ1&2 variant (Figure 21 A). Western blot analysis of ZEBOV GP_RRTRRΔgly/mucΔ1&2 expressed in HeLa cells revealed, that this highly truncated version of GP was still very efficiently expressed. However, cleavage by endogenous furin was abolished (Figure 21 B). The close proximity of the RRTRR sequence to the C511 forming the disulfide bond with C556 essential for the fusion loop formation might lead to a conformational change in the $GP_2$ subunit of this highly truncated GP variant. Therefore, furin might no longer be able to access the R501 for proteolytic cleavage. The insertion of 4, 5 or 9 alanine downstream of the RRTRR motif restored the recognition and processing of GP by endogenous furin, but cleavage was insufficient with only faint $GP_2$ product bands detectable (Figure 21 B). As the inserted alanine residues possibly led to incorrect folding in this region, the downstream EVIVNAQPK wildtype sequence (ZEBOV GP_RRTRRΔgly/mucΔ1) was restored to ensure a native GP folding structure in the $GP_2$ subunit. Unfortunately, the introduction of the wildtype aa from position 502 to 510 did not enhance the processing of GP by furin. Thus, further ten wildtype aa residues with the AGVAGLITGG sequence (ZEBOV GP_RRTRRΔ190-486) were additionally inserted upstream of the RRTRR motif, to provide a more native substrate structure for furin. Nevertheless, this ZEBOV GP variant was also poorly processed by endogenous furin compared to the ZEBOV GP_RRTRR wildtype construct. Western blot analysis of the ZEBOV GP_AGTAA cleavage by TMPRSS2 also displayed reduced processing capacity compared to the highly efficient priming of ZEBOV GP_RRTRR by furin (Figure 15 B). However, trVLPs bearing ZEBOV GP_AGTAA with low amounts of detectable cleavage product were able to mediate membrane fusion and reporter genome release in all tested cells with no disadvantage compared to the wildtype GP (Figure 17 A and D), indicating that a small proportion of processed GP was sufficient for ZEBOV entry. Similar effects were observed in previous studies with IAV. Proteolytic activation of the HA of influenza viruses revealed that low amounts of cleavage product $HA_2$ were sufficient for infectivity and efficient replication (Li *et al.*, 1990; Limburg *et al.*, 2019). However, preliminary data from experiments with trVLPs bearing the ZEBOV GP_RRTRRΔgly/mucΔ1&2_5A construct, which presented the most efficient cleavage of

all glycan cap and MLD deletion variants, showed that no reporter activity could be detected in the infected P1 cells (data not shown). This was most likely due to a defect in trVLP incorporation of ZEBOV GP_RRTRRΔgly/mucΔ1&2_5A, as even though comparable levels of VP40 could be detected in the trVLP preparations almost no $preGP_{del/ins}$ appeared (data not shown). The disruptive effect of glycan cap and MLD deletion was surprising, as the previously described VSV ZEBOV GP variant with aa deletions from position 228 to 489 had no replication disadvantage *in vitro* (Bhatia *et al.*, 2021). The $GP_1$ residues 33-69, 95-104, 158-167 and 176-189 form the base of the structure consisting of a hydrophobic surface, interacting with the internal fusion loop of the $GP_2$. This clamp-like structure prevents the hydrophobic patch from inserting prematurely into intracellular membranes (Lee & Saphire, 2009). The deletion of the ZEBOV GP_RRTRRΔgly/mucΔ1&2_5A from position 190 of the $GP_1$ subunit left the aa responsible for the clamp function of the remaining $GP_1$ still intact. Thus, a premature fusion with cellular membranes should not be the reason for the defective incorporation of GP into trVLPs. Even though the ZEBOV GP was highly resilient towards single aa mutations and broad aa deletions around the $GP_{1/2}$ cleavage site, the $GP_1$ subunit seems to be more sensitive to aa changes. Mutation studies within the $GP_1$ subunit of ZEBOV GP (Mayinga, 1976) revealed that not all $GP_1$ regions were equally robust concerning alanine exchange mutations. While the relatively large stretch from position 266 to 476 was quite insensitive to alanine mutations, the residues of the N-terminal 230 aa seemed to be essential for the incorporation into HIV reporter viruses. Among the aa residues responsible for disruption of GP insertion into virions were the I218, Y220 and F225 (Manicassamy *et al.*, 2005). Sequence comparison of the ZEBOV strain Mayinga with the 2014 emerged Makona strain pointed out a relatively high sequence homology of $GP_1$ areas outside of the MLD with approximately 99 %, while the average percent identity of the MLD with about 90.3 % was lower (Ueda *et al.*, 2017). Hence, the aa deletion from position 190 to 227 in our ZEBOV GP_RRTRRΔgly/mucΔ1&2_5A variant differing from the previously described functional VSV ZEBOV GP aa 228 to 489 deletion mutant could as well be responsible for the defect incorporation as it has been observed for the Mayinga strain. The loss of protein function after deletion of aa 190 to 227 cathepsin cleavage site might hint toward a highly conserved role of processing for ZEBOV at this site. Hence, the ZEBOV GP seems to have been shielded from any circumstances obstructing proteolytic activation at this site, as neither furin or cathepsin nor the cleavage by other so far unknown proteases could be disrupted by mutations without destroying protein function.

## 5.2 Furin and TMPRSS2 processing of SARS-CoV-2 S is crucial for the multicycle replication and infectivity

As a part of this thesis the proteolytic processing of the 2019 newly emerged SARS-CoV-2 S protein, belonging to the class I fusion proteins, was investigated and characterized. Sequence analysis revealed that SARS-CoV-2 belongs, together with SARS-CoV, to the family of *Betacoronaviruses* and among them to the lineage B (*Sarbecoviruses*). Despite their close sequential relationship, there was a major difference present in the SARS-CoV-2 S protein, as it contains a 12 nucleotide insertion at the S1/S2 site that leads to the multibasic $_{681}$PRRAR$_{685}$ motif while the S2' remained monobasic with an R at position 815 (Coutard *et al.*, 2020; Walls *et al.*, 2020). Thus, indicating a possible proteolytic processing by furin with its R-X-R/K-R cleavage recognition motif (Hosaka *et al.*, 1991; Krysan *et al.*, 1999) at the S1/S2 site and S2' site processing of the monobasic R815 by the trypsin-like serine protease TMPRSS2, as previously described for MERS- and SARS-CoV (Matsuyama *et al.*, 2010; Glowacka *et al.*, 2011; Gierer *et al.*, 2013; Shirato *et al.*, 2013)

Transiently expressed SARS-CoV-2 S protein was efficiently processed by endogenous furin at the S1/S2 site in 293F cells (Figure 22 B). Treatment with the potent furin inhibitor MI-1851 led to the complete inhibition of the proteolytic cleavage. Furthermore, co-expression of the human serine protease TMPRSS2 resulted in an additional slightly smaller cleavage product that corresponded to the S2' processing (Figure 22 B, left panel). S1/S2 cleavage could not be altered by incubation with the broad serine protease inhibitor aprotinin, whereas there was a clear reduction of S2' band intensity (Figure 22 B, right panel). Hence, these first data indeed indicated a possible sequential proteolytic activation of SARS-CoV-2 S by furin and TMPRSS2. Noteworthy, even though the single treatment with MI-1851 efficiently blocked S processing, the co-expression of SARS-CoV-2 S together with TMPRSS2 under treatment with MI-1851 did not fully abrogate the detection of S1/S2 and S2' cleavage products. Thus, indicating that overexpressed TMPRSS2 was able to cleave SARS-CoV-2 S at the S1/S2 site, however, the cleavage was not highly efficient. Processing of the monobasic cleavage sites by other trypsin-like serine proteases, such as TMPRSS13/MSPL, has been demonstrated in vitro (Laporte *et al.*, 2021). Nevertheless, *in vivo* studies revealed that *tmprss2*$^{-/-}$ mice were protected from severe SARS-CoV, MERS-CoV and SARS-CoV-2 infections, implicating a crucial role of TMPRSS2 in CoV replication (Iwata-Yoshikawa *et al.*, 2019; Li *et al.*, 2021). Hence, processing of SARS-CoV-2 S at the S2' monobasic cleavage site was likely to be important for the infectivity and multiplicity of this novel zoonotic CoV.

Here, in order to address the question, of whether the co-expression findings could be transferred to the activation of the S protein upon SARS-CoV-2 replication, human bronchial epithelial Calu-3 cells were infected with the SARS-CoV-2 isolate Munich 929 (wildtype) under BSL-3 conditions. Even though Calu-3 cells are an immortalized cell line, they represent a robust model of human airway cells. Infection studies with human IAV revealed a high correlation between data collected in human primary bronchial epithelial and Calu-3 cells (Limburg *et al.*, 2019). Replication of SARS-CoV-2 was strongly reduced under the treatment with substrate analog furin inhibitor MI-1851, thereby proving that the unique multibasic insertion at the S1/S2 site was indeed processed by endogenous furin. Furthermore, inhibitors of trypsin-like proteases, namely aprotinin, as well as the peptidomimetic synthetic inhibitors MI-432 and MI-1900 had also a potent inhibitory effect on the SARS-CoV-2 replication (Figure 23 A). The data displayed that inhibition of both host cell proteases had a strong effect on SARS-CoV-2 replication and neither furin nor TMPRSS2 were able to compensate for each other. Hence, combined treatment of furin and TMPRSS2 inhibitors had a synergistic effect on virus titers in Calu-3 cells (Figure 23 C). Both cleavage events were essential for the efficient replication of SARS-CoV-2 in Calu-3 cells. Processing of SARS-CoV-2 S at the S1/2 site by furin has been proposed to result in a higher flexibility leading to conformational changes associated with enhanced ACE2 binding affinity (Wrobel *et al.*, 2020). Moreover, a direct engagement of ACE2 with TMPRSS2 has previously been described (Shulla *et al.*, 2011), bringing SARS-CoV-2 S and TMPRSS2 in close proximity to each other. The combined sequential proteolytic activation would be a well-coordinated activation mechanism for furin and TMPRSS2 expressing cells, like human bronchial epithelial cells.

Unlike described for SARS-CoV S processing in different epithelial cell cultures (Simmons *et al.*, 2004; Simmons *et al.*, 2005), growth kinetics in Calu3 cells treated with the cysteine cathepsin inhibitor E64d showed no dependency of the novel SARS-CoV-2 S on endosomal CatL activity for replication in human bronchial airway epithelial cells (Figure 23 A). Activation of HCoVs and SARS-CoV S protein by endosomal CatL is still controversially discussed with several hints that CatL processing might be a cell culture adaptation rather than a physiological activation used *in vivo* (Matsuyama *et al.*, 2005; Shirato *et al.*, 2017; Shirato *et al.*, 2018). The passaging of SARS-CoV-2 in Vero cells led to deletion mutations within the S1/S2 region of S, including the multibasic motif. However, infectivity was not reduced in these cells. This effect could be due to a conserved CatL cleavage site (QSI↓IAYT) located 7 aa downstream of the multibasic furin motif (Liu *et al.*, 2020). However, Calu-3 cells reportedly express low CatL levels non-sufficient for efficient MERS-CoV activation (Park *et al.*, 2016), which most likely also hindered efficient processing of SARS-CoV-2 S .

The emergence of a multibasic S1/S2 cleavage site motif in SARS-CoV-2 S is a unique feature among the *Sarbecovirus* family, as even its close relatives, including the bat RaTG13 with a sequence homology of 97.7 % and the pangolin CoV with up to 92.9 % homology, do not possess a multibasic cleavage site motif (Wu & Zhao, 2020). Early studies with IAV showed that the insertion of basic aa at the monobasic cleavage site of HA led to the emergence of HPAIV subtypes H5 and H7 (Brugh, 1988; Swayne & Suarez, 2000). These HPAIV subtypes are associated with changed cell tropism and infectivity, from local infections in the respiratory and intestinal tract to systemic and often lethal infections in poultry, due to the altered activation by ubiquitously expressed furin (Stieneke-Gröber *et al.*, 1992; Horimoto *et al.*, 1994; Böttcher-Friebertshäuser *et al.*, 2014). A study with the SARS-CoV-2 SΔPRRA deletion mutant displayed a higher fitness in VeroE6 cell culture, but slower replication in human respiratory cells (Johnson *et al.*, 2021). This finding was consistent with frequently occurring deletions of the furin cleavage motif during cell culture passages, compared to a low incidence in human isolates of SARS-CoV-2 (Liu *et al.*, 2020). Therefore, the multibasic insertion in the SARS-CoV-2 S and observed proteolytic processing by furin might be an adaptive process for sustained human infections, contributing to the higher infectivity and more efficient spread of SARS-CoV-2. This was further supported by transmission studies in ferrets, here, only the wildtype SARS-CoV-2 with the multibasic insertion was able to transmit to sentinel animals (Peacock *et al.*, 2021). Sequence analysis of other *Betacoronaviruses* clearly showed a frequent presence of basic furin cleavage motifs found in human MERS-CoV, HKU1, HCoV-OC43 and murine MHV A59 CoV at the S1/S2 site (Appendix Table 33) (Haan *et al.*, 2004; Wu & Zhao, 2020). As furin is ubiquitously expressed in mammalian tissue, the acquisition of a multibasic cleavage site could correspond with a broader host cell tropism and higher infectivity. Even though MERS-CoV possesses a dibasic R-X-X-R minimal furin cleavage motif at both the S1/S2 and the S2' site, which could be processed by overexpressed furin, the proteolytic activation of MERS-CoV S at the S1/S2 site during replication has been controversially discussed, as it was shown to be crucial for the infection of human Calu-3 cells but dispensable for the entry into other epithelial cells (Millet & Whittaker, 2014; Gierer *et al.*, 2015; Park *et al.*, 2016; Matsuyama *et al.*, 2018). This highlights the importance of combined cleavage and infectivity studies for the characterization of proteolytic activation of viral fusion proteins.

In CoV infections, the host cell proteases present during initial virus replication seem to determine the entry route upon cell infection. Studies with MERS-CoV and SARS-CoV-2 revealed that the expression of TMPRSS2 directs the viruses towards an endosomal- and pH-independent entry mechanism at or near the cell surface, while the lack of TMPRSS2 led to a CatL-driven entry within the lysosomal compartment in certain cell lines (Park *et al.*, 2016; Koch *et al.*, 2021). The

sequential activation of SARS-CoV-2 S by furin during protein synthesis and the subsequent processing by TMPRSS2 at or close to the plasma membrane seems to be a highly efficient activation mechanism for SARS-CoV-2, superior to the entry mechanism in TMPRSS2-deficient cell lines. Studies revealed that the enhanced replication was most likely due to an evasion of the endosomal compartment, which contains the interferon-induced antiviral proteins IFITIM2/3 that are able to substantially decrease viral replication (Peacock *et al.*, 2021). The previously shown data generated in Calu-3 cells confirmed these observations as the combined inhibition of furin and TMPRSS2 led to a highly efficient 500-fold decrease of viral titers (Figure 23 C). However, it remains to be investigated why the SARS-CoV-2 replication was never fully abrogated during the combined inhibitor treatment. Further infection experiments with higher concentrations of the respective inhibitors could elucidate whether residual activity of furin and TMPRSS2 is responsible for the remaining replication or an alternative endosomal entry route is possible in Calu-3 cells.

The characterization of proteolytic activation of CoV over the years has revealed that the sequential activation at two distinct sites seems to be an advantage rather than a disadvantage, as protease specificity is not as strict as for most IAV (Hatesuer *et al.*, 2013; Sakai *et al.*, 2014; Lambertz *et al.*, 2019; Limburg *et al.*, 2019; Lambertz *et al.*, 2020; Bestle *et al.*, 2021). All the more important is the characterization of CoV activation in order to develop suitable therapeutic strategies.

## 5.3 Subcellular localization of virus-activating host cell protease TMPRSS2

The previous data have shown that TMPRSS2 plays a crucial role in the proteolytic activation of the novel SARS-CoV-2 S. Furthermore, TMPRSS2 was involved in the proteolytic activation of rVSVΔG ZEBOV GP in the absence of the classical activating proteases furin and endosomal cathepsins and was able to alternatively process ZEBOV GP_AGTAA *in vitro*. However, the precise subcellular localization of TMPRSS2 activation is still not clear and has yet to be determined. The co-localization studies in TMPRSS2-overexpressing Huh-7 cells with cellular compartment marker proteins revealed an intracellular distribution of TMPRSS2, beyond the known TGN residence (Böttcher *et al.*, 2006), within the ERGIC and to a certain extent within the late and recycling endosome (Figure 24 C).

Even though overexpressed TMPRSS2 did co-localize with the ERGIC marker protein ERGIC53 in Huh-7 cells indicating a possible residence of TMPRSS2 in this compartment, authentic

SARS-CoV-2 isolates have been shown to contain only furin-processed S protein on the viral surface (Koch *et al.*, 2021; Peacock *et al.*, 2021). Hence, residing TMPRSS2 within the ERGIC did not process S at the S2' site, suggesting that the processing of S by TMPRSS2 occurs during the viral entry, which might be dependent on further co-factors, like ACE2-interaction. Moreover, certain human CoV isolates with monobasic S1/S2 sites, including HCoV-229E and SARS-CoV have been described to be released from the host cell after budding into the ERGIC with overall uncleaved S protein (Bisht *et al.*, 2004; Haan & Rottier, 2016) further implicating that even though TMPRSS2 could be present within the ERGIC, S processing does not occur in the CoV budding compartment.

The entry of SARS-CoV-2 into TMPRSS2-expressing target cells has been intensively studied and was shown to take place at or near the plasma membrane (Hoffmann *et al.*, 2020; Peacock *et al.*, 2021). Nevertheless, it is still not clear whether this processing step occurs extracellularly or shortly after the uptake into the endosomal compartments (Koch *et al.*, 2021). Additionally, the infection studies in Vero-TMPRSS2 cells displayed an efficient activation of rVSVΔG ZEBOV $GP_0$ upon viral entry, which led to the loss of the initial growth defect observed in VeroE6 cells (Figure 13 A). Hence, further indicating that TMPRSS2 could contribute to the proteolytic activation of enveloped viruses during entry. Previous studies with IAV showed only minor enzymatic activity of TMPRSS2 at the cellular surface, which was not sufficient to activate unprimed $HA_0$ (Böttcher-Friebertshäuser *et al.*, 2010), leaving the question whether the TMPRSS2 activation of SARS-CoV-2 S and ZEBOV GP takes place in the endosomal compartments. The IF data collected upon overexpression of TMPRSS2 in Huh-7 cells revealed a partial co-localization with the recycling endosome marker CD71 and the late endosome marker Rab7 but not with the early endosome marker EEA1 (Figure 24 C), suggesting that the trypsin-like serine protease could be found in certain endosomal compartments. However, virus activation by TMPRSS2 has previously been observed at predominantly neutral pH (Böttcher *et al.*, 2006; Glowacka *et al.*, 2011). Therefore, TMPRSS2 contribution to endosomal activation of SARS-CoV-2 S and ZEBOV GP upon entry has to be further investigated, as an activity under low pH conditions ranging from pH 6 to 4.9 has so far not been described.

ZEBOV GP and SARS-CoV-2 S both need to be processed at two cleavage sites at different time points during the infection in order to gain a fusion competent state. Thus, processing by TMPRSS2 could take place at different compartments during the respective viral replication cycle. Even though the overexpression data in Huh-7 cells showed localization of TMPRSS2 beyond the TGN within the ERGIC and certain endosomal compartments, proteolytic activity in

these subcellular locations as well as whether these data could be transferred to endogenous TMPRSS2 expression still needs to be assessed.

## 5.4 Host cell proteases as promising antiviral targets and their limitations

Targeting viral proteins has been an effective antiviral strategy against viral infectious diseases, including HIV, hepatitis C and influenza. Nevertheless, viral escape mutations bear a high risk of a loss of therapeutic efficacy (Hu *et al.*, 2013; Richman & Nathanson, 2016). To avoid the emergence of drug resistance in the treatment of virus infections, host cell factors used by viruses to enter and replicate efficiently can be targeted. As these cellular proteins and molecules are often involved in highly conserved and therefore essential viral pathways during the replication, viral escape mutations are less likely. Thus, the identification and characterization of host cell-virus interactions is a pivotal step toward efficient antiviral drug development.

In this study, the role of host cell proteases in the proteolytic activation of the class I fusion proteins of ZEBOV and SARS-CoV-2 was examined. For both viruses, major efforts have been made in order to identify and license drug candidates for the treatment of acute infections. Nevertheless, so far most compounds entering clinical trials, including viral polymerase and protease inhibitors as well as convalescence sera and monoclonal antibodies, target virus factors, thereby possibly building up selective pressure (Bixler *et al.*, 2017; Marzi & Mire, 2019; Drożdżal *et al.*, 2020; Tao *et al.*, 2021). Moreover, until now none of the tested antiviral therapeutics has been recommended for the treatment of ZEBOV or SARS-CoV-2 infections, due to a lack of efficacy in phase III clinical trials.

For ZEBOV a VSV-based vaccine (rVSVΔG ZEBOV-GP; ERVEBO) has passed phase III ring vaccination trials and has been approved by the FDA in December 2019. Nevertheless, a study conducted with 620 patients in an Ebola virus disease treatment center revealed, that even though there was a high efficacy in the rVSVΔG ZEBOV-GP ring vaccine trials, approximately 10 % of patients who tested positive for ZEBOV were vaccinated at least 10 days prior to the admission (Mulangu *et al.*, 2019). The emergency licensed SARS-CoV-2 vaccines have been proven to efficiently slow down the spread of COVID-19. However, the high mutation rates of SARS-CoV-2 challenge the limits of vaccine-induced immunity (Tao *et al.*, 2021). Moreover, certain risk groups, including pregnant women before the second trimester and severely immunocompromised persons, are not able to receive vaccinations. Thus, there is despite the

effort still an urgent need for the development of new antiviral compounds suitable for the treatment of acute ZEBOV and SARS-CoV-2 infections. Accordingly, in 2013 the WHO issued a report highlighting among others the necessity of host-directed therapies in order to approach the battle against respiratory viruses (BRaVe) (Legand *et al.*, 2013).

Protease inhibitors have been extensively studied in the context of respiratory viral infections with influenza, parainfluenza, SARS-CoV and MERS-CoV. The airway protease TMPRSS2 has been shown to be essential for the proteolytic activation of influenza viruses and plays an important role in the processing of CoV S protein, including SARS-CoV, MERS-CoV and SARS-CoV-2 (Iwata-Yoshikawa *et al.*, 2019; Limburg *et al.*, 2019; Bestle *et al.*, 2021; Li *et al.*, 2021). Trypsin-like serine protease inhibitors, such as the peptide inhibitor aprotinin (Trasylol) and the small molecule S1 binder camostat (Foipan), have been licensed to reduce perioperative bleeding and to treat chronic pancreatitis, respectively. I*n vivo* studies in mice with aprotinin and camostat revealed the therapeutic potential of trypsin-like protease inhibitors for influenza, parainfluenza and SARS-CoV infections, suggesting these compounds are promising candidates for successful drug repurposing (Ovcharenko & Zhirnov, 1994; Lee *et al.*, 1996; Zhou *et al.*, 2015). Furthermore, aerosol application of aprotinin licensed for the use in clinical patients in Russia diminished severity and shortened the duration of influenza and parainfluenza symptoms in patients (Zhirnov *et al.*, 1996). In this thesis, it was shown that proteolytic processing of the novel SARS-CoV-2 S by TMPRSS2 at the S2' was important for efficient replication and was strongly reduced by TMPRSS2 inhibitors *in vitro* (Figure 23 A). Several clinical trials in COVID-19 patients have been investigating the value of TMPRSS2 as an antiviral target by the use of small-molecule inhibitors camostat and nafamostat. Hints for improvement of clinical outcome were found, although the data lacked to prove efficacy, due to low participant numbers and/or probable low bioavailability of administered inhibitors at the site of infection (Gunst *et al.*, 2021; Kitagawa *et al.*, 2021; Zhuravel *et al.*, 2021; Wettstein *et al.*, 2022). Consequently, treatment of acute SARS-CoV-2 infections could be supported by the use of locally administered aprotinin or other recently studied trypsin-like inhibitors with antiviral effects against SARS-CoV-2, including camostat, nafamostat, N-0385 and MI-1900 in an aerosolized form. Our data clearly showed that activation of SARS-CoV-2 S by TMPRSS2 and furin is crucial, as none could compensate for the lack of the other. Nevertheless, a combined inhibition of furin and TMPRSS2 would efficiently reduce SARS-CoV-2 replication and furthermore allow the treatment with low drug doses to avoid possible side effects.

Furin is involved in various physiological processes, with approximately 490 protein substrates within the human proteome (Shiryaev *et al.*, 2013). Targeting PCs might be more challenging,

with higher risks of side effects as they are participating in several physiological processes. While furin plays an important role during embryogenesis, as the lack of furin was lethal, conditional organ-specific knockouts were well tolerated (Roebroek *et al.*, 2004; Scamuffa *et al.*, 2006). Moreover, *in vivo* experiments in mice and rats with the substrate analog hexa-D-arginine (D6R) furin inhibitor showed no toxic effect with low dosages of 3.8 mg/kg. Furthermore, animals treated with D6R were significantly protected from anthrax toxin and *Pseudomonas* exotoxin pathology (Sarac *et al.*, 2002; Sarac *et al.*, 2004). A potent antiviral activity was observed for the substrate analog inhibitors MI-1148 and MI-1851. During its development, MI-1148 displayed substantial side effects in rodents probably due to its highly basic character. Therefore, the less basic canavanine-based derivate MI-1851 was designed, which was well tolerated in animal models and displayed a broad antiviral activity (van Lam van *et al.*, 2021). Hence, furin inhibition should be considered as an antiviral therapeutic approach, however, with precautious inhibitor design, application route and an optimal minimal treatment dosage.

Even though *tmprss2*$^{-/-}$ animals did not display a specific phenotype (Kim *et al.*, 2006), the experiences with aprotinin also revealed the importance of optimal inhibitor concentrations used for the treatment with trypsin-like protease inhibitors. High doses of aprotinin were used in heart surgery to prevent perioperative bleeding, however, studies revealed a higher risk of death compared to the standard antifibrinolytics (Fergusson *et al.*, 2008). The treatment with 2 times lower aprotinin concentrations resulted in a significantly reduced risk for intraoperative complications (Mangano *et al.*, 2006). The local administration of protease inhibitors could considerably lower the necessary inhibitor concentration and therefore reduce the risk of possible side effects. Aerosol delivery of aprotinin in mice infected with IAV and parainfluenza had a strong antiviral effect, whereas 15 times higher aprotinin doses were needed in intraperitoneally treated animals (Zhirnov *et al.*, 1982; Ovcharenko & Zhirnov, 1994). Hence, aprotinin concentrations needed for the previously described antiviral therapy in clinical patients were 1000-fold lower in the aerosol treatment, compared to the high-dose treatment used for cardiac surgery (Zhirnov *et al.*, 2011). A phase III clinical trial with SARS-CoV-2 patients admitted to hospitals in Spain demonstrated a beneficial effect of aprotinin inhalation on the length of treatment and hospitalization (Redondo-Calvo *et al.*, 2022). Thus, the topical application with sufficiently low concentrations of a combination of trypsin-like serine protease and furin inhibitors could therefore be a promising approach to efficiently treat SARS-CoV-2 infections without the risk of severe side effects.

To further minimize the risk of off-target effects the development of highly specific synthetic inhibitors of TMPRSS2 or furin such as phosphorodiamidate morpholino oligomers (PMO) have

been shown to efficiently block protease expression. The PMO T-ex5 conjugated to a cell-penetrating peptide (PPMO) is complementary to the spliceosome acceptor site of exon 5 within the TMPRSS2 pre-mRNA. The T-ex5 PPMO interferes with correct mRNA splicing, which is followed by the translation of a truncated enzymatically inactive protein (Böttcher-Friebertshäuser *et al.*, 2011). The PPMO-mediated knockdown of active TMPRSS2 inhibited the replication of influenza A and B viruses in human airway cells and very efficiently decreased SARS-CoV-2 titers in combination with MI-1851 (Limburg *et al.*, 2019; Bestle *et al.*, 2020). In recent years two PMO molecules have been licensed by the FDA targeting the exon 51 and 53 of the dystrophin gene and thereby restoring the function of the protein in patients with Duchenne muscular dystrophy (DMD) (Sun *et al.*, 2020). Hence, the further testing and development of PPMO T-ex5 is a promising approach toward highly selective protease inhibitors directed against a variety of enveloped viruses, among them the still pandemic SARS-CoV-2.

The ZEBOV GP shares with the SARS-CoV-2 S its two activation sites. However, while SARS-CoV-2 S processing predominantly takes place at the distinct S1/2 and S2' site by furin and TMPRSS2, respectively, the activation of ZEBOV GP appeared to be more complex depending on the protease repertoire present in the infected cell. In this study in addition to the previously described processing by furin at position R501 of RRTRR motif and trimming of $GP_1$ by endosomal CatB and CatL (Volchkov *et al.*, 1998; Wool-Lewis & Bates, 1999; Schornberg *et al.*, 2006; Kaletsky *et al.*, 2007), enhance replication of rVSVΔG ZEBOV $GP_0$ in Vero-TMPRSS2 cells and cleavage of ZEBOV GP_AGTAA by TMPRSS2 at a so far unknown position was observed.

Moreover, a new probably more efficient activation mechanism of ZEBOV GP_AGTAA at or near the mutated non-basic motif by human recombinant CatL could be shown (Figure 19). Alternative processing of ZEBOV GP by CatL at both cleavage sites could further explain the furin-independent replication observed in several infection studies (Wool-Lewis & Bates, 1999; Neumann *et al.*, 2002; Neumann *et al.*, 2007). The potent cysteine protease inhibitor E64d is a derivate of the epoxysuccinate-based inhibitor E64 first isolated from *Aspergillus japonicus*, which forms irreversible thioester bonds with the active site cysteine (Hanada *et al.*, 1978; Tamai *et al.*, 1986). Due to the lipophilic character, E64d was readily distributed systemically after oral administration of 100 mg/kg in Syrian hamsters. There, E64d was non-toxic and efficiently inhibited CatB and CatL over 3 h in the skeletal muscle, heart and liver. The efficacy of E64d in DMD animal models was very promising, leading to phase III clinical trial studies in DMD patients in Japan (Tamai *et al.*, 1986; Tamai *et al.*, 1987). The administration of Loxistatin (E64d) in these patients was well tolerated. Even though the results of the studies were inconclusive regarding

the benefit of Loxistatin in the treatment of DMD, it still showed that targeting cysteine cathepsins was possible without severe side effects (Satoyoshi, 1992).

The dependency of ZEBOV GP on endosomal cathepsins seemed to vary in different cell types with only a mild effect on viral replication by the use of cysteine protease inhibitors (Gnirss *et al.*, 2012; Marzi *et al.*, 2012). In this study, a synergistic effect of combined furin and cathepsin inhibition on rVSVΔG ZEBOV GP replication in Huh-7, VeroE6 and Vero-TMPRSS2 cells was observed (Figure 11 B, Figure 13 C and Figure 18 C). Due to the (i) apparent complex proteolytic activation mechanism of ZEBOV GP and (ii) differences in the protease repertoire in the used cell lines, rVSVΔG ZEBOV GP replication was only completely blocked in Huh-7 cells. The data suggested that in contrast to IAV and SARS-CoV-2 infections, different host cell proteases, including TMPRRS2, were able to alternatively activate ZEBOV GP in the absence of the classical processing host cell proteases furin and endosomal cathepsins. The treatment of ZEBOV infections with host cell protease inhibitors could therefore be challenging and at worst inefficient in the context of systemic infections with replication in various tissues and cell types. Hence, a combined treatment with compounds targeting additional host cell factors should be considered. The NPC1 cholesterol transporter has been shown to be the endosomal/lysosomal entry receptor for ZEBOV virus binding to the RBR after trimming of $GP_1$. Furthermore, replication of rVSVΔG ZEBOV GP was strongly suppressed *in vitro* under the treatment with the NPC1 inhibitor imipramine (Rodriguez-Lafrasse *et al.*, 1990; Carette *et al.*, 2011). Additional infection studies with mouse-adapted ZEBOV in knockout mice further suggested an essential role of NPC1 in viral replication, as all homozygote $NPC1^{-/-}$ animals were protected from lethal infections. Nevertheless, treatment of wildtype animals with 20 mg/kg intraperitoneally administered imipramine only slightly reduced weight loss and increased survival. However, viral replication in the liver, spleen and serum was significantly reduced compared to the untreated control group (Herbert *et al.*, 2015).

A combined treatment regime with up to three antiviral drugs, like it is known for antiviral therapy of HIV, could allow lower drug doses and therefore help to overcome unwanted side effects and could prevent resistance development (Cihlar & Fordyce, 2016; Sun *et al.*, 2017). Thus, the thorough investigation, characterization and consideration of virus-activating host cell factors, including host cell proteases, is important in the process of antiviral drug development and treatment.

## 5.5 Concluding remarks and future prospects

Shedding light on the proteolytic activation of SARS-CoV-2 S and ZEBOV GP, each possessing two host cell protease cleavage sites, revealed very distinct cleavage processes. Activation of SARS-CoV-2 S was predominantly performed by furin and TMPRSS2 in Calu-3 cells, making these proteases promising drug targets for the development of antiviral COVID-19 treatment. In contrast, the processing of ZEBOV GP was shown to be more complex with different proteases involved, depending on the protease repertoire present in the infected cell type. Thus, antiviral strategy development for Ebola virus disease appeared to be more difficult. Nevertheless, the data still emphasize the need for proper characterization of host cell factors crucial for viral replication in order to develop potent host-directed antiviral therapeutics. Especially the identification of the possible unusual processing site of TMPRSS2 within the ZEBOV GP_AGTAA could reveal a broader substrate specificity of this important virus-activating protease. Hence, ZEBOV $GP_2$ from TMPRSS2 co-expression experiments should be analyzed by Edman N-terminal protein sequencing or mass spectrometry, in order to identify the cleavage site.

In this study all data on ZEBOV GP activation were generated in pseudovirus or VLP background, incorporating high levels of GP into their respective membranes. The vast expression of GP on the particle surface could distort the level of virus entry into the host cells. Hence, the effect of a combined furin and cathepsin inhibitor treatment should be further assessed by the use of authentic ZEBOV under BSL-4 conditions. Furthermore, studies with recombinant ZEBOV containing the ZEBOV GP_AGTAAΔ1&2 variant could shed more light on the entry capacity of this cleavage site mutant. ZEBOV has been shown to enter a broad range of host cells including epithelial, endothelial, neuronal and immune cells. As tissue-resident macrophages seem to be the first site of viral entry, it would be interesting to determine the effect of protease inhibition in THP-1 cells infected with ZEBOV. Moreover, mRNA sequencing analysis of the respective host cell protease repertoire in Huh-7, VeroE6 and Vero-TMPRSS2 cells could provide further insight and help to identify the so far unknown protease(s) involved in the ZEBOV GP processing, especially in VeroE6 and Vero-TMPRSS2 cells.

Neither for SARS-CoV-2 S nor ZEBOV GP, the inhibitor approach was sufficient to pinpoint the location of TMPRSS2 processing within the cell. Nevertheless, first co-localization data revealed the presence of TMPRSS2 not only as previously described in the TGN, but as well in the ERGIC and to some degree in the endosomal compartments. Hence, future TMPRSS2 co-localization studies should be extended to ZEBOV and SARS-CoV-2 infected cells, in order to detect possible subcellular TMPRSS2-processing sites of GP and S.

# 6 References


Afar, D.E., Vivanco, I., Hubert, R.S., Kuo, J., Chen, E. & Saffran, D.C. et al. (2001) Catalytic cleavage of the androgen-regulated TMPRSS2 protease results in its secretion by prostate and prostate cancer epithelia. *Cancer Research*, 61(4), 1686–1692. Available from: https://cancerres.aacrjournals.org/content/61/4/1686.short.

Ascenzi, P., Bocedi, A., Bolognesi, M., Spallarossa, A., Coletta, M. & Cristofaro, R. de et al. (2003) The bovine basic pancreatic trypsin inhibitor (Kunitz inhibitor): a milestone protein. *Current Protein & Peptide Science*, 4(3), 231–251. Available from: https://doi.org/10.2174/1389203033487180.

Barrett, A.J., Woessner, J.F. & Rawlings, N.D. (2012) *Handbook of proteolytic enzymes*, 2nd edition. Elsevier Academic Press: London.

Belouzard, S., Chu, V.C. & Whittaker, G.R. (2009) Activation of the SARS coronavirus spike protein via sequential proteolytic cleavage at two distinct sites. *Proceedings of the National Academy of Sciences of the United States of America*, 106(14), 5871–5876. Available from: https://doi.org/10.1073/pnas.0809524106.

Belouzard, S., Millet, J.K., Licitra, B.N. & Whittaker, G.R. (2012) Mechanisms of coronavirus cell entry mediated by the viral spike protein. *Viruses*, 4(6), 1011–1033. Available from: https://doi.org/10.3390/v4061011.

Berry, D.M. & Almeida, J.D. (1968) The morphological and biological effects of various antisera on avian infectious bronchitis virus. *The Journal of General Virology*, 3(1), 97–102. Available from: https://doi.org/10.1099/0022-1317-3-1-97.

Bertram, S., Heurich, A., Lavender, H., Gierer, S., Danisch, S. & Perin, P. et al. (2012) Influenza and SARS-coronavirus activating proteases TMPRSS2 and HAT are expressed at multiple sites in human respiratory and gastrointestinal tracts. *PloS One*, 7(4), e35876. Available from: https://doi.org/10.1371/journal.pone.0035876.

Bestle, D., Heindl, M.R., Limburg, H., van Lam van, T., Pilgram, O. & Moulton, H. et al. (2020) TMPRSS2 and furin are both essential for proteolytic activation of SARS-CoV-2 in human airway cells. *Life Science Alliance*, 3(9). Available from: https://doi.org/10.26508/lsa.202000786.

Bestle, D., Limburg, H., Kruhl, D., Harbig, A., Stein, D.A. & Moulton, H. et al. (2021) Hemagglutinins of Avian Influenza Viruses Are Proteolytically Activated by TMPRSS2 in Human and Murine Airway Cells. *Journal of Virology*, 95(20), e0090621. Available from: https://doi.org/10.1128/JVI.00906-21.

Bhatia, B., Furuyama, W., Hoenen, T., Feldmann, H. & Marzi, A. (2021) Ebola Virus Glycoprotein Domains Associated with Protective Efficacy. *Vaccines*, 9(6). Available from: https://doi.org/10.3390/vaccines9060630.

Bier, C., Knauer, S.K., Klapthor, A., Schweitzer, A., Rekik, A. & Krämer, O.H. et al. (2011) Cell-based analysis of structure-function activity of threonine aspartase 1. *Journal of Biological Chemistry*, 286(4), 3007–3017. Available from: https://doi.org/10.1074/jbc.M110.161646.

Bimboim, H.C. & Doly, J. (1979) A rapid alkaline extraction procedure for screening recombinant plasmid DNA. *Nucleic Acids Research*, 7(6), 1513–1523. Available from: https://doi.org/10.1093/nar/7.6.1513.

Bisht, H., Roberts, A., Vogel, L., Bukreyev, A., Collins, P.L. & Murphy, B.R. et al. (2004) Severe acute respiratory syndrome coronavirus spike protein expressed by attenuated vaccinia virus protectively immunizes mice. *Proceedings of the National Academy of Sciences*, 101(17), 6641–6646. Available from: https://doi.org/10.1073/pnas.0401939101.

Bixler, S.L., Duplantier, A.J. & Bavari, S. (2017) Discovering Drugs for the Treatment of Ebola Virus. *Current Treatment Options in Infectious Diseases*, 9(3), 299–317. Available from: https://doi.org/10.1007/s40506-017-0130-z.

Bock, M. de, Wang, N., Decrock, E., Bultynck, G. & Leybaert, L. (2015) Intracellular Cleavage of the Cx43 C-Terminal Domain by Matrix-Metalloproteases: A Novel Contributor to Inflammation? *Mediators of Inflammation*, 2015, 257471. Available from: https://doi.org/10.1155/2015/257471.

Bosch, B.J., Bartelink, W. & Rottier, P.J.M. (2008) Cathepsin L functionally cleaves the severe acute respiratory syndrome coronavirus class I fusion protein upstream of rather than adjacent to the fusion peptide. *Journal of Virology*, 82(17), 8887–8890. Available from: https://doi.org/10.1128/JVI.00415-08.

Bosch, B.J., van der Zee, R., Haan, C.A.M. de & Rottier, P.J.M. (2003) The coronavirus spike protein is a class I virus fusion protein: structural and functional characterization of the fusion core complex. *Journal of Virology*, 77(16), 8801–8811. Available from: https://doi.org/10.1128/jvi.77.16.8801-8811.2003.

Böttcher, E., Matrosovich, T., Beyerle, M., Klenk, H.-D., Garten, W. & Matrosovich, M. (2006) Proteolytic activation of influenza viruses by serine proteases TMPRSS2 and HAT from human airway epithelium. *Journal of Virology*, 80(19), 9896–9898. Available from: https://doi.org/10.1128/JVI.01118-06.

Böttcher-Friebertshäuser, E., Freuer, C., Sielaff, F., Schmidt, S., Eickmann, M. & Uhlendorff, J. et al. (2010) Cleavage of influenza virus hemagglutinin by airway proteases TMPRSS2 and HAT differs in subcellular localization and susceptibility to protease inhibitors. *Journal of Virology*, 84(11), 5605–5614. Available from: https://doi.org/10.1128/JVI.00140-10.

Böttcher-Friebertshäuser, E., Garten, W. & Klenk, H.D. (2018) *Activation of Viruses by Host Proteases*. Springer International Publishing: Cham.

Böttcher-Friebertshäuser, E., Garten, W., Matrosovich, M. & Klenk, H.D. (2014) The Hemagglutinin: A Determinant of Pathogenicity. In: *Influenza Pathogenesis and Control - Volume I.* Springer, Cham, pp. 3–34.

Böttcher-Friebertshäuser, E., Klenk, H.-D. & Garten, W. (2013) Activation of influenza viruses by proteases from host cells and bacteria in the human airway epithelium. *Pathogens and Disease*, 69(2), 87–100. Available from: https://doi.org/10.1111/2049-632X.12053.

Böttcher-Friebertshäuser, E., Lu, Y., Meyer, D., Sielaff, F., Steinmetzer, T. & Klenk, H.-D. et al. (2012) Hemagglutinin activating host cell proteases provide promising drug targets for the treatment of influenza A and B virus infections. *Vaccine*, 30(51), 7374–7380. Available from: https://doi.org/10.1016/j.vaccine.2012.10.001.

Böttcher-Friebertshäuser, E., Stein, D.A., Klenk, H.-D. & Garten, W. (2011) Inhibition of influenza virus infection in human airway cell cultures by an antisense peptide-conjugated morpholino oligomer targeting the hemagglutinin-activating protease TMPRSS2. *Journal of Virology*, 85(4), 1554–1562. Available from: https://doi.org/10.1128/JVI.01294-10.

Brandsdal, B.O., Aqvist, J. & Smalås, A.O. (2001) Computational analysis of binding of P1 variants to trypsin. *Protein Science : a Publication of the Protein Society*, 10(8), 1584–1595. Available from: https://doi.org/10.1110/ps.940101.

Bray, M. & Geisbert, T.W. (2005) Ebola virus: the role of macrophages and dendritic cells in the pathogenesis of Ebola hemorrhagic fever. *The International Journal of Biochemistry & Cell Biology*, 37(8), 1560–1566. Available from: https://doi.org/10.1016/j.biocel.2005.02.018.

Brecher, M., Schornberg, K.L., Delos, S.E., Fusco, M.L., Saphire, E.O. & White, J.M. (2012) Cathepsin cleavage potentiates the Ebola virus glycoprotein to undergo a subsequent fusion-relevant conformational change. *Journal of Virology*, 86(1), 364–372. Available from: https://doi.org/10.1128/JVI.05708-11.

Bright, R.A., Medina, M., Xu, X., Perez-Oronoz, G., Wallis, T.R. & Davis, X.M. et al. (2005) Incidence of adamantane resistance among influenza A (H3N2) viruses isolated worldwide from 1994 to 2005: a cause for concern. *The Lancet*, 366(9492), 1175–1181. Available from: https://doi.org/10.1016/S0140-6736(05)67338-2.

Brix, K. (2005) Lysosomal Proteases. In: Saftig, P. (Ed.) *Lysosomes.* Landes Bioscience/Eurekah.com; Springer: Georgetown, Tex., New York, N.Y., Heidelberg, pp. 50–59.

Brix, K. (2018) Host Cell Proteases: Cathepsins. In: *Activation of Viruses by Host Proteases.* Springer, Cham, pp. 249–276.

Brix, K., Dunkhorst, A., Mayer, K. & Jordans, S. (2008) Cysteine cathepsins: cellular roadmap to different functions. *Biochimie*, 90(2), 194–207. Available from: https://doi.org/10.1016/j.biochi.2007.07.024.

Brix, K. & Jordans, S. (2005) Watching proteases in action. *Nature Chemical Biology*, 1(4), 186–187. Available from: https://doi.org/10.1038/nchembio0905-186.

Brugh, M. (1988) Highly Pathogenic Virus Recovered from Chickens Infected with Mildly Pathogenic 1986 Isolates of H5N2 Avian Influenza Virus. *Avian Diseases*, 32(4), 695. Available from: https://doi.org/10.2307/1590987.

Buck, M.R., Karustis, D.G., Day, N.A., Honn, K.V. & Sloane, B.F. (1992) Degradation of extracellular-matrix proteins by human cathepsin B from normal and tumour tissues. *Biochemical Journal*, 282 (Pt 1)(1), 273–278. Available from: https://doi.org/10.1042/bj2820273.

Bugge, T.H., Antalis, T.M. & Wu, Q. (2009) Type II transmembrane serine proteases. *The Journal of Biological Chemistry*, 284(35), 23177–23181. Available from: https://doi.org/10.1074/jbc.R109.021006.

Burnette, W. (1981) "Western Blotting": Electrophoretic transfer of proteins from sodium dodecyl sulfate-polyacrylamide gels to unmodified nitrocellulose and radiographic detection with antibody and radioiodinated protein A. *Analytical Biochemistry*, 112(2), 195–203. Available from: https://doi.org/10.1016/0003-2697(81)90281-5.

Cai, Y., Zhang, J., Xiao, T., Peng, H., Sterling, S.M. & Walsh, R.M. et al. (2020) Distinct conformational states of SARS-CoV-2 spike protein. *Science (New York, N.Y.)*, 369(6511), 1586–1592. Available from: https://doi.org/10.1126/science.abd4251.

Carette, J.E., Raaben, M., Wong, A.C., Herbert, A.S., Obernosterer, G. & Mulherkar, N. et al. (2011) Ebola virus entry requires the cholesterol transporter Niemann-Pick C1. *Nature*, 477(7364), 340–343. Available from: https://doi.org/10.1038/nature10348.

Cauwe, B. & Opdenakker, G. (2010) Intracellular substrate cleavage: a novel dimension in the biochemistry, biology and pathology of matrix metalloproteinases. *Critical Reviews in Biochemistry and Molecular Biology*, 45(5), 351–423. Available from: https://doi.org/10.3109/10409238.2010.501783.

CDC (2003) Revised U.S. Surveillance Case Definition for Severe Acute Respiratory Syndrome (SARS) and Update on SARS Cases --- United States and Worldwide, December 2003. *MMWR,* 12 December, pp. 1202–1206.

CDC (2019) *Ebola Virus Disease Distribution Map: Cases of Ebola Virus Disease in Africa Since 1976; 2019*.

Chandran, K., Sullivan, N.J., Felbor, U., Whelan, S.P. & Cunningham, J.M. (2005) Endosomal proteolysis of the Ebola virus glycoprotein is necessary for infection. *Science (New York, N.Y.)*, 308(5728), 1643–1645. Available from: https://doi.org/10.1126/science.1110656.

Chassy, B.M., Mercenier, A. & Flickinger, J. (1988) Transformation of bacteria by electroporation. *Trends in Biotechnology*, 6(12), 303–309. Available from: https://doi.org/10.1016/0167-7799(88)90025-X.

Cihlar, T. & Fordyce, M. (2016) Current status and prospects of HIV treatment. *Current Opinion in Virology*, 18, 50–56. Available from: https://doi.org/10.1016/j.coviro.2016.03.004.

Cohen, S.N., Chang, A.C. & Hsu, L. (1972) Nonchromosomal antibiotic resistance in bacteria: genetic transformation of Escherichia coli by R-factor DNA. *Proceedings of the National Academy of Sciences*, 69(8), 2110–2114. Available from: https://doi.org/10.1073/pnas.69.8.2110.

Collins, L.T., Elkholy, T., Mubin, S., Hill, D., Williams, R. & Ezike, K. et al. (2021) Elucidation of SARS-Cov-2 Budding Mechanisms through Molecular Dynamics Simulations of M and E Protein Complexes. *The Journal of Physical Chemistry Letters*, 12(51), 12249–12255. Available from: https://doi.org/10.1021/acs.jpclett.1c02955.

Côté, M., Misasi, J., Ren, T., Bruchez, A., Lee, K. & Filone, C.M. et al. (2011) Small molecule inhibitors reveal Niemann-Pick C1 is essential for ebolavirus infection. *Nature*, 477(7364), 344–348. Available from: https://doi.org/10.1038/nature10380.

Coutard, B., Valle, C., Lamballerie, X. de, Canard, B., Seidah, N.G. & Decroly, E. (2020) The spike glycoprotein of the new coronavirus 2019-nCoV contains a furin-like cleavage site absent in CoV of the same clade. *Antiviral Research*, 176, 104742. Available from: https://doi.org/10.1016/j.antiviral.2020.104742.

Deu, E., Verdoes, M. & Bogyo, M. (2012) New approaches for dissecting protease functions to improve probe development and drug discovery. *Nature Structural & Molecular Biology*, 19(1), 9–16. Available from: https://doi.org/10.1038/nsmb.2203.

Diederich, S., Moll, M., Klenk, H.-D. & Maisner, A. (2005) The nipah virus fusion protein is cleaved within the endosomal compartment. *Journal of Biological Chemistry*, 280(33), 29899–29903. Available from: https://doi.org/10.1074/jbc.M504598200.

Diederich, S., Sauerhering, L., Weis, M., Altmeppen, H., Schaschke, N. & Reinheckel, T. et al. (2012) Activation of the Nipah virus fusion protein in MDCK cells is mediated by cathepsin B within the endosome-recycling compartment. *Journal of Virology*, 86(7), 3736–3745. Available from: https://doi.org/10.1128/JVI.06628-11.

Dolnik, O., Volchkova, V., Garten, W., Carbonnelle, C., Becker, S. & Kahnt, J. et al. (2004) Ectodomain shedding of the glycoprotein GP of Ebola virus. *The EMBO Journal*, 23(10), 2175–2184. Available from: https://doi.org/10.1038/sj.emboj.7600219.

Donaldson, S.H., Hirsh, A., Li, D.C., Holloway, G., Chao, J. & Boucher, R.C. et al. (2002) Regulation of the epithelial sodium channel by serine proteases in human airways. *Journal of Biological Chemistry*, 277(10), 8338–8345. Available from: https://doi.org/10.1074/jbc.M105044200.

Dong, E., Du, H. & Gardner, L. (2020) An interactive web-based dashboard to track COVID-19 in real time. *The Lancet Infectious Diseases*, 20(5), 533–534. Available from: https://doi.org/10.1016/S1473-3099(20)30120-1.

Drosten, C., Günther, S., Preiser, W., van der Werf, S., Brodt, H.-R. & Becker, S. et al. (2003) Identification of a novel coronavirus in patients with severe acute respiratory syndrome. *The New England Journal of Medicine*, 348(20), 1967–1976. Available from: https://doi.org/10.1056/NEJMoa030747.

Drożdżal, S., Rosik, J., Lechowicz, K., Machaj, F., Kotfis, K. & Ghavami, S. et al. (2020) FDA approved drugs with pharmacotherapeutic potential for SARS-CoV-2 (COVID-19) therapy. *Drug Resistance Updates : Reviews and Commentaries in Antimicrobial and Anticancer Chemotherapy*, 53, 100719. Available from: https://doi.org/10.1016/j.drup.2020.100719.

Dube, D., Brecher, M.B., Delos, S.E., Rose, S.C., Park, E.W. & Schornberg, K.L. et al. (2009) The primed ebolavirus glycoprotein (19-kilodalton GP1,2): sequence and residues critical for host cell binding. *Journal of Virology*, 83(7), 2883–2891. Available from: https://doi.org/10.1128/JVI.01956-08.

Duve, C. de & Wattiaux, R. (1966) Functions of lysosomes. *Annual Review of Physiology*, 28, 435–492. Available from: https://doi.org/10.1146/annurev.ph.28.030166.002251.

ECDC (2022) *Geographical distribution of confirmed MERS-CoV cases by reporting country from April 2012 to 3 May 2022*. Available from: https://www.ecdc.europa.eu/en/publications-data/geographical-distribution-confirmed-mers-cov-cases-reporting-country-april-2012-1.

Erickson, A.H., Isidoro, C., Mach, L. & Mort, J.S. (2013) Cathepsins: Getting in Shape for Lysosomal Proteolysis. In: Brix, K. (Ed.) *Proteases: Structure and function.* Springer: Wien, Heidelberg, pp. 127–173.

Felbor, U., Kessler, B., Mothes, W., Goebel, H.H., Ploegh, H.L. & Bronson, R.T. et al. (2002) Neuronal loss and brain atrophy in mice lacking cathepsins B and L. *Proceedings of the National Academy of Sciences*, 99(12), 7883–7888. Available from: https://doi.org/10.1073/pnas.112632299.

Feldmann, H. & Geisbert, T.W. (2011) Ebola haemorrhagic fever. *The Lancet*, 377(9768), 849–862. Available from: https://doi.org/10.1016/S0140-6736(10)60667-8.

Feldmann, H., Klenk, H.D. & Sanchez, A. (1993) Molecular biology and evolution of filoviruses. *Archives of Virology. Supplementum*, 7, 81–100. Available from: https://doi.org/10.1007/978-3-7091-9300-6_8.

Fergusson, D.A., Hébert, P.C., Mazer, C.D., Fremes, S., MacAdams, C. & Murkin, J.M. et al. (2008) A comparison of aprotinin and lysine analogues in high-risk cardiac surgery. *The New England Journal of Medicine*, 358(22), 2319–2331. Available from: https://doi.org/10.1056/NEJMoa0802395.

Fraser, B.J., Beldar, S., Seitova, A., Hutchinson, A., Mannar, D. & Li, Y. et al. (2022) Structure and activity of human TMPRSS2 protease implicated in SARS-CoV-2 activation. *Nature Chemical Biology*. Available from: https://doi.org/10.1038/s41589-022-01059-7.

Fuller, R.S., Brake, A.J. & Thorner, J. (1989) Intracellular targeting and structural conservation of a prohormone-processing endoprotease. *Science (New York, N.Y.)*, 246(4929), 482–486. Available from: https://doi.org/10.1126/science.2683070.

Funkelstein, L., Toneff, T., Mosier, C., Hwang, S.-R., Beuschlein, F. & Lichtenauer, U.D. et al. (2008) Major role of cathepsin L for producing the peptide hormones ACTH, beta-endorphin, and alpha-MSH, illustrated by protease gene knockout and expression. *Journal of Biological Chemistry*, 283(51), 35652–35659. Available from: https://doi.org/10.1074/jbc.M709010200.

Galloway, S.E., Liang, B. & Steinhauer, D.A. (2018) Activation of the Hemagglutinin of Influenza Viruses. In: *Activation of Viruses by Host Proteases.* Springer, Cham, pp. 3–26.

Garten, W. (2018) Characterization of Proprotein Convertases and Their Involvement in Virus Propagation. In: *Activation of Viruses by Host Proteases.* Springer, Cham, pp. 205–248.

Garten, W., Hallenberger, S., Ortmann, D., Schäfer, W., Vey, M. & Angliker, H. et al. (1994) Processing of viral glycoproteins by the subtilisin-like endoprotease furin and its inhibition by specific peptidylchloroalkylketones. *Biochimie*, 76(3-4), 217–225. Available from: https://doi.org/10.1016/0300-9084(94)90149-X.

Gierer, S., Bertram, S., Kaup, F., Wrensch, F., Heurich, A. & Krämer-Kühl, A. et al. (2013) The spike protein of the emerging betacoronavirus EMC uses a novel coronavirus receptor for entry, can be activated by TMPRSS2, and is targeted by neutralizing antibodies. *Journal of Virology*, 87(10), 5502–5511. Available from: https://doi.org/10.1128/JVI.00128-13.

Gierer, S., Müller, M.A., Heurich, A., Ritz, D., Springstein, B.L. & Karsten, C.B. et al. (2015) Inhibition of proprotein convertases abrogates processing of the middle eastern respiratory syndrome coronavirus spike protein in infected cells but does not reduce viral infectivity. *The Journal of Infectious Diseases*, 211(6), 889–897. Available from: https://doi.org/10.1093/infdis/jiu407.

Glowacka, I., Bertram, S., Müller, M.A., Allen, P., Soilleux, E. & Pfefferle, S. et al. (2011) Evidence that TMPRSS2 activates the severe acute respiratory syndrome coronavirus spike protein for membrane fusion and reduces viral control by the humoral immune response. *Journal of Virology*, 85(9), 4122–4134. Available from: https://doi.org/10.1128/JVI.02232-10.

Gnirss, K., Kühl, A., Karsten, C., Glowacka, I., Bertram, S. & Kaup, F. et al. (2012) Cathepsins B and L activate Ebola but not Marburg virus glycoproteins for efficient entry into cell lines and macrophages independent of TMPRSS2 expression. *Virology*, 424(1), 3–10. Available from: https://doi.org/10.1016/j.virol.2011.11.031.

Gregory, S.M., Harada, E., Liang, B., Delos, S.E., White, J.M. & Tamm, L.K. (2011) Structure and function of the complete internal fusion loop from Ebolavirus glycoprotein 2. *Proceedings of the National Academy of Sciences of the United States of America*, 108(27), 11211–11216. Available from: https://doi.org/10.1073/pnas.1104760108.

Grimm, C., Holdt, L.M., Chen, C.-C., Hassan, S., Müller, C. & Jörs, S. et al. (2014) High susceptibility to fatty liver disease in two-pore channel 2-deficient mice. *Nature Communications*, 5, 4699. Available from: https://doi.org/10.1038/ncomms5699.

Groot, R.J. de, Baker, S.C., Baric, R., Enjuanes, L., Gorbalenya, A.E. & Holmes, K.V. et al. (2011) *Family coronaviridae*.

Gunst, J.D., Staerke, N.B., Pahus, M.H., Kristensen, L.H., Bodilsen, J. & Lohse, N. et al. (2021) Efficacy of the TMPRSS2 inhibitor camostat mesilate in patients hospitalized with Covid-19-a double-blind randomized controlled trial. *EClinicalMedicine*, 35, 100849. Available from: https://doi.org/10.1016/j.eclinm.2021.100849.

Haan, C.A. de & Rottier, P.J. (2016) Molecular Interactions in the Assembly of Coronaviruses. In: Ziebuhr, J. (Ed.) *Advances in Virus Research : Coronaviruses.* Academic Press, pp. 165–230.

Haan, C.A.M. de, Stadler, K., Godeke, G.-J., Bosch, B.J. & Rottier, P.J.M. (2004) Cleavage inhibition of the murine coronavirus spike protein by a furin-like enzyme affects cell-cell but not virus-cell fusion. *Journal of Virology*, 78(11), 6048–6054. Available from: https://doi.org/10.1128/JVI.78.11.6048-6054.2004.

Hammami, M., Rühmann, E., Maurer, E., Heine, A., Gütschow, M. & Klebe, G. et al. (2012) New 3-amidinophenylalanine-derived inhibitors of matriptase. *MedChemComm*, 3(7), 807. Available from: https://doi.org/10.1039/C2MD20074K.

Hanada, K., Tamai, M., Yamagishi, M., Ohmura, S., Sawada, J. & Tanaka, I. (1978) Isolation and Characterization of E–64, a New Thiol Protease Inhibitor. *Agricultural and Biological Chemistry*, 42(3), 523–528. Available from: https://doi.org/10.1080/00021369.1978.10863014.

Hardes, K., Becker, G.L., Lu, Y., Dahms, S.O., Köhler, S. & Beyer, W. et al. (2015) Novel Furin Inhibitors with Potent Anti-infectious Activity. *ChemMedChem*, 10(7), 1218–1231. Available from: https://doi.org/10.1002/cmdc.201500103.

Harrison, A.G., Lin, T. & Wang, P. (2020) Mechanisms of SARS-CoV-2 Transmission and Pathogenesis. *Trends in Immunology*, 41(12), 1100–1115. Available from: https://doi.org/10.1016/j.it.2020.10.004.

Hatesuer, B., Bertram, S., Mehnert, N., Bahgat, M.M., Nelson, P.S. & Pöhlmann, S. et al. (2013) Tmprss2 is essential for influenza H1N1 virus pathogenesis in mice. *PLoS Pathogens*, 9(12), e1003774. Available from: https://doi.org/10.1371/journal.ppat.1003774.

Helenius, A., Marsh, M. & White, J. (1980) The entry of viruses into animal cells. *Trends in Biochemical Sciences*, 5(4), 104–106. Available from: https://doi.org/10.1016/0968-0004(80)90260-1.

Hellstern, P., Stürzebecher, U., Wuchold, B., Haubelt, H., Seyfert, U.T. & Bauer, M. et al. (2007) Preservation of in vitro function of platelets stored in the presence of a synthetic dual inhibitor of factor Xa and thrombin. *Journal of Thrombosis and Haemostasis : JTH*, 5(10), 2119–2126. Available from: https://doi.org/10.1111/j.1538-7836.2007.02716.x.

Herbert, A.S., Davidson, C., Kuehne, A.I., Bakken, R., Braigen, S.Z. & Gunn, K.E. et al. (2015) Niemann-pick C1 is essential for ebolavirus replication and pathogenesis in vivo. *MBio*, 6(3), e00565-15. Available from: https://doi.org/10.1128/mBio.00565-15.

Hierholzer, J.C. & Killington, R.A. (1996) 2 - Virus isolation and quantitation. In: Mahy, B.W.J. & Kangro, H.O. (Eds.) *Virology Methods Manual.* Academic Press: London, pp. 25–46.

Hoenen, T. & Feldmann, H. (2014) Reverse genetics systems as tools for the development of novel therapies against filoviruses. *Expert Review of Anti-Infective Therapy*, 12(10), 1253–1263. Available from: https://doi.org/10.1586/14787210.2014.948848.

Hoenen, T., Groseth, A., Kolesnikova, L., Theriault, S., Ebihara, H. & Hartlieb, B. et al. (2006) Infection of naive target cells with virus-like particles: implications for the function of ebola virus VP24. *Journal of Virology*, 80(14), 7260–7264. Available from: https://doi.org/10.1128/JVI.00051-06.

Hoffmann, M., Hofmann-Winkler, H. & Pöhlmann, S. (2018) Priming Time: How Cellular Proteases Arm Coronavirus Spike Proteins. In: *Activation of Viruses by Host Proteases.* Springer, Cham, pp. 71–98.

Hoffmann, M., Kleine-Weber, H., Schroeder, S., Krüger, N., Herrler, T. & Erichsen, S. et al. (2020) SARS-CoV-2 Cell Entry Depends on ACE2 and TMPRSS2 and Is Blocked by a Clinically Proven Protease Inhibitor. *Cell*, 181(2), 271-280.e8. Available from: https://doi.org/10.1016/j.cell.2020.02.052.

Honey, K. & Rudensky, A.Y. (2003) Lysosomal cysteine proteases regulate antigen presentation. *Nature Reviews Immunology*, 3(6), 472–482. Available from: https://doi.org/10.1038/nri1110.

Horimoto, T., Nakayama, K., Smeekens, S.P. & Kawaoka, Y. (1994) Proprotein-processing endoproteases PC6 and furin both activate hemagglutinin of virulent avian influenza viruses. *Journal of Virology*, 68(9), 6074–6078. Available from: https://doi.org/10.1128/JVI.68.9.6074-6078.1994.

Hosaka, M., Nagahama, M., Kim, W.S., Watanabe, T., Hatsuzawa, K. & Ikemizu, J. et al. (1991) Arg-X-Lys/Arg-Arg motif as a signal for precursor cleavage catalyzed by furin within the constitutive secretory pathway. *Journal of Biological Chemistry*, 266(19), 12127–12130. Available from: https://doi.org/10.1016/S0021-9258(18)98867-8.

Hu, Y., Lu, S., Song, Z., Wang, W., Hao, P. & Li, J. et al. (2013) Association between adverse clinical outcome in human disease caused by novel influenza A H7N9 virus and sustained viral shedding and emergence of antiviral resistance. *The Lancet*, 381(9885), 2273–2279. Available from: https://doi.org/10.1016/S0140-6736(13)61125-3.

Huotari, J. & Helenius, A. (2011) Endosome maturation. *The EMBO Journal*, 30(17), 3481–3500. Available from: https://doi.org/10.1038/emboj.2011.286.

Hussain, M., Galvin, H.D., Haw, T.Y., Nutsford, A.N. & Husain, M. (2017) Drug resistance in influenza A virus: the epidemiology and management. *Infection and Drug Resistance*, 10, 121–134. Available from: https://doi.org/10.2147/IDR.S105473.

Ito, H., Watanabe, S., Takada, A. & Kawaoka, Y. (2001) Ebola virus glycoprotein: Proteolytic processing, acylation, cell tropism, and detection of neutralizing antibodies. *Journal of Virology*, 75(3), 1576–1580. Available from: https://doi.org/10.1128/JVI.75.3.1576-1580.2001.

IUPAC-IUB Joint Commission on Biochemical Nomenclature (JCBN). (1984) Nomenclature and symbolism for amino acids and peptides. Recommendations 1983. *European Journal of Biochemistry*, 138(1), 9–37. Available from: https://doi.org/10.1111/j.1432-1033.1984.tb07877.x.

Iwata-Yoshikawa, N., Okamura, T., Shimizu, Y., Hasegawa, H., Takeda, M. & Nagata, N. (2019) TMPRSS2 contributes to virus spread and immunopathology in the airways of murine models after coronavirus infection. *Journal of Virology*. Available from: https://doi.org/10.1128/JVI.01815-18.

Janko, M., Zink, A., Gigler, A.M., Heckl, W.M. & Stark, R.W. (2010) Nanostructure and mechanics of mummified type I collagen from the 5300-year-old Tyrolean Iceman. *Proceedings. Biological Sciences*, 277(1692), 2301–2309. Available from: https://doi.org/10.1098/rspb.2010.0377.

Jeffers, S.A., Sanders, D.A. & Sanchez, A. (2002) Covalent Modifications of the Ebola Virus Glycoprotein. *Journal of virology*, 76(24), 12463–12472. Available from: https://doi.org/10.1128/JVI.76.24.12463-12472.2002.

Jiang, A., Lehti, K., Wang, X., Weiss, S.J., Keski-Oja, J. & Pei, D. (2001) Regulation of membrane-type matrix metalloproteinase 1 activity by dynamin-mediated endocytosis. *Proceedings of the National Academy of Sciences*, 98(24), 13693–13698. Available from: https://doi.org/10.1073/pnas.241293698.

Jobin, P.G., Butler, G.S. & Overall, C.M. (2017) New intracellular activities of matrix metalloproteinases shine in the moonlight. *Biochimica Et Biophysica Acta (BBA) - Molecular Cell Research*, 1864(11 Pt A), 2043–2055. Available from: https://doi.org/10.1016/j.bbamcr.2017.05.013.

Johnson, B.A., Xie, X., Bailey, A.L., Kalveram, B., Lokugamage, K.G. & Muruato, A. et al. (2021) Loss of furin cleavage site attenuates SARS-CoV-2 pathogenesis. *Nature*, 591(7849), 293–299. Available from: https://doi.org/10.1038/s41586-021-03237-4.

Kaletsky, R.L., Simmons, G. & Bates, P. (2007) Proteolysis of the Ebola virus glycoproteins enhances virus binding and infectivity. *Journal of Virology*, 81(24), 13378–13384. Available from: https://doi.org/10.1128/JVI.01170-07.

Kassell, B., Radicevic, M., Ansfield, M.J. & Laskowski, M. (1965) The basic trypsin inhibitor of bovine pancreas IV. The linear sequence of the 58 amino acids. *Biochemical and biophysical research communications*, 18(2), 255–258. Available from: https://doi.org/10.1016/0006-291X(65)90749-7.

Kawase, M., Shirato, K., Matsuyama, S. & Taguchi, F. (2009) Protease-mediated entry via the endosome of human coronavirus 229E. *Journal of Virology*, 83(2), 712–721. Available from: https://doi.org/10.1128/JVI.01933-08.

Khailany, R.A., Safdar, M. & Ozaslan, M. (2020) Genomic characterization of a novel SARS-CoV-2. *Gene Reports*, 19, 100682. Available from: https://doi.org/10.1016/j.genrep.2020.100682.

Kim, T.S., Heinlein, C., Hackman, R.C. & Nelson, P.S. (2006) Phenotypic analysis of mice lacking the Tmprss2-encoded protease. *Molecular and Cellular Biology*, 26(3), 965–975. Available from: https://doi.org/10.1128/MCB.26.3.965-975.2006.

Kirchdoerfer, R.N., Cottrell, C.A., Wang, N., Pallesen, J., Yassine, H.M. & Turner, H.L. et al. (2016) Pre-fusion structure of a human coronavirus spike protein. *Nature*, 531(7592), 118–121. Available from: https://doi.org/10.1038/nature17200.

Kitagawa, J., Arai, H., Iida, H., Mukai, J., Furukawa, K. & Ohtsu, S. et al. (2021) A phase I study of high dose camostat mesylate in healthy adults provides a rationale to repurpose the TMPRSS2 inhibitor for the treatment of COVID-19. *Clinical and Translational Science*, 14(5), 1967–1976. Available from: https://doi.org/10.1111/cts.13052.

Klein, T., Eckhard, U., Dufour, A., Solis, N. & Overall, C.M. (2018) Proteolytic Cleavage-Mechanisms, Function, and "Omic" Approaches for a Near-Ubiquitous Posttranslational Modification. *Chemical Reviews*, 118(3), 1137–1168. Available from: https://doi.org/10.1021/acs.chemrev.7b00120.

Kleine-Weber, H., Elzayat, M.T., Hoffmann, M. & Pöhlmann, S. (2018) Functional analysis of potential cleavage sites in the MERS-coronavirus spike protein. *Scientific Reports*, 8(1), 1–11. Available from: https://doi.org/10.1038/s41598-018-34859-w.

Klenk, H.-D., Rott, R., Orlich, M. & Blödorn, J. (1975) Activation of influenza A viruses by trypsin treatment. *Virology*, 68(2), 426–439. Available from: https://doi.org/10.1016/0042-6822(75)90284-6.

Koch, J., Uckeley, Z.M., Doldan, P., Stanifer, M., Boulant, S. & Lozach, P.-Y. (2021) TMPRSS2 expression dictates the entry route used by SARS-CoV-2 to infect host cells. *The EMBO Journal*, 40(16), e107821. Available from: https://doi.org/10.15252/embj.2021107821.

Krijnse-Locker, J., Ericsson, M., Rottier, P.J. & Griffiths, G. (1994) Characterization of the budding compartment of mouse hepatitis virus: evidence that transport from the RER to the Golgi complex requires only one vesicular transport step. *Journal of Cell Biology*, 124(1-2), 55–70. Available from: https://doi.org/10.1083/jcb.124.1.55.

Krysan, D.J., Rockwell, N.C. & Fuller, R.S. (1999) Quantitative characterization of furin specificity. Energetics of substrate discrimination using an internally consistent set of hexapeptidyl methylcoumarinamides. *Journal of Biological Chemistry*, 274(33), 23229–23234. Available from: https://doi.org/10.1074/jbc.274.33.23229.

Kuzmin, P.I., Zimmerberg, J., Chizmadzhev, Y.A. & Cohen, F.S. (2001) A quantitative model for membrane fusion based on low-energy intermediates. *Proceedings of the National Academy of Sciences*, 98(13), 7235–7240. Available from: https://doi.org/10.1073/pnas.121191898.

Laemmli, U.K. (1970) Cleavage of structural proteins during the assembly of the head of bacteriophage T4. *Nature*, 227(5259), 680–685.

Lakadamyali, M., Rust, M.J. & Zhuang, X. (2006) Ligands for clathrin-mediated endocytosis are differentially sorted into distinct populations of early endosomes. *Cell*, 124(5), 997–1009. Available from: https://doi.org/10.1016/j.cell.2005.12.038.

Lambertz, R.L.O., Gerhauser, I., Nehlmeier, I., Gärtner, S., Winkler, M. & Leist, S.R. et al. (2020) H2 influenza A virus is not pathogenic in Tmprss2 knock-out mice. *Virology Journal*, 17(1), 56. Available from: https://doi.org/10.1186/s12985-020-01323-z.

Lambertz, R.L.O., Gerhauser, I., Nehlmeier, I., Leist, S.R., Kollmus, H. & Pöhlmann, S. et al. (2019) Tmprss2 knock-out mice are resistant to H10 influenza A virus pathogenesis. *Journal of General Virology*, 100(7), 1073–1078. Available from: https://doi.org/10.1099/jgv.0.001274.

Lan, J., Ge, J., Yu, J., Shan, S., Zhou, H. & Fan, S. et al. (2020) Structure of the SARS-CoV-2 spike receptor-binding domain bound to the ACE2 receptor. *Nature*, 581(7807), 215–220. Available from: https://doi.org/10.1038/s41586-020-2180-5.

Laporte, M., Raeymaekers, V., van Berwaer, R., Vandeput, J., Marchand-Casas, I. & Thibaut, H.-J. et al. (2021) The SARS-CoV-2 and other human coronavirus spike proteins are fine-tuned towards temperature and proteases of the human airways. *PLoS Pathogens*, 17(4), e1009500. Available from: https://doi.org/10.1371/journal.ppat.1009500.

Laursen, R.A. (1971) Solid-phase Edman degradation. An automatic peptide sequencer. *European Journal of Biochemistry*, 20(1), 89–102. Available from: https://doi.org/10.1111/j.1432-1033.1971.tb01366.x.

Lazarowitz, S.G., Compans, R.W. & Choppin, P.W. (1973) Proteolytic cleavage of the hemagglutinin polypeptide of influenza virus. Function of the uncleaved polypeptide HA. *Virology*, 52(1), 199–212. Available from: https://doi.org/10.1016/0042-6822(73)90409-1.

Leduc, R., Molloy, S.S., Thorne, B.A. & Thomas, G. (1992) Activation of human furin precursor processing endoprotease occurs by an intramolecular autoproteolytic cleavage. *Journal of Biological Chemistry*, 267(20), 14304–14308. Available from: https://doi.org/10.1016/S0021-9258(19)49712-3.

Lee, J.E., Fusco, M.L., Hessell, A.J., Oswald, W.B., Burton, D.R. & Saphire, E.O. (2008) Structure of the Ebola virus glycoprotein bound to an antibody from a human survivor. *Nature*, 454(7201), 177–182. Available from: https://doi.org/10.1038/nature07082.

Lee, J.E. & Saphire, E.O. (2009) Ebolavirus glycoprotein structure and mechanism of entry. *Future Virology*, 4(6), 621–635. Available from: https://doi.org/10.2217/fvl.09.56.

Lee, K.K. (2010) Architecture of a nascent viral fusion pore. *The EMBO Journal*, 29(7), 1299–1311. Available from: https://doi.org/10.1038/emboj.2010.13.

Lee, M.G., Kim, K.H., Park, K.Y. & Kim, J.S. (1996) Evaluation of anti-influenza effects of camostat in mice infected with non-adapted human influenza viruses. *Archives of Virology*, 141(10), 1979–1989. Available from: https://doi.org/10.1007/BF01718208.

Leendertz, S.A.J., Gogarten, J.F., Düx, A., Calvignac-Spencer, S. & Leendertz, F.H. (2016) Assessing the Evidence Supporting Fruit Bats as the Primary Reservoirs for Ebola Viruses. *EcoHealth*, 13(1), 18–25. Available from: https://doi.org/10.1007/s10393-015-1053-0.

Legand, A., Briand, S., Shindo, N., Brooks, W.A., Jong, M.D. de & Farrar, J. et al. (2013) Addressing the public health burden of respiratory viruses: the Battle against Respiratory Viruses (BRaVe) Initiative. *Future virology*, 8(10), 953–968. Available from: https://doi.org/10.2217/fvl.13.85.

Lenz, O., Meulen, J. ter, Klenk, H.D., Seidah, N.G. & Garten, W. (2001) The Lassa virus glycoprotein precursor GP-C is proteolytically processed by subtilase SKI-1/S1P. *Proceedings of the National Academy of Sciences*, 98(22), 12701–12705. Available from: https://doi.org/10.1073/pnas.221447598.

Leroy, E.M., Kumulungui, B., Pourrut, X., Rouquet, P., Hassanin, A. & Yaba, P. et al. (2005) Fruit bats as reservoirs of Ebola virus. *Nature*, 438(7068), 575–576. Available from: https://doi.org/10.1038/438575a.

Letko, M., Marzi, A. & Munster, V. (2020) Functional assessment of cell entry and receptor usage for SARS-CoV-2 and other lineage B betacoronaviruses. *Nature Microbiology*, 5(4), 562–569. Available from: https://doi.org/10.1038/s41564-020-0688-y.

Li, F., Han, M., Dai, P., Xu, W., He, J. & Tao, X. et al. (2021) Distinct mechanisms for TMPRSS2 expression explain organ-specific inhibition of SARS-CoV-2 infection by enzalutamide. *Nature Communications*, 12(1), 866. Available from: https://doi.org/10.1038/s41467-021-21171-x.

Li, F., Li, W., Farzan, M. & Harrison, S.C. (2005) Structure of SARS coronavirus spike receptor-binding domain complexed with receptor. *Science (New York, N.Y.)*, 309(5742), 1864–1868. Available from: https://doi.org/10.1126/science.1116480.

Li, S.Q., Orlich, M. & Rott, R. (1990) Generation of seal influenza virus variants pathogenic for chickens, because of hemagglutinin cleavage site changes. *Journal of Virology*, 64(7), 3297–3303. Available from: https://doi.org/10.1128/JVI.64.7.3297-3303.1990.

Li, W., Moore, M.J., Vasilieva, N., Sui, J., Wong, S.K. & Berne, M.A. et al. (2003) Angiotensin-converting enzyme 2 is a functional receptor for the SARS coronavirus. *Nature*, 426(6965), 450–454. Available from: https://doi.org/10.1038/nature02145.

Limburg, H., Harbig, A., Bestle, D., Stein, D.A., Moulton, H.M. & Jaeger, J. et al. (2019) TMPRSS2 Is the Major Activating Protease of Influenza A Virus in Primary Human Airway Cells and Influenza B Virus in Human Type II Pneumocytes. *Journal of Virology*, 93(21). Available from: https://doi.org/10.1128/JVI.00649-19.

Liu, Z., Zheng, H., Lin, H., Li, M., Yuan, R. & Peng, J. et al. (2020) Identification of Common Deletions in the Spike Protein of Severe Acute Respiratory Syndrome Coronavirus 2. *Journal of Virology*, 94(17). Available from: https://doi.org/10.1128/JVI.00790-20.

Lu, R., Zhao, X., Li, J., Niu, P., Yang, B. & Wu, H. et al. (2020) Genomic characterisation and epidemiology of 2019 novel coronavirus: implications for virus origins and receptor binding. *The Lancet*, 395(10224), 565–574. Available from: https://doi.org/10.1016/S0140-6736(20)30251-8.

Lucas, J.M., Heinlein, C., Kim, T., Hernandez, S.A., Malik, M.S. & True, L.D. et al. (2014) The androgen-regulated protease TMPRSS2 activates a proteolytic cascade involving components of the tumor microenvironment and promotes prostate cancer metastasis. *Cancer Discovery*, 4(11), 1310–1325. Available from: https://doi.org/10.1158/2159-8290.CD-13-1010.

Lucas, J.M., True, L., Hawley, S., Matsumura, M., Morrissey, C. & Vessella, R. et al. (2008) The androgen-regulated type II serine protease TMPRSS2 is differentially expressed and mislocalized in prostate adenocarcinoma. *The Journal of Pathology*, 215(2), 118–125. Available from: https://doi.org/10.1002/path.2330.

Mahoney, M., Damalanka, V.C., Tartell, M.A., Chung, D.H., Lourenço, A.L. & Pwee, D. et al. (2021) A novel class of TMPRSS2 inhibitors potently block SARS-CoV-2 and MERS-CoV viral entry and protect human epithelial lung cells. *Proceedings of the National Academy of Sciences*, 118(43). Available from: https://doi.org/10.1073/pnas.2108728118.

Maiwald, A., Hammami, M., Wagner, S., Heine, A., Klebe, G. & Steinmetzer, T. (2016) Changing the selectivity profile - from substrate analog inhibitors of thrombin and factor Xa to potent matriptase inhibitors. *Journal of Enzyme Inhibition and Medicinal Chemistry*, 31(sup1), 89–97. Available from: https://doi.org/10.3109/14756366.2016.1172574.

Mangano, D.T., Tudor, I.C. & Dietzel, C. (2006) The risk associated with aprotinin in cardiac surgery. *The New England Journal of Medicine*, 354(4), 353–365. Available from: https://doi.org/10.1056/NEJMoa051379.

Manicassamy, B., Wang, J., Jiang, H. & Rong, L. (2005) Comprehensive analysis of ebola virus GP1 in viral entry. *Journal of Virology*, 79(8), 4793–4805. Available from: https://doi.org/10.1128/JVI.79.8.4793-4805.2005.

Martines, R.B., Ng, D.L., Greer, P.W., Rollin, P.E. & Zaki, S.R. (2015) Tissue and cellular tropism, pathology and pathogenesis of Ebola and Marburg viruses. *The Journal of Pathology*, 235(2), 153–174. Available from: https://doi.org/10.1002/path.4456.

Marzi, A. & Mire, C.E. (2019) Current Ebola Virus Vaccine Progress. *BioDrugs*, 33(1), 9–14. Available from: https://doi.org/10.1007/s40259-018-0329-7.

Marzi, A., Reinheckel, T. & Feldmann, H. (2012) Cathepsin B & L are not required for ebola virus replication. *PLoS Neglected Tropical Diseases*, 6(12), e1923. Available from: https://doi.org/10.1371/journal.pntd.0001923.

Matsuyama, S., Nagata, N., Shirato, K., Kawase, M., Takeda, M. & Taguchi, F. (2010) Efficient activation of the severe acute respiratory syndrome coronavirus spike protein by the transmembrane protease TMPRSS2. *Journal of Virology*, 84(24), 12658–12664. Available from: https://doi.org/10.1128/JVI.01542-10.

Matsuyama, S., Shirato, K., Kawase, M., Terada, Y., Kawachi, K. & Fukushi, S. et al. (2018) Middle East Respiratory Syndrome Coronavirus Spike Protein Is Not Activated Directly by Cellular Furin during Viral Entry into Target Cells. *Journal of Virology*, 92(19). Available from: https://doi.org/10.1128/JVI.00683-18.

Matsuyama, S., Ujike, M., Morikawa, S., Tashiro, M. & Taguchi, F. (2005) Protease-mediated enhancement of severe acute respiratory syndrome coronavirus infection. *Proceedings of the National Academy of Sciences*, 102(35), 12543–12547. Available from: https://doi.org/10.1073/pnas.0503203102.

McWilliams, I.L., Kielczewski, J.L., Ireland, D.D.C., Sykes, J.S., Lewkowicz, A.P. & Konduru, K. et al. (2019) Pseudovirus rVSVΔG-ZEBOV-GP Infects Neurons in Retina and CNS, Causing Apoptosis and Neurodegeneration in Neonatal Mice. *Cell Reports*, 26(7), 1718-1726.e4. Available from: https://doi.org/10.1016/j.celrep.2019.01.069.

Meyer, D., Sielaff, F., Hammami, M., Böttcher-Friebertshäuser, E., Garten, W. & Steinmetzer, T. (2013) Identification of the first synthetic inhibitors of the type II transmembrane serine protease TMPRSS2 suitable for inhibition of influenza virus activation. *Biochemical Journal*, 452(2), 331–343. Available from: https://doi.org/10.1042/BJ20130101.

Mijanović, O., Branković, A., Panin, A.N., Savchuk, S., Timashev, P. & Ulasov, I. et al. (2019) Cathepsin B: A sellsword of cancer progression. *Cancer Letters*, 449, 207–214. Available from: https://doi.org/10.1016/j.canlet.2019.02.035.

Millet, J.K. & Whittaker, G.R. (2014) Host cell entry of Middle East respiratory syndrome coronavirus after two-step, furin-mediated activation of the spike protein. *Proceedings of the National Academy of Sciences of the United States of America*, 111(42), 15214–15219. Available from: https://doi.org/10.1073/pnas.1407087111.

Millet, J.K. & Whittaker, G.R. (2015) Host cell proteases: Critical determinants of coronavirus tropism and pathogenesis. *Virus Research*, 202, 120–134. Available from: https://doi.org/10.1016/j.virusres.2014.11.021.

Moestrup, S.K., Cui, S., Vorum, H., Bregengård, C., Bjørn, S.E. & Norris, K. et al. (1995) Evidence that epithelial glycoprotein 330/megalin mediates uptake of polybasic drugs. *Journal of Clinical Investigation*, 96(3), 1404–1413. Available from: https://doi.org/10.1172/jci118176.

Moller-Tank, S. & Maury, W. (2015) Ebola virus entry: A curious and complex series of events. *PLoS Pathogens*, 11(4), e1004731. Available from: https://doi.org/10.1371/journal.ppat.1004731.

Molloy, S.S., Anderson, E.D., Jean, F. & Thomas, G. (1999) Bi-cycling the furin pathway: from TGN localization to pathogen activation and embryogenesis. *Trends in cell biology*, 9(1), 28–35. Available from: https://doi.org/10.1016/s0962-8924(98)01382-8.

Molloy, S.S., Bresnahan, P.A., Leppla, S.H., Klimpel, K.R. & Thomas, G. (1992) Human furin is a calcium-dependent serine endoprotease that recognizes the sequence Arg-X-X-Arg and efficiently cleaves anthrax toxin protective antigen. *Journal of Biological Chemistry*, 267(23), 16396–16402. Available from: https://doi.org/10.1016/s0021-9258(18)42016-9.

Morrow, J.F., Cohen, S.N., Chang, A.C., Boyer, H.W., Goodman, H.M. & Helling, R.B. (1974) Replication and transcription of eukaryotic DNA in Escherichia coli. *Proceedings of the National Academy of Sciences*, 71(5), 1743–1747. Available from: https://doi.org/10.1073/pnas.71.5.1743.

Mühlberger, E., Lötfering, B., Klenk, H.D. & Becker, S. (1998) Three of the four nucleocapsid proteins of Marburg virus, NP, VP35, and L, are sufficient to mediate replication and transcription of Marburg virus-specific monocistronic minigenomes. *Journal of Virology*, 72(11), 8756–8764. Available from: https://doi.org/10.1128/JVI.72.11.8756-8764.1998.

Mukherjee, S. & Maxfield, F.R. (2004) Lipid and cholesterol trafficking in NPC. *Biochimica Et Biophysica Acta*, 1685(1-3), 28–37. Available from: https://doi.org/10.1016/j.bbalip.2004.08.009.

Mulangu, S., Dodd, L.E., Davey, R.T., Tshiani Mbaya, O., Proschan, M. & Mukadi, D. et al. (2019) A Randomized, Controlled Trial of Ebola Virus Disease Therapeutics. *The New England Journal of Medicine*, 381(24), 2293–2303. Available from: https://doi.org/10.1056/NEJMoa1910993.

Mullis, K., Faloona, F., Scharf, S., Saiki, R., Horn, G. & Erlich, H. (1986) Specific enzymatic amplification of DNA in vitro: the polymerase chain reaction. *Cold Spring Harbor Symposia on Quantitative Biology*, 51 Pt 1, 263–273.

Nelson, C.A. (1971) The Binding of Detergents to Proteins. *Journal of Biological Chemistry*, 246(12), 3895–3901. Available from: https://doi.org/10.1016/S0021-9258(18)62118-0.

Netzel-Arnett, S., Currie, B.M., Szabo, R., Lin, C.-Y., Chen, L.-M. & Chai, K.X. et al. (2006) Evidence for a matriptase-prostasin proteolytic cascade regulating terminal epidermal differentiation. *Journal of Biological Chemistry*, 281(44), 32941–32945. Available from: https://doi.org/10.1074/jbc.C600208200.

Neumann, G., Feldmann, H., Watanabe, S., Lukashevich, I. & Kawaoka, Y. (2002) Reverse Genetics Demonstrates that Proteolytic Processing of the Ebola Virus Glycoprotein Is Not Essential for Replication in Cell Culture. *Journal of virology*, 76(1), 406–410. Available from: https://doi.org/10.1128/JVI.76.1.406-410.2002.

Neumann, G., Geisbert, T.W., Ebihara, H., Geisbert, J.B., Daddario-DiCaprio, K.M. & Feldmann, H. et al. (2007) Proteolytic processing of the Ebola virus glycoprotein is not critical for Ebola virus replication in nonhuman primates. *Journal of Virology*, 81(6), 2995–2998. Available from: https://doi.org/10.1128/JVI.02486-06.

Ovcharenko, A.V. & Zhirnov, O.P. (1994) Aprotinin aerosol treatment of influenza and paramyxovirus bronchopneumonia of mice. *Antiviral Research*, 23(2), 107–118. Available from: https://doi.org/10.1016/0166-3542(94)90038-8.

Pager, C.T. & Dutch, R.E. (2005) Cathepsin L is involved in proteolytic processing of the Hendra virus fusion protein. *Journal of Virology*, 79(20), 12714–12720. Available from: https://doi.org/10.1128/JVI.79.20.12714-12720.2005.

Paoloni-Giacobino, A., Chen, H., Peitsch, M.C., Rossier, C. & Antonarakis, S.E. (1997) Cloning of the TMPRSS2 gene, which encodes a novel serine protease with transmembrane, LDLRA, and SRCR domains and maps to 21q22.3. *Genomics*, 44(3), 309–320. Available from: https://doi.org/10.1006/geno.1997.4845.

Park, J.-E., Li, K., Barlan, A., Fehr, A.R., Perlman, S. & McCray, P.B. et al. (2016) Proteolytic processing of Middle East respiratory syndrome coronavirus spikes expands virus tropism. *Proceedings of the National Academy of Sciences of the United States of America*, 113(43), 12262–12267. Available from: https://doi.org/10.1073/pnas.1608147113.

Peacock, T.P., Goldhill, D.H., Zhou, J., Baillon, L., Frise, R. & Swann, O.C. et al. (2021) The furin cleavage site in the SARS-CoV-2 spike protein is required for transmission in ferrets. *Nature Microbiology*, 6(7), 899–909. Available from: https://doi.org/10.1038/s41564-021-00908-w.

Peisajovich, S.G. & Shai, Y. (2003) Viral fusion proteins: multiple regions contribute to membrane fusion. *Biochimica et Biophysica Acta (BBA) - Biomembranes*, 1614(1), 122–129. Available from: https://doi.org/10.1016/S0005-2736(03)00170-6.

Pérez-Silva, J.G., Español, Y., Velasco, G. & Quesada, V. (2016) The Degradome database: expanding roles of mammalian proteases in life and disease. *Nucleic Acids Research*, 44(D1), D351-5. Available from: https://doi.org/10.1093/nar/gkv1201.

Phillips, J.M., Gallagher, T. & Weiss, S.R. (2017) Neurovirulent Murine Coronavirus JHM.SD Uses Cellular Zinc Metalloproteases for Virus Entry and Cell-Cell Fusion. *Journal of Virology*, 91(8). Available from: https://doi.org/10.1128/JVI.01564-16.

Plaimauer, B., Mohr, G., Wernhart, W., Himmelspach, M., Dorner, F. & Schlokat, U. (2001) 'Shed' furin: mapping of the cleavage determinants and identification of its C-terminus. *Biochemical Journal*, 354(Pt 3), 689–695. Available from: https://doi.org/10.1042/0264-6021:3540689.

Radzicka, A. & Wolfenden, R. (1996) Rates of Uncatalyzed Peptide Bond Hydrolysis in Neutral Solution and the Transition State Affinities of Proteases. *Journal of the American Chemical Society*, 118(26), 6105–6109. Available from: https://doi.org/10.1021/ja954077c.

Rawlings, N.D., Barrett, A.J. & Bateman, A. (2010) MEROPS: the peptidase database. *Nucleic Acids Research*, 38(Database issue), D227-33. Available from: https://doi.org/10.1093/nar/gkp971.

Rawlings, N.D. & Salvesen, G. (Eds.) (2013) *Handbook of proteolytic enzymes*. Elsevier Academic Press: Amsterdam, Heidelberg.

Redondo-Calvo, F.J., Padín, J.F., Muñoz-Rodríguez, J.R., Serrano-Oviedo, L., López-Juárez, P. & Porras Leal, M.L. et al. (2022) Aprotinin treatment against SARS-CoV-2: A randomized phase III study to evaluate the safety and efficacy of a pan-protease inhibitor for moderate COVID-19. *European Journal of Clinical Investigation*, 52(6), e13776. Available from: https://doi.org/10.1111/eci.13776.

Reinheckel, T., Deussing, J., Roth, W. & Peters, C. (2001) Towards Specific Functions of Lysosomal Cysteine Peptidases: Phenotypes of Mice Deficient for Cathepsin B or Cathepsin L. *Biological Chemistry*, 382(5), 735–742. Available from: https://doi.org/10.1515/bchm.2001.382.5.735.

Remacle, A., Murphy, G. & Roghi, C. (2003) Membrane type I-matrix metalloproteinase (MT1-MMP) is internalised by two different pathways and is recycled to the cell surface. *Journal of Cell Science*, 116(Pt 19), 3905–3916. Available from: https://doi.org/10.1242/jcs.00710.

Richman, D.D. & Nathanson, N. (2016) Antiviral Therapy. *Viral Pathogenesis*, 271–287. Available from: https://doi.org/10.1016/B978-0-12-800964-2.00020-3.

Roche, S. & Gaudin, Y. (2002) Characterization of the equilibrium between the native and fusion-inactive conformation of rabies virus glycoprotein indicates that the fusion complex is made of several trimers. *Virology*, 297(1), 128–135. Available from: https://doi.org/10.1006/viro.2002.1429.

Rodriguez-Lafrasse, C., Rousson, R., Bonnet, J., Pentchev, P.G., Louisot, P. & Vanier, M.T. (1990) Abnormal cholesterol metabolism in imipramine-treated fibroblast cultures. Similarities with Niemann-Pick type C disease. *Biochimica et Biophysica Acta (BBA) - Lipids and Lipid Metabolism*, 1043(2), 123–128. Available from: https://doi.org/10.1016/0005-2760(90)90284-5.

Roebroek, A.J., Schalken, J.A., Leunissen, J.A., Onnekink, C., Bloemers, H.P. & van de Ven, W.J. (1986) Evolutionary conserved close linkage of the c-fes/fps proto-oncogene and genetic sequences encoding a receptor-like protein. *The EMBO Journal*, 5(9), 2197–2202. Available from: https://doi.org/10.1002/j.1460-2075.1986.tb04484.x.

Roebroek, A.J.M., Taylor, N.A., Louagie, E., Pauli, I., Smeijers, L. & an Snellinx et al. (2004) Limited redundancy of the proprotein convertase furin in mouse liver. *Journal of Biological Chemistry*, 279(51), 53442–53450. Available from: https://doi.org/10.1074/jbc.M407152200.

Rossi, A., Deveraux, Q., Turk, B. & Sali, A. (2004) Comprehensive search for cysteine cathepsins in the human genome. *Biological Chemistry*, 385(5), 363–372. Available from: https://doi.org/10.1515/BC.2004.040.

Saeed, M.F., Kolokoltsov, A.A., Albrecht, T. & Davey, R.A. (2010) Cellular entry of ebola virus involves uptake by a macropinocytosis-like mechanism and subsequent trafficking through early and late endosomes. *PLoS Pathogens*, 6(9), e1001110. Available from: https://doi.org/10.1371/journal.ppat.1001110.

Saiki, R.K., Gelfand, D.H., Stoffel, S., Scharf, S.J., Higuchi, R. & Horn, G.T. et al. (1988) Primer-directed enzymatic amplification of DNA with a thermostable DNA polymerase. *Science (New York, N.Y.)*, 239(4839), 487–491.

Sakai, K., Ami, Y., Tahara, M., Kubota, T., Anraku, M. & Abe, M. et al. (2014) The host protease TMPRSS2 plays a major role in in vivo replication of emerging H7N9 and seasonal influenza viruses. *Journal of Virology*, 88(10), 5608–5616. Available from: https://doi.org/10.1128/JVI.03677-13.

Sakurai, Y., Kolokoltsov, A.A., Chen, C.-C., Tidwell, M.W., Bauta, W.E. & Klugbauer, N. et al. (2015) Ebola virus. Two-pore channels control Ebola virus host cell entry and are drug targets for disease treatment. *Science (New York, N.Y.)*, 347(6225), 995–998. Available from: https://doi.org/10.1126/science.1258758.

Sanger, F. & Coulson, A.R. (1975) A rapid method for determining sequences in DNA by primed synthesis with DNA polymerase. *Journal of Molecular Biology*, 94(3), 441–448.

Sanjuán, R., Nebot, M.R., Chirico, N., Mansky, L.M. & Belshaw, R. (2010) Viral mutation rates. *Journal of Virology*, 84(19), 9733–9748. Available from: https://doi.org/10.1128/JVI.00694-10.

Sarac, M.S., Cameron, A. & Lindberg, I. (2002) The furin inhibitor hexa-D-arginine blocks the activation of Pseudomonas aeruginosa exotoxin A in vivo. *Infection and Immunity*, 70(12), 7136–7139. Available from: https://doi.org/10.1128/IAI.70.12.7136-7139.2002.

Sarac, M.S., Peinado, J.R., Leppla, S.H. & Lindberg, I. (2004) Protection against anthrax toxemia by hexa-D-arginine in vitro and in vivo. *Infection and Immunity*, 72(1), 602–605. Available from: https://doi.org/10.1128/IAI.72.1.602-605.2004.

Satoyoshi, E. (1992) Therapeutic trials on progressive muscular dystrophy. *Internal Medicine (Tokyo, Japan)*, 31(7), 841–846. Available from: https://doi.org/10.2169/internalmedicine.31.841.

Scamuffa, N., Calvo, F., Chrétien, M., Seidah, N.G. & Khatib, A.-M. (2006) Proprotein convertases: lessons from knockouts. *FASEB Journal : Official Publication of the Federation of American Societies for Experimental Biology*, 20(12), 1954–1963. Available from: https://doi.org/10.1096/fj.05-5491rev.

Schechter, I. & Berger, A. (1967) On the size of the active site in proteases. I. Papain. *Biochemical and biophysical research communications*, 27(2), 157–162. Available from: https://doi.org/10.1016/S0006-291X(67)80055-X.

Scheid, A. & Choppin, P.W. (1974) Identification of biological activities of paramyxovirus glycoproteins. Activation of cell fusion, hemolysis, and infectivity by proteolytic cleavage of an inactive precursor protein of Sendai virus. *Virology*, 57(2), 475–490. Available from: https://doi.org/10.1016/0042-6822(74)90187-1.

Schornberg, K., Matsuyama, S., Kabsch, K., Delos, S., Bouton, A. & White, J. (2006) Role of endosomal cathepsins in entry mediated by the Ebola virus glycoprotein. *Journal of Virology*, 80(8), 4174–4178. Available from: https://doi.org/10.1128/JVI.80.8.4174-4178.2006.

Schornberg, K.L., Shoemaker, C.J., Dube, D., Abshire, M.Y., Delos, S.E. & Bouton, A.H. et al. (2009) Alpha5beta1-integrin controls ebolavirus entry by regulating endosomal cathepsins. *Proceedings of the National Academy of Sciences of the United States of America*, 106(19), 8003–8008. Available from: https://doi.org/10.1073/pnas.0807578106.

Seidah, N.G., Mayer, G., Zaid, A., Rousselet, E., Nassoury, N. & Poirier, S. et al. (2008) The activation and physiological functions of the proprotein convertases. *The International Journal of Biochemistry & Cell Biology*, 40(6), 1111–1125. Available from: https://doi.org/10.1016/j.biocel.2008.01.030.

Shirahama-Noda, K., Yamamoto, A., Sugihara, K., Hashimoto, N., Asano, M. & Nishimura, M. et al. (2003) Biosynthetic processing of cathepsins and lysosomal degradation are abolished in asparaginyl endopeptidase-deficient mice. *Journal of Biological Chemistry*, 278(35), 33194–33199. Available from: https://doi.org/10.1074/jbc.M302742200.

Shirato, K., Kanou, K., Kawase, M. & Matsuyama, S. (2017) Clinical Isolates of Human Coronavirus 229E Bypass the Endosome for Cell Entry. *Journal of Virology*, 91(1). Available from: https://doi.org/10.1128/JVI.01387-16.

Shirato, K., Kawase, M. & Matsuyama, S. (2013) Middle East respiratory syndrome coronavirus infection mediated by the transmembrane serine protease TMPRSS2. *Journal of Virology*, 87(23), 12552–12561. Available from: https://doi.org/10.1128/JVI.01890-13.

Shirato, K., Kawase, M. & Matsuyama, S. (2018) Wild-type human coronaviruses prefer cell-surface TMPRSS2 to endosomal cathepsins for cell entry. *Virology*, 517, 9–15. Available from: https://doi.org/10.1016/j.virol.2017.11.012.

Shiryaev, S.A., Chernov, A.V., Golubkov, V.S., Thomsen, E.R., Chudin, E. & Chee, M.S. et al. (2013) High-resolution analysis and functional mapping of cleavage sites and substrate proteins of furin in the human proteome. *PloS One*, 8(1), e54290. Available from: https://doi.org/10.1371/journal.pone.0054290.

Shulla, A., Heald-Sargent, T., Subramanya, G., Zhao, J., Perlman, S. & Gallagher, T. (2011) A transmembrane serine protease is linked to the severe acute respiratory syndrome coronavirus receptor and activates virus entry. *Journal of Virology*, 85(2), 873–882. Available from: https://doi.org/10.1128/JVI.02062-10.

Sielaff, F., Böttcher-Friebertshäuser, E., Meyer, D., Saupe, S.M., Volk, I.M. & Garten, W. et al. (2011) Development of substrate analogue inhibitors for the human airway trypsin-like protease HAT. *Bioorganic & Medicinal Chemistry Letters*, 21(16), 4860–4864. Available from: https://doi.org/10.1016/j.bmcl.2011.06.033.

Simmons, G., Gosalia, D.N., Rennekamp, A.J., Reeves, J.D., Diamond, S.L. & Bates, P. (2005) Inhibitors of cathepsin L prevent severe acute respiratory syndrome coronavirus entry. *Proceedings of the National Academy of Sciences of the United States of America*, 102(33), 11876–11881. Available from: https://doi.org/10.1073/pnas.0505577102.

Simmons, G., Reeves, J.D., Rennekamp, A.J., Amberg, S.M., Piefer, A.J. & Bates, P. (2004) Characterization of severe acute respiratory syndrome-associated coronavirus (SARS-CoV) spike glycoprotein-mediated viral entry. *Proceedings of the National Academy of Sciences of the United States of America*, 101(12), 4240–4245. Available from: https://doi.org/10.1073/pnas.0306446101.

Simmons, J.A., D'Souza, R.S., Ruas, M., Galione, A., Casanova, J.E. & White, J.M. (2016) Ebolavirus Glycoprotein Directs Fusion through NPC1+ Endolysosomes. *Journal of Virology*, 90(1), 605–610. Available from: https://doi.org/10.1128/JVI.01828-15.

Skehel, J.J. & Wiley, D.C. (1998) Coiled Coils in Both Intracellular Vesicle and Viral Membrane Fusion. *Cell*, 95(7), 871–874. Available from: https://doi.org/10.1016/S0092-8674(00)81710-9.

Song, W., Gui, M., Wang, X. & Xiang, Y. (2018) Cryo-EM structure of the SARS coronavirus spike glycoprotein in complex with its host cell receptor ACE2. *PLoS Pathogens*, 14(8), e1007236. Available from: https://doi.org/10.1371/journal.ppat.1007236.

Spence, J.S., Krause, T.B., Mittler, E., Jangra, R.K. & Chandran, K. (2016) Direct Visualization of Ebola Virus Fusion Triggering in the Endocytic Pathway. *MBio*, 7(1), e01857-15. Available from: https://doi.org/10.1128/mBio.01857-15.

Steinmetzer, T. & Hardes, K. (2018) The Antiviral Potential of Host Protease Inhibitors. In: *Activation of Viruses by Host Proteases.* Springer, Cham, pp. 279–325.

Stertz, S., Reichelt, M., Spiegel, M., Kuri, T., Martínez-Sobrido, L. & García-Sastre, A. et al. (2007) The intracellular sites of early replication and budding of SARS-coronavirus. *Virology*, 361(2), 304–315. Available from: https://doi.org/10.1016/j.virol.2006.11.027.

Stieneke-Gröber, A., Vey, M., Angliker, H., Shaw, E., Thomas, G. & Roberts, C. et al. (1992) Influenza virus hemagglutinin with multibasic cleavage site is activated by furin, a subtilisin-like endoprotease. *The EMBO Journal*, 11(7), 2407–2414. Available from: https://doi.org/10.1002/j.1460-2075.1992.tb05305.x.

Sun, C., Shen, L., Zhang, Z. & Xie, X. (2020) Therapeutic Strategies for Duchenne Muscular Dystrophy: An Update. *Genes*, 11(8), 837. Available from: https://doi.org/10.3390/genes11080837.

Sun, W., He, S., Martínez-Romero, C., Kouznetsova, J., Tawa, G. & Xu, M. et al. (2017) Synergistic drug combination effectively blocks Ebola virus infection. *Antiviral Research*, 137, 165–172. Available from: https://doi.org/10.1016/j.antiviral.2016.11.017.

Sure, F., Bertog, M., Afonso, S., Diakov, A., Rinke, R. & Madej, M.G. et al. (2022) Transmembrane serine protease 2 (TMPRSS2) proteolytically activates the epithelial sodium channel (ENaC) by cleaving the channel's γ-subunit. *Journal of Biological Chemistry*, 298(6), 102004. Available from: https://doi.org/10.1016/j.jbc.2022.102004.

Swayne, D.E. & Suarez, D.L. (2000) Highly pathogenic avian influenza. *Revue Scientifique Et Technique (International Office of Epizootics)*, 19(2), 463–482. Available from: https://doi.org/10.20506/rst.19.2.1230.

Tamai, M., Matsumoto, K., Omura, S., Koyama, I., Ozawa, Y. & Hanada, K. (1986) In vitro and in vivo inhibition of cysteine proteinases by EST, a new analog of E-64. *Journal of Pharmacobio-Dynamics*, 9(8), 672–677. Available from: https://doi.org/10.1248/bpb1978.9.672.

Tamai, M., Omura, S., Kimura, M., Hanada, K. & Sugita, H. (1987) Prolongation of life span of dystrophic hamster by cysteine proteinase inhibitor, loxistation (EST). *Journal of Pharmacobio-Dynamics*, 10(11), 678–681. Available from: https://doi.org/10.1248/bpb1978.10.678.

Tao, K., Tzou, P.L., Nouhin, J., Bonilla, H., Jagannathan, P. & Shafer, R.W. (2021) SARS-CoV-2 Antiviral Therapy. *Clinical Microbiology Reviews*, 34(4), e0010921. Available from: https://doi.org/10.1128/CMR.00109-21.

Tarnow, C., Engels, G., Arendt, A., Schwalm, F., Sediri, H. & Preuss, A. et al. (2014) TMPRSS2 is a host factor that is essential for pneumotropism and pathogenicity of H7N9 influenza A virus in mice. *Journal of Virology*, 88(9), 4744–4751. Available from: https://doi.org/10.1128/JVI.03799-13.

Tortorici, M.A. & Veesler, D. (2016) Chapter Four - Structural insights into coronavirus entry. In: Ziebuhr, J. (Ed.) *Advances in Virus Research : Coronaviruses.* Academic Press, pp. 93–116.

Towbin, H., Staehelin, T. & Gordon, J. (1979) Electrophoretic transfer of proteins from polyacrylamide gels to nitrocellulose sheets: procedure and some applications. *Proceedings of the National Academy of Sciences*, 76(9), 4350–4354. Available from: https://doi.org/10.1073/pnas.76.9.4350.

Tseng, C.-T.K., Tseng, J., Perrone, L., Worthy, M., Popov, V. & Peters, C.J. (2005) Apical entry and release of severe acute respiratory syndrome-associated coronavirus in polarized Calu-3 lung epithelial cells. *Journal of Virology*, 79(15), 9470–9479. Available from: https://doi.org/10.1128/JVI.79.15.9470-9479.2005.

Turk, D., Guncar, G., Podobnik, M. & Turk, B. (1998) Revised Definition of Substrate Binding Sites of Papain-Like Cysteine Proteases. *undefined*. Available from: https://www.semanticscholar.org/paper/Revised-Definition-of-Substrate-Binding-Sites-of-Turk-Guncar/1d1a31eaefe7db2a9b56a48a8f46837c67834430.

Turk, V., Stoka, V., Vasiljeva, O., Renko, M., Sun, T. & Turk, B. et al. (2012) Cysteine cathepsins: From structure, function and regulation to new frontiers. *Biochimica Et Biophysica Acta*, 1824(1), 68–88. Available from: https://doi.org/10.1016/j.bbapap.2011.10.002.

Tyrell, D.A. & Bynoe, M.L. (1965) CULTIVATION OF A NOVEL TYPE OF COMMON-COLD VIRUS IN ORGAN CULTURES. *British Medical Journal*, 1(5448), 1467–1470. Available from: https://doi.org/10.1136/bmj.1.5448.1467.

Ueda, M.T., Kurosaki, Y., Izumi, T., Nakano, Y., Oloniniyi, O.K. & Yasuda, J. et al. (2017) Functional mutations in spike glycoprotein of Zaire ebolavirus associated with an increase in infection efficiency. *Genes to Cells*, 22(2), 148–159. Available from: https://doi.org/10.1111/gtc.12463.

Vaarala, M.H., Porvari, K.S., Kellokumpu, S., Kyllönen, A.P. & Vihko, P.T. (2001) Expression of transmembrane serine protease TMPRSS2 in mouse and human tissues. *The Journal of Pathology*, 193(1), 134–140. Available from: https://doi.org/10.1002/1096-9896(2000)9999:9999<::AID-PATH743>3.0.CO;2-T.

van Doremalen, N., Bushmaker, T., Morris, D.H., Holbrook, M.G., Gamble, A. & Williamson, B.N. et al. (2020) Aerosol and Surface Stability of SARS-CoV-2 as Compared with SARS-CoV-1. *The New England Journal of Medicine*, 382(16), 1564–1567. Available from: https://doi.org/10.1056/NEJMc2004973.

van Lam van, T., Heindl, M.R., Schlutt, C., Böttcher-Friebertshäuser, E., Bartenschlager, R. & Klebe, G. et al. (2021) The Basicity Makes the Difference: Improved Canavanine-Derived Inhibitors of the Proprotein Convertase Furin. *ACS Medicinal Chemistry Letters*, 12(3), 426–432. Available from: https://doi.org/10.1021/acsmedchemlett.0c00651.

Vey, M., Orlich, M., Adler, S., Klenk, H.-D., Rott, R. & Garten, W. (1992) Hemagglutinin activation of pathogenic avian influenza viruses of serotype H7 requires the protease recognition motif R-X-K/R-R. *Virology*, 188(1), 408–413. Available from: https://doi.org/10.1016/0042-6822(92)90775-K.

Vey, M., Schäfer, W., Berghöfer, S., Klenk, H.D. & Garten, W. (1994) Maturation of the trans-Golgi network protease furin: compartmentalization of propeptide removal, substrate cleavage, and COOH-terminal truncation. *Journal of Cell Biology*, 127(6 Pt 2), 1829–1842. Available from: https://doi.org/10.1083/jcb.127.6.1829.

Volchkov, V.E., Feldmann, H., Volchkova, V.A. & Klenk, H.-D. (1998) Processing of the Ebola virus glycoprotein by the proprotein convertase furin. *Proceedings of the National Academy of Sciences*, 95(10), 5762–5767. Available from: https://doi.org/10.1073/pnas.95.10.5762.

Volchkov, V.E., Volchkova, V.A., Dolnik, O., Feldmann, H. & Klenk, H.-D. (2016) Polymorphism of Filovirus Glycoproteins. In: Ziebuhr, J. (Ed.) *Advances in Virus Research : Coronaviruses.* Academic Press, pp. 359–381.

Walls, A.C., Park, Y.-J., Tortorici, M.A., Wall, A., McGuire, A.T. & Veesler, D. (2020) Structure, Function, and Antigenicity of the SARS-CoV-2 Spike Glycoprotein. *Cell*, 181(2), 281-292.e6. Available from: https://doi.org/10.1016/j.cell.2020.02.058.

Weissenhorn, W., Wharton, S.A., Calder, L.J., Earl, P.L., Moss, B. & Aliprandis, E. et al. (1996) The ectodomain of HIV-1 env subunit gp41 forms a soluble, alpha-helical, rod-like oligomer in the absence of gp120 and the N-terminal fusion peptide. *The EMBO journal*, 15(7), 1507–1514. Available from: https://doi.org/10.1002/j.1460-2075.1996.tb00494.x.

Wettstein, L., Kirchhoff, F. & Münch, J. (2022) The Transmembrane Protease TMPRSS2 as a Therapeutic Target for COVID-19 Treatment. *International Journal of Molecular Sciences*, 23(3). Available from: https://doi.org/10.3390/ijms23031351.

White, J. & Helenius, A. (1980) pH-dependent fusion between the Semliki Forest virus membrane and liposomes. *Proceedings of the National Academy of Sciences*, 77(6), 3273–3277. Available from: https://doi.org/10.1073/pnas.77.6.3273.

White, J., Kartenbeck, J. & Helenius, A. (1980) Fusion of Semliki forest virus with the plasma membrane can be induced by low pH. *Journal of Cell Biology*, 87(1), 264–272. Available from: https://doi.org/10.1083/jcb.87.1.264.

White, J., Kartenbeck, J. & Helenius, A. (1982) Membrane fusion activity of influenza virus. *The EMBO Journal*, 1(2), 217–222. Available from: https://doi.org/10.1002/j.1460-2075.1982.tb01150.x.

White, J.M., Delos, S.E., Brecher, M. & Schornberg, K. (2008) Structures and mechanisms of viral membrane fusion proteins: Multiple variations on a common theme. *Critical Reviews in Biochemistry and Molecular Biology*, 43(3), 189–219. Available from: https://doi.org/10.1080/10409230802058320.

White, J.M. & Whittaker, G.R. (2016) Fusion of Enveloped Viruses in Endosomes. *Traffic (Copenhagen, Denmark)*, 17(6), 593–614. Available from: https://doi.org/10.1111/tra.12389.

Wool-Lewis, R.J. & Bates, P. (1999) Endoproteolytic processing of the ebola virus envelope glycoprotein: Cleavage is not required for function. *Journal of Virology*, 73(2), 1419–1426.

Wrobel, A.G., Benton, D.J., Xu, P., Roustan, C., Martin, S.R. & Rosenthal, P.B. et al. (2020) SARS-CoV-2 and bat RaTG13 spike glycoprotein structures inform on virus evolution and furin-cleavage effects. *Nature Structural & Molecular Biology*, 27(8), 763–767. Available from: https://doi.org/10.1038/s41594-020-0468-7.

Wu, Y. & Zhao, S. (2020) Furin cleavage sites naturally occur in coronaviruses. *Stem Cell Research*, 50, 102115. Available from: https://doi.org/10.1016/j.scr.2020.102115.

Yasuda, Y., Kageyama, T., Akamine, A., Shibata, M., Kominami, E. & Uchiyama, Y. et al. (1999) Characterization of new fluorogenic substrates for the rapid and sensitive assay of cathepsin E and cathepsin D. *Journal of Biochemistry*, 125(6), 1137–1143. Available from: https://doi.org/10.1093/oxfordjournals.jbchem.a022396.

Zaki, A.M., van Boheemen, S., Bestebroer, T.M., Osterhaus, A.D.M.E. & Fouchier, R.A.M. (2012) Isolation of a novel coronavirus from a man with pneumonia in Saudi Arabia. *The New England Journal of Medicine*, 367(19), 1814–1820. Available from: https://doi.org/10.1056/NEJMoa1211721.

Zhirnov, O.P., Kirzhner, L.S., Ovcharenko, A.V. & Malyshev, N.A. (1996) Klinicheskaia éffektivnost' aérozolia aprotinina pri grippe i paragrippe. *Vestnik Rossiiskoi akademii meditsinskikh nauk*, (5), 26–31. Available from: https://doi.org/Trial.

Zhirnov, O.P., Klenk, H.D. & Wright, P.F. (2011) Aprotinin and similar protease inhibitors as drugs against influenza. *Antiviral Research*, 92(1), 27–36. Available from: https://doi.org/10.1016/j.antiviral.2011.07.014.

Zhirnov, O.P., Ovcharenko, A.V. & Bukrinskaya, A.G. (1982) Protective effect of protease inhibitors in influenza virus infected animals. *Archives of Virology*, 73(3-4), 263–272. Available from: https://doi.org/10.1007/BF01318080.

Zhou, A., Martin, S., Lipkind, G., LaMendola, J. & Steiner, D.F. (1998) Regulatory roles of the P domain of the subtilisin-like prohormone convertases. *Journal of Biological Chemistry*, 273(18), 11107–11114. Available from: https://doi.org/10.1074/jbc.273.18.11107.

Zhou, P., Yang, X.-L., Wang, X.-G., Hu, B., Zhang, L. & Zhang, W. et al. (2020) A pneumonia outbreak associated with a new coronavirus of probable bat origin. *Nature*, 579(7798), 270–273. Available from: https://doi.org/10.1038/s41586-020-2012-7.

Zhou, Y., Vedantham, P., Lu, K., Agudelo, J., Carrion, R. & Nunneley, J.W. et al. (2015) Protease inhibitors targeting coronavirus and filovirus entry. *Antiviral Research*, 116, 76–84. Available from: https://doi.org/10.1016/j.antiviral.2015.01.011.

Zhu, C., He, G., Yin, Q., Zeng, L., Ye, X. & Shi, Y. et al. (2021) Molecular biology of the SARs-CoV-2 spike protein: A review of current knowledge. *Journal of Medical Virology*, 93(10), 5729–5741. Available from: https://doi.org/10.1002/jmv.27132.

Zhu, N., Zhang, D., Wang, W., Li, X., Yang, B. & Song, J. et al. (2020) A Novel Coronavirus from Patients with Pneumonia in China, 2019. *The New England Journal of Medicine*, 382(8), 727–733. Available from: https://doi.org/10.1056/NEJMoa2001017.

Zhuravel, S.V., Khmelnitskiy, O.K., Burlaka, O.O., Gritsan, A.I., Goloshchekin, B.M. & Kim, S. et al. (2021) Nafamostat in hospitalized patients with moderate to severe COVID-19 pneumonia: a randomised Phase II clinical trial. *EClinicalMedicine*, 41, 101169. Available from: https://doi.org/10.1016/j.eclinm.2021.101169.

# 7 List of figures

# 8 List of tables

# 9 Abbreviations

| | |
|---|---|
| Δ | Deletion |
| α | Anti |
| aa | Amino acid |
| ACE2 | Angiotensin converting enzyme 2 |
| AFC | 7-amino-4-trifluormethyl-coumarin |
| APS | Ammonium persulfate |
| BDBV | *Bundibugyo ebolavirus* |
| BOMV | *Bombali ebolavirus* |
| bp | Base pair |
| BPTI | Bovine pancreatic trypsin inhibitor |
| BSA | Bovine serum albumin |
| BSL | Biosafety level |
| C | Celsius |
| $Ca^{2+}$ | Calcium ion |
| CatB | Cathepsin B |
| CatL | Cathepsin L |
| CDC | Center of Disease Control |
| CD-MPR | Cation-dependent mannose 6-phosphate receptor |
| cDNA | Complementary/copy DNA |
| CoV | Coronavirus |
| COVID-19 | Coronavirus infectious disease 2019 |
| CPE | Cytopathic effect |
| Da | Dalton |
| DMD | Duchenne muscular dystrophy |
| DMEM | *Dulbecco`s Modified Eagle`s Medium* |
| DNA | Desoxyribonucleic acid |
| DTT | DL-Dithiothreitol |
| EBOV | Ebola virus |
| EDTA | Ethylenediaminetetraacetic acid |
| EE | Early endosome |
| ENaC | Epithelium sodium channel |
| ER | Endoplasmic reticulum |
| ERGIC | ER-Golgi intermediate compartment |
| FCS | Fetal calf serum |
| FP | Fusion peptide |
| g | G-force |
| h | Hour |
| HA | Hemagglutinin |
| HAT | Human airway trypsin-like protease |
| HCoV | Human Coronavirus |
| HEK | Human embryonal kidney |
| HPAIV | Highly pathogenic avian influenza virus |
| HR | Heptad repeat |
| HRP | Horse radish peroxidase |
| IAV | Influenza A virus |
| ICC | Immunocytochemistry |
| IFM | Infection medium |
| KCl | Potassium chloride |
| $KH_2PO_4$ | Potassium dihydrogen phosphate |
| LB | Lysogeny broth |

| | |
|---|---|
| LDLRA | Low-density lipoprotein receptor class A |
| LE | Late endosome |
| LRP2 | Low-density lipoprotein receptor-related protein 2 |
| mA | Milliampere |
| MERS | Middle Eastern respiratory syndrome |
| MHV | Mouse hepatitis virus |
| min | Minute |
| MLD | Mucin-like domain |
| MMP | Matrix metalloproteinase |
| MOI | Multiplicity of infection |
| NaCl | Sodium chloride |
| NPC1 | Niemann-Pick disease, type C1 |
| NTD | N-terminal domain |
| p.i. | Postinfection |
| PAGE | Polyacrylamide gel electrophoresis |
| PBS | Phosphate buffered saline |
| PC | Proprotein convertase |
| PCR | Polymerase chain reaction |
| pH | Potentia hydrogneii |
| PPMO | Peptide-conjugated phosphorodiamidate morpholino oligomer |
| PtdSer | Phosphatidyl serine |
| PVDF | Polyvinylidene difluorid |
| RBD/R | Receptor binding domain/region |
| RE | Recycling endosome |
| REBOV | *Reston ebolavirus* |
| RFU | Relative fluorescence unit |
| RNA | Ribonucleic acid |
| RNP | Ribonucleoprotein |
| ROI | Region of interest |
| rpm | Revolutions per minute |
| RT | Room temperature |
| SARS | Severe acute respiratory syndrome |
| SARS-CoV-2 S | SARS-CoV-2 spike protein |
| SCRC | Scavenger receptor cysteine-rich |
| SDS | Sodium dodecyl sulfate |
| SEBOV | Sudan ebolavirus |
| sec | Second |
| ssRNA | Single-stranded RNA |
| TAE | Tris-acetate-EDTA |
| TAFV | *Taï Forest ebolavirus* |
| TCID | Tissue culture infectious dose |
| TGN | Trans-Golgi network |
| TMD | Transmembrane domain |
| TEMED | Tetramethylethylenediamine |
| TMPRSS2 | Transmembrane serine protease 2 |
| TNE | Tris-NaCl-EDTA |
| TPC2 | Two-pore calcium channel 2 |
| TPCK | Tosyl phenylalanyl chloromethyl ketone |
| trVLP | Transcription and replication-competent virus-like particles |
| TTSP | Type II transmembrane serine protease |
| UV | Ultraviolet |
| V | Volt |

| | |
|---|---|
| vRNA | Viral RNA |
| VSV | Vesicular stomatitis virus |
| WHO | World Health Organization |
| ZEBOV | *Zaire ebolavirus* |
| ZEBOV GP | ZEBOV glycoprotein |

## Amino acid abbreviations

After the 1984 recommendation of the Joint Commission on Biochemical Nomenclature (JCBN) (IUPAC-IUB Joint Commission on Biochemical Nomenclature (JCBN)., 1984).

| Amino acid | Three-letter code | One-letter code |
|---|---|---|
| Alanine | Ala | A |
| Arginine | Arg | R |
| Asparagine | Asn | N |
| Aspartic acid | Asp | D |
| Cysteine | Cys | C |
| Glutamic acid | Glu | E |
| Glutamine | Gln | Q |
| Glycine | Gly | G |
| Histidine | His | H |
| Isoleucine | Ile | I |
| Leucine | Leu | L |
| Lysine | Lys | K |
| Methionine | Met | M |
| Phenylalanine | Phe | F |
| Proline | Pro | P |
| Serine | Ser | S |
| Threonine | Thr | T |
| Tryptophan | Try | W |
| Tyrosine | Tyr | Y |
| Valine | Val | V |

# 10 Appendix

## I. Figures and tables

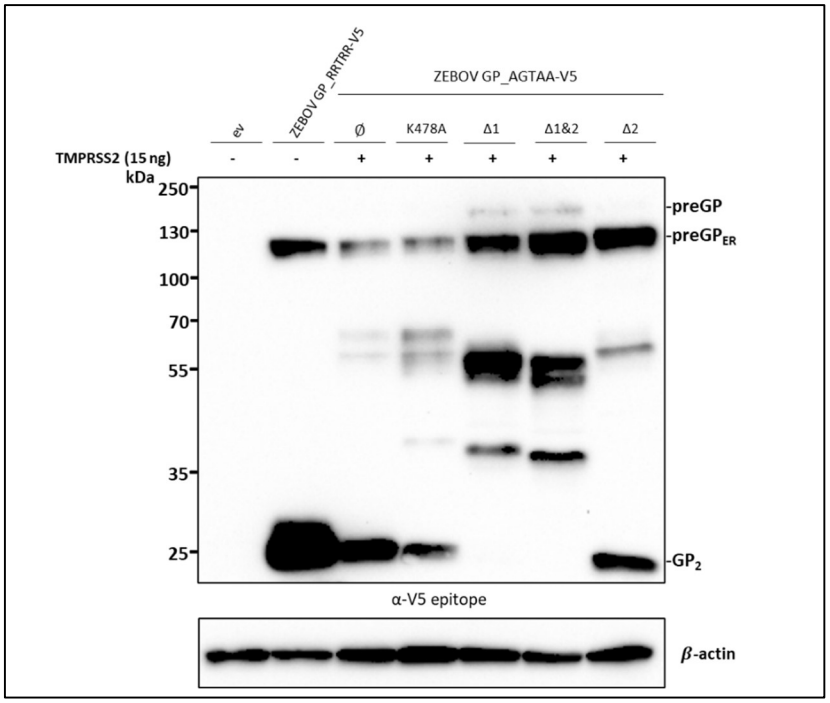


**Figure 26: Comparison of proteolytic cleavage product of ZEBOV GP_AGTAA variants by TMPRSS2**
HeLa cells were co-transfected with ZEBOV GP_RRTRR, ZEBOV GP_AGTAA without aa exchange (Ø), the single alanine exchange mutant K478A or the deletion variants ZEBOV GP_AGTAAΔ1, Δ2 and Δ1&2 and human TMPRSS2 plasmid for 24 h. Afterward, the cells were lysed and the samples were analyzed using a 10 % SDS-PAGE and immunoblotting. ZEBOV GP cleavage forms were detected with an antibody directed against the V5 epitope of ZEBOV GP. The ß-Actin staining was used as a loading control. Western blots shown are representative immunoblots from three independent experiments (n=3).

**Table 33: Sequence alignment of human CoV S1/2 and S2' cleavage sites.**

| Virus | S1/S2 site | S2′ site | GenBank sequence |
|---|---|---|---|
| SARS-CoV-2 | TNSP**RR**A**R**↓SVA | PSKPSK**R**↓SFIEDL | YP_009724390.1 |
| SARS-CoV | S----LL**R**↓STS | PLKPTK**R**↓SFIEDL | AAP13441.1 |
| MERS-CoV | TLTP**R**SV**R**↓SVP | TGS**R**SA**R**↓SAIEDL | QFQ59587.1 |
| HCoV-OC43 | SKT**RR**S**RR**↓AIT | CSKASS**R**↓SAIEDL | AMK59677.1 |
| HCoV-229E | SIIAVQP**R**↓NVS | GSRVAG**R**↓SAIEDI | APT69890.1 |
| HCoV-NL63 | SLIPVRP**R**↓NSS | SSRIAG**R**↓SALEDL | AFV53148.1 |
| HCoV-HKU1 | SSS**RRKRR**↓SIS | CGS-SS**R**↓SFFEDL | AAT98580.1 |
| MHV-A59 | -S**RR**AH**RR**↓SVS | PSAIRG**R**↓SAIEDL | NP_045300.1 |

# II. Inhibitors

### Trypsin-like protease inhibitors

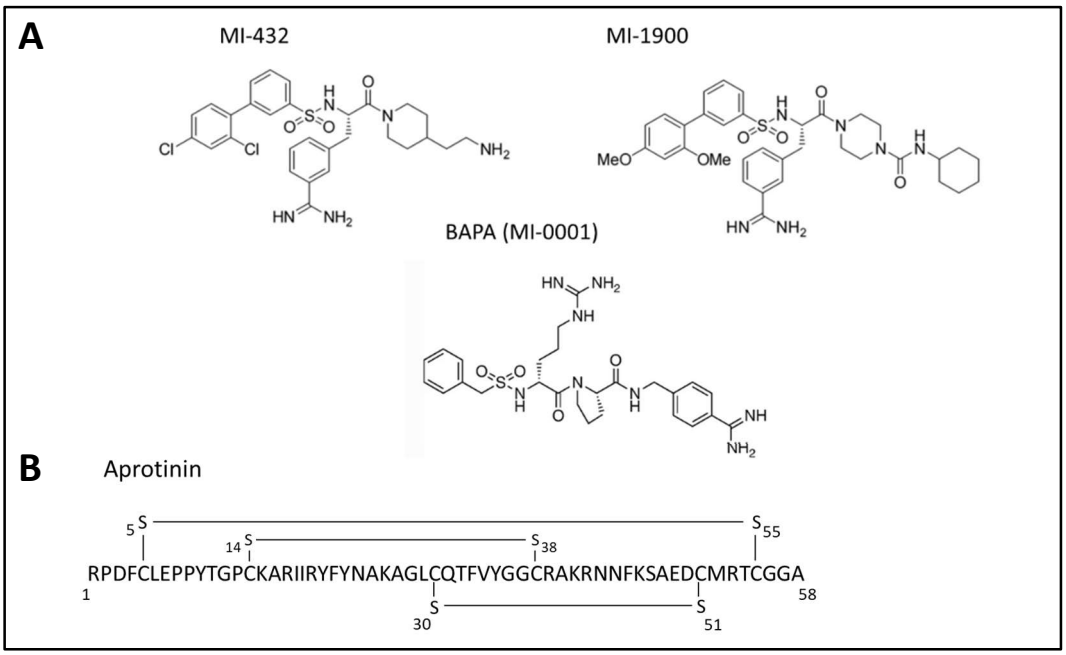


**A**) Structure of synthetic peptide mimetic broad range inhibitor BAPA (MI-0001) and structure-based inhibitors MI-432 and MI-1900 (Steinmetzer & Hardes, 2018). **B**) Amino acid sequence of the natural proteinaceous broad active inhibitor aprotinin (Kassell *et al.*, 1965).

### Furin protease inhibitors

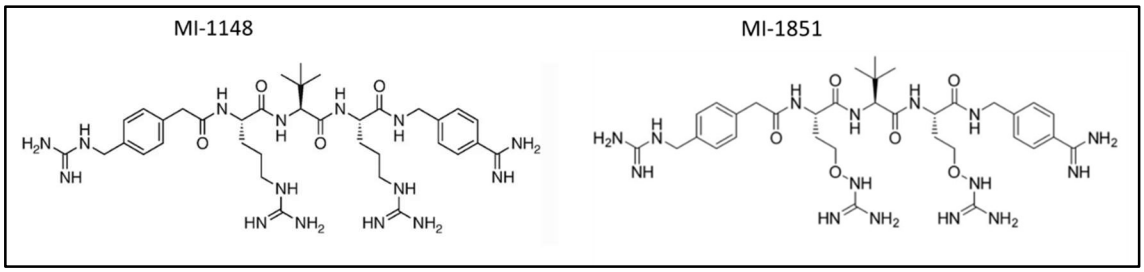


Structure of synthetic substrate analog inhibitors MI-1148 and MI-1851 (Hardes *et al.*, 2015; van Lam van *et al.*, 2021).

### Cysteine protease inhibitor

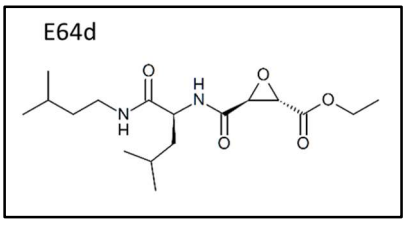


Structure of synthetic covalent irreversible epoxysuccinate-based inhibitor E64d (Tamai *et al.*, 1986).

## III. Amino acid sequences

**Human furin**: 794 aa (Uniport: P09958)

MELRPWLLWVVAATGTLVLLAADAQGQKVFTNTWAVRIPGGPAVANSVARKHGFLNLGQIFGDYYHFWHRGVTKR
SLSPHRPRHSRLQREPQVQWLEQQVAKRRTKRDVYQEPTDPKFPQQWYLSGVTQRDLNVKAAWAQGYTGHGIVVSI
LDDGIEKNHPDLAGNYDPGASFDVNDQDPDPQPRYTQMNDNRHGTRCAGEVAAVANNGVCGVGVAYNARIGGVR
MLDGEVTDAVEARSLGLNPNHIHIYSASWGPEDDGKTVDGPARLAEEAFFRGVSQGRGGLGSIFVWASGNGGREHDS
CNCDGYTNSIYTLSISSATQFGNVPWYSEACSSTLATTYSSGNQNEKQIVTTDLRQKCTESHTGTSASAPLAAGIIALTLEA
NKNLTWRDMQHLVVQTSKPAHLNANDWATNGVGRKVSHSYGYGLLDAGAMVALAQNWTTVAPQRKCIIDILTEPK
DIGKRLEVRKTVTACLGEPNHITRLEHAQARLTLSYNRRGDLAIHLVSPMGTRSTLLAARPHDYSADGFNDWAFMTTHS
WDEDPSGEWVLEIENTSEANNYGTLTKFTLVLYGTAPEGLPVPPESSGCKTLTSSQACVVCEEGFSLHQKSCVQHCPPG
FAPQVLDTHYSTENDVETIRASVCAPCHASCATCQGPALTDCLSCPSHASLDPVEQTCSRQSQSSRESPPQQQPPRLPP
EVEAGQRLRAGLLPSHLPEVVAGLSCAFIVLVFVTVFLVLQLRSGFSFRGVKVYTMDRGLISYKGLPPEAWQEECPSDSEE
DEGRGERTAFIKDQSAL

**Human TMPRSS2, isoform 2**: 492 aa (NCBI: NP_005647.3)

MALNSGSPPAIGPYYENHGYQPENPYPAQPTVVPTVYEVHPAQYYPSPVPQYAPRVLTQASNPVVCTQPKSPSGTVCT
SKTKKALCITLTLGTFLVGAALAAGLLWKFMGSKCSNSGIECDSSGTCINPSNWCDGVSHCPGGEDENRCVRLYGPNFIL
QVYSSQRKSWHPVCQDDWNENYGRAACRDMGYKNNFYSSQGIVDDSGSTSFMKLNTSAGNVDIYKKLYHSDACSSK
AVVSLRCIACGVNLNSSRQSRIVGGESALPGAWPWQVSLHVQNVHVCGGSIITPEWIVTAAHCVEKPLNNPWHWTAF
AGILRQSFMFYGAGYQVEKVISHPNYDSKTKNNDIALMKLQKPLTFNDLVKPVCLPNPGMMLQPEQLCWISGWGATE
EKGKTSEVLNAAKVLLIETQRCNSRYVYDNLITPAMICAGFLQGNVDSCQGDSGGPLVTSKNNIWWLIGDTSWGSGCA
KAYRPGVYGNVMVFTDWIYRQMRADG

**Bovine Cathepsin B**: 335 aa (Uniprot: P07688)

MWRLLATLSCLLVLTSARSSLYFPPLSDELVNFVNKQNTTWKAGHNFYNVDLSYVKKLCGAILGGPKLPQRDAFAADVV
LPESFDAREQWPNCPTIKEIRDQGSCGSCWAFGAVEAISDRICIHSNGRVNVEVSAEDMLTCCGGECGDGCNGGFPSG
AWNFWTKKGLVSGGLYNSHVGCRPYSIPPCEHHVNGSRPPCTGEGDTPKCSKTCEPGYSPSYKEDKHFGCSSYSVANN
EKEIMAEIYKNGPVEGAFSVYSDFLLYKSGVYQHVSGEIMGGHAIRILGWGVENGTPYWLVGNSWNTDWGDNGFFKI
LRGQDHCGIESEIVAGMPCTHQY

**ZEBOV GP Makona C7**: 676 aa (NCBI: AIW47462.1)

MGVTGILQLPRDRFKRTSFFLWVIILFQRTFSIPLGVIHNSTLQVSDVDKLVCRDKLSSTNQLRSVGLNLEGNGVATDVPS
ATKRWGFRSGVPPKVVNYEAGEWAENCYNLEIKKPDGSECLPAAPDGIRGFPRCRYVHKVSGTGPCAGDFAFHKEGA
FFLYDRLASTVIYRGTTFAEGVVAFLILPQAKKDFFSSHPLREPVNATEDPSSGYYSTTIRYQATGFGTNETEYLFEVDNLTY
VQLESRFTPQFLLQLNETIYASGKRSNTTGKLIWKVNPEIDTTIGEWAFWETKKNLTRKIRSEELSFTAVSNGPKNISGQS
PARTSSDPETNTTNEDHKIMASENSSAMVQVHSQGRKAAVSHLTTLATISTSPQPPTTKTGPDNSTHNTPVYKLDISEA
TQVGQHHRRADNDSTASDTPPATTAAGPLKAENTNTSKSADSLDLATTTSPQNYSETAGNNNTHHQDTGEESASSGK
LGLITNTIAGVAGLITGGRRTRREVIVNAQPKCNPNLHYWTTQDEGAAIGLAWIPYFGPAAEGIYTEGLMHNQNGLICG
LRQLANETTQALQLFLRATTELRTFSILNRKAIDFLLQRWGGTCHILGPDCCIEPHDWTKNITDKIDQIIHDFVDKTLPDQ
GDNDNWWTGWRQWIPAGIGVTGVIIAVIALFCICKFVF

**SARS-CoV-2 S Wuhan-Hu-1**: 1273 aa (NCBI: YP_009724390.1)

MFVFLVLLPLVSSQCVNLTTRTQLPPAYTNSFTRGVYYPDKVFRSSVLHSTQDLFLPFFSNVTWFHAIHVSGTNGTKRFD
NPVLPFNDGVYFASTEKSNIIRGWIFGTTLDSKTQSLLIVNNATNVVIKVCEFQFCNDPFLGVYYHKNNKSWMESEFRVY
SSANNCTFEYVSQPFLMDLEGKQGNFKNLREFVFKNIDGYFKIYSKHTPINLVRDLPQGFSALEPLVDLPIGINITRFQTLL
ALHRSYLTPGDSSSGWTAGAAAYYVGYLQPRTFLLKYNENGTITDAVDCALDPLSETKCTLKSFTVEKGIYQTSNFRVQP
TESIVRFPNITNLCPFGEVFNATRFASVYAWNRKRISNCVADYSVLYNSASFSTFKCYGVSPTKLNDLCFTNVYADSFVIR
GDEVRQIAPGQTGKIADYNYKLPDDFTGCVIAWNSNNLDSKVGGNYNYLYRLFRKSNLKPFERDISTEIYQAGSTPCNG
VEGFNCYFPLQSYGFQPTNGVGYQPYRVVVLSFELLHAPATVCGPKKSTNLVKNKCVNFNFNGLTGTGVLTESNKKFLP
FQQFGRDIADTTDAVRDPQTLEILDITPCSFGGVSVITPGTNTSNQVAVLYQDVNCTEVPVAIHADQLTPTWRVYSTGS
NVFQTRAGCLIGAEHVNNSYECDIPIGAGICASYQTQTNSPRRARSVASQSIIAYTMSLGAENSVAYSNNSIAIPTNFTISV
TTEILPVSMTKTSVDCTMYICGDSTECSNLLLQYGSFCTQLNRALTGIAVEQDKNTQEVFAQVKQIYKTPPIKDFGGFNFS
QILPDPSKPSKRSFIEDLLFNKVTLADAGFIKQYGDCLGDIAARDLICAQKFNGLTVLPPLLTDEMIAQYTSALLAGTITSG
WTFGAGAALQIPFAMQMAYRFNGIGVTQNVLYENQKLIANQFNSAIGKIQDSLSSTASALGKLQDVVNQNAQALNTL
VKQLSSNFGAISSVLNDILSRLDKVEAEVQIDRLITGRLQSLQTYVTQQLIRAAEIRASANLAATKMSECVLGQSKRVDFC
GKGYHLMSFPQSAPHGVVFLHVTYVPAQEKNFTTAPAICHDGKAHFPREGVFVSNGTHWFVTQRNFYEPQIITTDNTF
VSGNCDVVIGIVNNTVYDPLQPELDSFKEELDKYFKNHTSPDVDLGDISGINASVVNIQKEIDRLNEVAKNLNESLIDLQE
LGKYEQYIKWPWYIWLGFIAGLIAIVMVTIMLCCMTSCCSCLKGCCSCGSCCKFDEDDSEPVLKGVKLHYT

# IV. Publications

## Publications

*__Bestle, D__., *Limburg, H., Kruhl, D., Harbig, A., Stein, D. A., Moulton, H., Matrosovich, M., Abdelwhab, E. M., Stech, J., Böttcher-Friebertshäuser, E. (2021). *shared first authorship. *Hemagglutinins of Avian Influenza Viruses Are Proteolytically Activated by TMPRSS2 in Human and Murine Airway Cells*. Journal of virology 95 (20), e0090621. DOI: 10.1128/JVI.00906-21.

*__Bestle, D__.,*Heindl, M. R.,*Limburg, H., Van Lam van, T., Pilgram, O., Moulton, H. M., Stein, D. A., Hardes, K., Eickmann, M., Dolnik, O., Rohde, C., Klenk, H.-D., Garten, W., Steinmetzer, T., Böttcher-Friebertshäuser E. (2020). *shared first authorship. *TMPRSS2 and furin are both essential for proteolytic activation of SARS-CoV-2 in human airway cells*. Life Sci Alliance. 2020 Sep; 3(9): e202000786; DOI: 10.26508/lsa.202000786

Limburg, H., Harbig, A., **Bestle, D**., Stein, D. A., Moulton, H. M., Jaeger, J., Janga, H., Hardes, K., Koepke, J., Schulte, L., Koczulla A. R., Schmeck, B., Klenk, H.-D., and Böttcher-Friebertshäuser, E. (2019). *TMPRSS2 is the major activating protease of influenza A virus in primary human airway cells and influenza B virus in human type II pneumocytes*. Journal of Virology 93:e00649-19; https://doi.org/10.1128/JVI.00649-19.

## Oral presentations

*Hemagglutinins of Avian Influenza Viruses are proteolytically activated by TMPRSS2 in Human and Murine Airway Cells.* 4 th Retreat of the LOEWE Center DRUID. „Novel Drug Targets against Poverty-Related and Neglected Tropical Infectious Diseases“ at Rauischholzhausen Castle, 18.-19. November 2021

*Inhibition of virus-activating host cell proteases.* 1st Retreat of the LOEWE Center DRUID „Novel Drug Targets against Poverty-Related and Neglected Tropical Infectious Diseases“ at Rauischholzhausen Castle, 26-27. November 2018

## Poster

**Bestle, D.**, Bittel, L.; Steinmetzer, T; Böttcher-Friebertshäuser, E.: *Characterization of Proteolytic Activation of Ebola Virus GP by different Host Cell Proteases.* 30th Annual Meeting of the Society for Virology, digital, 24.-26. March 2021

**Bestle, D.**, Bittel, L.; Steinmetzer, T; Böttcher-Friebertshäuser, E.: *Characterization of Proteolytic Activation of Ebola Virus GP by different Host Cell Proteases.* 2nd Retreat of the LOEWE Center DRUID. „Novel Drug Targets against Poverty-Related and Neglected Tropical Infectious Diseases" at Rauischholzhausen Castle, 25 –26. November 2019

Limburg, H., **Bestle, D**., Janga, H.; Schulte, L., Moulton, H. M., Stein, D. A., Böttcher-Friebertshäuser, E.: *TMPRSS2 is essential for proteolytic activation and spread of influenza A virus in bronchial cells and for both influenza A and B virus in human type II pneumocytes*. 7th Meeting of the European Congress of Virology (ECV), Rotterdam, 28. April – 01. May 2019

Limburg, H., **Bestle, D**., Janga, H.; Schulte, L., Moulton, H. M., Stein, D. A., Böttcher-Friebertshäuser, E.: *TMPRSS2 is essential for proteolytic activation and spread of influenza A virus in human airway epithelial cells*. 28th Annual Meeting of the Society for Virology, Würzburg, 14.-17. March 2018

## V. List of academic teachers

Meine akademischen Lehrer*innen an der Philipps-Universität Marburg waren die Damen und Herren Professoren bzw. Privat-Dozenten:

S. Bauer, U. Bauer, S. Becker, M. Conrad, D. Brandt, A. Brehm, J. Daut, O. Dolnik, M. Eickmann, P. Elsässer, B. Feuser, E. Friebertshäuser, B. Fritz, M. Huber, R. Jakob, L. Kolesnikova, R. Lill, M. Lohoff, A. Maisner, W. Milani, U. Mühlenhoff, D. Oliver, T. Plant, R. Preisig-Müller, B. Schmeck, M. Schnare, L. Schulte, M. Schween, U. Steinhoff, D. Strauer, G. Suske, W. Slenzka, A. Visekruna, K. Westermann, C. Wrocklage, P. Yu,

## VI. Acknowledgements

Zum Schluss möchte ich mich ganz herzlich bei allen Menschen bedanken, die mich in den Jahren meiner Doktorarbeit begleitet und unterstützt haben. Ein ganz besonderer Dank gilt natürlich meiner Betreuerin und Erstgutachterin Prof. Dr. Eva Friebertshäuser. Liebe Eva, du hast immer ein offenes Ohr für alle Fragen, Probleme und vor allem Ideen. Ich danke dir, dass du mir ermöglicht hast unglaublich frei an meinem Projekt zu arbeiten. Während Corona hast du unserer Arbeitsgruppe zudem die einmalige Chance eröffnet, direkt an diesem unglaublich spannenden Thema mitzuwirken, vielen Dank dafür.

Unserem Institutsleiter Prof. Dr. Stephan Becker danke ich für die besondere arbeitsgruppenübergreifende Zusammenarbeit und tolle Atmosphäre am Institut für Virologie. Dem LOEWE Zentrum DRUID danke ich für die Finanzierung und dafür, dass ich ein Teil dieses spannenden Konsortiums zur Erforschung von vernachlässigten Erkrankungen sein durfte.

Darüber hinaus danke ich meinen Kooperationspartnern, die mich im Laufe meiner Arbeit unterstützt haben. Prof. Dr. Torsten Steinmetzer und seiner Arbeitsgruppe möchte ich für die großzügige Bereitstellung und stetige Weiterentwicklung der Proteaseinhibitoren danken, ohne die meine Arbeit nicht möglich gewesen wäre. Aber auch ein großes Dankeschön an meine Institutskollegen und hier besonders Dr. Olga Dolnik für die Bereitstellung der rekombinanten VSV-Pseudoviren, Dr. Cornelius Rhode und Lennart Kämper für die Bereitstellung und Hilfe mit dem trVLP System und Dr. Sandro Halwe für die Einarbeitung und die Hilfe am KLSM, sowie für das Coloc-Makro. Nicht zu vergessen, vielen Dank an das BSL-3 Team, hier vor allem Prof. Dr. Marcus Eickmann für die tatkräftige Unterstützung bei den SARS-CoV-2-Projekten und die Überwachung unserer Sicherheit. Aber auch ein großer Dank an Anne, Hannah und Ruth, es war eine sehr anstrengende, aber auch unvergessliche Zeit im BSL-3 unter Pandemiebedingungen, die ich mit niemand anderen hätte erleben wollen.

Ein ganz besonderer Dank gilt meiner Arbeitsgruppe, der AG Friebertshäuser (Aka der eitrige Appendix), mit allen ehemaligen und aktuellen Mitgliedern. Ich kann mich sehr glücklich schätzen, dass ich euch damals zugelost wurde (Obwohl ich nie in die Virologie wollte!). Anne, Hannah, Ruth, Marie, Elisa, Diana, Aline, Julia, Anna-Lena, Moritz, Anki, Linda und wen ich möglicherweise noch vergessen habe, vielen Dank für die tolle Zusammenarbeit und die ausgelassene Stimmung im Labor. Ich verdanke euch eine unglaublich schöne Zeit mit unermüdlichen wissenschaftlichen Input, so wie absolut unwissenschaftlichen Mittagspausen und Trash-TV Abenden. Liebe Anne, du warst über viele Jahre mein treuer, zuweilen zuckersüchtiger Sitznachbar, und meine persönliche wandelnde Protease-Expertin. Vielen Dank für die vielen Diskussionen über meine Blots und, dass du noch dazu meine Freude am Bouldern

teilst (mit der wir Hannah und Marie auch angesteckt haben). Liebe Ruth, ich danke dir für deine überschwängliche gute Laune, deinen Optimismus vor allem bei neuen Projekten und natürlich deine Backleidenschaft, von der wir regelmäßig profitieren. Ich danke dir, liebe Marie für dein immer offenes Ohr und dafür, dass du meine Leidenschaft für das Aufräumen und die Ordnung im Labor teilst (Zusammen könnten wir das effizienteste Freezersystem der Welt erschaffen!). Liebe Hannah, ich gehe mit dir gern als „Hasi & Schatzi“ auf Tour und ich bin sehr glücklich, dass aus der anfänglichen Praktikumsbetreuung eine tolle Freundschaft gewachsen ist, die auch nach deinem Weggang aus der AG anhält. Deine falschen Zitate haben den Laboralltag unendlich versüßt und ich freue mich jedes Jahr auf das beste Festival unter spanischer Sonne mit dir.

Zu guter Letzt möchte ich noch meinen Freunden und Familie danken. Meine Mädels aus KF, Toni, Immo und Billy danke, dass ihr mich immer unterstützt habt und ich bei meinen seltenen Besuchen in der Heimat darauf zählen kann mit euch eine tolle Zeit zu haben. Liebste Billy, ohne dich hätte ich meine Studienbewerbung nie abgeschickt und du würdest mich immer noch auf dem Erlenhof besuchen.

Meine Familie Ma, Pa, Hena, Felix (inklusive Armin und Johanna) auf eure Unterstützung kann ich mich immer verlassen, egal welchen Weg ich in meinem Leben eingeschlagen habe und noch einschlagen werde. Mir hat in den letzten Jahren meiner Doktorarbeit sehr geholfen, dass ihr mich immer wieder bestärkt habt weiter zu machen, auch wenn es mir manchmal schwerfällt das Positive zu sehen. Zusätzlich war ich viele Jahre glücklicher Empfänger des Ma&Pa-Stipendiums, vielen Dank dafür. Leni, ich bin sehr stolze Tante-Todi und freu mich jedes Mal, wenn ich dich Besuchen komme und wir zusammen Unfug machen, währenddessen sind alle Probleme und Anstrengungen der Doktorarbeit vergessen. Robert, du bist seit meinem Neuanfang in Marburg an meiner Seite und wir haben alle Höhen und Tiefen, die das Studium und das Leben an sich bieten zusammen gemeistert. Du bist mein aktiver und gut gelaunter Gegenpol, verstehst meine Daten und hast mich auch in meinen schlimmsten Zweifelphasen immer wieder aufgebaut. Ein großes Dankeschön an dich und Hannah, dass ihr trotz eurer stressigen Jobs noch die Zeit gefunden habt, meine Arbeit Korrektur zu lesen.

Ganz zum Schluss möchte ich meiner Oma und meinem Opa danken, ihr habt mir mein erstes Kindermikroskop geschenkt und meine Leidenschaft für die Natur und vor allem für die Naturwissenschaften geweckt. Opa, dass ich mit dir über meine Forschung sprechen kann und sehe wie stolz du bist, macht mich sehr glücklich.